STRENGTH OF HOLLOW CONCRETE BLOCK MASONRY WALLS

SUBJECT TO

LATERAL (OUT-OF-PLANE) LOADING

By

© AHMED SHERIF ALY AHMED ESSAWY, B.Sc., M.Sc.

A Thesis

Submitted to the School of Graduate Studies

in Partial Fulfillment of the Requirements

for the Degree

Doctor of Philosophy

McMaster University

September 1986

STRENGTH OF BLOCK MASONRY WALLS

SUBJECT TO LATERAL LOADING

To my kind parents,

my patient wife

and

my daughter

DOCTOR OF PHILOSOPHY (1986)
(Civil Engineering and
Engineering Mechanics)

McMASTER UNIVERSITY
Hamilton, Ontario

TITLE: Strength of Hollow Concrete Block Masonry Walls
             Subject to Lateral (Out-of-Plane) Loading

AUTHOR: Ahmed Sherif Aly Ahmed Essawy, B.Sc.   (Ain Shams University)

                                          M.Sc.   (Ain Shams University)

SUPERVISOR: Dr. R. G. Drysdale

NUMBER OF PAGES: xxvii, 426

ABSTRACT

Provisions for the design of masonry walls subject to uniformly distributed pressure normal to the surface of the, wall differ significantly from country to country. These differences may be attributed both to differences in design philosophy and to a general lack of conclusive or widely accepted experimental and analytical research. Most of the previous research in this area was concerned with brick masonry and with practical rather than well defined support conditions. Also, the available design methods were not accurate or rational. Therefore, this study was initiated to investigate the flexural behaviour of hollow concrete block masonry both experimentally and analytically and to assess the design methods for laterally loaded walls.

The experimental program included 30 full scale wall tests representing different support conditions and aspect ratios. In addition, stack bonded prisms and wallettes were used to determine the flexural tensile strengths. The full scale tests were performed using a test facility designed to accommodate tests of masonry panels up to 6.0 m long by 3.6 m high and to provide well defined support conditions. The observed behaviours of the walls were compared to other walls of the same series and to other tests to investigate the effects of variability, aspect ratio, support conditions, and the presence of either precompression along the top of the panel or precracking near the panel center.

iii

A nonlinear finite element model capable of reproducing the observed behaviour of the walls was developed and used to extend the knowledge of masonry wall behaviour to include untested conditions and configurations. In this model, the anisotropic nature of masonry, the nonlinearity due to cracking, and the effects of the transverse shear deformations due to the presence and the discontinuity of the core webs were taken into consideration. Also, the existing biaxial failure criteria were examined and a proposed macroscopic biaxial failure criterion was incorporated in the finite element model to predict the strengths and the failure modes for masonry assemblages. This criterion accounted for the anisotropic and composite nature of masonry and was based on physical interpretations rather than being strictly a phenomenological criterion.

Finally, the available design methods were compared using the extended data from the analytical model and a design method based on elastic plate theory was proposed. This method was rationally developed to predict first cracking and failure capacities for masonry panels simply supported on three and four sides for a wide range of aspect ratios.

ACKNOWLEDGEMENTS.

help, patience, deep understanding, and encouragement towards the completion of this thesis.

Finally, praise be to God who bestowed on me the faith which has been the nourishing source of all my activities including this present work.

TABLE OF CONTENTS

ix

x

LIST OF FIGURES

xiv

xv

LIST OF TABLES

NOTATION

$2a$, b	nominal length and height of the masonry unit, respectively.
D	flexural rigidity of plate.
dt	arbitrary shell thickness.
E_b, G_b	modulus of elasticity and shear modulus of the masonry units, respectively.
E_m, G_m	equivalent or apparent linear modulus of elasticity and shear modulus of the mortar joints, respectively.
E_n, E_p, G_{np}	respectively, modulii of elasticity normal and parallel to the bed joints and the in-plane shear modulus for the equivalent masonry material.
E'_p, G'_{np}	respectively, reduced modulus of elasticity parallel to the bed joints and reduced shear modulus for the equivalent masonry material after head joint strength limit.
E_w	modulus of elasticity for the web material.
E_x, E_y	modulii of elasticity in the x and y directions, respectively.
E_{xf}, E_{yf}	modulii of elasticity for the orthotropic face shell material.
f'_{tn}	uniaxial tensile strength of the masonry assemblage normal to the bed joints.
f'_{tpI}, f'_{tpII}	uniaxial tensile strengths parallel to the bed joints for vertical splitting and vertically toothed failure patterns, respectively.
f'_{snpI}, f'_{snpII}	pure shear strength for diagonal splitting and diagonally stepped failure modes, respectively.
$f'_{t\theta}$	flexural tensile strength of assemblages for direction of bending oriented at θ° from the bed joints.
G_f	shear modulus of the face shell material.

G_w	shear modulus of the web material.
G_{xy}, G_{xz}, G_{yz}	shear modulii in the x-y, x-z, and y-z planes, respectively.
h	height of the cellular plate measured between center lines of the face shells (see Figure 6.6).
h_b, l_b	height and length of the masonry unit, respectively.
L, H	length and height of masonry panel, respectively.
M_h, M_v	maximum moments of the horizontal and vertical strips due to uniform loads of p_h and p_v, respectively.
M_n, M_p, M_θ	bending moment capacities per unit length normal, parallel, and at an angle θ with respect to the bed joints, respectively.
M_{xo}, M_{yo}	maximum moments of simply supported beams subjected to the total load of the panel, p, in the horizontal and vertical directions, respectively.
N_i, N_i^o, N_i^s	I-shape functions for the 12 DOF nonconforming plate bending, 8 DOF plane stress and 8 DOF transverse shear rectangular elements, respectively.
n	number of layers in the multilayer plate.
p	uniformly distributed load on the panel or plate.
p_h, p_v	equivalent loads on the horizontal and vertical strips, respectively.
R	orthogonal strength ratio
r	panel length to height or aspect ratio; L/H
R_I, R_{II}	orthogonal strength ratios for vertical splitting and vertically stepped patterns in tension parallel to the bed joints, respectively.
t_f, t_w	respectively, thickness of the face shell and the web of cellular plate or hollow block.
t_m	thickness of mortar joint
u, v, w	displacements in the coordinate directions x, y, z, respectively.
u^o, v^o	middle surface displacements in the coordinate

	directions x and y, respectively.
x, y, z	cartisian coordinate directions.
α, β	coefficients which define the ratios of load on the vertical and horizontal equivalent strips, respectively, to determine moments at plate center.
α_s	factor introduced to account for non-uniform shear deformations.
α_c, β_c	reduction factors for the modulii of elasticity and the shear modulii, respectively, for cracked elements.
$\gamma_{xy}, \gamma_{xz}, \gamma_{yz}$	shear strains in x-y, x-z, and y-z planes, respectively.
γ_{xy}^o	shear strain in the xy plane (the middle surface).
Δ_b, Δ_m	total displacements occurring in the units and mortar joints, respectively.
Δ_s, Δ_t	total displacements due to shear and tension, respectively.
$\varepsilon_x, \varepsilon_y$	strains in the x and y directions, respectively.
$\varepsilon_x^o, \varepsilon_y^o$	middle surface strains in the x and y directions, respectively.
ξ, η	nondimensional coordinates with the origin at the left bottom corner (see Figure 6.4).
θ^o	angle between the direction of tension or bending and the bed joint orientation.
θ_x, θ_y	total section rotations about the y and x axes, respectively.
λ	cross web spacing.
μ	coefficient of friction between mortar and masonry units.
ν_b	Poisson's ratio of the masonry units.
ν_{np}	Poisson's ratio of the equivalent masonry material in the direction parallel to the bed joints.
ν_w	Poisson's ratio of the web material.

ν_{xy}, ν_{yx}	Poisson's ratios of an orthotropic material in the y and x directions, respectively.
σ_c	compressive stresses normal to the crack.
σ_{cbm}, σ_{tbm}, σ_{sbm}	respectively, compressive, tensile, and shear bond stresses on mortar joints at failure.
σ_{cbmo}	normal stress at zero shear according to Coulomb's straight line assumption (see Figure 5.2).
σ_n, σ_p, τ_{np}	stresses at the extreme fibers of the assemblage normal and parallel to the bed joints and shear stresses, respectively.
σ_{sbl}, σ_{tbl}	shear stresses on masonry units and tensile strength of the units, respectively.
σ_{sbmo}, σ_{tbmo}	respectively, shear and tensile bond strengths of mortar joints.
σ_x, σ_y, σ_z	normal stresses in the x, y, and z directions, respectively.
τ_{xy}, τ_{xz}, τ_{yz}	shear stresses in the x-y, x-z, and y-z planes, respectively.
ϕ_x, ϕ_y	uniform shear deformations in the x-z and y-z planes, respectively.
x_x, x_y, x_{xy}	respectively, curvatures due to flexure in the x direction, flexure in the y direction, and due to torsion including the effects of the shear deformations.
$[\bar{B}]$ 8x28	generalized strain matrix relating the generalized strain vector to the displacement vector.
$[D]^k$ 5x5	elasticity matrix for layer k.
$[D_{cr}]$ 5x5	modified elasticity matrix for the cracked element.
$[D_{ef}]$ 3x3	extension/flexure elasticity submatrix.
$[D_s]$ 2x2	shear elasticity submatrix.

$[\bar{D}]$ 8x8	total rigidity matrix.
$[\bar{D}_c]$ 3x3	extension/flexure coupling rigidity submatrix.
$[\bar{D}_e]$, $[\bar{D}_f]$, 3x3 3x3	extension and flexure rigidity submatrices, respectively.
$[\bar{D}_s]$ 2x2	shear rigidity submatrix.
$[K_e]$ 28x28	element stiffness matrix.
$\{M\}$, $\{N\}$, $\{Q\}$	internal bending moment, in-plane force, and shear force vectors, respectively.
$\{u\}$	displacement vector.
$\{\varepsilon\}$, $\{\bar{\varepsilon}\}$, $\{d\varepsilon\}$	strain, generalized strain, and incremental strain vectors, respectively.
$\{\varepsilon_s\}$	shear strain vector.
$\{\sigma\}$, $\{\bar{\sigma}\}$, $\{d\sigma\}$	stress, generalized stress, and incremental stress vectors, respectively.
$\{x\}$	vector containing the curvatures including the shear deformations.

CHAPTER 1

INTRODUCTION

1.1 GENERAL

Masonry has been used as a building material since the early days of man. However, significant research and engineered design of masonry structures has really only occurred in the last three decades. Specifically, masonry walls subjected to lateral loads did not receive the attention of masonry researchers because walls for domestic buildings were relatively thick. It was not until the development of modern wall construction, with the use of larger column spacings, greater column heights and thinner masonry units, that the potential for failure due to out-of-plane bending existed.

Provisions for the design of masonry walls subject to uniformly distributed pressure normal to the surface of the wall differ significantly from country to country. These differences may be attributed both to differences in design philosophy and to a general lack of conclusive or widely accepted experimental and analytical research. The low flexural tensile strength of masonry and its high variability make it difficult to identify the effects of different factors on the flexural behaviour of masonry panels and necessitate many replications of experiments. Also, the time and cost associated with testing full scale walls make it impractical to consider testing sufficient combinations of conditions to provide or confirm adequate

1

design provisions or procedures. On the other hand, rational analysis was not an easy task because of the non-homogeneous and anisotropic nature of masonry assemblages. Furthermore, the available design methods were not accurate or rational. Therefore, it was apparent that much more research was required before alternative design provisions and procedures can be proposed and justified by adequate evidence.

Concentrated efforts of researchers in England, Scotland, Sweden and Australia over the last two decades were made in this area but most of the research was concerned with brick masonry and with practical rather than well defined support conditions. However, this existing work is beneficial in understanding the behaviour of masonry as a whole regardless of the masonry units used. Nonetheless, the body of test data, particularly with well defined support conditions is very small and for North American conditions is almost non-existent.

In this chapter, the available research work for laterally loaded brick and block masonry panels is reviewed. Then, the objectives of the research program and the scope of this dissertation are outlined.

1.2 LATERALLY LOADED MASONRY PANELS- "LITERATURE REVIEW"

The literature review of the behaviour of laterally loaded masonry walls would have been lengthy and difficult task without the available extensive reviews provided by Baker [22], Lawrence [71], Cajdert [30], Gairns [44] and recently the state of the art report by Baker, Gairns, Lawrence and Scrivener [24]. Therefore, in this chapter only the essential material for this study is reported while the readers are referred to the above mentioned reviews for more complete

information.

It should also be noted that this review deals primarily with the flexural behaviour of single leaf plain masonry panels. Therefore, arching action, reinforced masonry, grouted blockwork and high level of precompression are all considered to be outside the scope of this review and generally outside the scope of this study. The review reported in this section includes flexural behaviour of brick and block masonry assemblages, flexural behaviour of masonry panels, design methods and masonry codes. These four subsections are discussed individually below.

1.2.1. Flexural Behaviour of Brick and Block Masonry Assemblages

The flexural behaviour of masonry assemblages is well known to be different for different orientations of moments with respect to the critical bed and head mortar joints. Therefore, in this section, the flexural behaviour of masonry assemblages is discussed for different cases of bending orientation.

The flexural tensile strength normal to the bed joints is characterized as flexural bond strength since the failure occurs at the mortar/unit interfaces. Different standard tests specified for determination of this strength include third point loads [5,96] and uniformly distributed loads [5] on unit wide stack bonded prisms tested horizontally. Also, this strength can be determined using two unit wide vertical panels subjected to two line loads according to the British Code [28]. Single joint tests are also specified in some codes [4] using couplet specimens. Comparisons of test results are difficult in most cases due to the differences in the loading configurations, number

of units per specimen, bond pattern, joint tooling, and the required number of specimens [44,56]. Accordingly, the suggestion of the direct measurement of single joint strengths [19,22] and the proposed simple test method using the bond wrench [62] can lead to significant improvement of this situation. This test method provides economical and uniform results with the smallest possible specimen size.

Baker [12 to 22 inclusive] investigated the statistical aspects of the flexural tensile strength normal to the bed joints for brickwork. He experimentally evaluated the statistical distribution of joint strengths, differentiated between beam and joint strengths, and investigated four possible failure mechanisms for failure of walls spanning vertically between top and bottom supports. These mechanisms were brittle, successive cracking, partially plastic, and plastic types of failure. Based on the existing experimental evidence, Baker recommended the partially plastic mechanism for brickwork with the plasticity or the sharing of the strengths taking place over three bricks in the panel width. He also produced some curves to evaluate the mean joint strengths and the coefficients of variation from beam test results. His proposal was then used in a computer simulation technique [22] to predict mean panel strengths and the coefficients of variation.

Lawrence and Morgan [67] used Baker's proposal to predict the failure of nine brick high piers and indicated good agreement with experimental results. Gairns [44], based on his experimental research, reported that the load sharing proposed by Baker [22] for brickwork seems to be also applicable to blockwork.

Various load-deflection relationships for specimens in flexure with tension normal to the bed joints have been reported. Fishburn reported a linear relationship for full size concrete masonry walls built with strong mortars and a distinctly nonlinear relationship for weak mortars [44]. However, Lawrence and Morgan [67] indicated a linear relationship up to failure for brick masonry. Anderson found it to be nonlinear for small panels of blockwork (no material details were provided) [44]. Recently, Gairns [44] reported an initial linear relationship up to a limit ranging between 1/3 to 1/2 of the failure load for blockwork piers and thereafter an increasingly nonlinear relationship. The different relationships reported in the literature indicate the need for further investigations to reach a firm conclusion.

Masonry assemblages, tested in flexure with tension parallel to the bed joints, failed in several different modes. These were failure in the head joints and the units of the alternate courses in a single failure plane, debonding along bed and head joints in a vertically toothed pattern, and a combination of the above mentioned modes. The critical mode of failure and the flexural tensile strength parallel to the bed joints are affected by many factors. These include the relative values of the unit flexural tensile strength and the flexural tensile and torsional shear bond strengths of the mortar/unit interfaces, the bond pattern, number of courses in the specimen and the method of loading [44].

The reported test methods for determination of the assemblage flexural tensile strength parallel to the bed joints were beam tests for wallette specimens under central line load [67], two line loads with

nearly constant moment zone [9,37,39,67], or uniformly distributed load [56]. The wallette specimens were tested either in vertical [37,56] or horizontal planes [9,39,67]. Drysdale and Hamid [39] pointed out that the criterion for wallette configuration was to have equal regions of head joints and face shells and to allow for different crack patterns. However, their four course high specimens lacked symmetry of strength with respect to the wallette longitudinal axis.

The effect of using light bed joint reinforcement on the flexural tensile strength was investigated [29,44,56] and was not found to cause significant increases in the capacities before cracking. Also, for the ultimate moment capacities no increases [44] or only minor increases [29,56] were reported.

The reported load-deflection relationships in the literature for wallettes in flexure with tension parallel to the bed joints were similar for both brickwork [70] and blockwork [44]. These load-deflection relationships were characterized by a sudden decrease in the stiffness at 1/3 to 1/2 of the ultimate load with nearly linear behaviour before and after this change. For clay brickwork, based on the experimental evidence, Baker suggested that this decrease in stiffness was not due to head joint cracking but rather he attributed it to the nonlinear behaviour of the head mortar joints [30]. However, Lawrence [70] supported the alternate explanation of head joint cracking. Gairns [44] reported behaviour for concrete blockwork similar to that of Baker and suggested that a combination of plastic redistribution of load due to and associated with the cracking of the head joints may be involved. He also suggested that the relationship

between the elastic modulii before and after the stiffness change may be predicted using the lines of best fit of the available brickwork data provided by Lawrence [70]. He also concluded that load sharing behaviour may also occur in blockwork in flexure with tension parallel to the bed joints.

As reported by Cajdert [30], early proposals for predicting the flexural tensile strength parallel to the bed joints were suggested by Royen and Sahlin [84]. These proposals faced several objections [22] for neglecting the contribution of the head joint strength for the vertically toothed failure mode [30] and for assuming that both units and head joints reach their ultimate strengths simultaneously for the vertical splitting failure mode [84].

The ratio of the flexural tensile strengths parallel and normal to the bed joints, which is known as the orthogonal strength ratio, was studied for both clay brickwork [18,66,86] and concrete blockwork [37,44]. Ratios up to 7.0 and 6.25 were reported for brickwork [86] and blockwork [37], respectively. However, most masonry codes [8,33,96] specify a value of 2 for the orthogonal strength ratio. Lawrence [66] proposed an expression for predicting the orthogonal strength ratio for different flexural tensile strengths normal to the bed joints. This expression was derived using the regression analysis to best fit most of the available brickwork data regardless of the observed failure mode in flexure parallel to the bed joints. Baker [18] considered the difference in modes of failure and produced two expressions to predict the orthogonal strength ratio for the vertical splitting and the vertically toothed modes. His expression for the vertical splitting

mode was proposed on a theoretical basis and then logically adjusted to account for the limited nonlinear behaviour of the head mortar joints. However, the expression for the vertically toothed mode was completely empirical. Baker verified these expressions using available clay brickwork data and later Gairns [44] utilized them and reported reasonably good estimates for concrete blockwork.

The orthogonal stiffness ratio or the degree of orthotropy is defined as the ratio of the modulii of elasticity parallel (before sudden stiffness change) and normal to the bed joints. Reported values in the literature ranged from 0.6 to 1.2 for brickwork [70] and blockwork [44] in most studies. However, Sinha [92] reported an average value of 1.4 for clay brickwork prisms. To best fit his clay brickwork data, Lawrence [70] derived an expression for the relationship between the modulii of elasticity parallel and normal to the bed joints. Anderson suggested a similar relationship [44] for concrete blockwork. From his experimental evidence, Gairns [44] confirmed this for concrete blockwork.

The interaction of the flexural tensile stresses normal and parallel to the bed joints in brickwork was investigated experimentally by Baker [18] who then suggested an elliptical interaction relationship. For concrete blockwork, Gazzola, Drysdale and Essawy [46] discussed this interaction and considered the influence of the different modes of failure. Aspects of stress interactions and failure criteria will be discussed in detail later in Chapter 5 of this thesis.

For off-axis bending of masonry assemblages relating to cases where the longitudinal axis is oriented at various angles to the bed joints, Hedstrom in an early publication [56] reported different strength ratios using different mortars for concrete blockwork wallettes with angles of 0°, 45° and 90° degrees between the longitudinal axis and the bed joint orientation. Then, Satti and Hendry [86] found the strength of brickwork wallettes, having the longitudinal axis oriented at 45° to the bed joints, to be between 1/3 to 1/2 of the strength parallel to the bed joints for a range of orthogonal strength ratios up to 7. On the same topic, Losberg and Johansson as reported by Cajdert [30] concluded that the strength at any orientation can be determined through the vectorial addition of the strengths normal and parallel to the bed joints. This suggestion was confirmed by means of limited experimental results from clay brickwork wallette tests. Baker [22] proposed another expression for determination of the strength for bending at different orientations with respect to the bed joints. This was derived to best fit available brickwork data in the literature. Both of these expressions lacked the symmetry requirements for strengths for bending at 0° and 90° degrees to the bed joints.

Recently, Gazzola [47] reported test results for off-axis bending of concrete blockwork wallettes and prisms. The wallette series were beam type tests which included five different orientations of the longitudinal axis with respect to the bed joints. The prism series included seven orientations and these were tested using the bond wrench test method [62]. At least five specimens were tested for every orientation in each series. These test results form a large part of the

available data for the strengths and the failure modes of concrete blockwork wallettes for different orientations of bending.

1.2.2 FLexural Behaviour of Masonry Panels

In this section, only the flexural behaviour of masonry panels supported on three and four sides are considered. However, behaviour of panels supported only on two sides, where the flexural action is one way action, was considered to be included in the preceding section. Most investigations of the flexural behaviour of masonry panels were experimental rather than theoretical. This stems from the nature of the material which is anisotropic, non-homogeneous and highly variable in most of its properties. Also, by far the majority of the research in this area was concerned with clay brick masonry and very little was related to concrete block masonry or the comparative study of both. In spite of the concentrated efforts of the researchers in the last two decades, the flexural behaviour of masonry panels is not completely understood even for clay brickwork panels.

In an overview of the problem of lateral loading of masonry panels, Baker [15] compared the test results of research work performed in different laboratories and quantitatively investigated some secondary effects. These secondary effects included scale, loading, self weight, arching, rotational restraints at supports, translational yielding of supports, estimates of material properties, failure criterion, and various human factors. He concluded that these secondary effects may be present and are likely to be quite significant compared to the primary flexural action of the panel.

Early investigations for brickwork panels prior to 1970, reviewed by Cajdert [30], showed linear behaviour prior to first cracking followed by gradually increasing deformations. A considerable reserve of strength after first cracking and failure patterns similar to the yield line patterns were reported. Since the early 70's, research interest in this area significantly increased in several countries and many reports have been published. In the next part of this section, most of this work will be reviewed in a chronological order.

In 1972, a series of tests on laterally loaded one-sixth scale model brickwork panels were presented in Satti's Ph.D. thesis and reviewed by Hendry [57]. These panels showed a clearly nonlinear behaviour and failed in a distinct yield line pattern. Baker also presented his work on one-third scale model brickwork panels with simple or rotationally restrained supports [44]. He also compared the test results with analytical and empirical theories and recommended the empirical strip method as the best available at that time.

In 1973, Cajdert and Losberg [29] reported their test results on reinforced and unreinforced light expanded clay block panels. They reported reasonable predictions of first cracking load and failure load using elastic plate theory and yield line theory, respectively, for both unreinforced and reinforced panels. In their yield line analysis, an averaged moment of resistance was used which was obtained by averaging the strengths normal, parallel and at $45°$ with respect to the bed joint orientation.

In the same year, West, Hodgkinson, and Webb [103] presented test results of brickwork panels performed by the British Ceramic Research Association, B.C.R.A. These tests included panels built using different bricks and mortars, different support conditions, and several sizes of window and door openings. Haseltine and Hodgkinson [53] compared the above test results to panel capacity predictions calculated using both elastic plate and yield line theories. Unlike Cajdert and Losberg [29]; they found that both the elastic plate analysis and the yield line method underestimated panel capacities. Also, in another paper, Haseltine [54] used the above mentioned and other B.C.R.A. test results to verify the use of the yield line theory with a limit state approach and characteristic strengths for design of laterally loaded masonry walls.

In 1976, Hendry and Kheir [58] reported on tests of one-sixth scale model brickwork panels with different aspect ratios. Test results were compared to results of theoretical analyses using different methods. They reported fair predictions using the yield line method yet they noted that there was no rational basis for its application to masonry. In the same year, Anderson [9] reported a series of full scale concrete blockwork panels with different horizontal spans. These panels were supported on three sides with tops free and the two ends of the walls were either simply supported or restrained by a T return walls. Different reserve strengths after first cracking were recorded according to the horizontal span and the edge conditions.

In 1977, the extensive test program performed by the B.C.R.A. on brickwork panels since 1972 was presented by West, Hodgkinson and

Haseltine [107]. These test results were compared with various design methods by Haseltine, West and Tutt [55]. In the latter paper, a modified yield line approach to fit data better was proposed for design. Provisions in the British Code BS 5628 [28] for the design of laterally loaded panels were based mainly on the work reported in these papers. A number of criticisms of these papers were published in their discussion [108] and by Lawrence [71].

In 1978, Sinha [92] reported test results of brickwork panels and compared these results with his fracture line theory which indicated good agreement. In his paper of 1980 [93], this theory was then applied to walls with openings and having various shapes. Good agreement with test results was reported. In the same year, Lawrence [72] provided some interim recommendations on lateral load design and he recommended empirical design moment coefficients based on his experimental data for different support conditions. He also compared various design methods such as elastic plate analysis for first cracking predictions and yield line and the empirical strip methods for ultimate load predictions. It was concluded that none of these methods provides consistent predictions of cracking or ultimate loads.

In a publication by the Cement and Concrete Association of Australia, Baker [21] presented a revised version of the empirical strip method together with his early work on the statistical aspects of the joint, beam and panel properties and the load sharing concept. Design curves were included in this document to determine the mean panel capacity and its coefficient of variation for different support

conditions. This procedure was confirmed by his experimental work on brickwork and recommended for blockwork [44].

In the 80's, three very significant research projects in this area were reported in three comprehensive theses. Cajdert [30] presented a Ph.D. thesis on lateral loading of brickwork and blockwork masonry panels. His tests included plain single leaf walls, arching tests, reinforced masonry panels, brick cavity walls, and auxiliary assemblage tests to determine the strength and deformation characteristics in the different directions. He reported linear brittle failure in beam tests and a nonlinear behaviour prior to cracking in walls supported on three sides due to the plasticity or the rotational capacity of the mortar joints in the statically indeterminate panels. He also discussed the behaviour of walls at uncracked, cracked, and failure stages. He stated that the crack pattern and reserve strength after first cracking depend on the orthogonal strength ratio, aspect ratio, support conditions, and the effect of forced crack propagation. This forced crack propagation relates to cases where crack lines take another route other than that corresponding to the minimum of the internal work. He reported that elastic plate theory underestimated the cracking load which he attributed to elasto-plastic behaviour of the mortar joints. Also, he supported use of the yield line method for predicting wall behaviour on the grounds that the moment redistribution seems to occur in the future crack line prior to cracking. He also reported higher experimental capacities than those predicted by the yield line analysis and attributed this to arching action.

Another comprehensive Ph.D. thesis in this area was presented by Baker [22] who summarized his previously published work on lateral loading. In this thesis, he extended his proposed failure criterion based on stresses in the two principal material directions [18] to a principal stress failure criterion and proposed an expression for the determination of the strength at different directions based on available data for off axis bending of masonry assemblages. He then incorporated this failure criterion in a finite difference computer simulation, using elastic plate analysis. The analysis included the variation of the strengths and the load sharing concept to predict first cracking and panel capacity (both mean value and its coefficient of variation). The good predictions obtained using this principal stress theory were confirmed by Baker's full scale and model brickwork panel tests [22] as well as by Lawrence's tests [24] on brickwork panels. Similar rational proposals were reported by Seward [89] and Drysdale and Essawy [42]. However, in both proposals no consideration for the variability was included since they were deterministic analyses.

Recently, a third thesis in this area was presented by Gairns [44] where he reported test results of ten single leaf and four cavity walls using concrete block units. These panels represented three different aspect ratios and were supported on three or four sides. It was reported that the test frame did not achieve the full translational restraint at the horizontal supports in all tests. The test results showed a reserve of strength after first cracking for panels supported on four sides with the highest aspect ratio (1.38) whereas panels with the smaller aspect ratio (0.92) failed at first cracking in both cases

of panels supported on three or four sides. Gairns compared his test results to the predicted capacities using elastic plate theory for uncracked panels, Baker's principal stress theory, yield line theory, fracture line theory, and the empirical methods by Baker and Lawrence. He reported that all methods significantly underestimated the magnitude of the relevant cracking or ultimate loads. The secondary effects, particularly the horizontal support yielding, was thought to be the probable reason for this discrepancy.

1.2.3 Available Methods For the Design and Analysis of Laterally Loaded Masonry Walls

The available methods for the design and analysis of laterally loaded masonry walls included universally available and acceptable methods and other methods specifically developed for masonry. Of the universally available methods were the elastic plate theory assuming isotropic or orthotropic properties and the yield line method [63]. However, the other methods included the fracture line theory [92] and the empirical methods such as Baker's strip method [21,23] and Lawrence's moment coefficients [72].

The elastic plate analysis was first limited to predict only the cracking loads or the failure loads where the panels showed no reserve strength after first cracking. Some researchers [22,29] reported negligible differences in the magnitudes for the modulii of elasticity in the two orthogonal directions and hence suggested isotropic plate solutions. However, others [69,89] reported considerable anisotropy and accordingly proposed orthotropic plate solutions. It should also be

noted that the modulus of elasticity parallel to the bed joints was inconsistently reported to be higher [89] or lower [69] than the corresponding modulus normal to the bed joints. Added to uncertainty regarding the elastic constants of brickwork were the markedly nonlinear behaviour of the walls, the lack of knowledge about the failure criterion for brickwork in biaxial bending, and the difficulty of dealing with irregularly shaped walls. These were identified by Hendry [57] as complications in the application of the elastic theory to brickwork panels.

Many researchers [30,54,55,57,58] have proposed the yield line method and reported good agreement with test results to predict the failure load of laterally loaded masonry panels. However, most of them [54,55,58] have admitted that there is no rational justification for the use of a theory based on ductile behaviour for a brittle material like masonry. An arbitrarily modified yield line method [55] has also been used as the basis for design in the current British Code [28]. Discussion of the applicability of the yield line theory has led to the argument that the good results for the yield line method in some cases were mainly due to the fact that for favorable loading and support conditions, both the theory of elasticity and the theory of plasticity may have practically identical predictions [30]. It should also be noted that the yield line method was reported to be conservative in some investigations [30,69] whereas other investigations [55,72] reported nonconservative predictions. Gairns [44] suggested that some of the secondary effects discussed by Baker [15] may be the probable reason for

these conflicts.

The fracture line theory was proposed and verified by Sinha [92,93] for brickwork panels of different shapes and support conditions. This theory was basically yield line theory but modified to include the anisotropy of the panels. Therefore, ft faced all the criticism, objections and problems of the yield line method [22].

Of the empirical methods for the design of laterally loaded masonry panels are the empirical strip method [21,23] and Lawrence's moment coefficients [72]. The strip method was proposed by Baker and then modified to account for the variability of the masonry strengths [21]. Although it is a semi-empirical method, it provided reasonable predictions for brickwork panels [21,22]. The other empirical method was proposed by Lawrence [72] in the form of moment coefficients based on analysis of his test results for brickwork panels with different support conditions.

In a more recent approach, Baker [22] proposed his principal stress theory reviewed in the preceding section. This rationally developed theory yielded reasonable predictions for model and full scale brickwork panels tested by Baker [22] and the full scale panels tested by Lawrence [24]. Independently, similar analyses using the finite element method were reported by Seward [89] and Drysdale and Essawy [42] but with the use of other failure criteria and not considering the random variation of masonry properties. Although the principal stress theory and these similar analyses were rationally developed, none is yet available in a suitable form for design purposes.

1.2.4 Provisions For the Design of Laterally Loaded Panels in Masonry Codes

Provisions for the design of laterally loaded walls differ greatly from country to country. These differences may be attributed both to differences in design philosophy and to a general lack of conclusive (or widely accepted) experimental and analytical research. In North America, the Canadian design Code [33] and the ACI Code [8] do not provide specific instructions for the analysis but rather specify allowable flexural tensile stresses. The designer is responsible for performing an appropriate analysis. These codes are open to criticism mainly because it is difficult to justify the relatively high values for some of the allowable tensile stresses. Nonetheless, there is no indication that any significant number of masonry walls have collapsed and therefore, there has not been any widespread concern in North America about these provisions. However, it is reasonably argued that for low rise construction, very few walls will have ever been subjected to their full design wind pressure. Recent reductions in the wind pressures for such buildings [76] support this argument. This change in loading means that rationalizing of design methods by taking account of the previous service history of masonry walls may not be valid. This warning may not only be appropriate because of changes in design loads but also because the evolution of masonry has resulted in walls with different support conditions, less redundancy, and which more often border on the limits of slenderness and allowable stress.

More comprehensive treatments of lateral load design are found in the current British Code [28] and the new Australian Draft Code [97].

Therefore, in this section, only these two codes will be reviewed. The current British Code [28] incorporates design based on the ultimate limit state, where the characteristic ultimate flexural strengths (either determined experimentally or taken from the code) are substantially reduced by a partial safety factor for material strength. This factor depends on manufacturing quality control for the units and construction quality control. The design process is based on providing structural resistance which is equal or larger than the loading effects. These loading effects were calculated using tabulated moment coefficients based on the yield line method and modified to best fit some available experimental results. This code was heavily based on the work in B.C.R.A. reported earlier [55,107]. Therefore, most of the criticisms in the discussion of this work [108] and those by Lawrence [71] for this work are also applicable to this code. Lawrence [71] also reported some unsatisfactory features of this code such as the relationship of characteristic flexural strengths to brick absorption and mortar composition, the assumption of constant orthogonal strength ratio, and construction of the moment coefficients table based on limited experimental work. However, he commended some features of this code such as the use of a limit state format, the guidance on practical support conditions, and the guidance on treatment of cavity walls.

The current Australian Codes [95,96] incorporate very low allowable stresses which are of the same order of magnitude as the reduced values in the British Code. However, the yield line based moment coefficients have not been adopted. This has led to either

restrictions on the sizes of wall panels or difficulty in justifying sizes of panels currently in use. Recently, a unified Draft Code [97] for both brickwork and blockwork was issued in Australia and the code is expected to be issued in 1986. Unlike the current Australian brickwork and blockwork Codes, the unified Draft Code was expressed in a limit states format. Masonry construction was classified in this Draft Code as either normal, calculated, or special masonry. This classification helped defining the quality of the supervision and allowed different masonry elements on the same job or even particular element to be classified differently for different actions. For strength requirements, again, the design structural resistance has to be larger than the load effects. For lateral load design, the Draft Code recommended the use of the empirical strip method [23] for the determination of the design panel resistance.

With the foregoing as background, it seemed clear that the existing codes contain provisions for design of walls subjected to out-of-plane bending which are not consistent with each other and which are difficult to justify individually. However, it was also apparent that much more research was required before alternative design provisions and procedures can be proposed and justified by adequate evidence.

1.3 OBJECTIVES AND SCOPE

The survey of the available literature reported in the previous section revealed the need for research on the lateral load resistance of concrete block masonry walls. To meet this need, the investigation reported herein was initiated with the following objectives:

1. To have a good understanding of the behaviour of masonry walls subjected to out-of-plane loading and to judge the adequacy of the methods of design and analysis, it was necessary to study the behaviour of concrete masonry walls with well defined support conditions at different stages (uncracked, cracked and failure). This also required investigating the effects of aspect ratio, support conditions, and presence of precompression on the behaviour of full scale walls .

2. To verify a generalized design method, it was necessary to extend the wall test results to include untested conditions by means of an analytical model. Therefore, it was required to construct an acceptable nonlinear model for masonry which is capable of handling different masonry elements subjected to different loading conditions.

3. After meeting the first two objectives, it was feasible to assess the available design methods and to propose an easy to use design method for walls subjected to lateral loading which is both rational and accurate.

The scope of the proposed research was limited to simply supported non-loadbearing walls subjected primarily to lateral out-of-plane loading and fabricated using hollow concrete blocks. Therefore, reinforced or grouted masonry walls subjected to considerable in-plane loading and arching action of panels were all considered to be outside the scope of this research.

This dissertation includes three main parts after this Introductory Chapter. Part II is concerned with the experimental

portion of this investigation which is given in Chapters 2,3, and 4. In Chapter 2, the experimental test program and the different test procedures are described together with the test facility which was specifically developed for this study. Chapter 3 deals with the materials used and the fabrication of the test specimens (both full scale walls and control specimens). Finally, the experimental results are reported and discussed in Chapter 4.

Part III, which is the part concerned with the theoretical study, consists of Chapters 5,6 and 7. In Chapter 5, the biaxial failure criterion developed in this study was derived and verified using different cases of reported masonry test results. In Chapter 6, the nonlinear finite element model proposed for masonry is presented and verified against available linear elastic and nonlinear solutions as well as masonry wall behaviour available through the experimental work in this study. In Chapter 7, some of the available design methods are compared to a wide range of data generated using the developed model. Then, a proposed design method is presented and compared to this data.

Part IV consists of only Chapter 8. This chapter contains a summary of the investigation and presents the final conclusions drawn from this study. It also includes recommended areas for further research related to this study.

CHAPTER 2

EXPERIMENTAL TEST PROGRAM

2.1 INTRODUCTION

The experimental test program conducted in this investigation was designed to meet the objectives of this study as mentioned earlier in Chapter 1. This test program included both full scale testing of masonry walls and the associated auxiliary control specimens.

In this chapter, the design of experiments for full scale walls is presented. Then, the experimental test program performed in this study is described. It also contains a description of the recently constructed test facility for lateral loading of masonry walls of sizes up to 3.60 m high by 6.00 m long. Finally, arrangements, procedures and instrumentation for the different tests performed are summarized.

2.2 EXPERIMENTAL TEST PROGRAM

The program consisted chiefly of two main parts, full scale walls and auxiliary tests. The auxiliary tests were considered to serve as control tests and for the determination of the required strength values for both masonry assemblages and the component materials (mortars and blocks).

2.2.1 Design of Wall Tests

The published experimental tests for laterally loaded brick and block walls have been tested mainly with practical rather than well

defined support conditions. Because practical support conditions are generally difficult to define and model, the interpretation of these results using analytical models is subject to some judgement. Therefore, the main uses for these test results were to serve as an evaluation for the adequacy of various design procedures. In this regard, the fact that they were tested under conditions representative of actual construction is desirable. However, the time and cost associated with testing full scale masonry walls make it impractical to consider testing sufficient combinations of conditions to fully confirm the adequacy of design procedures.

Considering the above situation, it was concluded that it was necessary to develop an accurate analytical model to assist in the development of design procedures and to provide information to supplement test data. Therefore, in order to be able to verify the analytical model it was necessary to produce test data with well defined support conditions. Accordingly, it was decided that lateral load testing of hollow concrete block walls for this study should have pin and roller types of supports to provide well defined conditions which in themselves do not introduce in-plane membrane action or ill defined, partial rotational restraint.

The results of wall tests performed on small scale models may contain some sources of inaccuracy. These inaccuracies are due to the possibilities of different workmanship of small scale specimens and different characteristics of small size blocks which are manufactured differently from full sized ones. These can result in altogether

different mortar to block bond characteristics. Also, the inaccuracies in test arrangements and the forces exerted by measuring devices may be quite significant. Accordingly, it was decided to test full scale wall panels in spite of the cost and time associated with full scale testing.

The strengths of masonry walls are influenced by many factors. However, in order to limit the number of full scale walls in this program, the effects of only the aspect ratio and support conditions were investigated. The reason was that only these two factors need to be investigated on the full scale level. Most of the other factors affecting the panel strength may be investigated on assemblage specimens smaller than full scale walls.

The expected high variability in masonry test results, in general, necessitated the repetitions of tests. However, in the case of full scale walls, the expected variability is less than that of individual joints or beams which resulted in a smaller number of required repetitions. Also, the cost and time associated with full scale testing of masonry walls makes it desirable to limit the number of wall tests to a minimum. Therefore, three repetitions were used in most full scale wall tests and the test results reported later confirmed the consistency and the acceptable level of variability for the repetitions of each test.

2.2.2 Full Scale Walls

The types of full scale walls used in the test program are categorized and listed in Table 2.1 on the next page. The table includes nine different full scale wall test series with each of them

Table 2.1   Wall Test Program

Group	Series	Dimensions		Aspect Ratio	N*	Description
		Wall $L_o \times H_o$ m	Frame $L \times H$ m	L/H		
W	WI	3.6 X 2.8	3.4 X 2.8	1.21	3	Simply supported on all four sides with no pre-compression.
	WII	5.2 X 2.8	5.0 X 2.8	1.79	3	
	WIII	6.0 X 2.8	5.8 X 2.8	2.07	3	
WC	WC	5.2 X 2.8	5.0 X 2.8	1.79	3	As WII, but having central horizontal crack prior to loading.
WP	WP	5.2 X 2.8	5.0 X 2.8	1.79	3	As WII, but having pre-compression of 0.20 MPa
WF	WF	5.2 X 2.8	5.0 X 2.85	1.75	3	Free at top and simply supported on the other three sides.
WH	WH	5.2 X 2.8	5.0		3	Simply supported only on the sides and free at top and bottom.
WV	WV	5.2 X 2.8	2.8		3	Simply supported only on the top and bottom and free at both sides
	WVV	2.6 X 2.8	2.8		6	

* Number of repetitions

having three repetitions except the last test series which had six repetitions. Therefore, the total number of full scale wall tests in this program was thirty.

For Group W, the full scale wall test program consisted of three different aspect ratios for walls simply supported on all four sides. These ratios were chosen to theoretically give the three different failure patterns according to the yield line analysis which are as follows:

1. Diagonal cracks originating from the four corners with upper and lower pairs connecting to a vertical center crack (Series WI)

2. Only diagonal cracking (Series WII)

3. Diagonal cracks originating from the four corners with end pairs connecting to a horizontal center crack (Series WIII)

A sketch of these patterns is given in Figure 2.1.

Wall WII, with only diagonal cracking, was taken as the basic wall since it represented the case of a panel having equal potential of transmitting load in the two orthogonal directions. It was hoped that using this wall type as the basic wall would clearly show the effect of any changes made in the other wall tests. The dimensions of all other wall groups included in this program were the same as those of WII walls except Series WVV walls where they were approximately half the length of the WII walls.

There were two more wall groups included in which the walls were simply supported on all four sides. The first was Group WP which was the same as Series WII but with the additions of an external in-plane loading(precompression) applied along the tops of the walls. The value
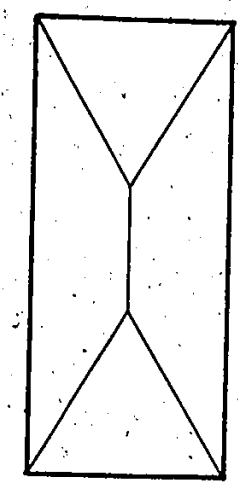
Pattern c
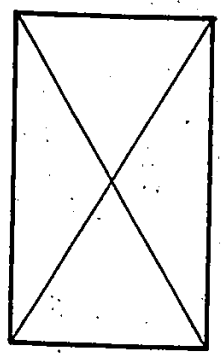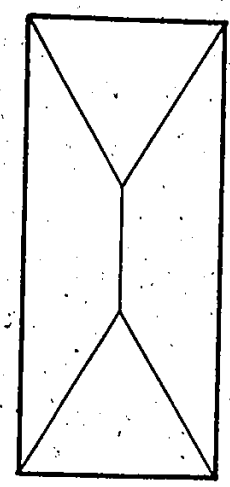
Pattern b

Pattern a

Figure 2.1   Theoretical Yield Line Failure Patterns for Panels
Supported on All Four Sides

of this preload was chosen to give a precompression along the top of the wall of 0.20 MPa which is roughly equivalent to the roof loads carried by the wall of the top floor in a load bearing wall construction system. The other group with supports on all sides was Group WC which was the same as Series WII except that the walls had a full length horizontal precrack near the mid height of the walls. The reason for including this series was to compare its behaviour with WII walls to show the effect of precracking on wall capacity.

The remaining wall tests were grouped according to support conditions other than that of being simply supported on all four sides. They included walls simply supported on three sides and free at the top, Group WF. These WF walls together with the other five test series for walls supported on all four sides form the body of test data for two-way action in that program.

One-way action was investigated in this program through Group WH, which had walls supported only on the two sides with the top and bottom free for lateral deflection. As well there were walls supported only on the top and bottom edges, Group WV.

Due to the expected high variability of the capacity and strength of the walls supported only on the top and the bases, the last test series (Series WVV) was included to increase the sample size and consequently to have more confidence in the experimental results.

For the one-way action walls (Series WH, WV, and WVV), the expected failure pattern was as simple as a nearly straight line crack. This crack was observed along the whole wall near the center, either

vertically at about wall mid-length in the case of the WH walls, or horizontally at about wall mid-height in the case of the WV or WVV walls. The undamaged parts (halves) of the walls in these groups were large enough to be tested again. In this way, the total number of walls required for the proposed program was reduced and the most possible information was obtained from the limited number of walls. In this program, the failed halves of WH walls supported on the sides were retested as Series WVV walls supported only at the top and bottom and having approximately half the length of the basic wall. Also, after the failure of Series WV walls supported at top and bottom, they were retested as Group WC walls supported on all four sides with a precrack near mid-height.

The other factors such as type of mortar and type of block which might influence flexural tensile strength were kept constant for all walls. Moreover, all the walls also had joint reinforcement (standard truss type) embedded in mortar bed joints at the first and every other course. The inclusion of this joint reinforcement was made not only because it is common practice, but also to avoid destruction of the wall parts at failure. Keeping the wall together in almost one piece after failure facilitated safely removing the wall from the test frame. Since cracks parallel to the head joints were consistently reported to develop only at failure, the effect of joint reinforcement on the moment capacity of walls in bending with tension parallel to the bed joints could be estimated using elastic properties of the uncracked section. This yielded an increase of 2% in the horizontal moment capacity of the walls which was considered to be negligible.

2.2.3 Auxiliary Tests

Auxiliary test specimens were constructed at the same time as the walls to serve as control tests and to determine the strength values of block masonry assemblages and component materials. These tests can be divided into two separate categories which are the component material tests and the assemblage tests as given below.

2.2.3.1 Component Material Tests

Since the research work was restricted to plain ungrouted masonry and only one type of mortar and one size of blocks were used, the component materials tested were limited to this mortar and block. Three standard 2 in. (50.8 mm) mortar cubes were constructed from each mortar batch used in building the full scale walls or the auxiliary assemblage specimens. These cubes were used to provide the mortar compressive strength at the time of testing of the full scale walls and at the time of testing of the auxiliary assemblage specimens. They simply served as a measure of quality and consistency of the mortar.

The 190 mm standard normal weight hollow concrete blocks, which were used throughout the program, were tested to provide various measures of strength of the concrete blocks. The different tests performed had from 5 to 10 repetitions in order to have a reasonable statistical sample. The number of repetitions in these tests was chosen according to the statistical design of experiments to guarantee a 95% confidence level for test results according to the expected variations in each test and the acceptable tolerable error in the mean values of strength. These tests and their results are discussed in detail in Appendix A.

2.2.3.2 Assemblage Tests

The auxiliary tests for blockwork assemblages were done to determine the strength of blockwork in flexure at different orientations from the bed joint. This was required to facilitate the development of a failure criterion for masonry in biaxial bending and to verify it experimentally.

In this program, only the two basic orientations of bending normal and parallel to bed joint directions were considered since these are the basic strengths needed for the construction of the failure criterion. The strength values at other orientations which were needed for the verification of the criterion, were available through another McMaster Masonry research project [47]. The test specimens for this project were constructed using the same materials and at the same time as the author's experimental program.

The flexural tensile bond strength normal to the bed joints was determined by means of the bond wrench test method [62] which has the merit of testing every joint. This results in a larger statistical sample with the smallest possible specimen size when compared to beam specimens. The stack pattern prism specimen and test equipment are shown in Figure 2.2.a where the stack pattern was used for ease of construction. However, the minimum face shell thickness was used in strength calculations. It was found that, for face shell bedding, use of the possible increased section properties due to the alignment of the block's cross webs would have resulted in a decrease in the calculated strength of 4.5%. Since the specimens were built with nominally face shell mortared joints, this effect was thought to be so small that it

5 BLOCKS
=990

390
SPECIMEN

LOAD BY
SAND BIN
OR JACK

BOND WRENCH TEST SET-UP

(a) Flexure Normal to Bed Joints

1590

400

SPECIMEN

SUPPORT LINE

LOAD LINE
FAILURE MODE I

FAILURE MODE II

LOAD LINE

SUPPORT LINE

HYDRAULIC JACK
LOAD CELL
SHIMS
LOAD DISTRIBUTION
BEAM
BALL & ROLLER
SPREADER BEAMS
PLYWOOD STRIPS
SPECIMEN
ROLLERS

160
115
215
190
115

400 | 300 | 300 | 400
95 | 1400 | 95
1590

b) TEST SET UP
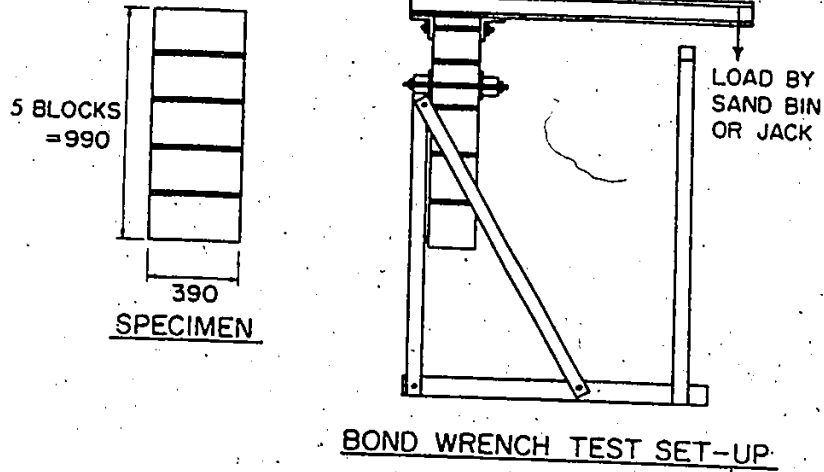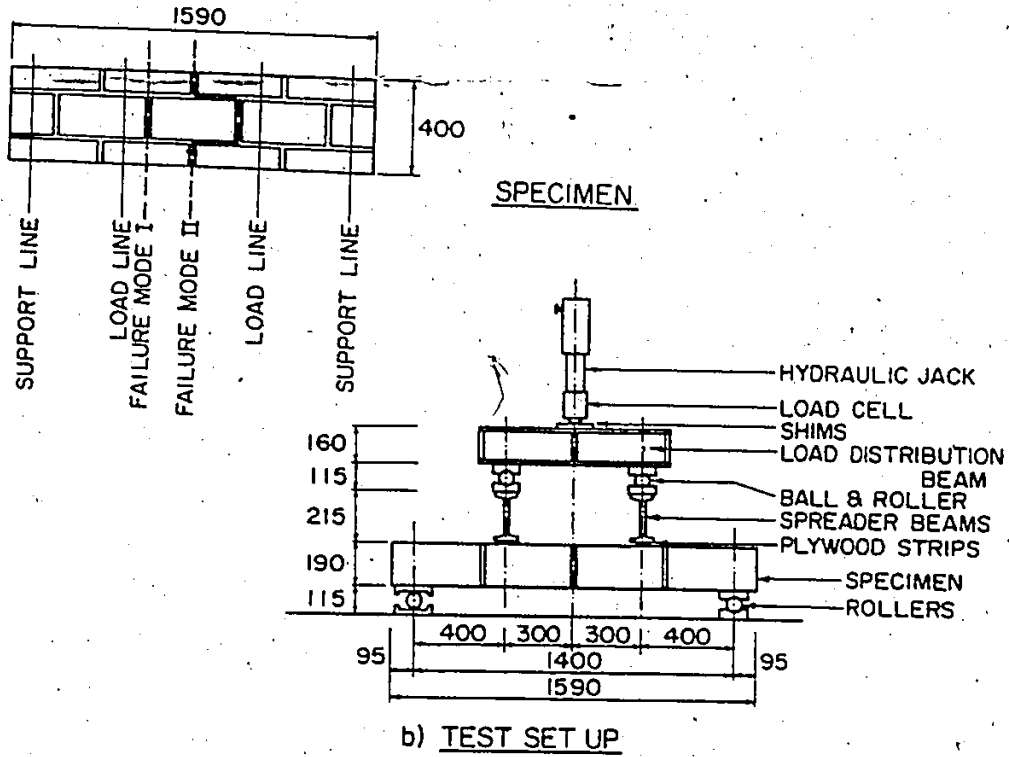
(b) Flexure Parallel to Bed Joints

Figure 2.2   Details of Tests for Flexural Tensile Strength

can be neglected without introducing any significant error in stress calculations.

For flexural tension parallel to the bed joints, the test specimens and the test set-up are shown in Figure 2.2.b. The four block long specimens were constructed in running bond with full height blocks sandwiched between half height blocks. This configuration was chosen to provide the following:

1. Equal regions of head joints and face shells at locations of potential cracking.

2. The possibility of crack patterns following the path of least resistance around the blocks or passing through blocks at alternate courses.

3. Sufficient length to permit the failure to occur in the nearly constant bending moment region.

4. Sufficient length to develop the bending moments without correspondingly high shears which might tend to cause shear affected failures in the shear span.

5. Equal lengths of head and bed joints which results in the same head joint flexure to bed joint torsion ratio irrespective of the specimen width.

6. Symmetrical specimen with respect to the longitudinal axis with the minimum possible number of courses in the wallette height.

In order to have a larger statistical sample, some of the failed parts of these wallettes or beam specimens were tested by means of the bond wrench. The experimental results of these tests were used to evaluate the bond wrench as a method of testing for flexure parallel to

the bed joint.

2.3 TEST FACILITY

A test apparatus was specially constructed for this study. It was designed to accommodate tests of full scale walls up to 6.00 m long and 3.60 m high. This test setup consisted of the supporting frame for masonry walls, the backup wall to support the pressure on the other side of the air bag, and the air bag itself to simulate uniform wind pressure. Moreover, there were some other auxiliary parts in that setup. The different parts of the apparatus are described in the following sections.

2.3.1 Supporting Frame

The supporting frame was designed not only to be strong enough to support the masonry walls but also to be rigid enough to minimize the relative deflection of the frame members. This rigidity of the frame was essential since deflection of the supporting frame greatly affects the panel capacity under lateral loading due to the low tensile strength and high stiffness of the masonry walls. The member sizes and configuration of the reaction frame were chosen so that at a lateral load of 12.5 kPa on the largest possible panel dimensions, the differential deflection between any points on the reaction frame would be less than 1 mm.

Different views of the reaction frame are shown in Figure 2.3. It consisted of the following:

1. Four W250x67 beams (Beams A) to laterally support the test specimen when it was supported on all four sides. For other

SECTIONAL PLAN FOR EXPERIMENTAL SETUP

3m

DETAIL A

VERTICAL SECTION FOR EXPERIMENTAL SET UP

SPECIMEN

SUPPORT FRAME

REACTION BEAM

CONCRETE SUPPORT

AIR BAG

BACKUP WALL

DETAIL A

VARIABLE UP TO 3.6 m

VARIABLE UP TO 6.0 m

ELEVATION OF SUPPORTING FRAME

ELEVATION OF BACKUP WALL
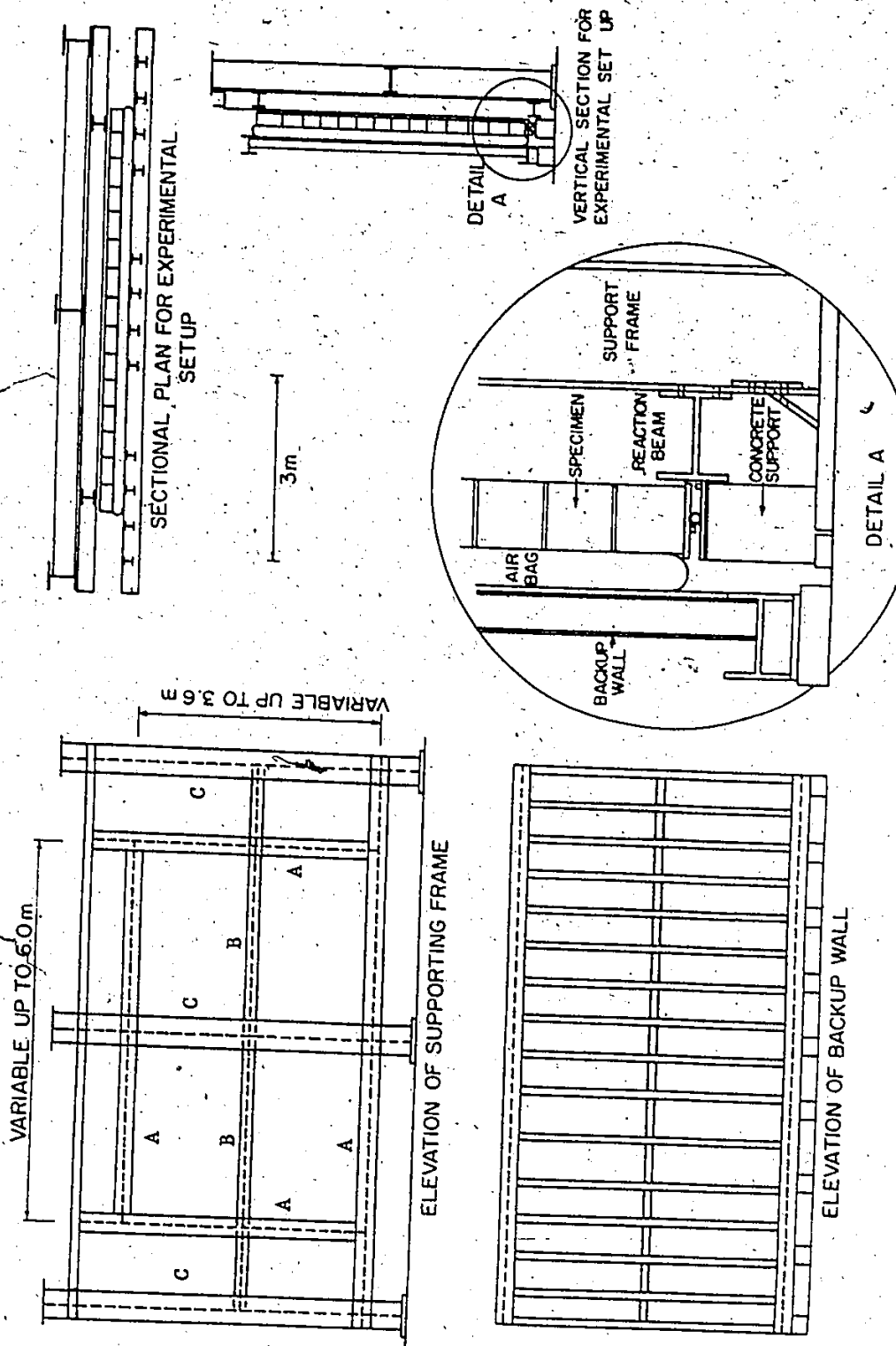
Figure 2.3   Details of the Experimental Set-Up

37

support conditions, each of these beams could be excluded or positioned differently. These beams connected together by angles and bolts so that they can be easily modified to support any combination of panel dimensions at 200 mm increments.

2. Two W310x39 beams (Beams B) to act as lateral support for the two vertical sides of the frame at mid-height.

3. Three W360x134 columns (Columns C) which were bolted to the strong floor of the Applied Dynamics Laboratory. These columns provided lateral support for the two horizontal frame members (top and bottom supports) at mid-length as well as support for the vertical self weight of the whole reaction frame which was elevated at 408 mm above the laboratory floor level.

4. A C250x23 top channel was used to link the top of the two vertical sides of the frame to the three W360x134 columns.

5. All these members were connected together by means of bolts and angles to facilitate frame adjustments to different panel sizes. Moreover, due to the hole spacing and base details of the W360x134 columns, the bottom horizontal beam of the supporting frame was connected to the end columns by means of two brackets having the details shown in Figure 2.4.

2.3.2 Backup Wall

This backup wall supported air pressure on the other side of the air bag. It was made out of steel beams and plywood panelling. The steel frame was composed of two W250x67 beams at the top and the bottom, 18 standard S130x15 I-beams spanning between the two beams plus two

W360x134
Column

180

40 | 100 | 40

4x2ϕ25

241

Pl.365x180x10

Pl. (t=10)

L110x110x10

2ϕ16

2ϕ16

250

W250x67

(b) Side View

W360x134
Column

55

365
254

2ϕ16

50

100

200

55

50

50

2ϕ25

2ϕ25

W250x67

(a) Front View
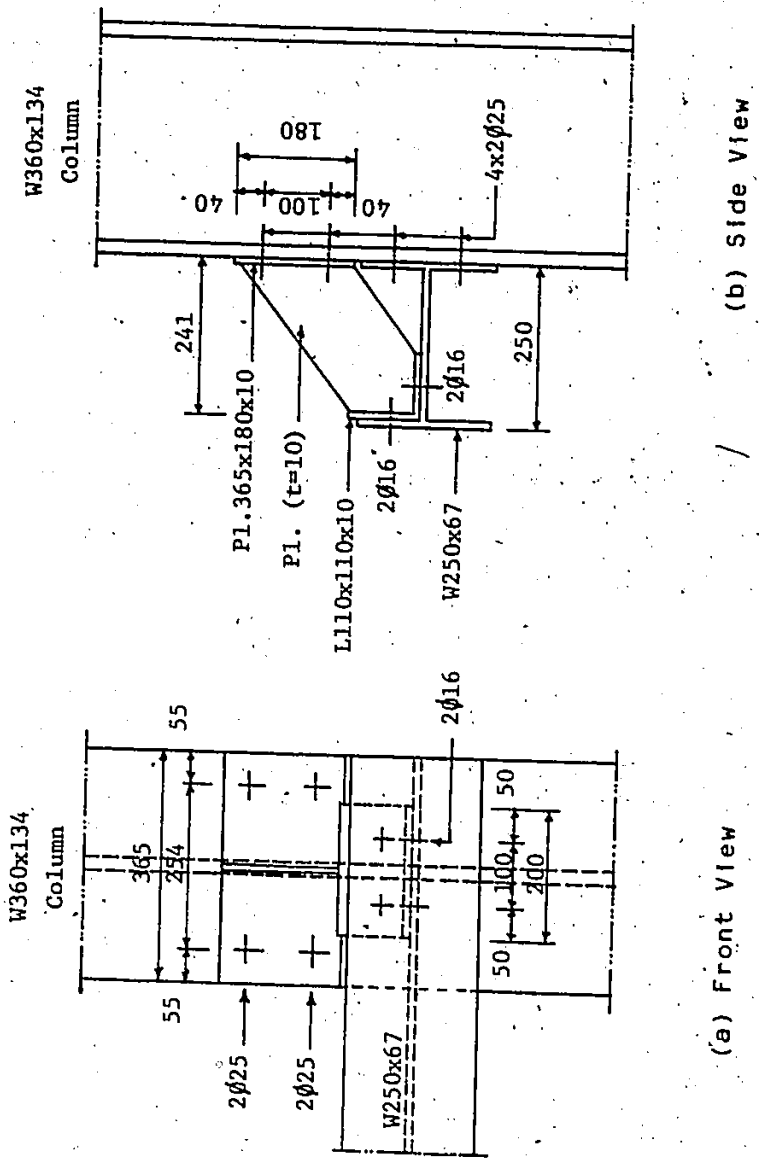
Figure 2.4 Details of Bracket Connecting Bottom Beam to
W360x134 Column

C250x23 channels at the ends of the beams. The I-beams and the channels were linked together through a cross girder at mid-height which was built out of steel plates Pl 80x8 and Pl.109x8. The last part of the steel frame was diagonal bracing made out of steel plates Pl 80x8. All connections were made by welding. Then, 1/2 in. (12.7 mm) plywood panelling was used to cover the whole backup wall.

Different views of the wall are shown in Figure 2.3. This wall was tied back to the supporting frame by means of sets of threaded rods top and bottom. The 5/8 in. (15.9 mm) and 1 in. (25.4 mm) sizes of threaded rods were used as shown in Figure 2.3.

The backup wall was elevated at 205 mm from the laboratory floor and it was seated on two supports at its ends where 1/2 in. (12.7 mm)-thick steel plates were welded to the flanges of the bottom beam. The steel plates and seats are shown on Figure 2.3.

2.3.3 Air Bag and Air Supply System

A Vinyl coated polyethylene air bag with 100 mm side pieces was fabricated to cover the entire area of a wall of 2.80 m high and up to 6.00 m long. A sketch of the air supply system together with the air bag are shown in Figure 2.5. The air from a 100 psi (690 kPa) supply was used by incorporating a pressure reduction valve and a low pressure regulator on the intake. In addition, a manometer using water columns was included on the intake between the regulator and the air bag for accurate measurement of input pressure. A similar manometer was connected to the far end of the air bag to ensure no leakage in the bag and to double check the air pressure inside the bag.

100 psi (690 kPa)
Air Line

Low Pressure Regulator

Pressure Gauge (1/2 kPa Divisions)

Input Control Valve

Control Valve For
Intake Manometer

Air Scape Valve

Manometers

Air Bag
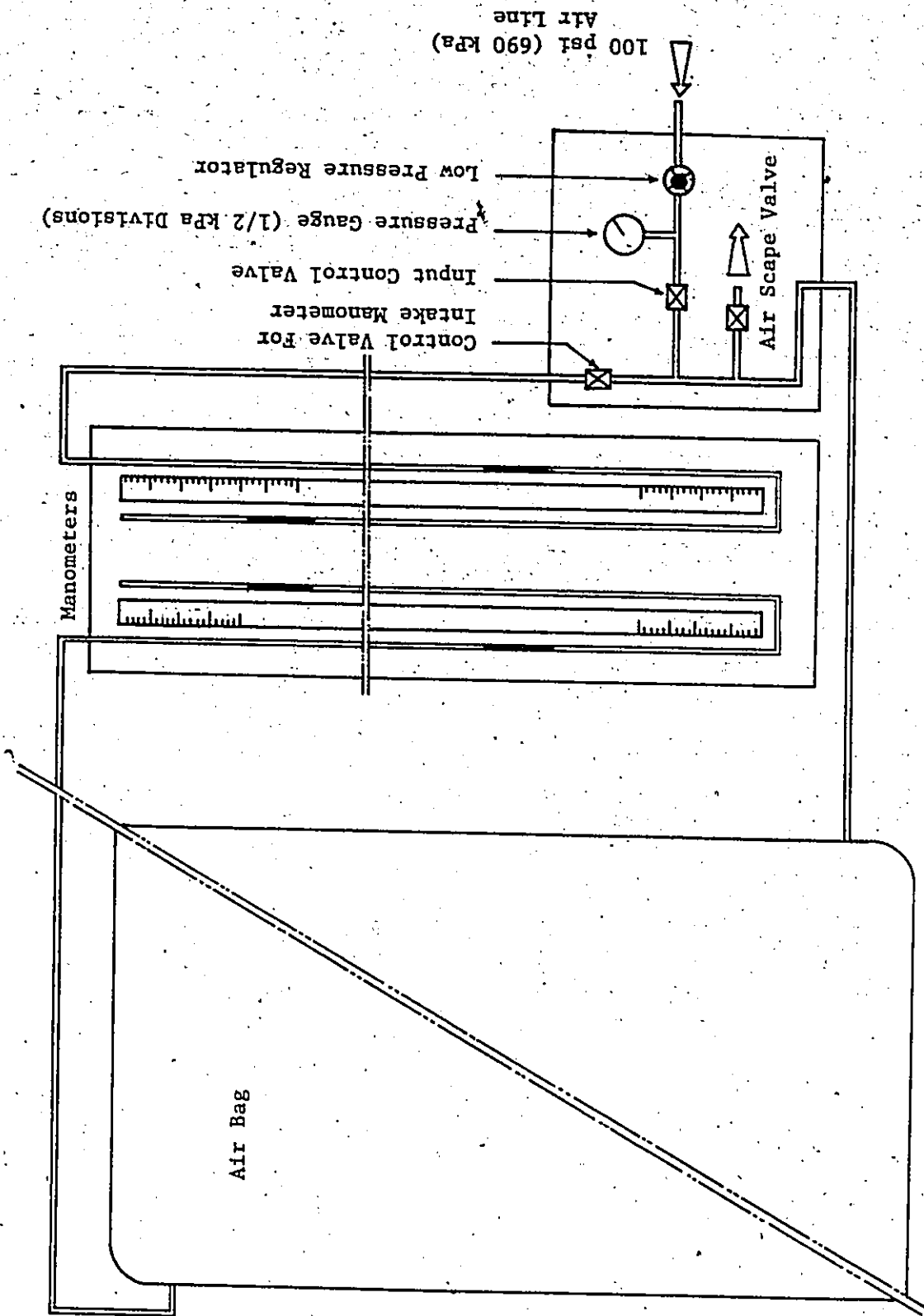
Figure 2.5.   Details of Air Supply

2.3.4 Edge Supports of Wall Panels

The simple supports for the sides and the top of the wall panels consisted of 1 in. (25.4 mm) steel rods welded to the reaction frame. Lateral load was transferred to these reactions through 3/16 in. (4.8 mm) thick, 1.5 in. (38.1 mm) wide steel strips which were held against the rods while plaster of Paris was placed in the gap between these strips and the wall specimen. This eliminated the effects of any imperfections in the alignment of either the wall or the reaction frame.

At the bottom of the wall specimens, it was necessary to support both lateral loads and vertical gravity loads due to the self weight of the masonry wall plus any surcharge or precompression applied on top of the wall. A single hinged support was chosen rather than two separate rollers in order to have a unique support point at the wall base for analysis purposes.

The base support shown in Figure 2.6 was fabricated using a 1.5 in. (38.1 mm) roller welded to a 3/4 in. (19.1 mm) thick steel plate. This steel plate was 9 in. (228.6 mm) wide and 20 ft (6096 mm) long. The lateral load was transferred to the bottom beam of the reaction frame through steel shear keys and wedges as shown in Figure 2.6. In order not to reinforce or stiffen the bottom edge of the wall panel, individual steel plates corresponding to the size of a block (390 mm long) were used to transfer the loads from each block in the wall bottom course to the roller. A milled slot with a 3/4 in. (19.1 mm) radius permitted rotation while a shear key welded to the bottom surface of these plates prevented lateral displacement. The masonry wall specimen was set on a full bed of mortar placed over the individual steel plates

220

190

Mid-Wall Axis

Lower Reaction Beam

40

10

15 10

4 6

Mortar Bed

Top Plates

20

5

20

26

26

10 16

C.L. of Lower

26

5

90°

6

Reaction Beam

30

40

26

Bottom Plate

20

20 5

Wedges

Reinforced Masonry Base

190

240

(a) Cross-Section

50

20

145

390

Circular Slot

R = 20

100

50

220

145

10

(b) Top Plate in Plan

240

20

165

50

40 mm Roller

165

165

50
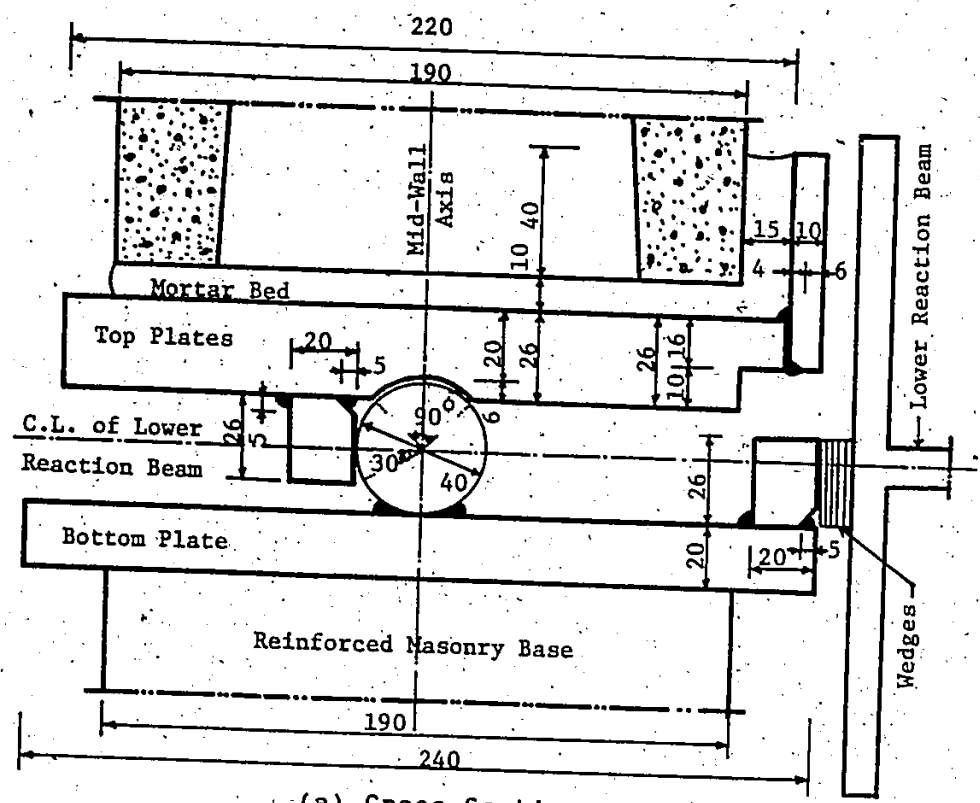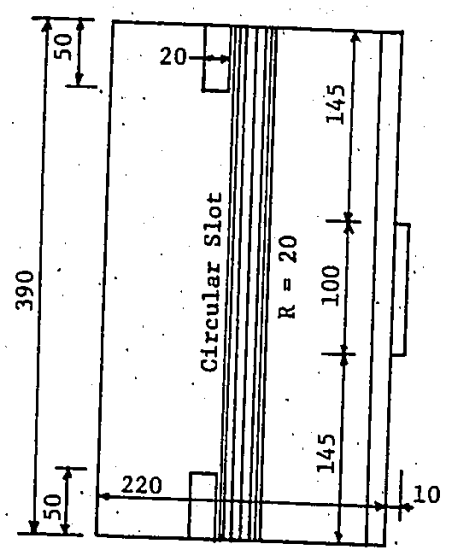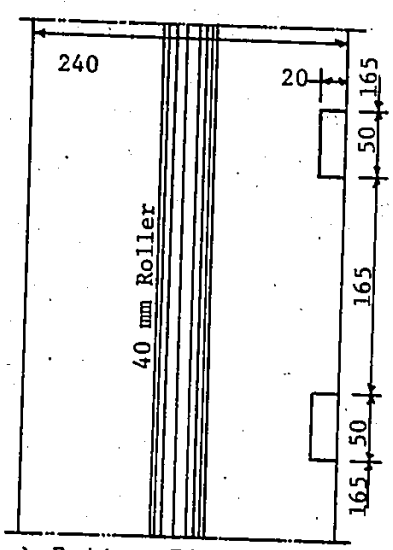
(c) Bottom Plate in Plan

Figure 2.6   Details of Bottom Wall Support

to ensure the bearing of the wall along its whole length. The lateral load was transferred from the masonry wall to the individual plates by means of friction and cohesion of mortar bed as well as bearing on the perpendicular steel strips welded at the center of the individual plate top edges. The gaps between these strips and the wall were filled with mortar.

Again, due to the hole spacing and base details of the W360x134 columns, the bottom support of wall specimens was placed at 370 mm from the laboratory floor on a continuous seat underneath the whole length of the bottom support. This seat was made of two reinforced and grouted masonry bases and a reinforced concrete beam bridging between the bases as shown in Figure 2.7. The need for this central beam was to avoid the interference with the steel base of the W360x134 center column.

The Group WH walls, which were laterally supported only on the sides, were to be free to displace laterally at their bottom edges. However, it was decided that the self weight of these walls should not be supported only at the bottom corners due to the relatively large span or length of the wall and the low tensile bond strength of masonry. Instead, a three point support system for wall self weight was used along the bottom edge. It was positioned at the center and the two corners as shown in Figure 2.8. A roller support was used at the center to permit the out-of-plane translation while ball supports were introduced at the corners to permit the out-of-plane rotations at these points.

Finally, lifting of the panel corners was prevented by special supports provided at the corners whenever corner lifting was expected.

Section X-X

Grouted Core

$2\#12$ (A)

Tie $\phi6$ mm $s=400$ mm

$2\#12$ (B)

370

190

$6.5\times390 + 6\times10 = 2595$ mm

$2\#12$ (A)

$2\#12$ (B)

$7\times390 + 6\times10 = 2790$ mm

3145 mm

3660 mm

370

190

170

10

195

550

R.C. Beam

305

355

160

170

40

Axis of Symmetry
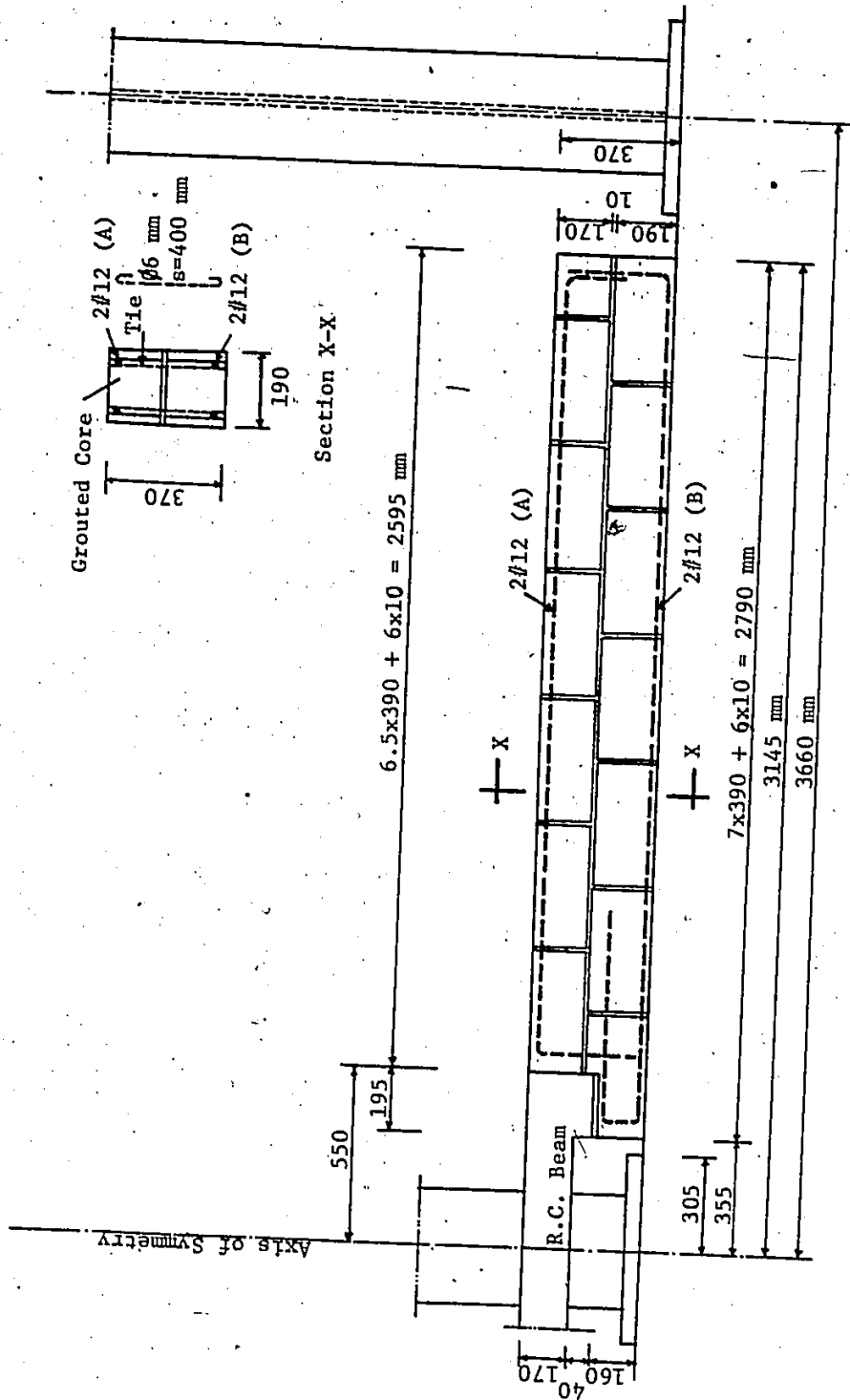
(a) Reinforced Masonry Base

Figure 2.7   Details of the Base Under Masonry Wall Bottom Support

Cross Section

2Ø12 mm

70
170 40
60
40
160
190

Stirrups
Ø6, s=60 mm
2Ø12 mm

Closed Stirrups
Ø6, S=60 mm

255 mm

Polyethlene
Sheets

210 mm
170

90 mm

2Ø12 mm

2 Holes
Ø40 mm

80 mm   2Ø12 mm

710 mm

1100 mm
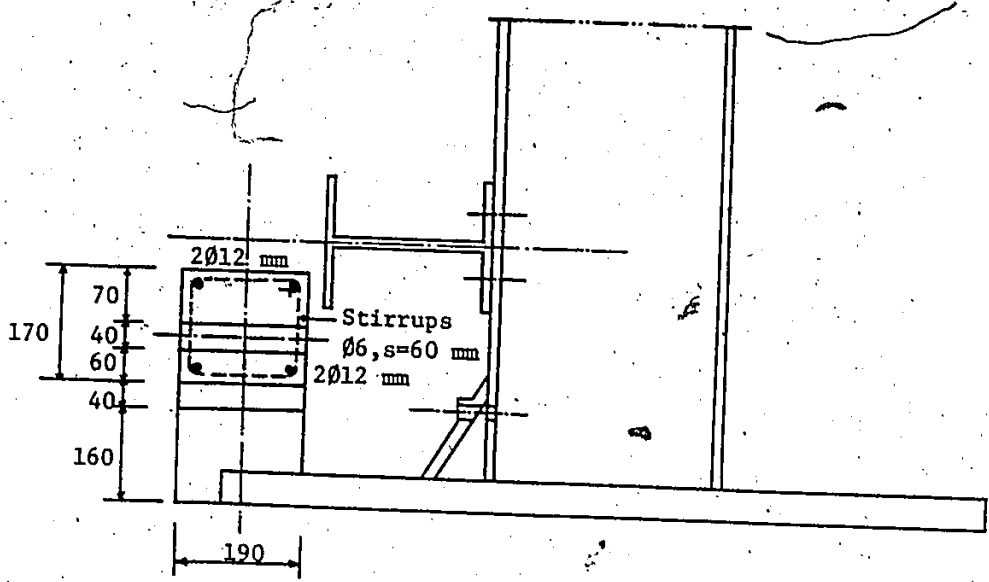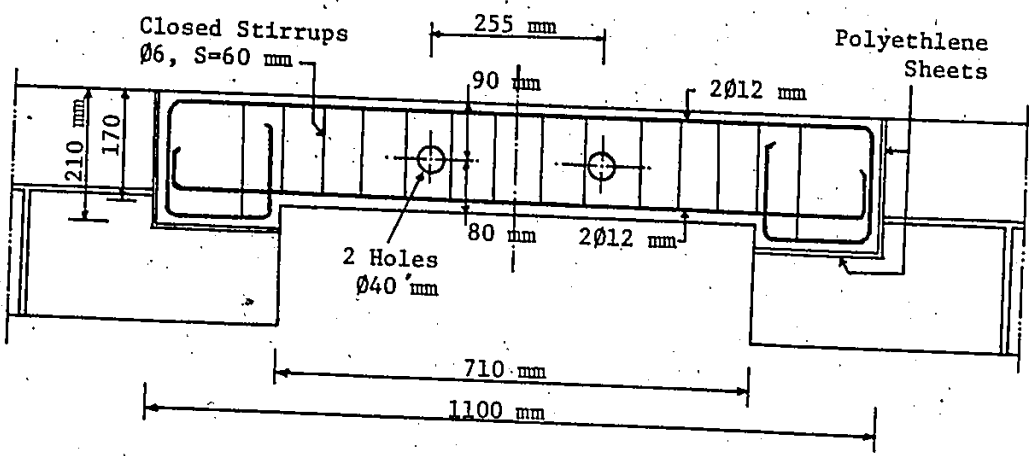
(b) Reinforced Concrete Beam

Figure 2.7   Continued

Full Bed of Mortar

40 mm Roller

20 mm Steel Plate

Front View

Side View

(a) Support at Wall Center

25 mm Roller
For Lateral Support

Full Bed of Mortar

50 mm Diameter Steel Ball

50 mm Thick Steel Plate

Front View

Side View
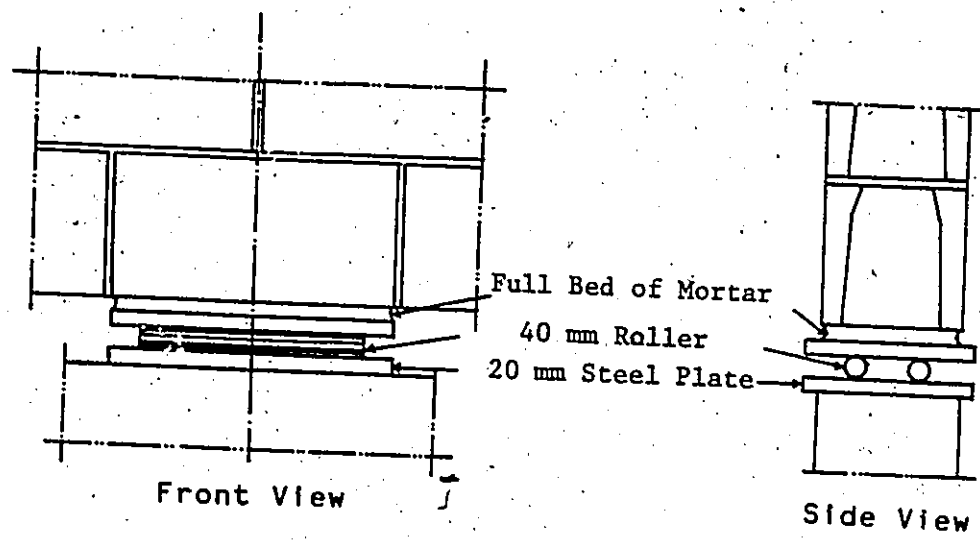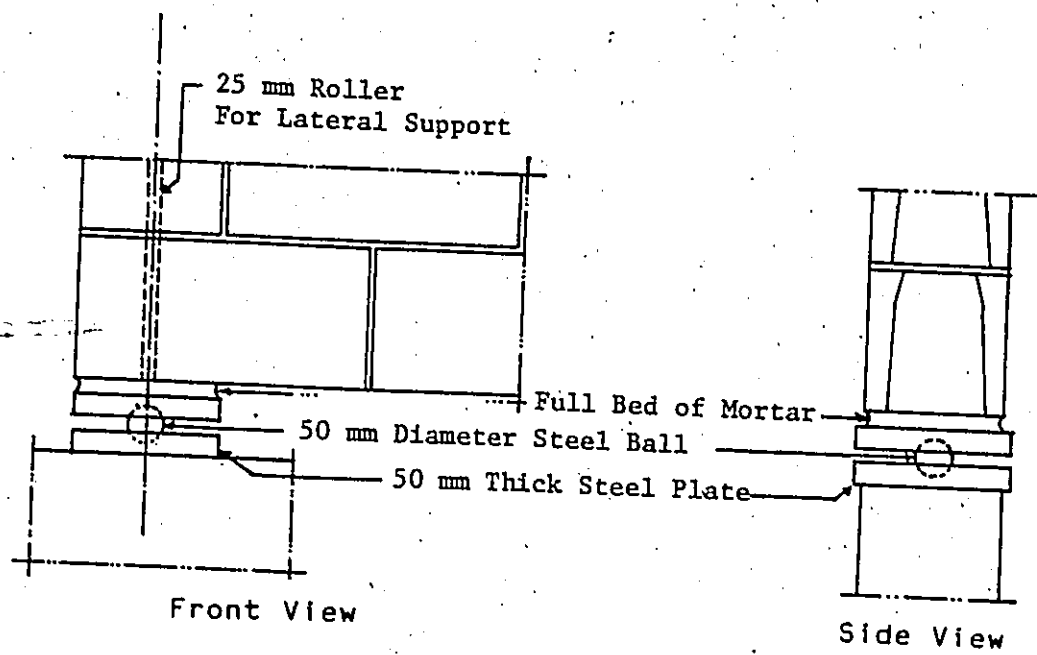
(b) Supports at Wall Ends

Figure 2.8   Self Weight Support for Series WH Walls

At the bottom corners, steel strips, similar to those provided to prevent slip of the wall off of the base plates were provided at the end of the first and last individual plates to prevent the masonry wall corner lifting with respect to the base support. Also, additional shear keys were welded to the end of the first and last individual plates and the roller of the base support was clamped to the reaction frame to assure that the panel corners would not lift relative to the reaction frame. For each upper corner, a 1/2 in. (12.7 mm) steel plate with a steel ball welded on the plate was placed against the wall and two 3/4 in. (19.1 mm) diameter threaded rods were used to tie the masonry wall back to the reaction frame. The ball in the plate against the wall was adjusted to correspond to the point of intersection of the horizontal top and vertical side support lines. The two types of corner lifting restraints are shown in Figure 2.9.

2.3.5 Precompression Loading System

Group WP wall specimens were subjected to in-plane uniformly distributed line load along the top of the walls. This in-plane surcharge or precompression was applied through a set of steel beams to distribute and spread the single point load of the hydraulic jack to an almost uniformly distributed load on the top of the wall.

The precompression loading system as shown in Figure 2.10 consisted of a hydraulic jack and load cell for the application of the load. This jack was hung from two channels cantilevered out from the central column of the supporting frame. To create a stiffer support, the free ends of these channels were tied back to the same column by two
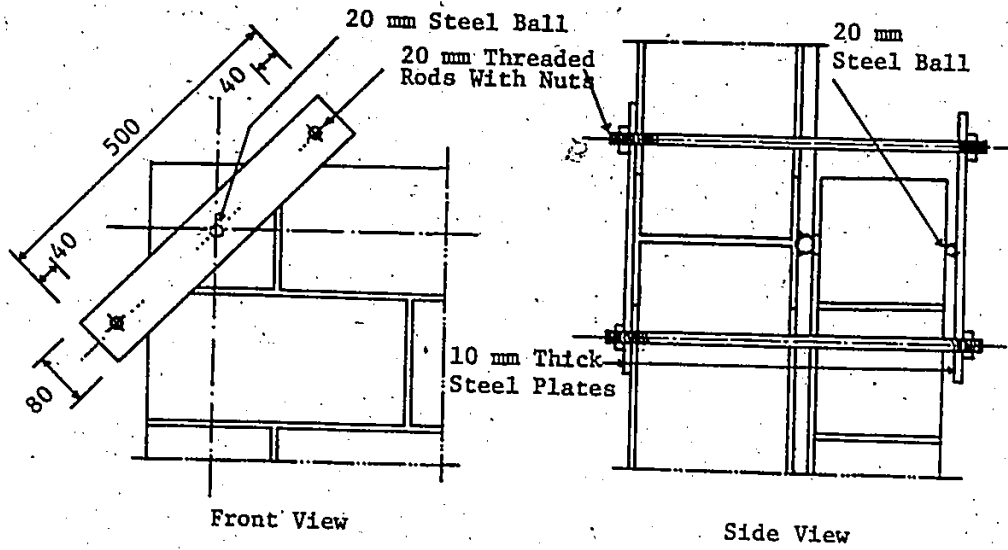
(a) Top Corner Support
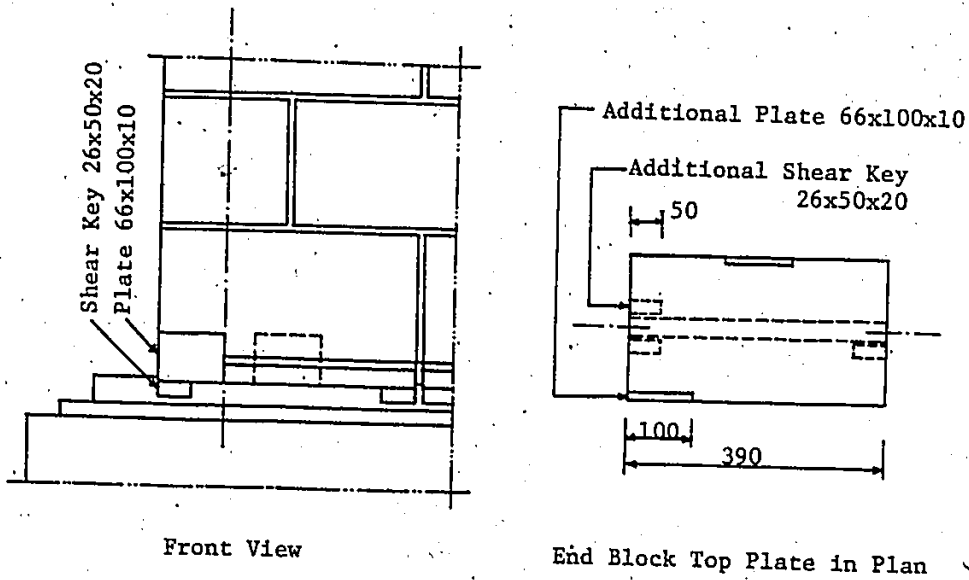
(b) Bottom Corner Support

Figure 2.9   Corner Lifting Restraints

Center W360x134 Column

25 mm Diameter Threaded Rod

Angle Ties

Load Distribution Beams

2 Channels

Hydraulic Jack

Load Cell

Short Column

Full Scale Masonry Wall

Full Bed of Mortar

.675

1.35

1.35

5.20

.675

.675

1.35

1.35

.675
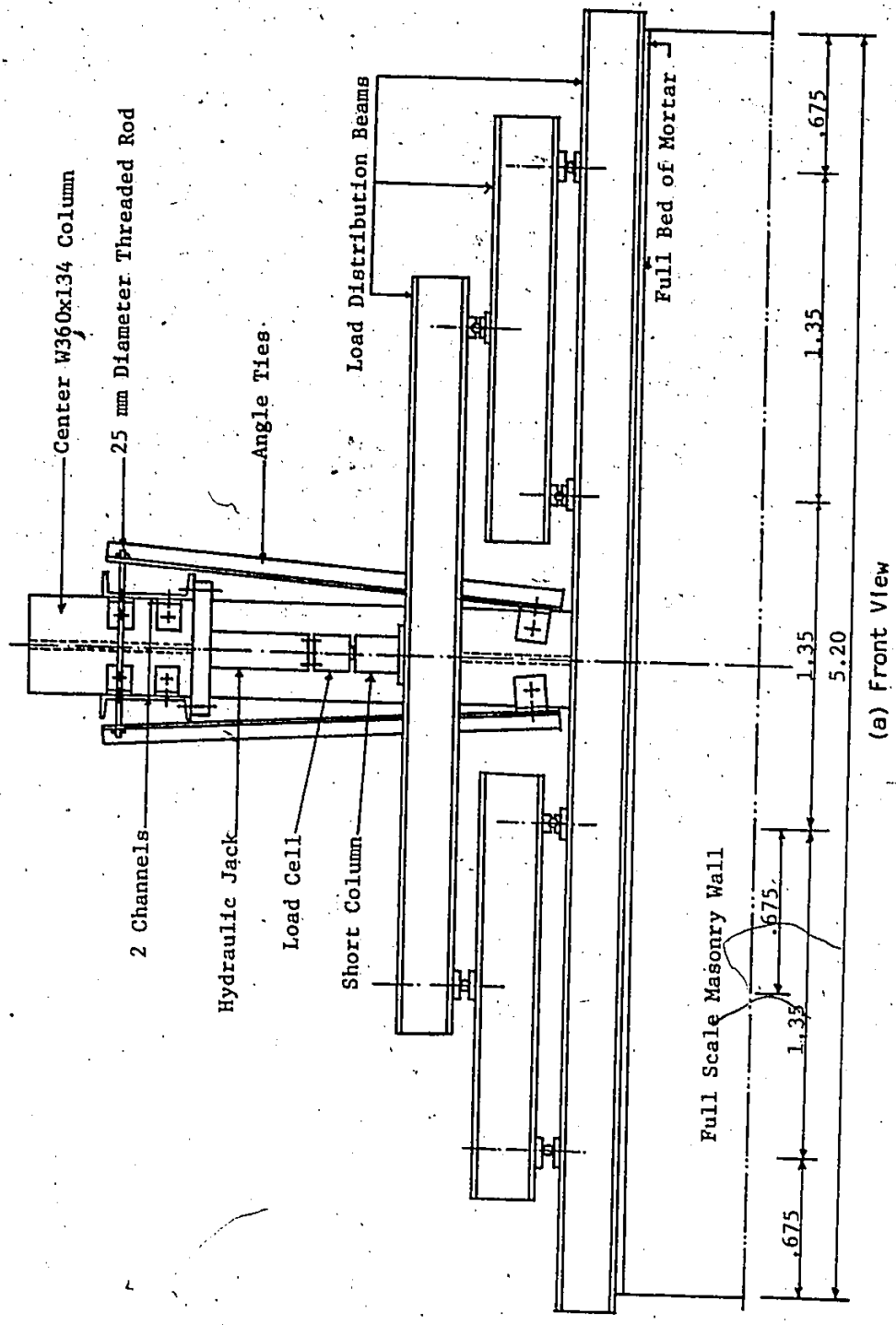
(a) Front View

Figure 2.10   Precompression Loading System

Hydraulic Jack

Load Cell

Short Column

Angle Ties

Top Reaction
Beam

W360x134
Center
Column

Backup Wall

Air Bag

Masonry Wall
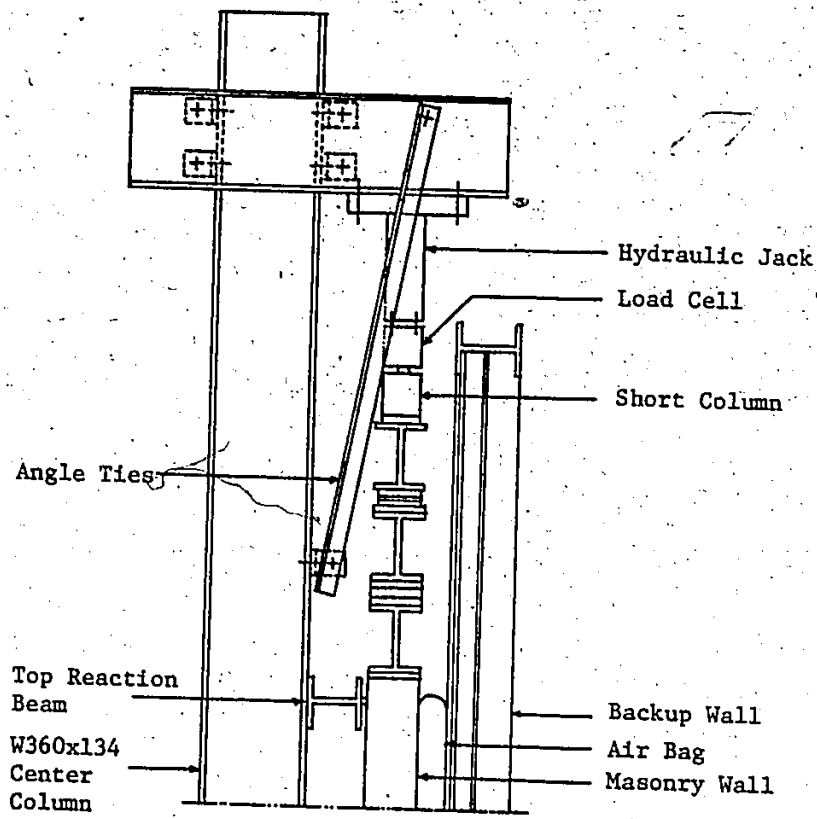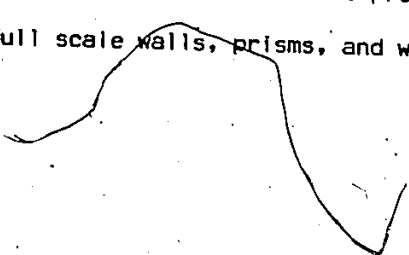
(b) Side View

Figure 2.10   Continued

angles, as shown in Figure 2.10. Then, through a set of beams the load was distributed into four point loads which were applied to a W250x67 beam set on a full bed of mortar to ensure the transfer of load along the whole wall length. It was thought that even if the load was not exactly a uniformly distributed line load along the top of the wall, an even distribution would be attained within the top part of the wall. It was considered that the presence of this continuous beam might influence or restrict the independent rotations of the top edge of the masonry wall. However, detailed analyses (using the finite element model described in Chapter 6) showed that, for the relatively small torsional stiffness of this beam compared to the wall, its effect on the top edge rotations and consequently the test results was insignificant. This finding was not applicable to the bottom support where the individual steel plates were within the supported wall area. Similar analyses showed that the use of continuous plate instead of the separate block length plates would have resulted in higher failure loads and generally stiffer post cracking behaviours.

2.4 TEST ARRANGEMENTS AND PROCEDURES

Tests of full scale walls using the previously described test facility as well as the other auxiliary tests were performed in the Applied Dynamics Laboratory according to different test procedures and using different instrumentation and measurements. In the following sections, the different test arrangements and test procedures will be discussed separately for full scale walls, prisms, and wallettes.

To Crane

Crane Chains

2 in.
Strap

1 in.
Pin

| a | b | c | b | a |

L
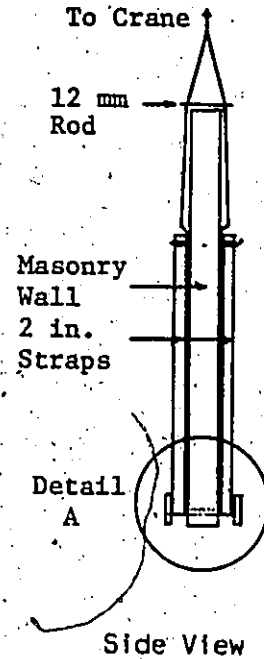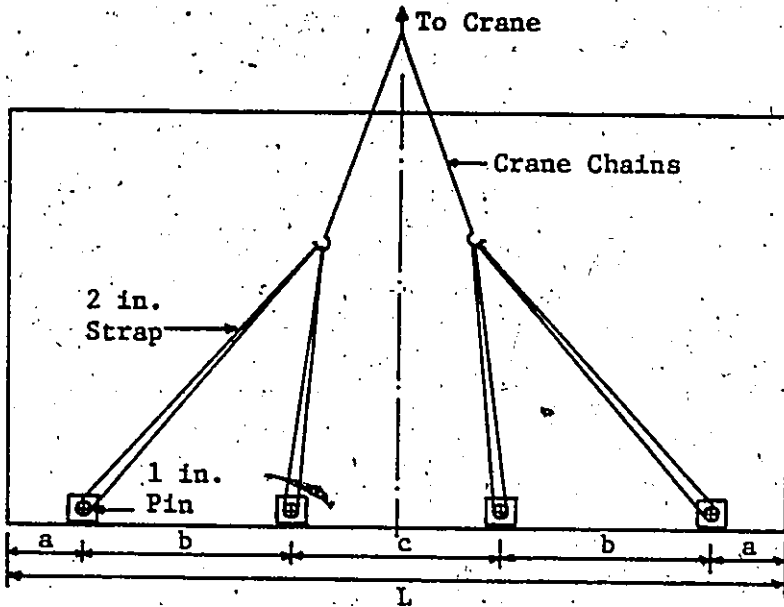
L (m)	3.60	5.20	6.00
a	0.51	0.51	0.68
b	0.80	1.37	1.60
c	0.97	1.43	1.43

Front View

To Crane

12 mm
Rod

Masonry
Wall
2 in.
Straps

Detail
A

Side View

2 in.
Strap

190 mm Block

2 in.
Strap

Plate
120x120x12 mm

1 in. Diam.
Pin

Washer

1 in.
Nut

1 in. Diam.
Holes in
Face Shells

95 mm

Tube Sleeve

50

330 mm

50

Detail A
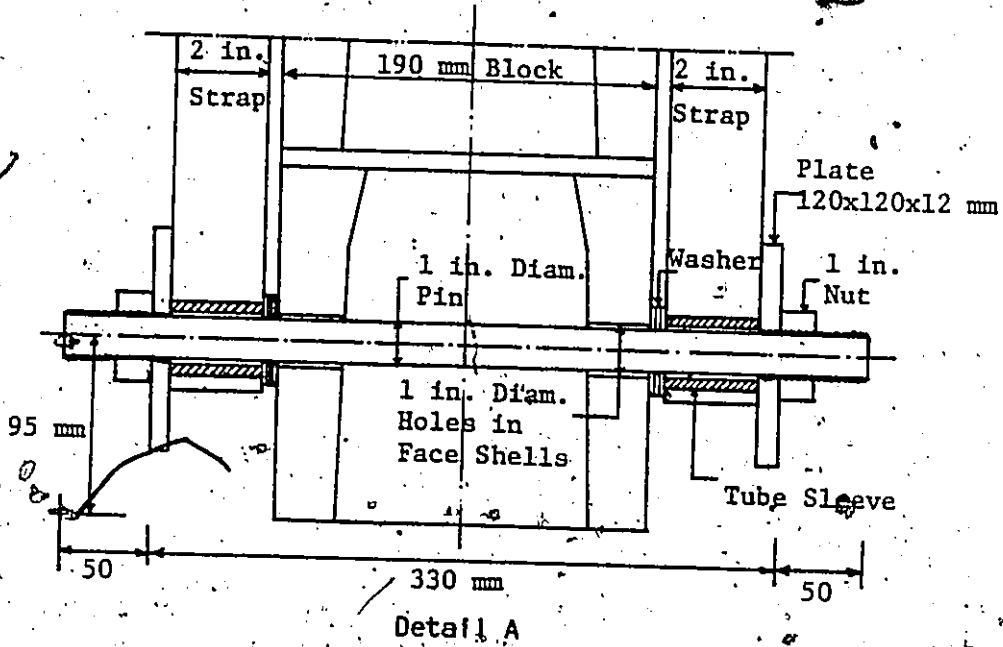
Figure 2.11   Lifting Walls Attachments

2.4.1 Testing of Full Scale Walls

2.4.1.1 Lifting and Moving the Walls

The full scale walls were fabricated at the same time which necessitated having a procedure for moving the walls from the fabrication area to the test setup and back again after testing.

In this procedure, full scale walls were carefully picked up at four points as shown in Figure 2.11. At each of these four locations, a high strength 1 in. (25.4 mm) diameter and 430 mm long steel pins were inserted through a predrilled hole in the masonry wall. The wall was lifted by these four pins using four 2 in. (50.8 mm) wide straps hooked to the four chains of the overhead crane. In order to ensure the stability of the wall during transportation, a set of washers, nuts and tube sleeves were included at the threaded ends of the pins. Also, the crane chains were tied together as shown in Figure 2.11.

It should be noted that pin size and pin spacing were chosen carefully to ensure the adequate safety of the wall for in-plane flexure, bearing and splitting as well as adequate safety of the pins with regard to shear and bending.

2.4.1.2 Instrumentation and Measurements

During testing of full scale walls, deflections and strain readings were recorded. Deflections of the test specimens with respect to the reaction frame were measured using 0.01 mm-dial gauges positioned in lines at panel center and quarter points both horizontally and vertically as shown in Figure 2.12 for wall supported on all four sides. Horizontal lines were positioned at third points in the case of walls
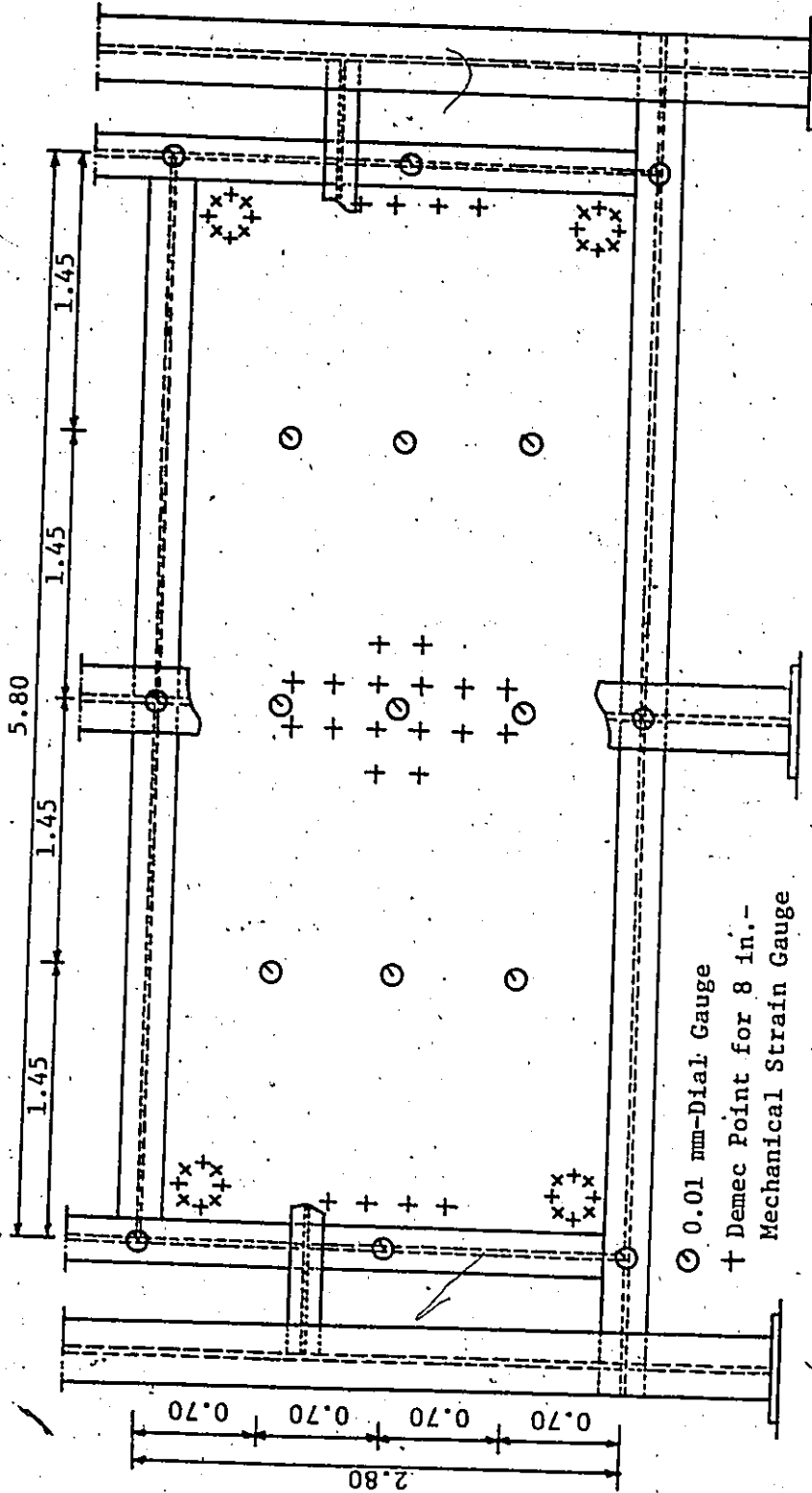
Figure 2.12 Instrumentation for Series WIII Walls
(Representative for Walls Supported on All Four Sides)

⊘ 0.01 mm-Dial Gauge
+ Demec Point for 8 in.-
  Mechanical Strain Gauge

5.80
1.45
1.45
1.45
1.45

2.80
0.70 0.70 0.70 0.70
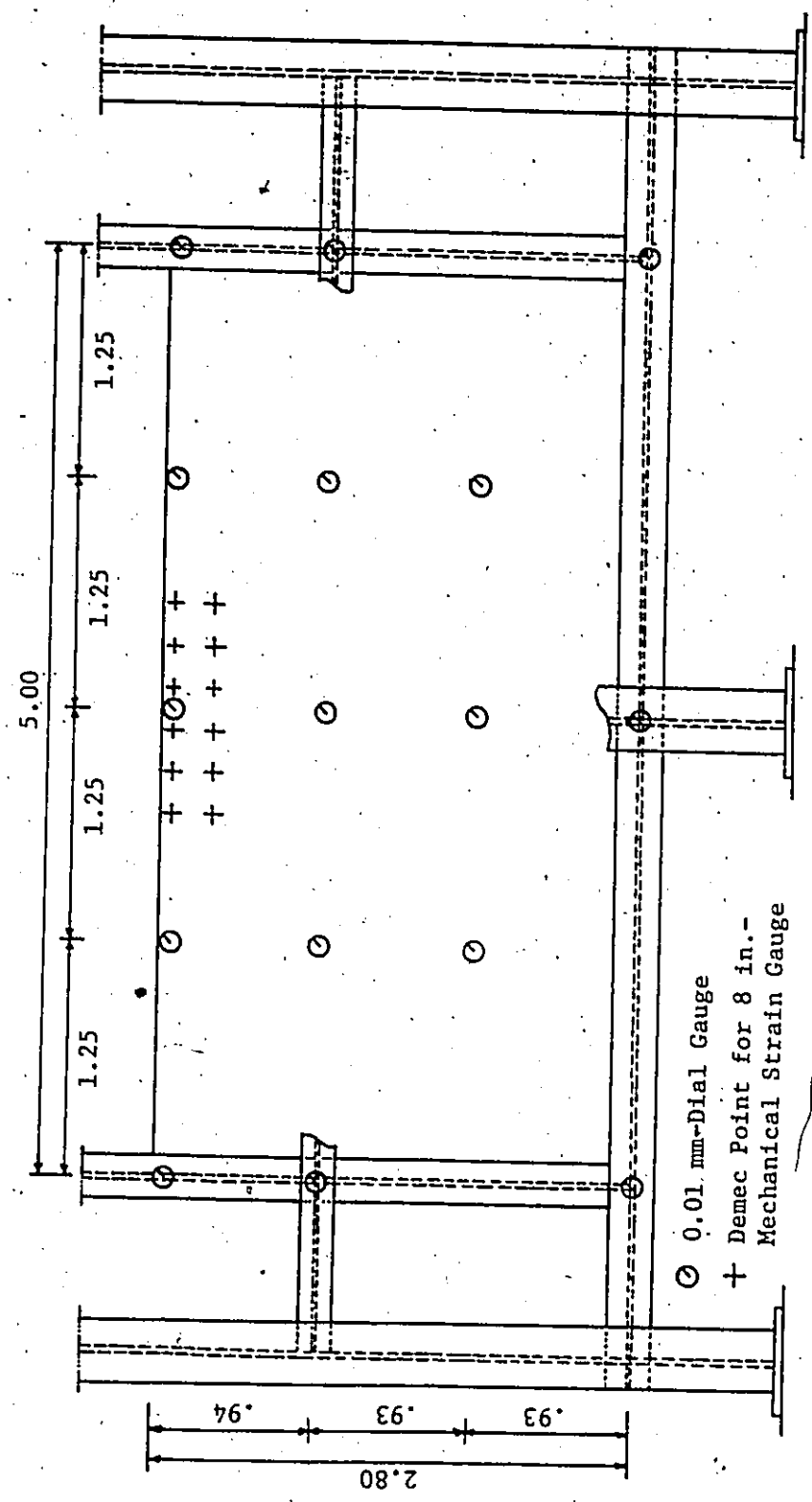
Figure 2.13   Instrumentation for Walls Supported on Three Sides
                With the Tops Free

⊘ 0.01 mm–Dial Gauge
+ Demec Point for 8 in.–
   Mechanical Strain Gauge

5.00
1.25
1.25
1.25
1.25

2.80
.94
.93
.93
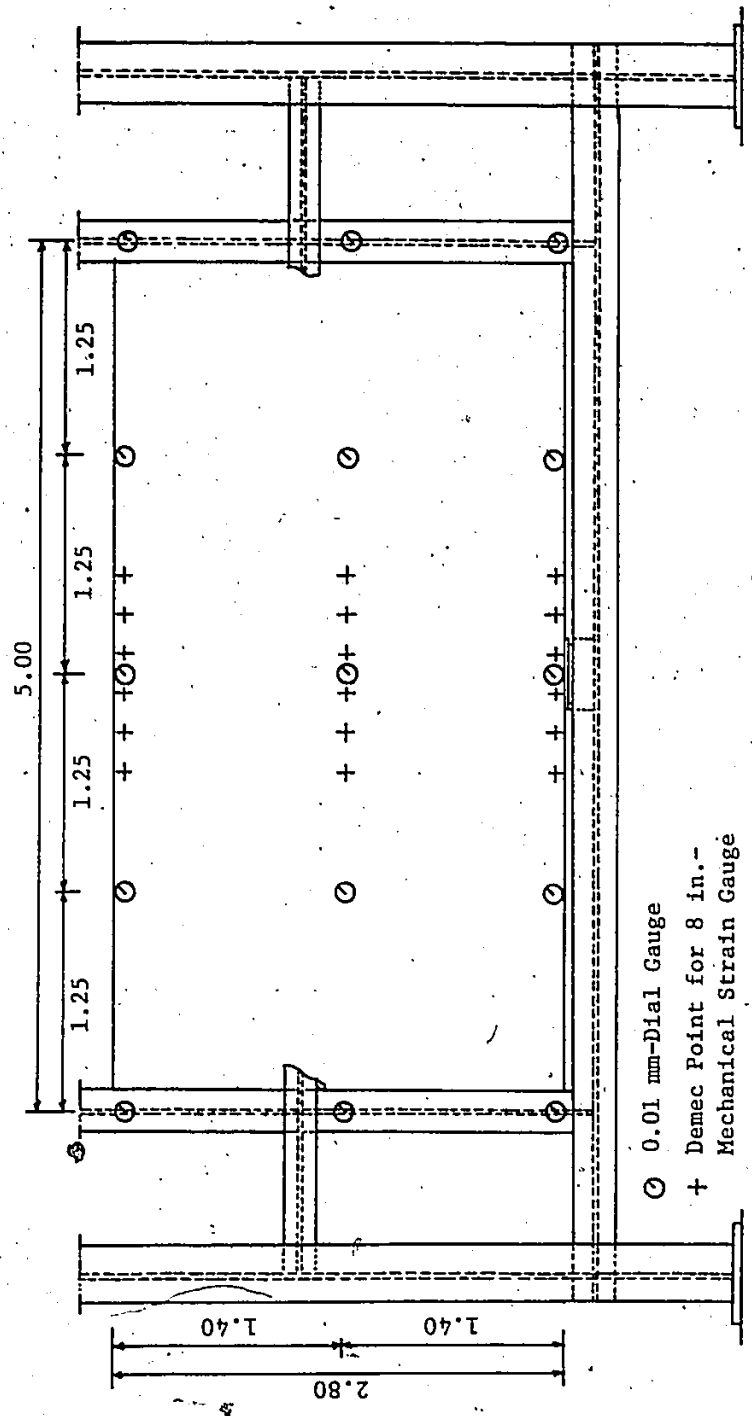
Figure 2.14   Instrumentation for Walls Supported Only on the Two Sides
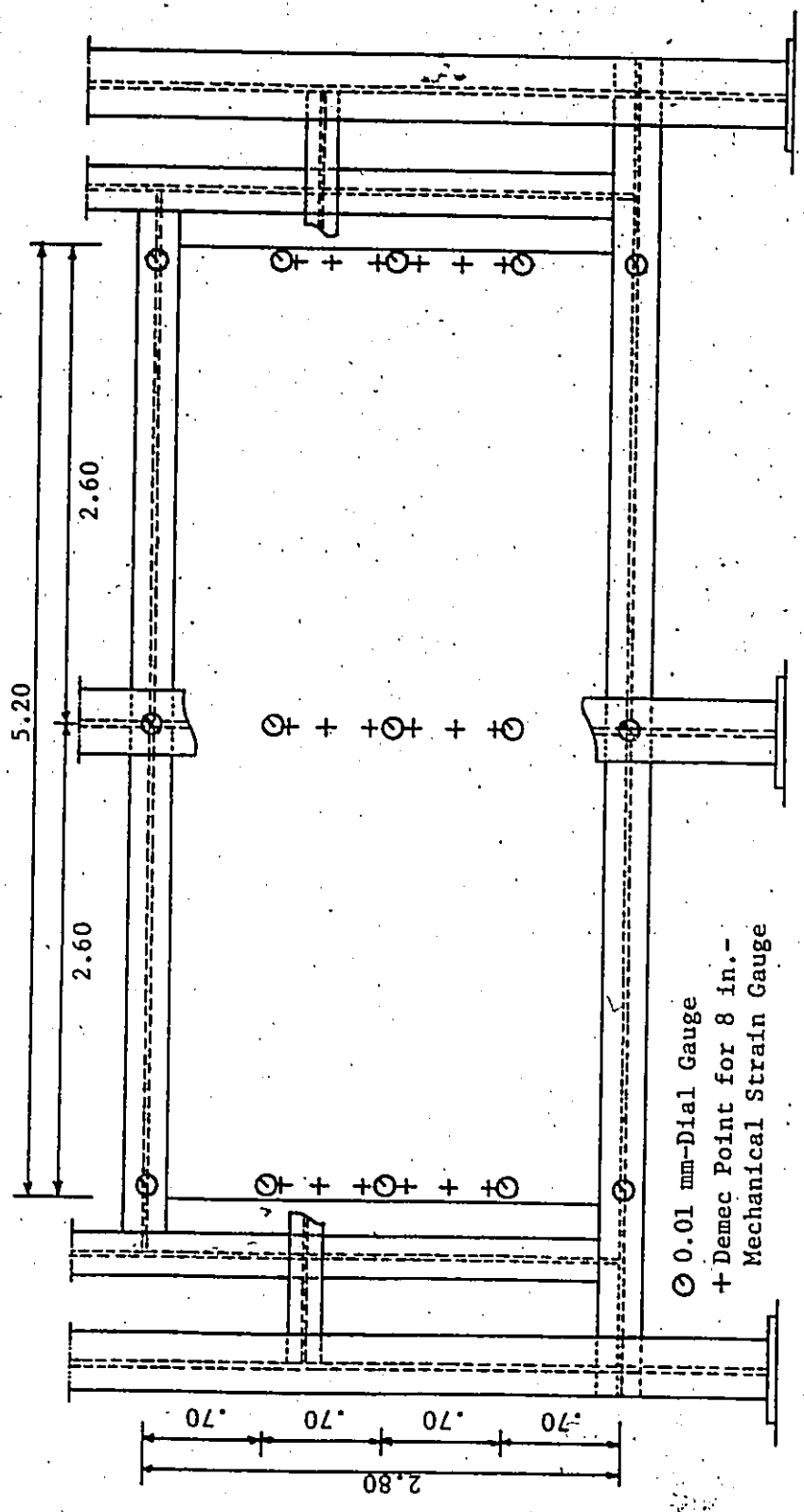
Figure 2.15   Instrumentation for Walls Supported Only
on the Top and Bottom

⊘ 0.01 mm-Dial Gauge
+ Demec Point for 8 in.-
Mechanical Strain Gauge

supported on three sides with a free top while these lines were positioned at mid height and the top and bottom edges for walls supported only on the vertical sides. These locations were identical in Figures 2.13 and 2.14. The dial gauge locations for walls supported on the top and bottom edges are shown in Figure 2.15 where the vertical lines of gauges were positioned at mid-length and the two vertical edges. These gauges were fixed on three light steel columns (angles) attached to the reaction frame at the appropriate locations.

The adequacy of the corner lifting supports was checked by monitoring the deflection of the wall with respect to the reaction frame by means of dial gauges placed near the respective corner.

Deflections of the support frame were also monitored at the corners and mid-length of supporting beams using dial gauges as shown in Figures 2.12 through 2.15. These gauges were attached to free standing steel columns placed at the proper locations behind the reaction frame.

Strains were measured using a mechanical strain gauge (Demec Strain Indicator) and demec points over 8 in (203 mm) gauge lengths. These points were located at the central, mid-edge and sometimes corner regions of the panels as shown in Figures 2.12 through 2.15 for different wall configurations.

2.4.1.3 Wall Test Procedure

At the beginning of each wall test series, the frame was first adjusted to accommodate the new wall dimensions or support conditions. Where top and bottom supporting beams were present, the 2.8 m vertical span was kept equal to the wall height by positioning the top roller a

distance below the top of the wall equal to the distance from the bottom of the wall to the center of the 1.5 in. (38.1 mm) bottom support roller. To accommodate bearing for the side supports, the horizontal spans were made 200 mm less than the nominal length of the wall.

Each wall was carefully picked up according to the procedure mentioned earlier and positioned over the individual bearing plates corresponding to the blocks on the bottom course. It was carefully lowered onto a full bed of mortar and leveled and adjusted vertically. Then, plaster of Paris was placed in the gap between the strips tied to the reaction frame and the wall along the vertical sides and the top support. The mortar and plaster were allowed to harden for several days, prior to testing. During this time, the different instrumentation was positioned , the backup wall was tied back to the reaction frame, the corner lifting restraints were tightened to ensure contact of wall specimen and the frame, and initial readings were recorded. For Group WP walls, the precompression load was applied gradually up to the designed level of preload prior to application of lateral load.

The lateral pressure was applied in increments by pressurizing the air bag and watching the far end manometer reading till it reached the required pressure level. At this time, the input air valve to the bag was shut off and the same readings of inlet and outlet manometers were watched to ensure no leakage in the air system. The size of the load increment was different from test to test in order to have a sufficient number of increments before failure (20 increments average) so that the behaviour and responce to loading could be clearly observed and first cracking and failure pressures more accurately determined.

After each load increment, the pressure was kept constant and deflection and strain readings were recorded and the wall surface was checked for cracks. Cracks were marked and the pressure level at which each crack had been observed was indicated. The pressure was increased in increments until failure. Failure was defined as a sudden drop in pressure and development of new cracks which with the earlier cracks formed a failure mechanism. At this stage, the pressure always kept on dropping even when the inlet valve was still open while the deflection was extensively increasing. Following failure, the air bag deflation valve was opened to release the pressure in the air bag in order to keep the wall in one piece so that it could be taken safely out of the test apparatus and photographed. The time spent in completing one wall test varied from one series to another with an average of about 6 hours. The mortar cubes belonging to each wall were tested on the day following the wall test.

2.4.2 Testing of Prisms For Flexural Tensile
Strength Normal to Bed Joints

The bond wrench apparatus used to determine flexural tensile strengths normal to the bed joints was shown in Figure 2.2.a. Prisms were fixed within the lower frame with only one joint positioned above that frame. Then, the wrench was clamped to the top of the block and the load applied at the other end of the wrench to rupture the top joint. The load was applied gradually either by filling a sand bin or using a hydraulic jack depending on the expected failure load. Only failure loads and failure modes were recorded. For all of these bond

wrench tests, the moment arm for the applied load was 1200 mm measured from the centroid of the block. The 15.15 kg mass of the bond wrench with its moment arm of 453 mm and the self weight of the top block were also considered in the calculation of stress. Each test took approximately 10 minutes with the load being applied gradually.

2.4.3 Testing of Wallettes For Flexural Tensile Strength Parallel to Bed Joints

The beam test shown in Figure 2.2.b for flexural tension parallel to the bed joints was used to provide a region of nearly constant bending moment in which all possible failure modes could occur. In these tests, the wallettes were carefully turned over to be in horizontal plane as shown. Specimens were set in plaster on the top of the support rollers to avoid any torsion due to lack of planeness of their bottom surface. For the same reason, the two spreader beams were set on plywood sheets and loaded through a combination of roller and ball seats.

The load was applied through a hydraulic jack in increments of 1 kN. After each load increment, deflections were recorded using dial gauges positioned at wallette mid-span near the two edges. Load was increased to failure at which time both the corresponding load and failure modes were recorded. The time required to test one specimen was approximately 30 minutes.

CHAPTER 3

MATERIALS AND FABRICATION
OF TEST SPECIMENS

3.1 INTRODUCTION

Full scale walls and auxiliary assemblage specimens were built by an experienced mason. The whole experimental program was fabricated in two phases. These were first a preliminary series and then, the remainder of the program. The materials used could not be kept the same in both phases since the preliminary series was fabricated a year earlier than the rest of the program. Moreover, during the second phase of the program, more than one order of sand was used due to the large amount of mortar needed and the available space limitations.

The physical and mechanical properties of the materials used throughout this program are reported in this chapter together with the specimen fabrication details for both full scale walls and auxiliary assemblage specimens.

3.2 MASONRY MATERIALS

In the construction of the full scale walls and auxiliary assemblage specimens, the masonry materials used were commercially available and were similar to those commonly used in building construction. The component masonry materials used were hollow concrete blocks, mortar and joint reinforcement.

63

3.2.1 Concrete Blocks

The concrete blocks used in this experimental program could not be kept the same for the preliminary tests and the main series. During the year between fabrication of the preliminary series and the main series, the block manufacturer changed manufacturing methods. Thus, the two kinds of blocks used were cured differently. The first blocks were autoclave cured normal weight hollow concrete blocks while the later ones were cured by the bubble curing technique.

The physical and mechanical properties of the autoclave cured blocks which were available through another McMaster masonry research project [110] are summarized in the following sections. The properties of the bubble cured blocks were investigated by the author in collaboration with two other graduate students engaged in masonry research at McMaster [47,99]. The results of this investigation are given in detail in Appendix A and are also summarized in the following sections.

3.2.1.1 Physical Properties

The masonry units used throughout the test program were the standard 190 mm normal weight hollow concrete blocks. This type of blocks had the nominal dimensions of 200x200x400 mm. The curing was done in an autoclave for the blocks used in the preliminary series while it was done by bubble curing in the main series blocks. In addition to the frogged end units used in most situations, the splitters or end units were used as edge units in the full scale walls and were also used to provide half blocks. The general views of the frogged end and

splitter units are shown in the photographs of Figure 3.1. The standard cross-sectional dimensions of the two block types are given in Figure 3.2. The average net cross-sectional area of this block as supplied by the manufacturer, based on the standard block dimensions, was 41500 mm^2 which resulted in a net to gross area ratio of 0.56.

The initial rate of absorption (IRA) was determined by performing the ASTM standard C67-85 [2] test on 6 autoclave cured blocks and 10 bubble cured blocks. In this test, the IRA is defined as the amount of water initially absorbed by a dry unit when it is partially immersed in water to a depth of 1/8 inch (3.2 mm) for a period of one minute. Accordingly, the mean initial rate of absorption was 1.13 kg/m^2/min with a coefficient of variation of 31.5% for autoclave cured blocks while the mean and coefficient of variation for bubble cured blocks were 2.96 kg/m^2/min and 28.5% , respectively. It should be noted that the IRA was determined for the bottom surface of the blocks. However, similar experimental results for the top surface yielded a mean value only 1% less than that for the bottom surface. This is considered to be an insignificant difference. Therefore, only the bottom surface value was reported as a material property. Based on weighing five dry specimens, the average density of the units and their coefficients of variation were 2109.0 kg/m^3 and 1.2% for autoclave cured blocks and 2120.0 kg/m^3 and 8.2% for bubble cured blocks, respectively.

3.2.1.2 Mechanical Properties

The compressive strength of autoclave cured blocks was determined experimentally for different specimen shapes or geometries,
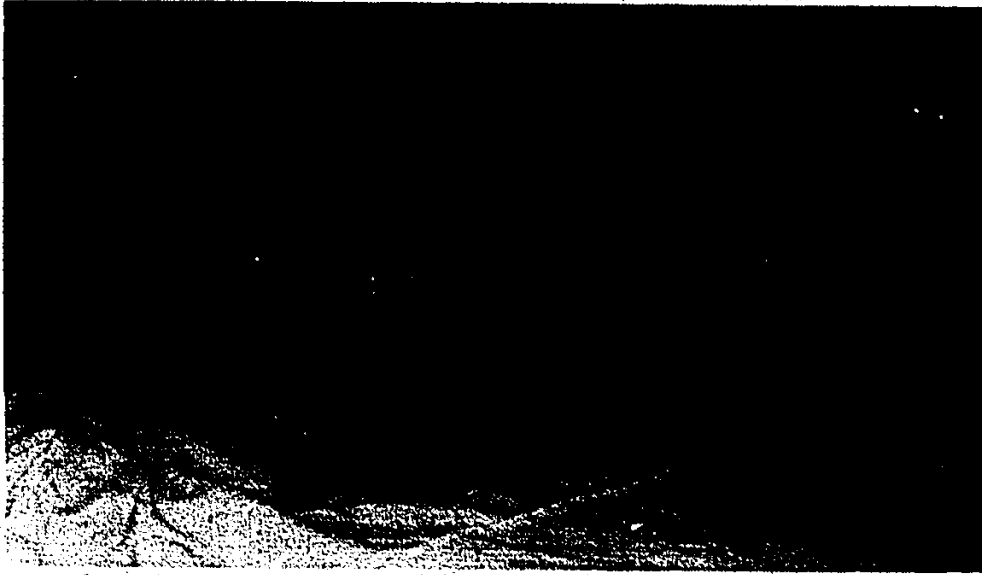
(a) Frogged End Unit
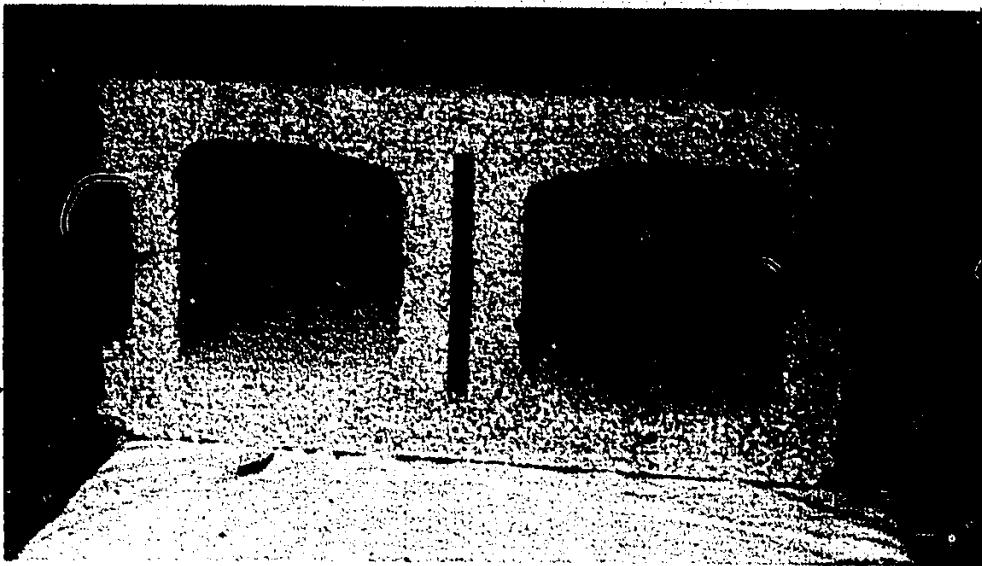
(b) Splitter Unit

Figure 3.1   Different Masonry Units Used

| | | | | |
| Section A-A | Section B-B | | | |

(a) Frogged End Unit

Section C-C

Section D-D

(b) Splitter Unit
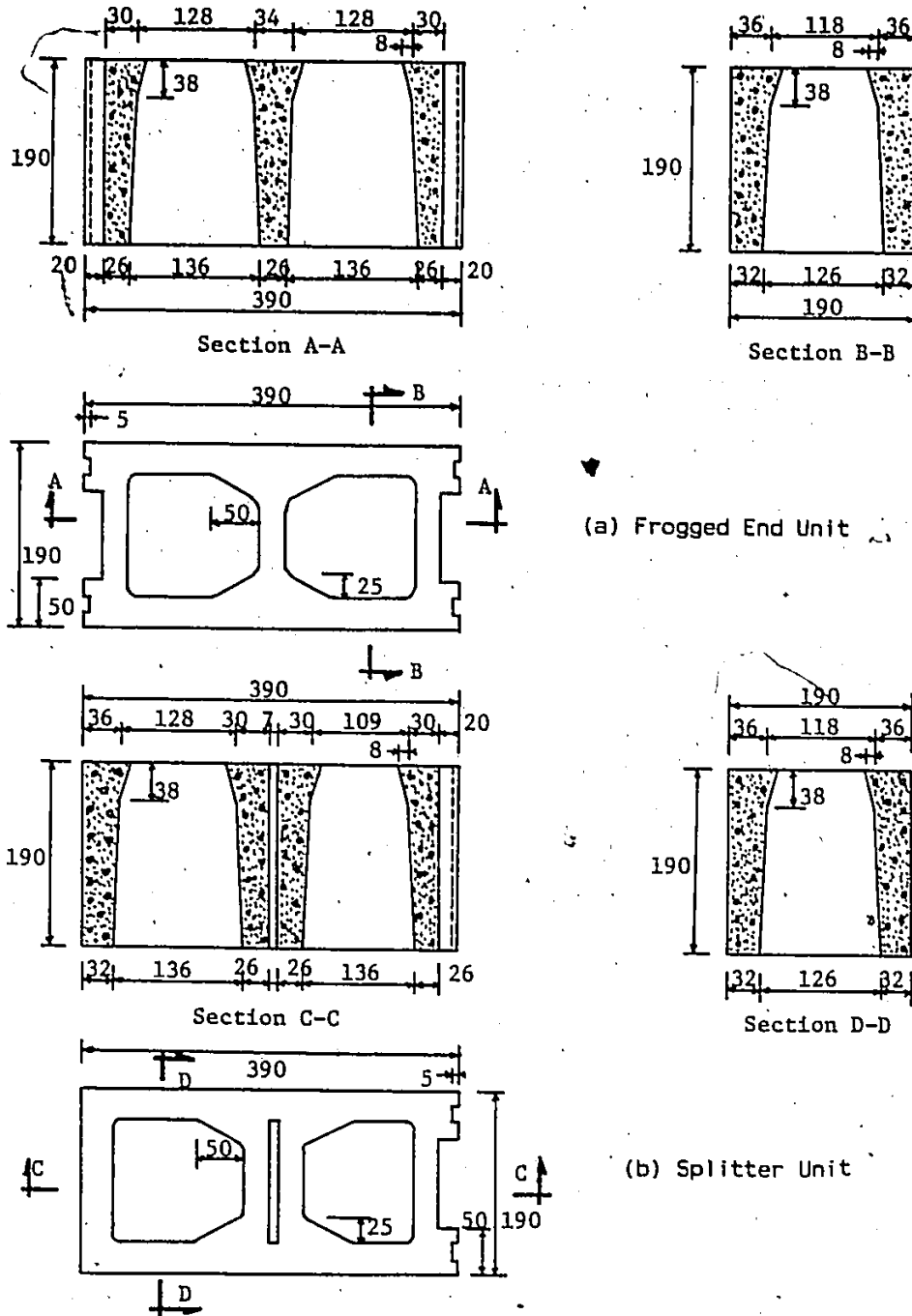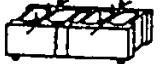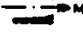
Figure 3.2   Standard Dimensions of Concrete Block Units Used

Table 3.1   Summary of Compression and Tension Test Results
for Autoclave Cured Concrete Blocks

TEST SERIES	TYPE OF TEST	DESCRIPTION	NUMBER OF SAMPLES	AVERAGE FAILURE STRESS (MPa)	COEFF. OF VARIATION (%)	AREA OF APPLIED STRESS
C 1	COMPRES-SION	FULL HOLLOW BLOCKS. HARD CAPPING ON FULL BEDDING. LOAD ALONG SHORT AXIS.	5	19.2	3.8	MINIMUM MEASURED AREA (M.M.A.)
C 2	COMP.	HALF HOLLOW SPLITTER BLOCKS. SAW CUT. HARD CAPPING ON FULL BEDDING. FACTORY-FLAT HALF USED.	5	17.26	4.9	M.M.A.
C 3	COMP.	HALF HOLLOW SPLITTER BLOCKS. SAW CUT HARD CAPPING ON FACE-SHELL ONLY. FACTORY-FLAT HALF USED.	5	21.05	7.8	MINIMUM MEASURED FACESHELL AREA (M.F.A.)
C 4	COMP.	HALF HOLLOW SPLITTER BLOCKS. SAW CUT. SOFT CAPPING ON FULL BEDDING. FACTORY-FLAT HALF USED.	5	15.61	5.9	M.M.A.
C 5	COMP.	HALF SOLID BLOCKS. SAW CUT. HARD CAPPING.	3	15.56	4.8	GROSS AREA
C 6	COMP.	FULL HOLLOW BLOCKS. HARD CAPPING ON THE ENDS OF FACESHELLS. LOAD ALONG LONG AXIS.	5	16.59	5.4	M.F.A.
T 1	SPLITTING TENSION	HALF HOLLOW BLOCKS. MIXED SAMPLE OF STD. AND SPLITTER UNITS. LINE LOAD PARALLEL TO CROSS WEBS.	9	2.03	9.2	FACESHELL AREA IN LOADING PLANE (F.A.L.P.)
T 2	SPLITTING TENSION	FACE SHELLS SAW CUT FROM HOLLOW UNITS WITH TAPERS REMOVED. LINE LOAD PERPENDICULAR TO SHELL PLANE.	9	2.09	5.9	F.A.L.P.
T 3	FLEXURAL TENSION IN-PLANE	TWO FULL HOLLOW BLOCKS EPOXIED AT FROGGED ENDS. THIN SIDE OF FACE SHELLS IN TENSION.	5	3.32	7.1	M.F.A.
T 4	FLEXURAL TENSION OUT-OF PLANE	FULL HOLLOW BLOCKS. FROGGED ENDS SAWED OFF. EPOXIED TO STEEL PLATES & BEAMS.	5	2.92	15.2	M.F.A.

different capping materials, and different capping configurations. The results of these tests, which were available through another masonry project[110], are summarized in Table 3.1. This included tests of full blocks hard capped on the full bedding area and tested flatwise,fully hard capped half blocks, half blocks with face shell hard capping, half blocks with full soft capping, hard capped half solid blocks, and full blocks with hard capping on the ends of the face shells and tested lengthwise.

The tensile strength of the autoclave cured blocks was determined by splitting tests of face shells either in half block specimens or face shell specimens sawn from blocks. Also, flexural tensile strength was determined by means of in-plane and out-of-plane flexure tests. These tensile strengths are also given in Table 3.1.

Table 3.2 contains a summary of the experimentally determined compressive and tensile strengths of the bubble cured blocks. The detailed test results for these blocks are given in Appendix A. In these tests, only the hard capping was used for compressive strength tests. All tests mentioned above for autoclave cured blocks were also performed for the bubble cured blocks with the exception of compression tests of solid blocks, tensile splitting of sawed face shells, and in-plane flexural tension tests. Additional tests included compression of specimens made of face shells glued together and splitting of webs in half block specimens. Not only were strength values determined but also the deformation characteristics (stress-strain relationships) were obtained from most tests for the bubble cured blocks. The stress-strain curves shown in Figure 3.3 were obtained by regression analysis of the

Table 3.2 Summary of Compression and Tension Test Results for Bubble Cured Concrete Blocks

TEST SERIES	TYPE OF TEST	DESCRIPTION		NUMBER OF TESTS	AVERAGE FAILURE STRESS (MPa)	COV (%)	AREA OF APPLIED STRESS	SECANT MODULUS OF ELASTICITY (MPa)	POISSON'S RATIO
C1	comp	full hollow block full capping		10	22.8	5.4	minimum net area		
C2	comp	half splitter block full capping		10	22.1	8.7	minimum net area	18.2×10^3	0.33
C3	comp	half splitter block face shell capping		10	26.8	4.4	min face shell area	15.5×10^3	0.30
C4	comp	4 glued faceshells full capping		10	18.5	6.1	measured area	19.6×10^3	0.34
C5	comp	full hollow block head joint capping tested endwise		10	18.7	13.6	average faceshell area	15.6×10^3	0.19
T1	splitting tens	half splitter block load face shells		10	1.60	11.4	avg face shell area		
T2	splitting tens	half splitter block load across webs		10	1.30	18.1	average web area		
T3	flexural tens	full hollow block tested out-of-plane		7	2.41	7.1	minimum faceshell area	$EI=1.82 \times 10^{12}$	

* determined at half the failure stress from only 5 specimens.
** determined from only 5 specimens for compressive strains up to 1000με.
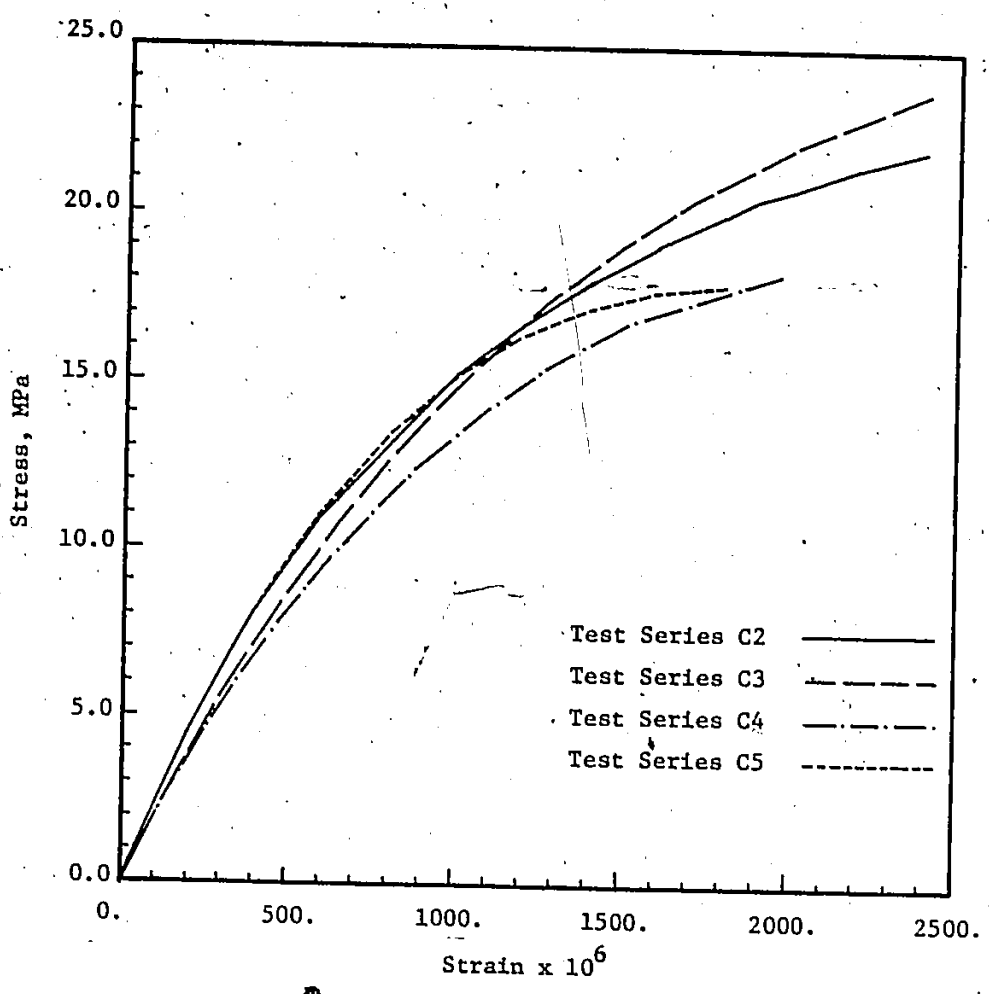
Figure 3.3   Stress-Strain Relationships for Different Block
              Tests in Compression (Regression Lines)

available data for the concrete blocks in compression from different tests.

The following observations have been drawn from the block test results :

1. The compression tests using soft capping material yielded relatively lower block compressive strengths with relatively larger coefficients of variation. It is thought that the lack of platen restraint by the soft capping allowed more lateral tensile strain and hence the reduced strength and changed mode of failure from a conical pattern to almost splitting failure along vertical planes. Also, the increase in lateral tensile strains and tensile splitting are consistent with larger variations in strength values. Therefore, the use of hard capping for compression tests was adopted to provide a more consistent measure for compressive strength of blocks.

2. The compression tests of full blocks tested flatwise yielded higher compressive strength and lower variability than the half blocks. The reason for this is thought to be that the confinement affected the strength of the full blocks more than the half blocks due to the larger area affected by this confinement. Although the half block tests seem to be more reliable in describing the compressive strength due to smaller associated effects of lateral confinement, the full block tests were performed since it is still most often used in practice to determine the compressive strength. The minimum confinement occurs in the case of full blocks tested lengthwise with the

load applied parallel to the longitudinal axis of the blocks.
Consequently, the compressive strength determined from these
tests was the lowest.

3. The compressive strength, as determined from half block
specimens or full blocks tested either flatwise or lengthwise,
reflects the material strength as well as the geometry of the
specimen. In order to isolate the material strength, specimens
made by gluing face shells together were tested. The reason for
using four face shells glued together was to avoid having very
slender specimens which would be the case if individual face
shells were tested. Comparison of the test results of these
specimens and the other compression tests shows that the
deformation characteristics of the half block specimens are
similar to those of the glued face shells while the failure
stress is slightly higher for the half block specimens. Also,
the strength of full blocks tested lengthwise were almost the
same as for the glued face shells while the derived modulus of
elasticity is considerably lower than for the glued face shell
specimens. It was concluded that the compressive strength and
deformation characteristics of the half block specimens could be
considered to represent the corresponding properties of the
block material.

4. The tensile strength of concrete blocks is of prime importance
since in most masonry assemblages, when the failure plane goes
through the blocks, the block failure is characterized to be
tension failure. This is due to the brittle nature of the

masonry material, its very small tensile strength compared to its compressive strength, and of course the presence of the softer mortar joints between the concrete blocks.

5. The splitting tensile strength has generally been considered to represent the axial tensile strength using a relatively easy test to perform [50]. Previous splitting tests always referred to splitting of face shells and this was considered to be the tensile strength of the block material. This was confirmed by splitting tests of sawed face shells to eliminate the effect of specimen geometry. The test results showed that the splitting strength of sawed face shells and of face shells in half blocks are similar which indicates that the splitting tensile strength as determined using half block specimens can reasonably be considered as a material property which is not affected by the specimen geometry.

6. The splitting of webs in half blocks was thought to be representative of the tensile strength controlling failure in masonry assemblages subjected mainly to in-plane compression. In these cases the experimentally observed failure is always described by splitting of block webs. The tensile splitting strength determined by web splitting was found to be almost 20% lower than that determined for face shell splitting and its variability is larger. A reason for this may be the observed indentation or defect at the bottom of the webs of most of the bubble cured blocks used in the block testing program. This would have the effect of reducing the actual splitting area and

made the calculated stress, based on the whole splitting area, smaller than the actual stress. In addition, there seemed to be some lack of compaction at the extremities of webs which would likely result in a weaker section.

7. The flexural tensile strength of blocks as determined from the in-plane flexure test was considerably higher than the splitting strength. This increase in the strength is attributed to the strain gradient effect. It should be noted here that the strain gradient in the case of this test is higher than the gradient in elements commonly used in practice such as shear walls or columns.

8. The flexural tensile strength of blocks from out-of-plane bending tests was higher than the splitting strength and less than the in-plane flexural tensile strength. In this case, the increase over the splitting strength is thought to be due to the small increase in strain gradient. Furthermore, the splitting strength is controlled by the weaker of the two face shells whereas the out-of-plane flexural strength is controlled by the strength of only the tension face shell. The decrease in strength for out-of-plane bending with respect to the in-plane bending is attributed to the comparatively small strain gradient over the tension face shell thickness for out-of-plane bending tests.

9. Although the testing of both autoclave cured and bubble cured blocks were performed at representative ages of several months, the comparison between the compressive and tensile strengths for

both types, indicated that generally the compressive strengths for the bubble cured blocks were about 20% higher than the corresponding strengths of the autoclave cured blocks. However, the different tensile strength tests for the bubble cured blocks yielded lower values by about 20% compared to those of the autoclave cured blocks.

3.2.2 Mortar

Code designated type S mortar was used in fabrication of all full scale walls, wallettes and prisms. It was chosen because of its common use in practice.

The mortar conformed to CSA Standard A 179M [32] using type 10 Portland cement and "white" type N hydrated lime as the cementitious materials. The mortar mixes were batched by weight instead of by volume in order to ensure better quality control and a more consistent mortar. The mix proportion of Portland cement to lime to sand was 1 : 0.21 : 4.24 by weight which corresponded to ·1 : 0.50 : 3.33 by volume. The water to cement ratio was kept consistent throughout the test program at about 0.9 by weight.

As reported earlier, materials and workmanship, representative of common practice, were chosen for this test program except where conformance with building standards was necessary. The masonry sand in stock was shown, by means of sieve analysis, to exceed the specified upper limits, due to the relatively high percentage passing 600 microns. Accordingly, it was rejected and the available concrete sand was used instead after sieving through a 4.75 mm sieve. The resulting gradation

satisfied the specifications. Furthermore, due to the time lag between the fabrication of the preliminary series and the main series, the large amount of mortar needed and the available space limitations, four different loads of concrete sand were used. The gradation of these different concrete sands used together with that of the rejected masonry sand are shown in Figure 3.4.

Mortar was prepared in 100 lbs (45 kg) batches and if any mortar batch was not used up within a half hour, the unused mortar was discarded rather than permitting retempering of the mortar with additional water. The fabrication of all the test specimens required a total of 215 batches.

The mortar initial flow was measured for each batch using the flow table according to the ASTM Standard C109-84 [3]. The mean initial flow for mortar batches used in each wall ranged from 100% to 118% with an overall mean value of 109%.

Three 2 inch (50.8 mm) mortar cubes were made from each mortar batch to be used for the determination of the mortar compressive strength. These cubes were air cured in the laboratory under the same conditions as the test specimens. The mortar cubes associated with each wall, wallette or prism were tested the same or the day following the assemblage test. When the same batch was used in fabricating more than one specimen, the mortar cubes belonging to this batch were divided between the different groups accompanying the different specimens.

The mean compressive strength of the mortar cubes tested are shown in Table 3.3 for each wall or control specimens fabricated using the same batches. The numbers of cubes tested and the corresponding
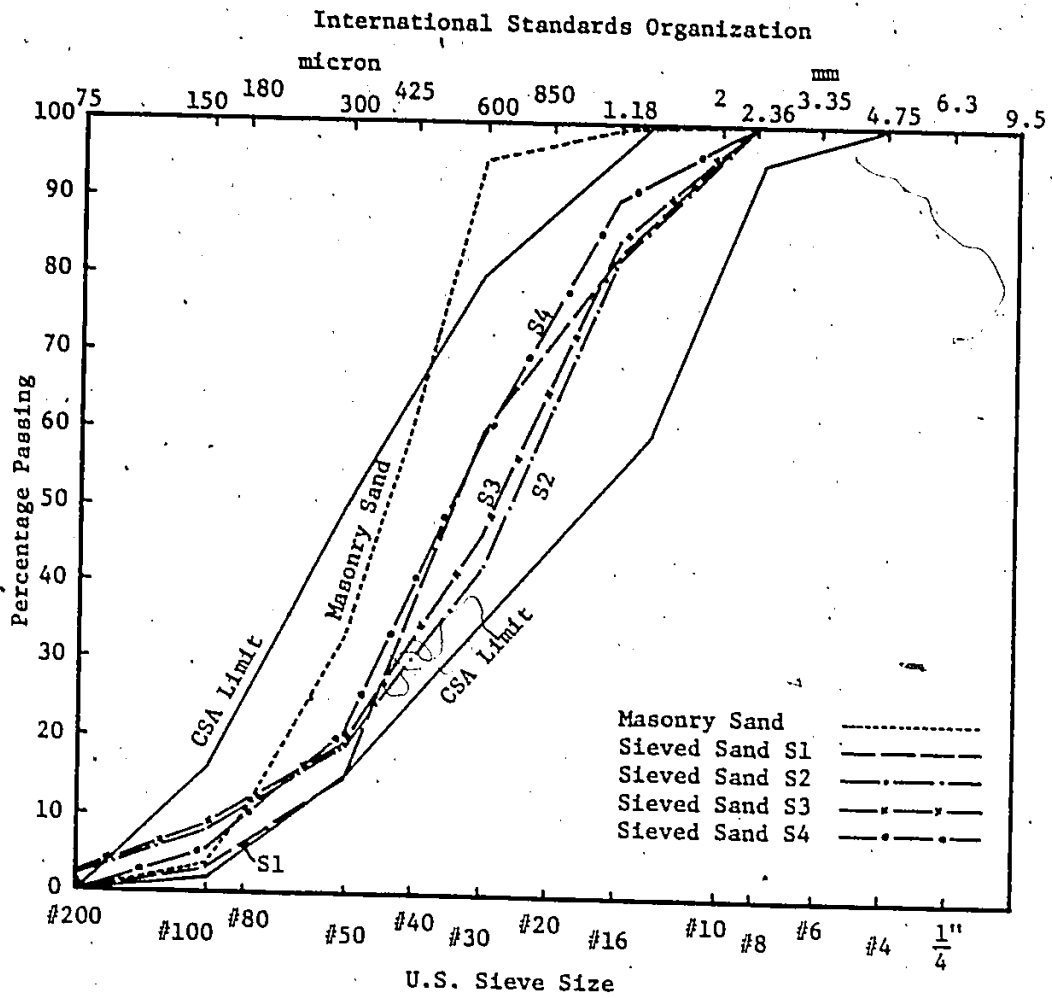
Figure 3.4   Sieve Analysis of Sand for Masonry Mortar

Table 3.3   Compressive Strength of Mortar Cubes

Series	Sand Type	Cubes Belong To	No. of Cubes	Age Days	Walls		Sands	Series
					Mean Strength MPa	C.O.V* %		
Preliminary Series	S1	WI-1	14	368	20.5	14.5	n=72 Mean= 17.3 C.O.V= 17.3%	n=72 Mean= 17.3 C.O.V= 17.3%
		WIII-1	29	265	16.9	16.		
		Prisms	9	85	17.3	7.5		
		Wall-ettes	20	162	15.5	13.		
Main Series	S2	WI-2	16	65	22.4	7.9	n=287 Mean= 24.1 C.O.V= 13.8%	
		WI-3	19	64	22.5	8.8		
		WII-1	28	102	26.5	7.1		
		WII-2	27	99	24.4	7.9		
		WII-3	28	98	24.4	10.5		
		WIII-2	33	92	21.8	10.6		
		WIII-3	25	110	28.7	18.7		
		WP-1	28	98	22.7	10.4		
		WP-2	30	111	25.3	4.2		
		WP-3	25	111	22.3	17.7		
		WV-3	28	140	22.9	6.8		
	S3	WH-1	28	126	24.3	12.4	n=164 Mean= 23.6 C.O.V= 13.8%	n=507 Mean= 23.4 C.O.V= 15.3%
		WH-2	27	128	21.6	13.7		
		WH-3	27	133	21.6	11.3		
		WF-1	27	114	21.9	6.4		
		WF-2	27	117	25.2	10.8		
		WF-3	28	116	26.7	10.1		
	S4	WV-1	28	128	18.5	14.4	n=56 Mean= 19.3 C.O.V= 16.2%	
		WV-2	28	132	20.	17.		
		Prisms & Wall-ettes	49	169	24.	17.6		

* coefficient of variation

coefficients of variation are also included. The number of cubes tested with each wall varied according to the number of mortar batches required for completing the wall. Therefore, the number of cubes for the short walls (Series WI) ranged between 14 and 19 cubes as shown in Table 3.3. While for the long walls (Series WIII) it ranged between 25 and 33 cubes and for all other walls it was 25 to 30 cubes per wall. Despite care in the batching procedure and the large number of cubes tested per wall, the mean mortar strengths listed in Table 3.3 show considerable variation. Also, for individual walls, the coefficient of variation of mortar cube strengths ranged from 4.2% to 18.7%.

Differences between mortar strengths for the preliminary series and the main series could be attributed to changes in sand and cement. The variation of mortar strengths of all the cubes of the main series was of the same order as that for the individual walls. This can be observed by comparing the 15.3% coefficient of variation for all of the main series cubes with the coefficients of variation for individual walls. This indicates that this scatter appears to be inherent for this material. It should be noted that the changes in sand within the main series did not appear to cause much difference in mortar strengths. This is thought to be due to the very similar gradation for sands S2 and S3 as shown in Figure 3.4 which were used for building most of the main series specimens.

The age of the mortar cubes at the test date listed in Table 3.3 ranged from 85 days to 368 days for the preliminary series and from 64 to 169 days for the main series. To study the effect of age on the mortar strength, the mean cube strengths are plotted versus the
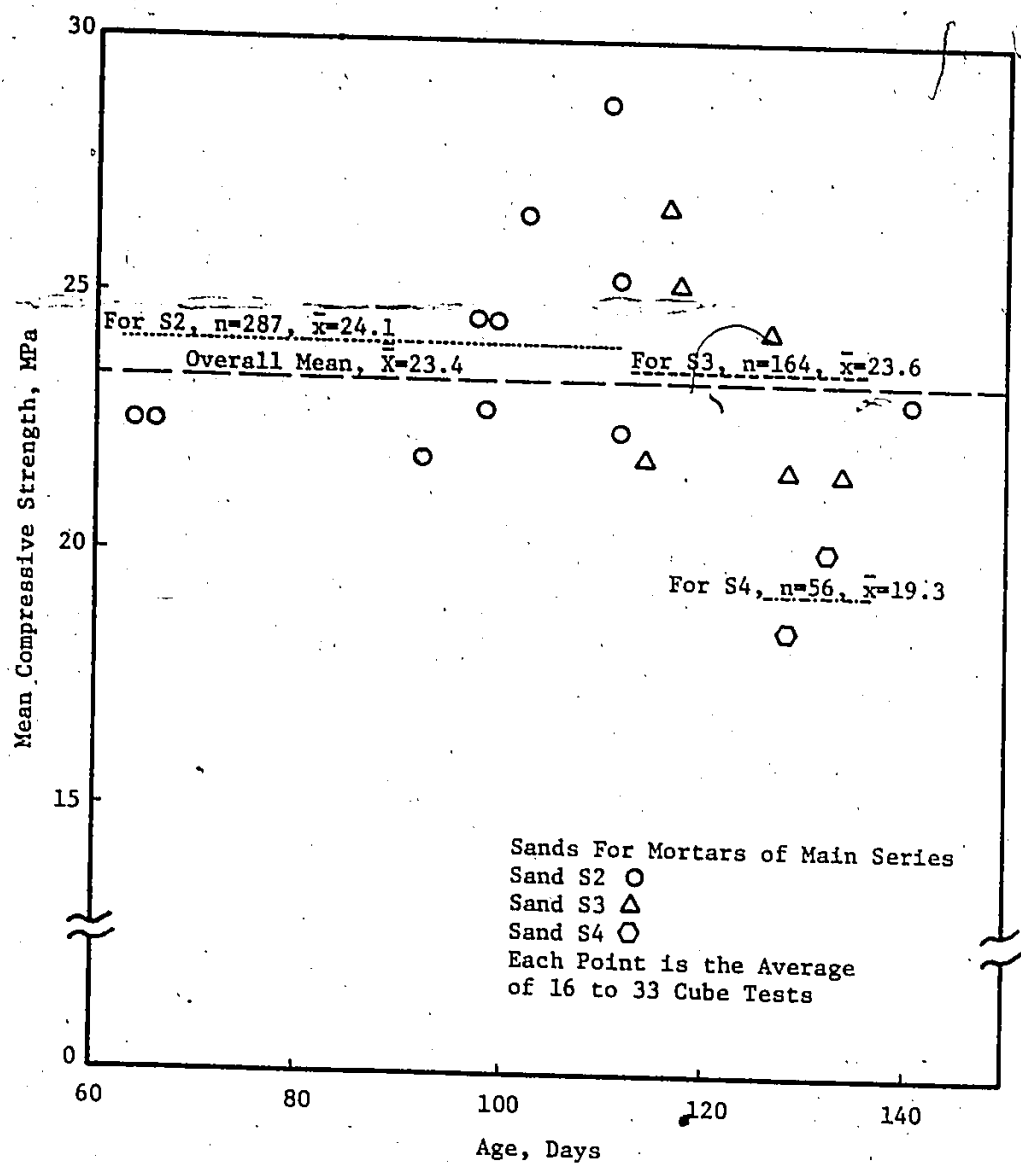
Figure 3.5   Compressive Strength of Mortar Cubes Tested With
Walls Versus Age

corresponding age at the test date in Figure 3.5. The scatter of the strengths with respect to mean strength suggests that at an age of 64 days or larger, the scatter of strengths due to the inherent variability is large enough to obscure any possible small increase in strength.

In conclusion, the mortar cube compressive strength as determined from the previously mentioned tests had a mean of 17.3 MPa and coefficient of variation of 17.3% for the preliminary series. For the main series, the mean strength and its coefficient of variation were 23.4 MPa and 15.3%, respectively.

3.2.3 Joint Reinforcement

All full scale walls had horizontal joint reinforcement embedded in mortar bed joints at every other course. The inclusion of such reinforcement was made to keep the wall together in almost one piece after failure and made it possible to lift the wall out of the testing frame safely. The standard truss configuration was used for that purpose. This reinforcement consisted of 9 gauges diameter (3.65 mm) side rods welded to a continuous diagonal formed cross rod of the same size as the side rods. The overall measurements was approximately 38 mm less than the nominal thickness of the wall. The side rods were manufactured with a four-sided knurled surface to develop bond. Flush welding of the side and cross rods was used which permitted full mortar cover .

. The steel wire used in the manufacture of the standard truss type joint reinforcement complies with the requirements of CSA G30.3 [31] and ASTM A82 [1] for cold drawn steel wire. The properties of the

wire as supplied by the manufacturer were yield strength of 80,000 psi (552 MPa), proportional limit of 70,000 psi (483 MPa), and a reduction of area of 30 percent.

3.3 FABRICATION OF TEST SPECIMENS

The experimental program was constructed in two phases as mentioned earlier. The preliminary series, which was constructed in the summer of 1982, included two full scale walls plus auxiliary specimens whereas the main series constructed in the summer of 1983, contained nineteen full scale walls plus auxiliary specimens. In each series, the full scale walls and the auxiliary assemblage specimens were constructed at the same time using the same materials.

The full scale walls included in the preliminary series were one of the Series WI walls which had the dimensions of 3.60x2.80 m (9 blocks long by 14 blocks high) and one of the Series WIII walls having dimensions of 6.00x2.80 m (15 blocks long by 14 blocks high). The auxiliary assemblage specimens for this series consisted of the following :

1. Six 5 blocks high stack bonded prisms used for the determination of the flexural tensile bond strength normal to the bed joints.

2. Twenty wallette specimens consisted of a full block and two half blocks high and four blocks long laid in running bond. These were used to determine the flexural tensile strength parallel to bed joints.

The main series included two of Series WI walls and two of Series WIII walls with the dimensions mentioned above plus fifteen walls

5.20x2.80 m (13 blocks long by 14 blocks high). The auxiliary assemblage specimens for the main series consisted of twenty three prisms for tensile strength normal to the bed joints and fourteen wallettes for tensile strength parallel to the bed joints. These specimens had the same configurations as the preliminary series specimens.

Fabrication of the full scale walls was done using the following procedure :

1. The wall was constructed on a polyethylene sheet in order to prevent the sticking of mortar to the laboratory floor.

2. The first course was laid using blocks with predrilled holes at the proper locations for wall lifting purposes.

3. After mixing each batch of mortar, the mortar flow was determined.

4. At the beginning, middle and end of building with a mortar batch, three 2 inch (50.8 mm) mortar cubes were made for mortar compressive strength tests.

5. Standard truss type joint reinforcement was placed in the first and then in every other bed joint. This reinforcement was available in 10 ft (3.05 m) long lengths. For longer walls the splices of the two steel lengths used were located alternately near the two sides in successive alternate courses.

6. All mortar joints on both sides were tooled with a 15 mm diameter jointer.

7. All the walls were fabricated and air cured within the laboratory at a temperature of about 20°C and 30 to 50% relative

.humidity.

The auxiliary specimens were built after the fabrication of each full scale wall and sometimes from the last mortar batch used for the wall. When this was not appropriate, separate batches were used for the auxiliary specimens.

Figure 3.6 is a photograph of the full scale walls and some of the auxiliary specimens in the Applied Dynamics laboratory of McMaster University during fabrication.
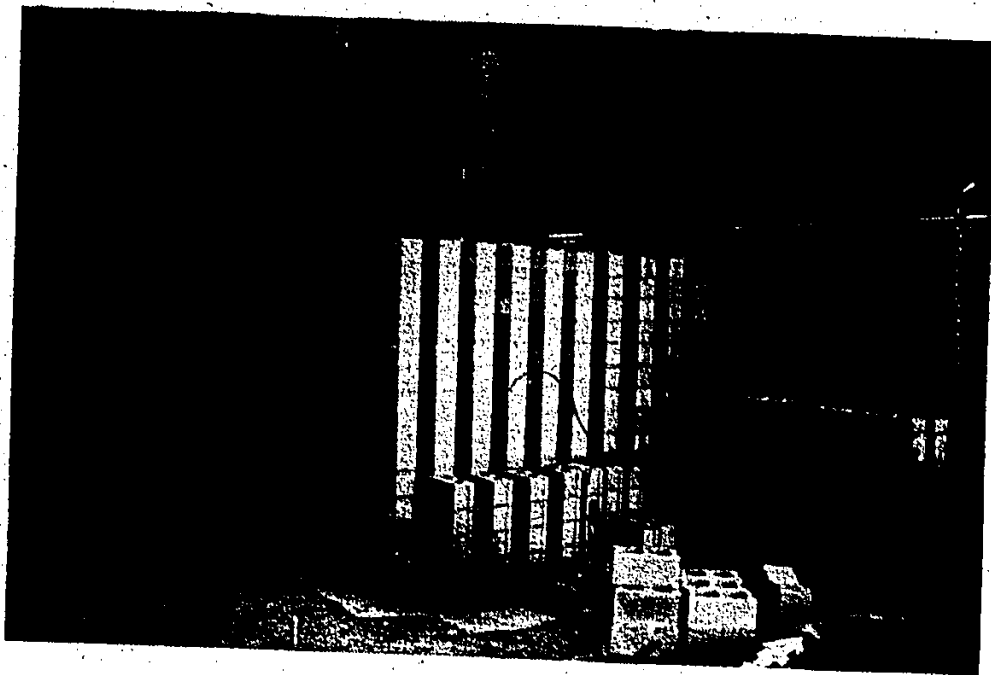
Figure 3.6 Fabrication of Test Specimens

CHAPTER 4

EXPERIMENTAL RESULTS

4.1 INTRODUCTION

Testing of the full scale walls and their auxiliary assemblage specimens was conducted according to the test procedures discussed in chapter 2. In this chapter, the experimental test results for the auxiliary assemblage specimens are reported for both the preliminary and main series. These included test results for flexural tensile strength normal and parallel to the bed joints. Also, the test results and observations from the 30 full scale wall tests are reported. The test conditions included different support conditions, different aspect ratios, presence or absence of precompression, and presence or absence of a precracking at the panel center.

4.2 AUXILIARY ASSEMBLAGE TESTS

4.2.1 Preliminary Series Tests

As stated before, the preliminary test series was conducted a year before the main series using different blocks and mortar sand. To be able to interpret or analyse the test results of the full scale walls, flexural tensile strengths for assemblages in the principal material directions normal and parallel to the bed joints were required. Even though the preliminary series included only two full scale walls, a sufficient number of auxiliary tests for strengths normal and parallel

87

to bed joints were performed to have an acceptable statistical sample of data. The results of these tests are described in the following sections.

4.2.1.1 Flexural Tensile Strength Normal to Bed Joints

The original specimens were six 5 block high stack bonded prisms. These prisms were tested at an age of 80 days by means of a bond wrench [62] and the results of 23 joints were obtained. The average flexural tensile strength normal to the bed joints was 0.31 MPa with a coefficient of variation of 28.0 %. These strength calculations were based on the net mortared section properties using the minimum, 32 mm, face shell thickness. The failure in most cases occurred at the bottom contact surface between the mortar joint and the flared end of the block beneath such joint.

The full scale walls of the preliminary series were tested at ages more than 250 days. It was thought that the flexural tensile strength normal to the bed joints might have become considerably larger over this time. For this reason, following testing of the first full scale wall, WIII-I, the undamaged parts were cut up to form more prisms. These new one block wide prisms for tension normal to the bed joints had a running bond pattern and were of various heights. The ten joints that were tested gave an average flexural tensile bond strength of 0.37 MPa with a coefficient of variation of 24.3%. The average age of these specimens at the time of testing was 260 days. Also, the same failure mode was applicable for these specimens.

4.2.1.2 Flexural Tensile Strength Parallel to the Bed Joints

A series of 20 wallette specimens were tested as horizontal beams under two line loads according to the procedure described in chapter 2 for wallette testing. The result was a mean tensile strength parallel to bed joints of 1.32 MPa with a coefficient of variation of 8.5%. The strengths of the individual specimens are listed in Table 4.1 together with the failure mode and the age of specimens at the time of testing. The failure of 85% of the tests occurred along a single plane through head joints and the face shells of alternating blocks which is failure mode I, according to Figure 2.2.b . Of these 17 tests, 13 failed through the head joint of the middle block and face shells of the two half blocks (Mode I). The other four specimens failed through the head joints of the outside half block courses and through the face shell of the center block (Mode I'). The failure mode for the remaining three specimens was Mode III which is a combination of Modes I and II where Mode II is a stepped or toothed pattern along head and bed joints.

Load-deflection data was recorded for all specimens using deflection readings at the center of the specimen. Typical curves are shown in Figure 4.1 for two specimens of this series. From these load-deflection curves, it appears that the first linear part ended at a sudden stiffness change and the curves continued in a nonlinear fashion with decreasing stiffness up to failure. It should be noted here that the load level at the first change in stiffness corresponded to stresses (based on homogeneous elastic analysis) in the order of the flexural tensile strength normal to the bed joints. Accordingly, the first and consequent changes in stiffness may be attributed to the loss of

Table 4.1   Flexural Tensile Strength Parallel to the Bed Joints from Preliminary Series Wallettes

Specimen	Age Days	Strength f_{tp}, MPa	Failure Mode[*]
H1	92	1.14	III
H2	92	1.27	III
H3	142	1.50	I
H4	142	1.31	I
H5	141	1.35	I
H6	141	1.25	I
H7	145	1.35	I
H8	146	1.20	III
H9	146	1.22	I
H10	147	1.46	I
H11	150	1.18	I
H12	151	1.48	I'
H13	152	1.23	I
H14	152	1.25	I
H15	153	1.25	I'
H16	156	1.24	I
H17	156	1.31	I
H18	157	1.42	I'
H19	157	1.46	I'
H20	156	1.45	I

[*] Mode I is the mode where failure occurred along the head joint of the middle block and the face shells of the two halfblocks.

Mode I' refers to the case of failure along the head joints of the outside half block courses and the face shells of the center block.

Mode II represents the case of toothed pattern along haed and bed joints.

Mode III is a combination of modes I and II.

Figure 4.1 Typical Load-Deflection Curves from Preliminary Series
Wallette Tests

stiffness at the head joint where the joint strength has been reached.

Again, following testing of the preliminary full scale wall WIII-1, a series of prisms for the flexural tensile strength parallel to bed joints were cut from the undamaged parts of the wall. These plus the undamaged parts of the previously tested wallettes were tested using the bond wrench test method. The 13 tests yielded a mean flexural tensile strength parallel to the bed joints of 1.47 MPa and a coefficient of variation of 12.0%. These results suggested that there was not as significant an increase in the strength parallel to the bed joints with the increase in age as was the case for strength normal to the bed joints. This was thought to be due to the fact that having the failure through the head joints and blocks in most cases, resulted in the strength being controlled mainly by the block strength and not the joint strength. The other conclusion from these test results was that the bond wrench test method can be successfully used to evaluate the strength parallel (or at any other orientation) to the bed joints. This has the advantage of a relatively simple test technique which also gives larger sample of data using the same amount of material as for the beam tests.

4.2.2 Main Series Tests

4.2.2.1 Flexural Tensile Strength Normal to the Bed Joints

The flexural tensile strength normal to bed joints was determined from bond wrench tests of the prisms built with the main series walls. The results of these tests are summarized in Table 4.2 and are shown also in Figure 4.2. The mean flexural tensile strengths

Table 4.2　Flexural Tensile Strength Normal to the Bed Joints from Main Series Prisms

Prism	Sand Type	Age Days	Mean Strength[a] MPa	Failure Mode[b]		
				I	II	III
P1	S2	156	0.25	2		1
P2		147	0.46	3		
P3		143	0.45	3	1	
P4		140	0.28	3		1
P5		136	0.39	1	2	1
P6		135	0.47	2		1
P7		134	0.46	4		
P8		133	0.45	4		
P9		136	0.62	4		
P10		153	0.63	4		
P11		150	0.52	4		
P12	S3	156	0.38	3	1	
P13		155	0.45	2	1	1
P14		154	0.41	3		
P15		153	0.27	3		
P16		152	0.45	4		
P17		151	0.48	3		1
P18	S4	147	0.65	1		3
P19		147	0.59	2	1	1
P20		147	0.58	3	1	
P21		146	0.53	2	2	
P22		146	0.52	2		1
P23		146	0.44	4		

a. Mean of 3 or 4 joint strengths for each prism
b. Number of joints failed along:
　(I)　the section of maximum contact area at the flared top of the block.
　(II)　the section of minimum contact area at the bottom of the block.
　(III) a combination of both.
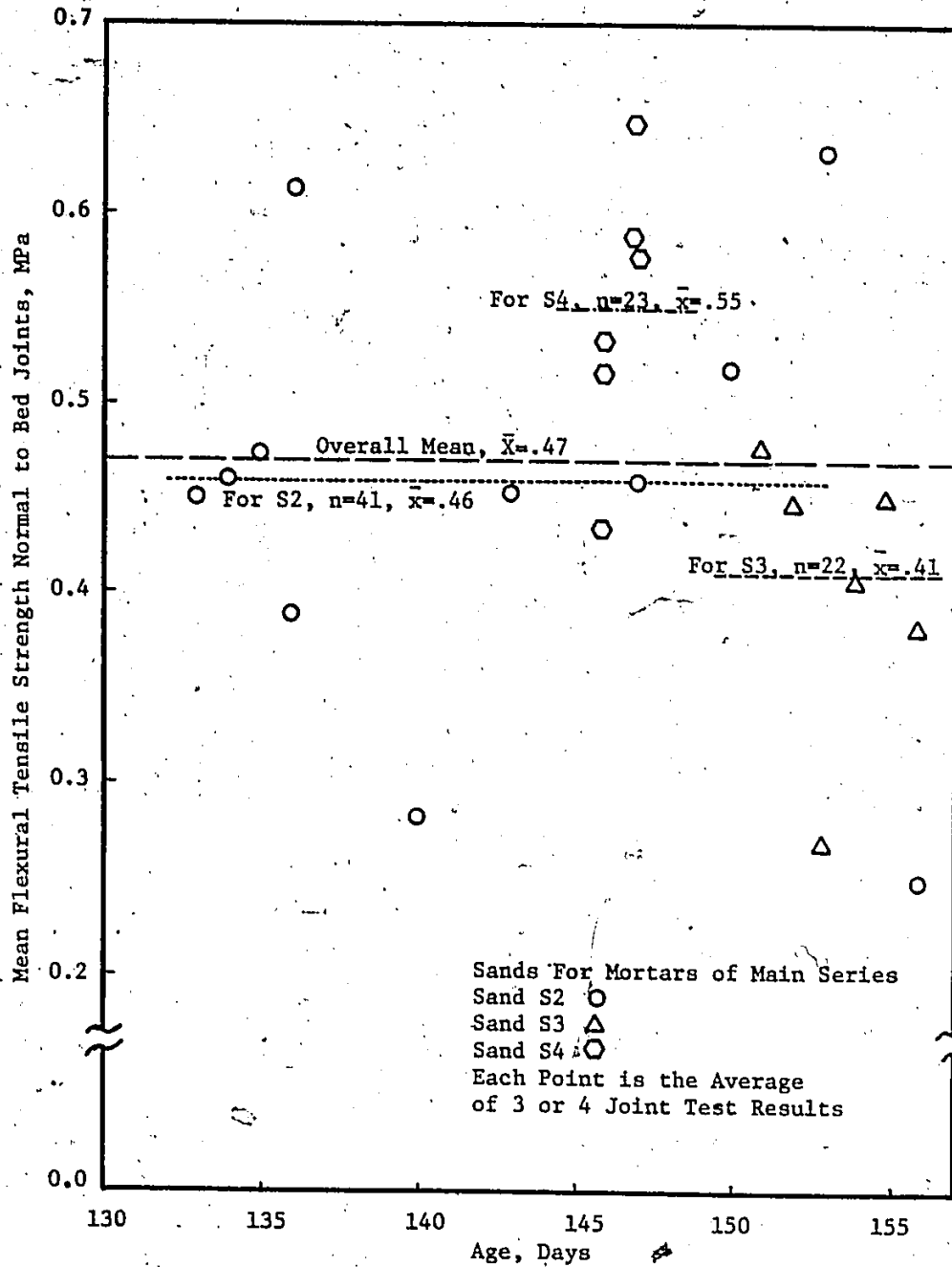
Figure 4.2   Flexural Tensile Strength Normal to Bed Joints Versus Age from Main Test Series

95_

of the prisms versus the age at the time of testing are shown in Figure 4.2 (each was the average strength of 3 or 4 joints). Also, prisms having mortars made using different sands are marked differently. The scatter of the results as shown in this figure, due to the inherent variability, indicated that there was no significant change of strength with the increase in age for the range of ages reported in these tests.

The mean flexural tensile strength and its coefficient of variation for all joints made using each type of sand were determined and indicated also on Figure 4.2. This yielded means and coefficients of variation of 0.46 MPa and 44.5% for sand S2; 0.41 MPa and 28.8% for sand S3; and 0.55 MPa and 24.4% for sand S4, respectively. The 0.47 MPa mean strength for all 86 joints irrespective of the type of sand used and the 37.0% coefficient of variation are also included in Figure 4.2. Changes of mortar sand from either Sand S2 or Sand S3 to Sand S4 were proven at the 95% confidence level to have a significant effect on the flexural tensile strength normal to bed joints. Unless otherwise stated, the overall mean strength of 0.47 MPa and 37.0% coefficient of variation were considered for flexural tensile strength normal to bed joints for the main series. This was thought to be appropriate since most of the full scale walls were fabricated using either Sand S2 or S3 and only two walls were fabricated using Sand S4.

The failure occurred in most cases (66 of 86 joints) at the section of maximum contact area between the mortar joint and the flared top of the block. This failure pattern was different from that observed previously by Drysdale and Hamid [39] at the minimum contact area.

However, recently, Gairns [44] reported a similar failure pattern for hollow blockwork. Based on experimental evidence, he [44] suggested that trapping of the mortar in block cores might led to failure at the section of maximum contact area. Although the cores of the concrete blocks used in this investigation were much wider than those reported by Gairns, it is believed that there was less but still significant effect of mortar trapping. This plus the probable dusty surfaces of the maximum block section and probable different surface texture were thought to be possible causes for the shift of the failure from the minimum contact area.

4.2.2.2 Flexural Tensile Strength Parallel to the Bed Joints

In the main series, there were 14 wallettes built to determine flexural tensile strength parallel to the bed joints. These were tested exactly as in the preliminary series. The individual test results given in Table 4.3 yielded a mean strength of 1.54 MPa with a coefficient of variation of 7.2%. Thirteen of the 14 tests failed along a single plane passing through the head joints and the face shells of blocks at alternate courses. The remaining specimen failed according to the so called combined mode.

A typical load versus center deflection curve is shown in Figure 4.3, for specimen H14, and has the same general description as that for the preliminary series curves given in Figure 4.1.

4.2.3 . The Orthogonal Strength Ratio

The orthogonal strength ratio is defined as the ratio between the strengths in the two principal material directions, namely parallel

Table 4.3   Flexural Tensile Strength Parallel to the Bed Joints
from Main Series Wallettes

Specimen	Age Days	Strength f_{tp}' MPa	Failure Mode[*][**]
H1	190	1.38	I
H2	199	1.46	I
H3	197	1.55	I
H4	199	1.64	I
H5	191	1.80	I
H6	191	1.58	I'
H7	188	1.53	I'
H8	188	1.60	I
H9	188	1.46	III
H10	184	1.56	I'
H11	186	1.49	I
H12	185	1.64	I
H13	181	1.46	I
H14	180	1.42	I

[*] Mode I is the mode where failure occurred along the head joint of the middle block and the face shells of the two halfblocks.

Mode I' refers to the case of failure along the head joints of the outside half block courses and the face shells of the center block.

Mode II represents the case of toothed pattern along haed and bed joints.

Mode III is a combination of modes I and II.
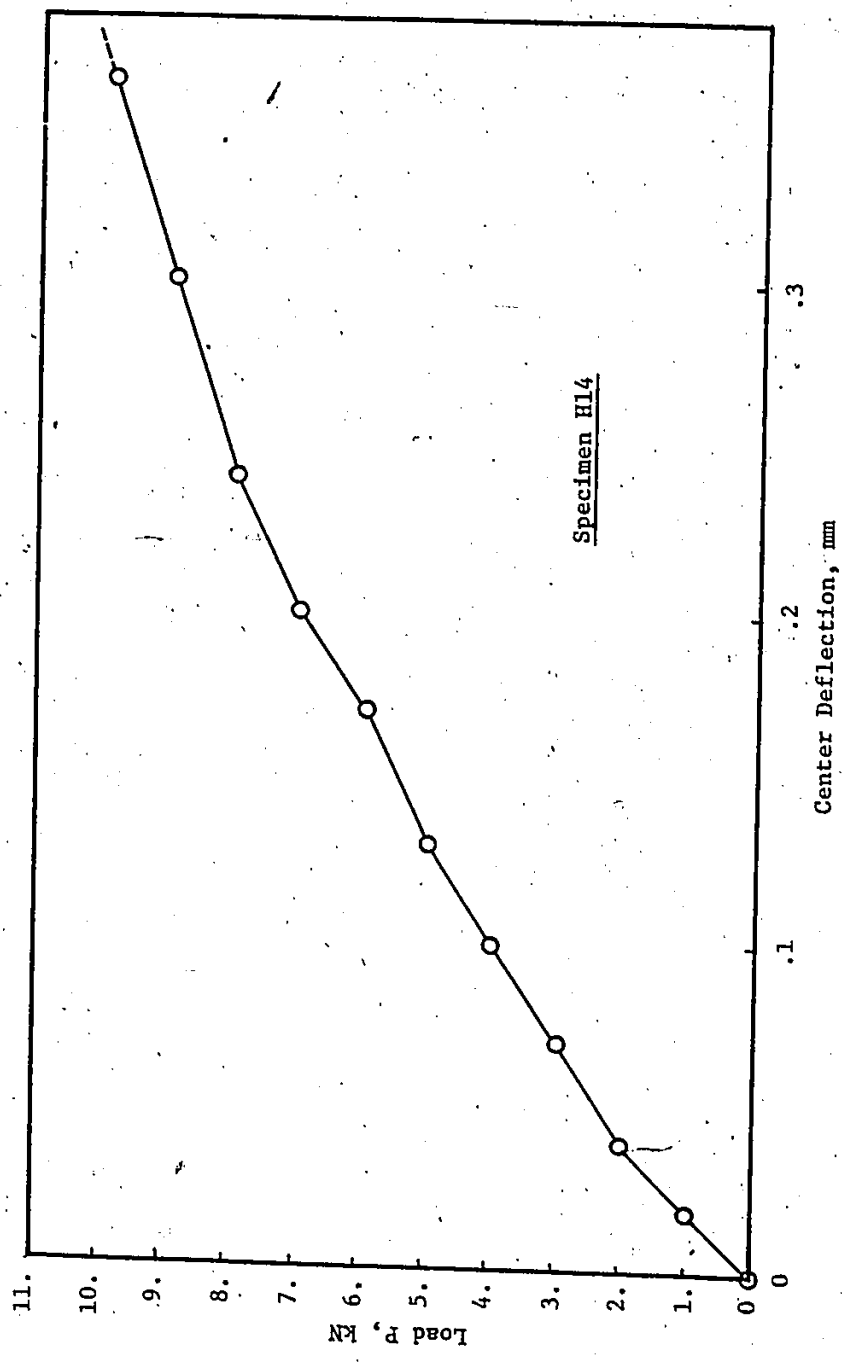
Figure 4.3   Typical Load-Deflection Curve from Main Series
Wallette Tests (Wallette H14)

and normal to the bed joint orientation. Considering the strengths parallel and normal to bed joints for the preliminary series as 1.32 MPa and 0.37 MPa, respectively, the orthogonal strength ratio for the preliminary tests was 3.5. However, for the main series having strengths parallel and normal to bed joints of 1.54 MPa and 0.47 MPa, respectively, the orthogonal strength ratio was found to be 3.3.

4.3   TEST RESULTS OF THE FULL SCALE WALLS

The full scale wall tests were performed according to the procedure described in Chapter 2. It should be noted that the supporting frame was found to be very rigid as it was designed and the maximum relative deflection of that frame recorded from all tests and all along the frame was less than 0.6 mm. In the next sections, the test results of all the full scale walls from both the preliminary and the main series are reported as one program. The two preliminary walls designated as WI-1 and WIII-1 were included in the WI and WIII series, respectively.

The full scale wall test results were grouped mainly to two categories. The first was walls in one-way action including Series WV and WVV which had walls supported only on top and bottom as well as Series WH which had walls supported only on the two vertical sides. The other category included two-way action which therefore include all the other test walls.

All the test results are summarized in Table 4.4 together with the different dimensions, mortar strengths, and test ages. Except for examples used in this chapter, the photographs of the other test walls

Table 4.4   Wall Test Results

Series		Dimensions		Aspect Ratio	Wall Test Results			
		Wall $L_o \times H_o$ m	Frame $L \times H$ m	L/H	Age Days	Mortar Cube Strength* MPa	Pressure at:	
							First Crack kPa	Failure kPa
	Wall							
WV	1	5.2 × 2.8	2.8		126	18.5		2.84
	2				132	20.0		3.38
	3				138	22.9		3.09
	Mean							3.10
WVV¹	1	2.6 × 2.8	2.8					2.94/3.19
	2							2.50
	3							1.32
	Mean							2.25
WH	1	5.2 × 2.8	5.0		115	24.3		2.04
	2				126	21.6		2.10
	3				126	21.6		1.96
	Mean							2.03
WF	1	5.2 × 2.8	5.0 × 2.85	1.75	113	21.9		3.97
	2				116	25.2		3.79
	3				116	26.7		3.95
	Mean							3.90
WI	1	3.6 × 2.8	3.4 × 2.8	1.21	358	20.5	5.50	11.0
	2				53	22.4	3.14	10.99
	3				64	22.5	3.14	8.63
	Mean						3.93	10.21
WII	1	5.2 × 2.8	5.0 × 2.8	1.79	88	26.5	5.10	6.67
	2				85	24.4	4.32	6.73
	3				90	24.4	3.53	7.06
	Mean						4.32	6.82
WIII	1	6.0 × 2.8	5.8 × 2.8	2.07	253	16.9	2.35	5.30
	2				86	21.8	2.16	4.32
	3				92	28.7	2.55	4.70
	Mean						2.35	4.77

Table 4.4   Continued

WC	1	5.2 × 2.8	5.0 × 2.8	1.79	127	18.5		6.62
	2				133	20.0		7.21
	3				139	22.9		7.36
	Mean							7.06
WP**	1	5.2 × 2.8	5.0 × 2.8	1.79	96	22.7	5.59	9.42
	2				109	25.3	5.59	8.75
	3				108ǰ	22.3	4.41	8.24
	Mean						5.20	8.80

* The number of mortar cubes per wall ranged between 25 and 33 except for Series WI where only 14 to 19 cubes were tested.
! The capacities of the two halves were recorded (if different).
** A concentric compression load providing a precompression of 0.20 MPa was applied to the tops of these walls.

after failure are given in Appendix B.

4.3.1 Walls In One-Way Action

4.3.1.1 Walls Supported Only On Top and Bottom (Series WV and WVV)

The failure pressures for these vertically spanning walls are listed in Table 4.4 for both the original Series WV and the supplementary Series WVV. The reason for including the supplementary series was, as mentioned earlier, to have a larger statistical sample and therefore an increased level of confidence for the relatively high variability associated with strength normal to the bed joints.

As can be seen in Table 4.4, the failure pressure for both halves of the WVV-3 wall was very low compared to the other WVV or WV walls. In order to understand what happened at this failed joint, first, the tests of mortar cubes taken from the two batches used in this bed joint were checked and found to have mean compressive strengths of 19.32 MPa and 21.59 MPa. These were not significantly less than the mean strength of 21.56 MPa for all batches used in this wall or the mean strength of 23.37 MPa for the overall program. In addition, bond wrench tests were performed for 8 individual joints from the bed joint directly above that in question and 4 joints from the bed joint directly below it. The resulting mean flexural tensile strengths normal to the bed joints were 0.42 MPa and 0.47 MPa respectively for the bed joint above and below the failed joint. Finally, since these checks did not point to any specific defect in wall WVV-3, it was concluded that these low strengths were the natural result of the known high variability of results for tensile strength normal to the bed joints.

Plots of the pressure versus panel center deflection are shown in Figure 4.4 for the three walls of Series WV. These clearly indicated the relatively linear relationship up to the pressure level at which failure occurred. Moreover, the effective flexural rigidities as shown in this figure were quite different. This might lead to large variations in the first cracking loads for walls supported on all four sides.

The cracking or failure patterns of all the walls in both series were typically a horizontal crack along a bed joint near the mid-height of the wall panels. This crack extended longitudinally for the whole wall length. Sketches of the failure patterns of the different walls are shown in Figure 4.5. In this figure, the deviation of the horizontal crack from the most highly stressed bed joint just above the panel mid-height is clearly indicated. This is, of course, due to the inherent variability of the flexural tensile bond strength normal to the bed joints and the possibility of having weaker joints outside the central bed joint.

The flexural tensile strength normal to the bed joints can be estimated from the full scale walls of Series WV and Series WVV. This panel strength was determined considering the following points :

1. These walls were fabricated using different types of sand. The mean flexural tensile strength of joints made from these sands were in some cases significantly different at the 95% confidence level. Therefore, to eliminate the effect of the differences in sand, the panel strength of each wall was normalized with respect to the overall mean joint strength of 0.47 MPa.
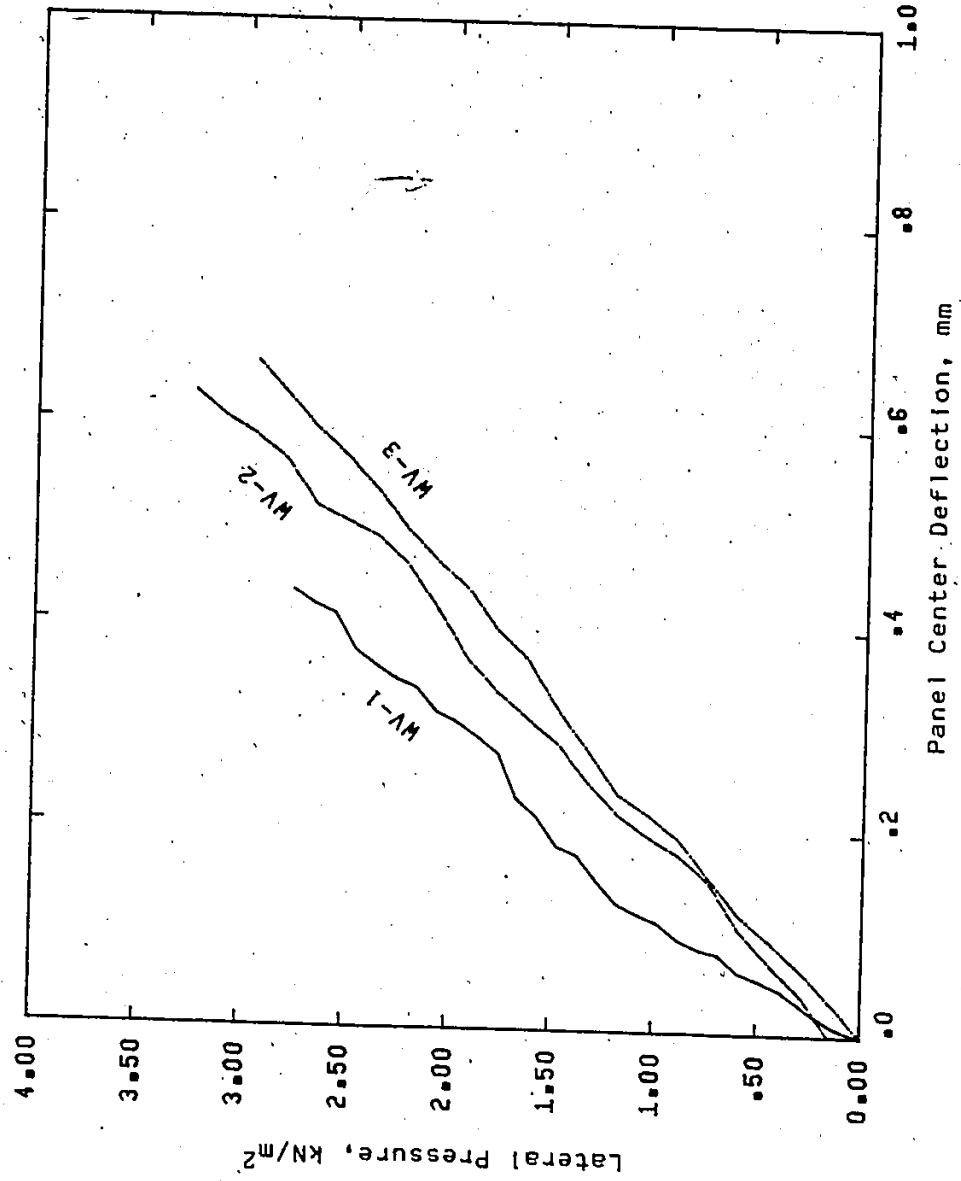
Figure 4.4   Deflection Data for Series WV Walls
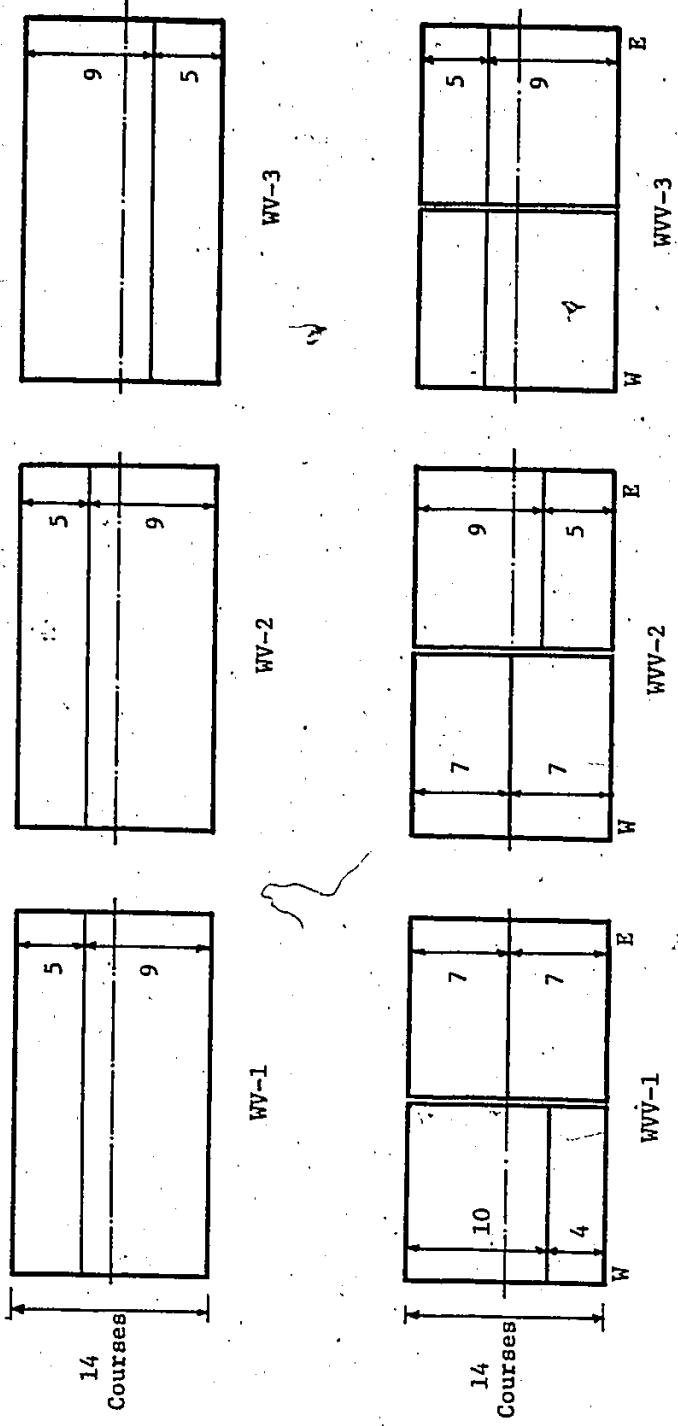
Figure 4. 5   Sketchs of Cracking Patterns for Walls Supported
at the Top and Bottom

2. The observed failure patterns indicated that the failed bed joint might not be the central one. However, the central bed joint may be considered for panel strength determination as it represents the average case where the mean panel capacity was obtained from a large number of wall tests. Moreover, the consideration of the failed bed joints may lead to an underestimation of the panel strength as it considers the weakest bed joint in each panel. Therefore, the central bed joint was considered here for panel strength determination.

3. Both halves of each wall of Series WVV were originally one wall of Series WH and only the WVV-1 halves had different failure loads. Since, it was thought that the strengths of each pair of half walls were dependent, only the lower capacity was used for the panel strength in the case where the halves failed at different loads. Therefore, the capacity of each pair of halves was considered to be for one wall.

Taking these points into consideration, an estimation of the panel flexural tensile strength normal to the bed joints was determined and yielded a mean strength of 0.570 MPa with a 27.0% coefficient of variation. However, including the results of all halves as independent results only changed the mean strength to 0.572 MPa. Also, the direct average of different wall strengths without normalization yielded a mean wall strength of 0.56 MPa with a 29.5% coefficient of variation.

The comparison of this panel strength and the joint strength reported earlier (0.47 MPa mean strength with 37.0% coefficient of variation) indicated that the panel strength was significantly higher and had a lower coefficient of variation than the joint strength.

According to Baker's theory [22] for panels in vertical flexure, both the mean and the coefficient of variation of the panel strength were expected to be less than for the individual joints. This increase in panel strength may be attributed to the possible increase in the joint strength in wall specimens due to two reasons. First, the possible improvement or increase in the mortar block bond strength in wall specimens due to the self weight pressure on the bed joints. An additional argument is that, for testing of bond along the length of a single block, the strength would be much more affected by local flaws. For several blocks acting together, they will force planar action which will allow the strength of the stronger areas to be fully developed.

Moreover, having a sample size of only 6 walls (3 walls of Series WV and 3 halves of Series WVV) resulted in an estimated mean panel strength which might have a tolerable error up to 16% at the 90% confidence level. Therefore, a more precise estimate of panel strength might be possible from a larger sample size and this might be also a source of the significant difference observed between the joint and panel strengths.

It should be noted that the actual failure mechanism in terms of load sharing along a bed joint cannot be easily identified. However, of the four different mechanisms suggested by Baker [22] for panels in vertical flexure, both brittle and successive cracking failure mechanisms might not be expected to be applicable due to the considerably higher panel strength than joint strength. Therefore, the probable failure mechanism for blockwork in this case might be either the partially or the fully plastic mechanism.

4.3.1.2 Walls Supported Only Along the Sides (Series WH)

The failure pressures for these walls spanning horizontally between the two sides are also given in Table 4.4. The typical vertical crack located near the middle of the horizontal span at failure is shown in the photograph of Figure 4.6. As can be seen in this figure, the crack alternately passed through head joints and blocks in a nearly straight line throughout the whole wall height. It should be noted here that the same failure pattern was observed in the wallette tests reported earlier.

The deflection data for Series WH walls given in Figure 4.7 indicated the nearly linear behaviour in the very early stages of loading. It also indicated the nonlinear behaviour thereafter with continuously decreasing stiffness up to the development of the center crack and, consequently, the failure mechanism. The end of the initial linear relation was observed at a stress level (based on elastic homogeneous analysis) corresponding to the head joint strength. This was also observed in the wallette tests as reported earlier.

The strength of concrete blockwork in flexure parallel to the bed joints can also be found from the full scale wall test results of Series WH walls. These test results yielded a mean wall strength of 1.49 MPa with a coefficient of variation of 3.5%. While, as mentioned earlier, the wallette tests yielded a mean strength of 1.54 with a 7.2% coefficient of variation. From the comparison of the wall and wallette strengths, it can be seen that both had essentially the same mean value with smaller coefficient of variation in the case of the wall strength.

A wall may be considered to consist of a set of adjacent
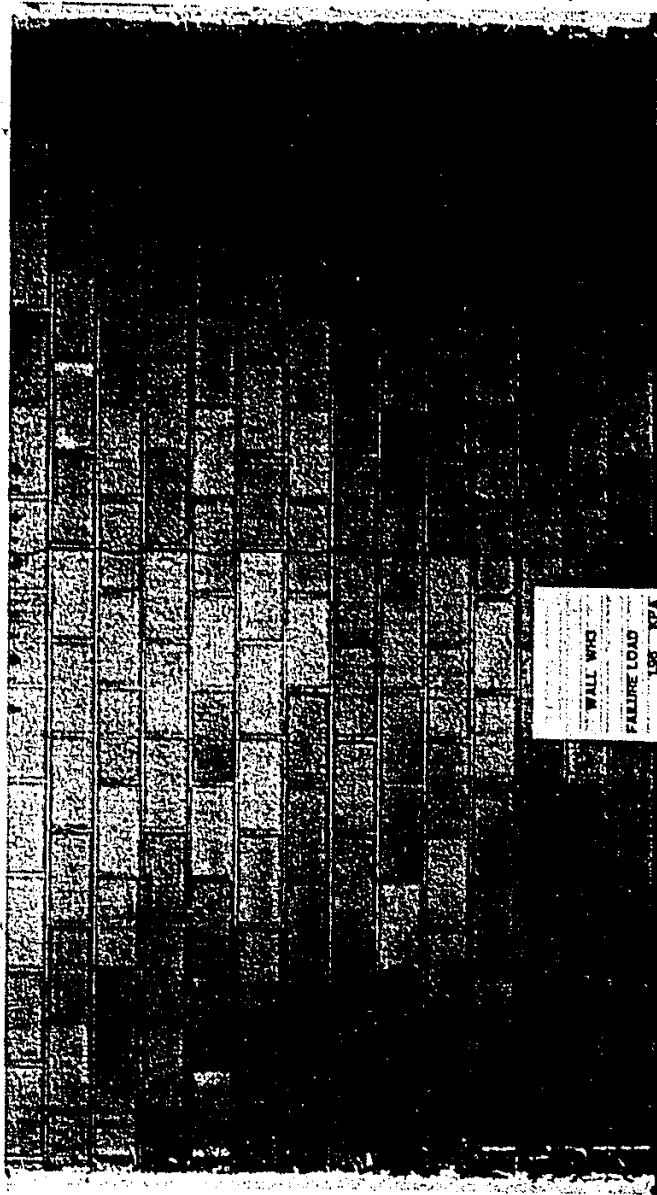
Figure 4.6 Crack Pattern for Wall WH-3
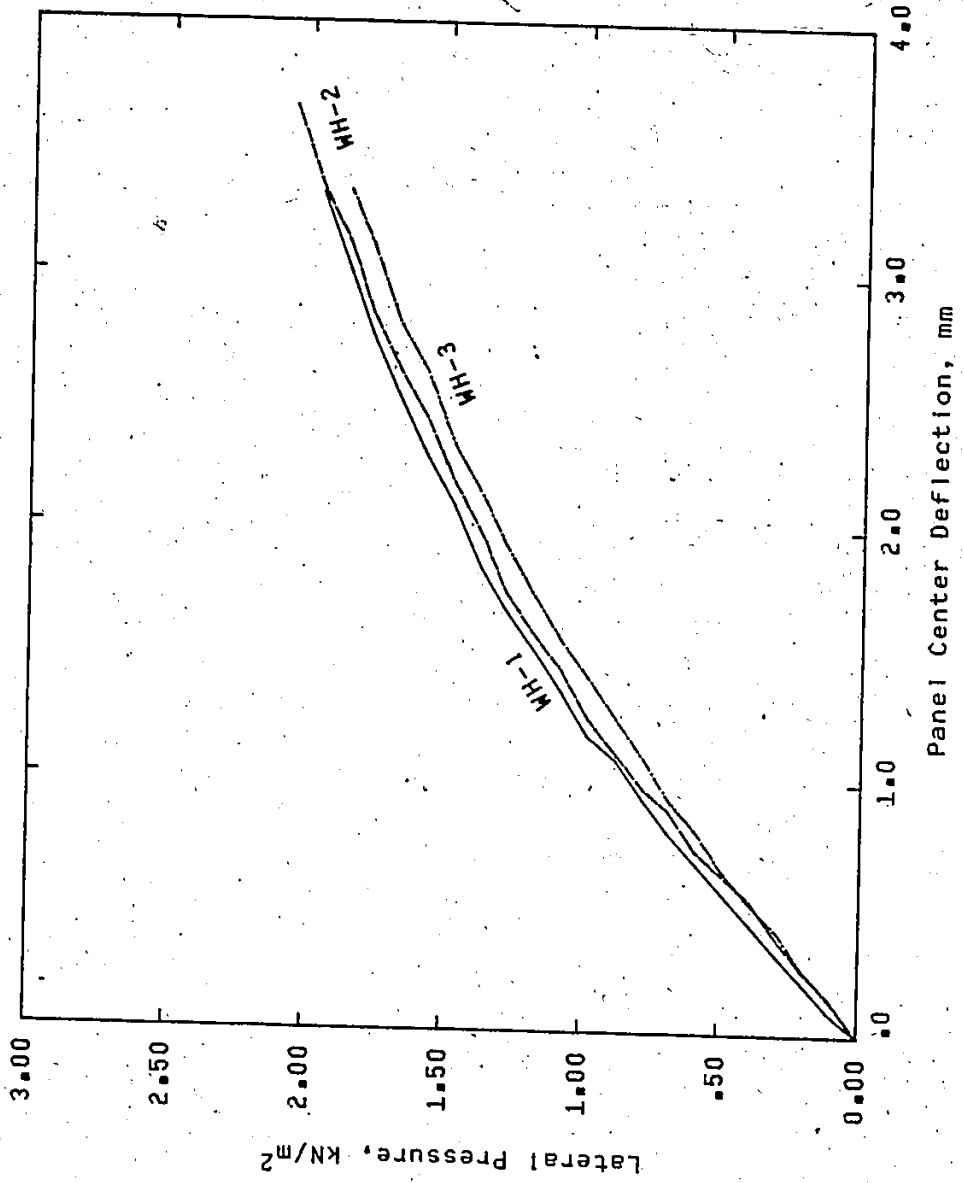
Figure 4.7   Deflection Data For Series WH Walls.

wallettes and the wall strength to be the mean of the wallette strengths. Then, the distribution of wall strengths has the same distribution as the means of wallette strengths. This indicates that the mean wall strength is equal to the mean wallette strength. However, the coefficient of variation of wall strength is equal to that of the wallettes divided by the square root of the possible number of wallettes in the wall height. Applying this hypothesis to the available data yielded a mean wall strength of 1.54 MPa with a 2.7% coefficient of variation. These are not significantly different from the values determined from the full scale wall test results.

It was assumed in this hypothesis that failure occurred only when all the wallettes in the wall height reached their respective strengths. This was known as the fully plastic mechanism [22]. However, it is believed that, due to the relatively low variability of the wallette strengths, the wall strength based on the partially plastic mechanism may not be significantly different from that for the case of the fully plastic mechanism. Accordingly, it may be concluded again that either the partially or the fully plastic mechanisms could be the failure mechanism for the walls of Series WH.

4.3.1.3 Orthogonal Strength and Rigidity Ratios

The mean flexural tensile strengths parallel and normal to the bed joint orientation, as found from the full scale walls in one-way action, were 1.49 MPa and 0.567 MPa, respectively. Accordingly, the orthogonal strength ratio from full scale wall tests was found to be 2.6. This was significantly different from the 3.3 ratio from the

control specimens and is mainly due to the differences in flexural bond normal to the bed joints.

The effective flexural rigidity of the concrete masonry walls can be estimated from the load-deflection curves given earlier for walls in one way bending. The flexural rigidity in the direction parallel to bed joints can be estimated from the initial linear part of the load-deflection curves for walls of Series WH. This yielded a mean flexural rigidity in horizontal bending of 6.56×10^{12} N.mm^2 with a coefficient of variation of 7.2%. Similarly, the flexural rigidity for the direction normal to the bed joints can be estimated from the test results of Series WV walls. This yielded a mean value of 4.19×10^{12} N.mm^2 with a coefficient of variation of 19.4%.

The orthogonal rigidity ratio or the degree of orthotropy is defined as the ratio of the flexural rigidity parallel to the bed joints to the flexural rigidity normal to the bed joints. The flexural rigidity values mentioned above yielded a rigidity ratio of 1.57. The relatively higher flexibility observed in the direction normal to the bed joints may be attributed to the presence of the continuous mortar bed joints. These mortar joints are considerably more flexible than the concrete blocks. However, the parallel direction to the bed joints has half the volume of such flexible joints. In addition, these joints are not continuous but rather comprise only half of the width.

4.3.2 Walls In Two-Way Action

There were 15 full scale walls tested in two-way action plus three more walls which were tested in vertical flexure (Series WV walls)

and then retested in two-way bending as Series WC walls. Thus, a total of 18 full scale wall tests in two-way bending were performed in this program. All these walls were supported along all four sides except the three walls forming Series WF which were supported only on three sides and had a free top edge.

The walls supported on all four sides were in five different series. These were three series of walls with different aspect ratios, a series with a precompression applied along the top edge and finally a series of walls with the preformed cracks near the mid-height of the panel.

The following are the detailed test results and observations for each of these wall series.

4.3.2.1 Walls Supported On Three Sides With Free Top (Series WF)

This series had the 5.20 m long by 2.80 m high (13 blocks long by 14 blocks high) dimensions of the basic wall with a 5.00 m horizontal span between the two side supports and it was supported along the bottom. The failure loads given in Table 4.4 for these walls were notably consistent.

The crack pattern for Wall WF-3 is shown in the photograph of Figure 4.8. This pattern is consistent with the yield line pattern for such walls. It was composed of two diagonal cracks originating from the bottom corners and meeting at a central vertical crack extending from the intersection of the diagonal cracks to the free top edge. The cracking patterns of the other two walls as shown in Appendix B were slightly different. In these walls, the diagonal cracks did not reach

WALL WF3
FAILURE LOAD
3.95 KPA
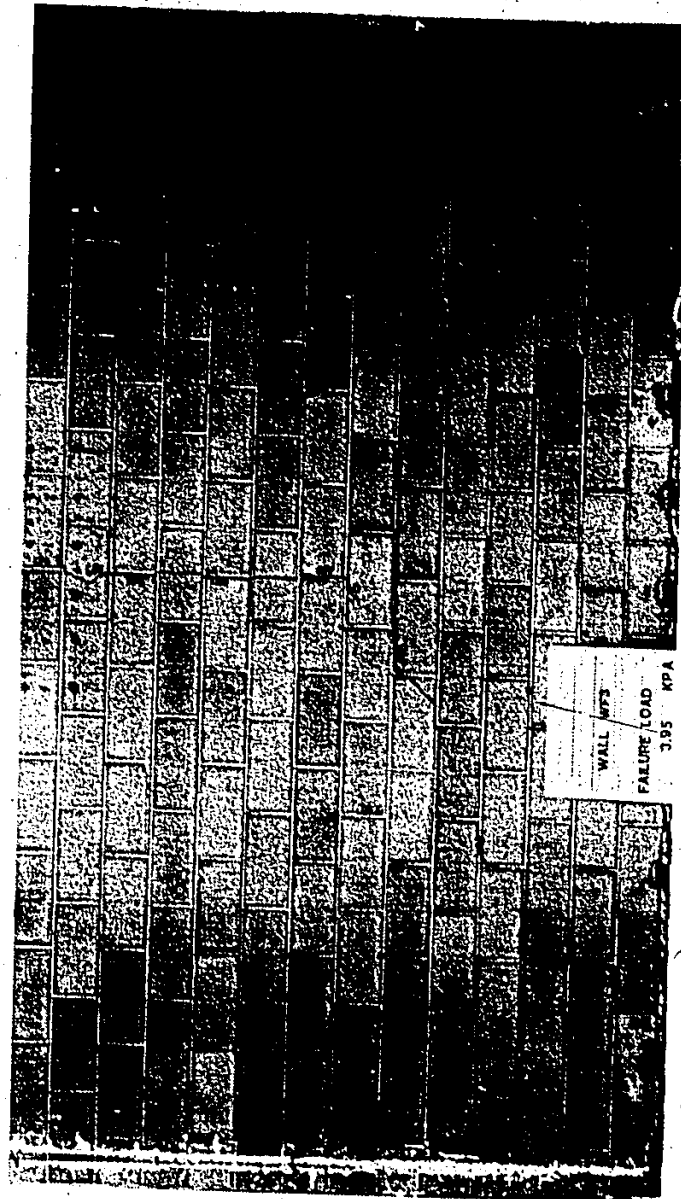
Figure 4.8   Crack Pattern for Wall WF-3

the center but a horizontal crack developed at a certain bed joint and the diagonal cracks above the horizontal one straighten to be vertical or nearly vertical cracks up to the free top edge. This change of pattern is attributed to the presence of a weak bed joint or joints where the horizontal crack developed. It should be noted that these cracks were developed right at failure where the equilibrium was not necessarily satisfied.

The load versus lateral deflection plotted in Figure 4.9 for the three walls of this series were relatively linear up to about half the failure load. Thereafter, a slight but continuous decrease in the stiffness was observed for the three walls. This may be attributed to the nonlinear behaviour of the head joints where their capacity had been reached. However, the decrease in the stiffness was less than that observed in the Series WH walls where the flexural rigidity of the direction parallel to the bed joints was the only source of stiffness. It should be noted also that the sharp change in the slope for WF-2 and WF-3 walls near failure as shown in Figure 4.9 is probably due to the development of the initial cracking.

4.3.2.2 Walls Supported On All Four Sides With the Smallest Aspect Ratio (Series WI)

The observed first cracking and failure capacities of this series of walls are listed in Table 4.4 together with all the experimental data for these walls.

The predicted yield line cracking pattern at failure for this series was the formation of a 500 mm long vertical crack over the mid-
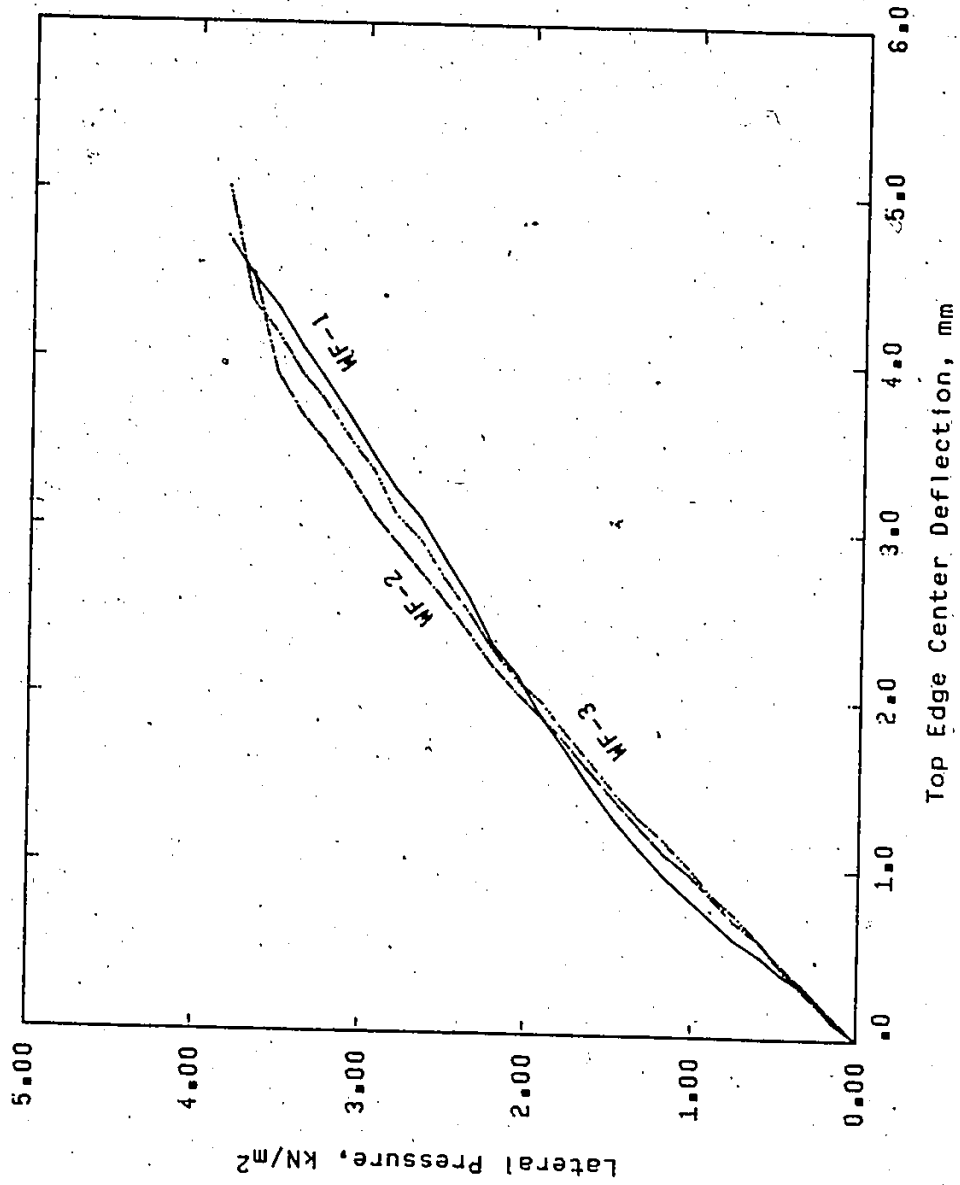
Figure 4.9   Deflection Data for Series WF Walls

height region of the panel at the middle of the horizontal span. In addition, diagonal cracks extending from the top and bottom of this vertical crack to the respective corners of the panel were predicted. In fact, as shown in Figure 4.10 for wall WI-2, what occurred was a vertical crack of 3 blocks height which is reasonably close to the predicted 500 mm. However, what had not been expected was the initial formation of a horizontal crack running nearly the full length of the panel along a bed joint near mid-height of the panel. The cracking pattern of the other two walls reflected almost the same pattern. The scatter of cracks other than these main ones forming the failure mechanism in this series was not surprising due to the statistical scatter of strengths. An additional factor was that the expected cracking pattern for these walls included both vertical and diagonal cracks which required high stresses to occur compared to the low strength of the bed joints. The existence of these high stresses increased the probability of having horizontal cracks and accordingly affected the expected diagonal cracks.

The loads versus panel center deflections for the three walls of this series are shown in Figure 4.11. The sharp changes in slope shown in this figure for each wall corresponded to the observed formation of the initial horizontal cracks. Also, the first part of each curve, before the sharp slope change, was reasonably linear.
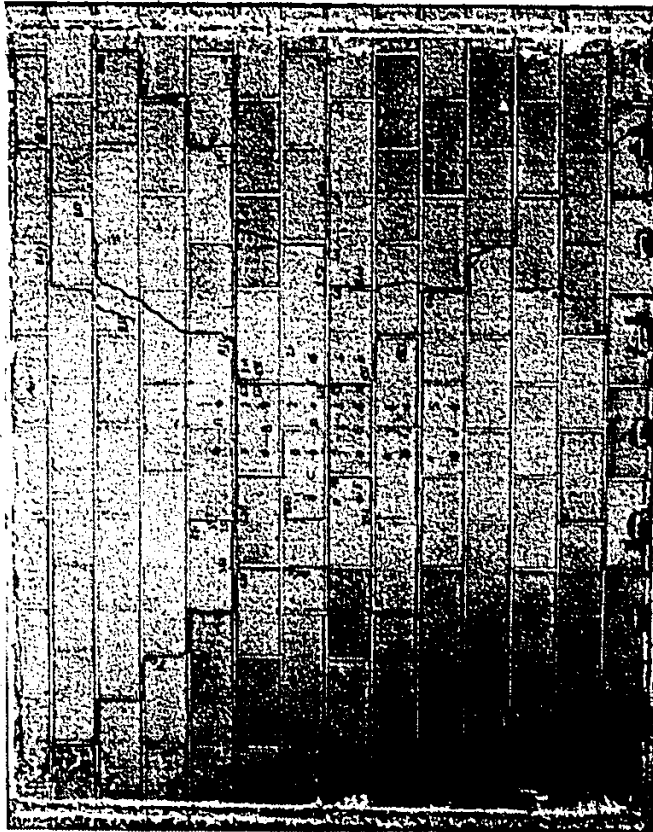
Figure 4.10 Crack Pattern for Wall WI-2
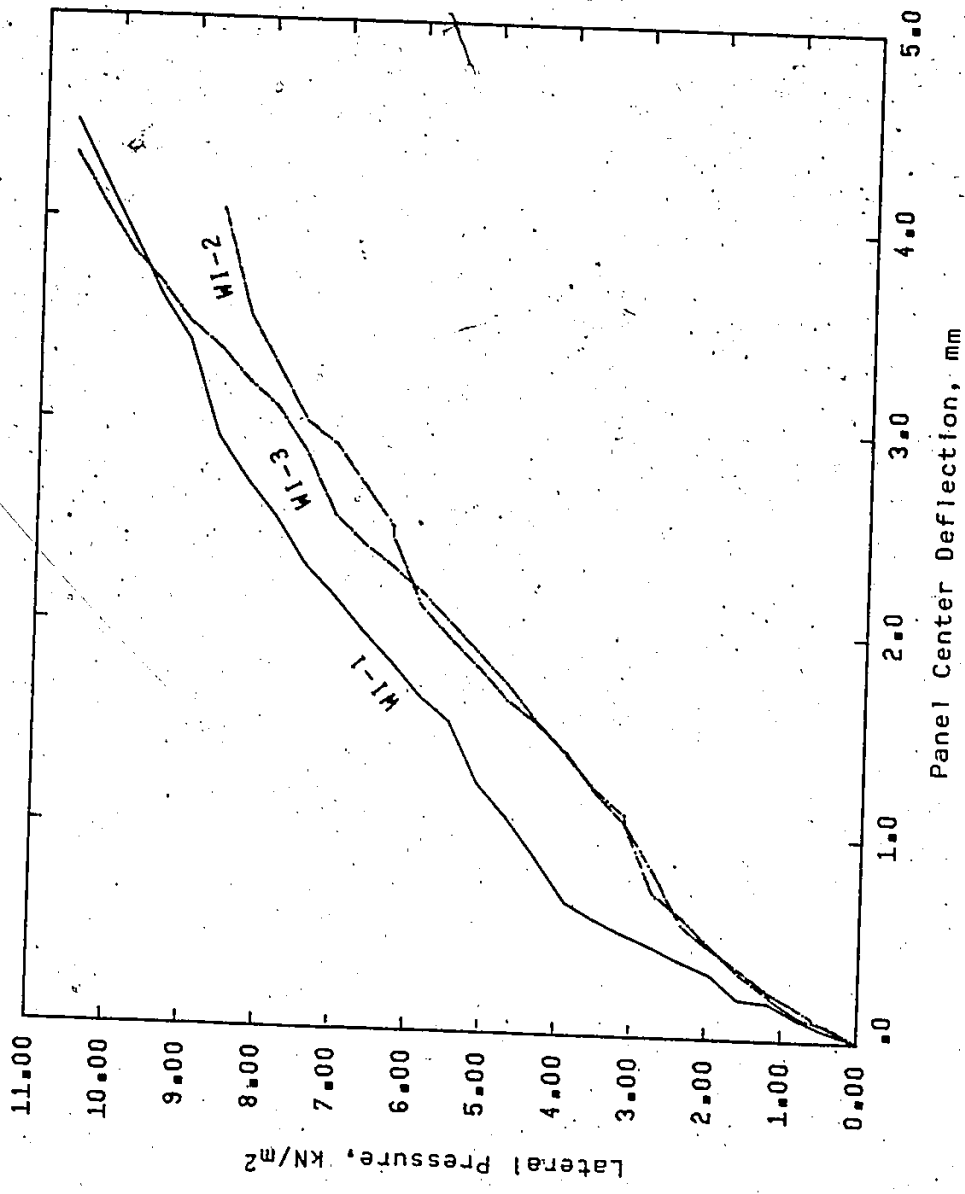
Figure 4.11   Deflection Data for Series WI Walls

4.3.2.3 Walls Supported On All Four Sides With Intermediate

Aspect Ratio (Series WII)

For the combination of flexural tensile strengths, the yield line analysis indicated that for this aspect ratio a X-shaped cracking pattern composed of two diagonal cracks joining opposite corners of the wall panel would be expected. However, again the initial crack was a horizontal crack running nearly the full length of the panel along a bed joint near mid-height. The collapse mechanism was formed when additional cracks extended diagonally from this horizontal crack to the corners of the panel. An example of this crack pattern is shown in Figure 4.12 for wall WII-2. Regarding the appearance of cracks other than those forming the failure mechanism, the same statement made for the WI walls is applicable.

The load level at which the initial horizontal crack was observed and the failure load are also tabulated in Table 4.4 for the three walls of this series.

The deflection results for the three walls are given in Figure 4.13. The plateau shown in each curve corresponded to the development of the initial horizontal crack. The three tests indicated a linear relationship up to first cracking and a nonlinear type of relationship after the plateau and up to failure.

4.3.2.4 Walls Supported On All Four Sides With the Largest

Aspect Ratio (Series WIII)

This series was expected and did produce cracking patterns similar to that for Series WII but with more distance between the two
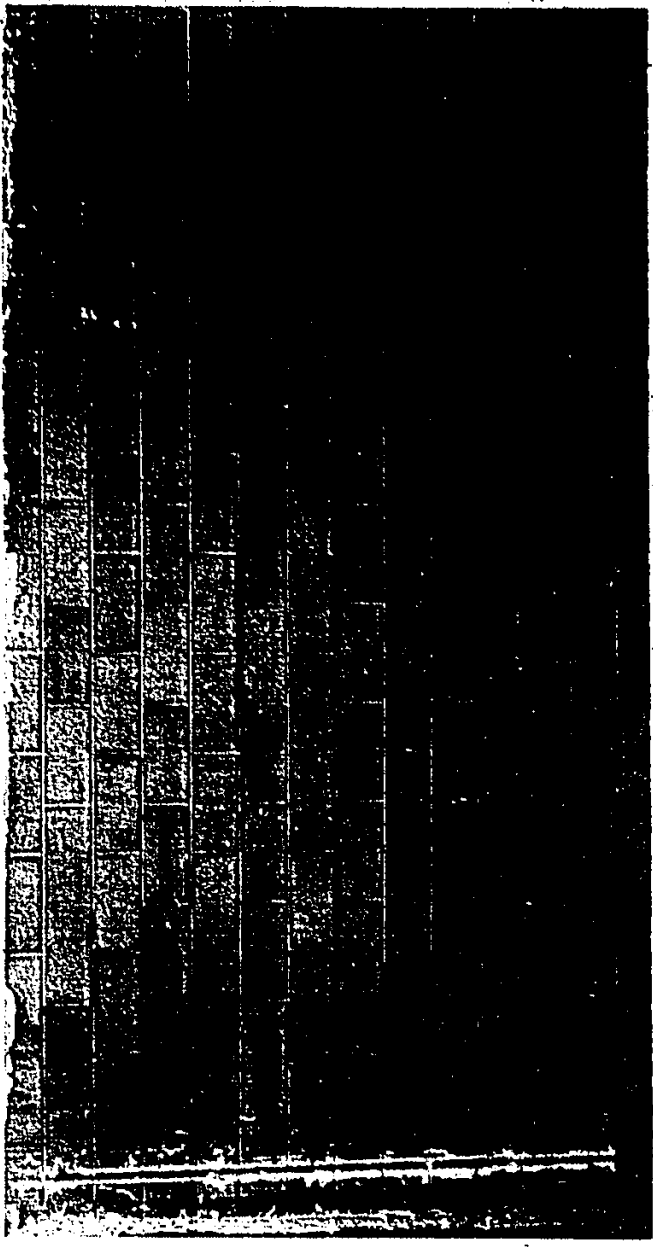
Figure 4.12   Crack Pattern for Wall W11-2
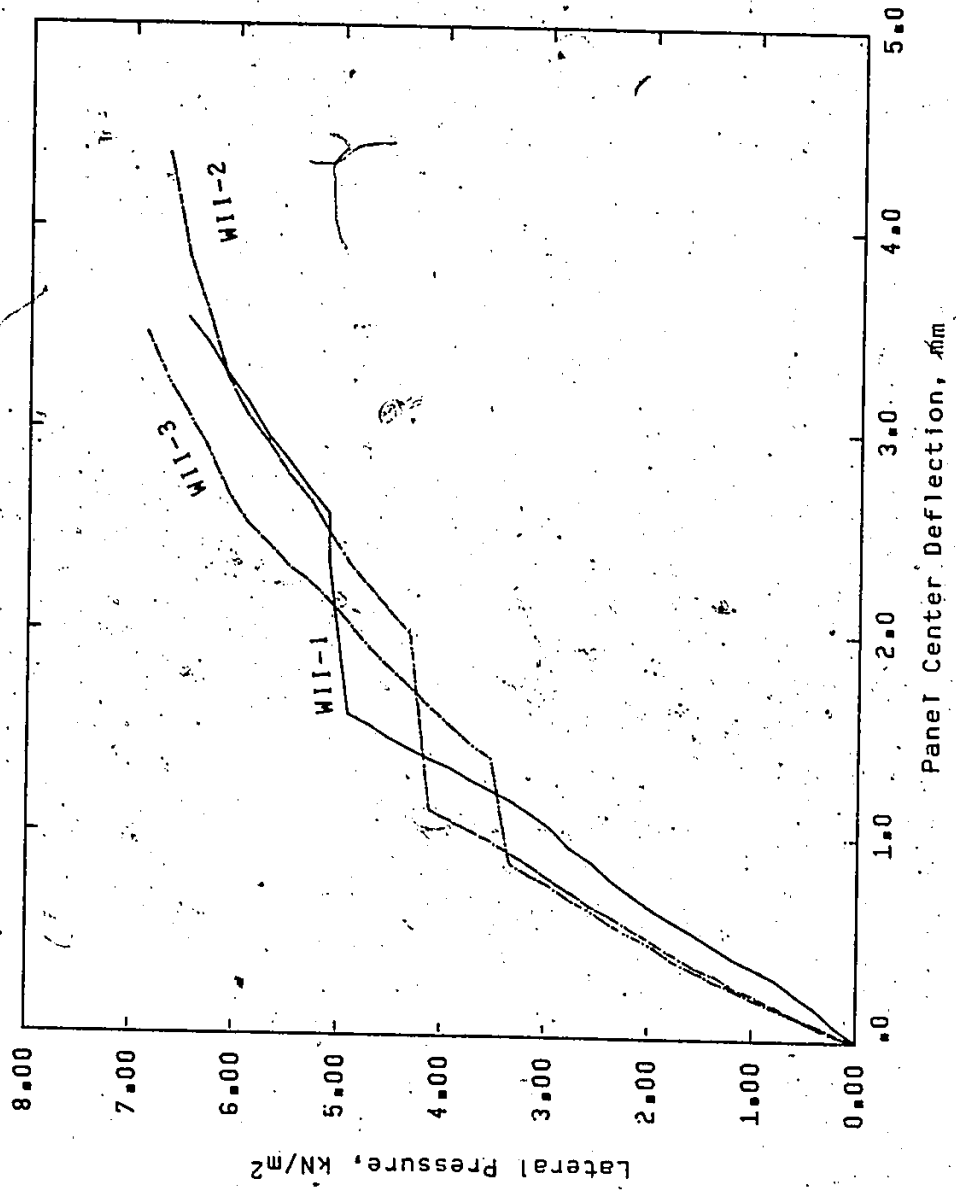
Figure 4.13 Deflection Data for Series WII Walls

sets of diagonal cracks. This can be clearly seen in Figure 4.14 for Wall WIII-3. The first cracking and failure loads for these walls are also given in Table 4.4.

It should be noted here that the cracking pattern for the first preliminary wall WIII-1, as shown in Figure 4.15 did not have the diagonal cracks originating from the bottom corners but instead a vertical and horizontal cracks formed around each corner. This was because of the inadequately restrained bottom corners against corner lifting plus the insufficiently restrained bottom edge of the wall against lateral displacement. This allowed the wall to slip off the individual steel plates at the base and therefore allowed the vertical crack to develop. It should be noted that Wall WIII-1 was the first preliminary wall tested and these inadequacies in the testing frame were corrected after this wall test.

The load-deflection results for the WIII walls are given in Figure 4.16. They were also similar to those for the WII walls as they were composed of a linear part up to the formation of the first horizontal crack which corresponds to a plateau in the load-deflection curve. Then, a nonlinear part up to failure completed the pattern.

4.3.2.5 Walls Supported On All Four Sides With a Precrack Near Panel Mid-Height (Series WC)

This series was a retest of the Series WV walls after their failure by a horizontal crack along wall length near the mid-height of the panels. This series was decided on to check a design method which considers the wall panel after first cracking as two separate walls each
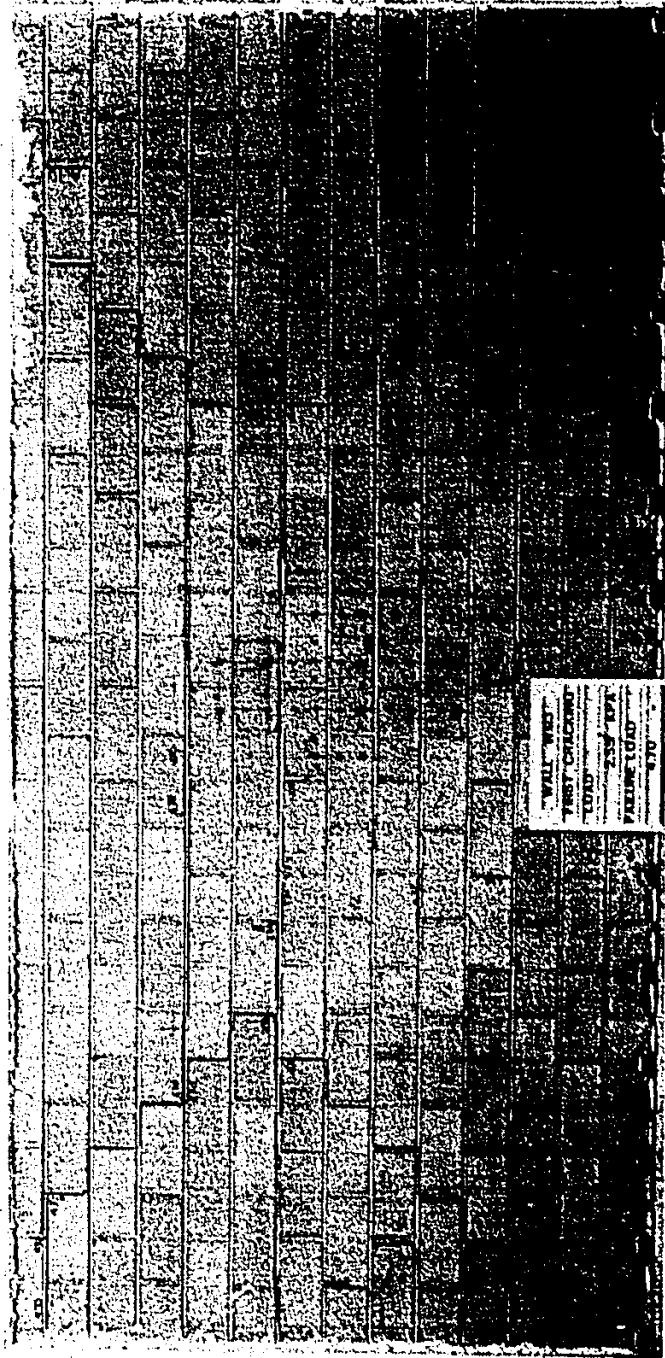
Figure 4.14 Crack Pattern for Wall WIII-3

Figure 4.15 Crack Pattern for Wall WIII-1
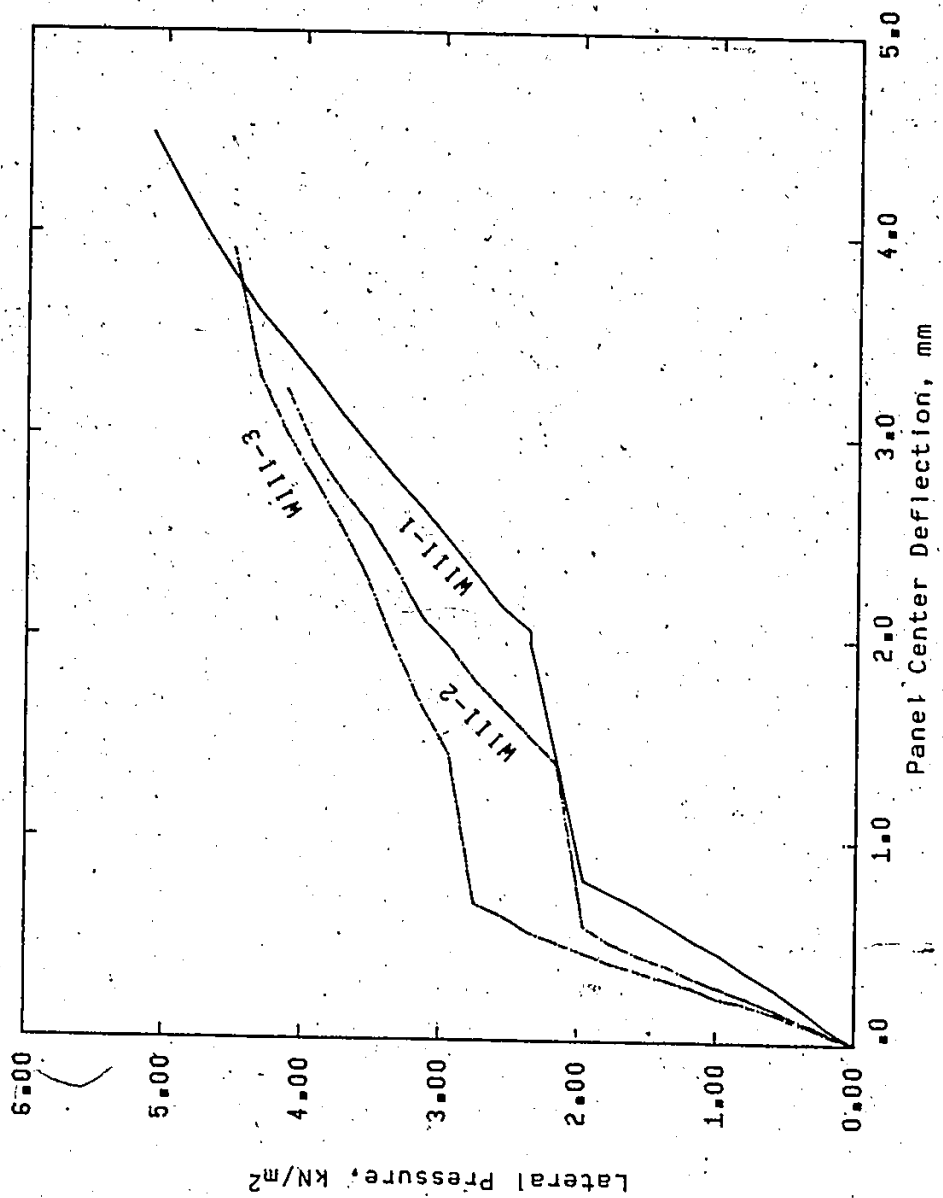
Figure 4.16   Deflection Data for Series WIII Walls

having a free edge at the horizontal crack and with different precompression due to the self weight of the wall.

The cracking pattern of such walls, as can be seen in Figure 4.17 for Wall WC-1, was formed by the extension of diagonal cracks from the horizontal precrack to the respective corner which is similar to Series WII. Also, the mean failure pressure for this wall series was reasonably close to that for the Wall Series WII as can be seen in Table 4.4.

The load-deflection results for the three walls are shown in Figure 4.18. They were nearly linear up to a pressure level of 50% to 60% of the failure pressure and nonlinear after that and up to failure.

4.3.2.6 Walls Supported On All Four Sides With Precompression
On the Top Edge (Series WP)

Series WP was similar to Series WII except that the precompression loading indicated in Table 4.4 was added. The first cracking and failure loads are also included in this table.

It is known that precompression should delay the development of cracking. Accordingly, the higher first cracking and failure pressures were expected. However, according to both elastic and yield line analyses, the observed large increase in failure pressure over that of Series WII would not only be due to the vertical prestressing. Instead, these analyses showed that this increase in failure pressure can be expected only if the precompression also increases the strength for bending in the horizontal direction. This is attributed to the fact that the vertical precompression increases the torsional strength of the bed

Figure 4.17   Crack Pattern for Wall WC-1

129
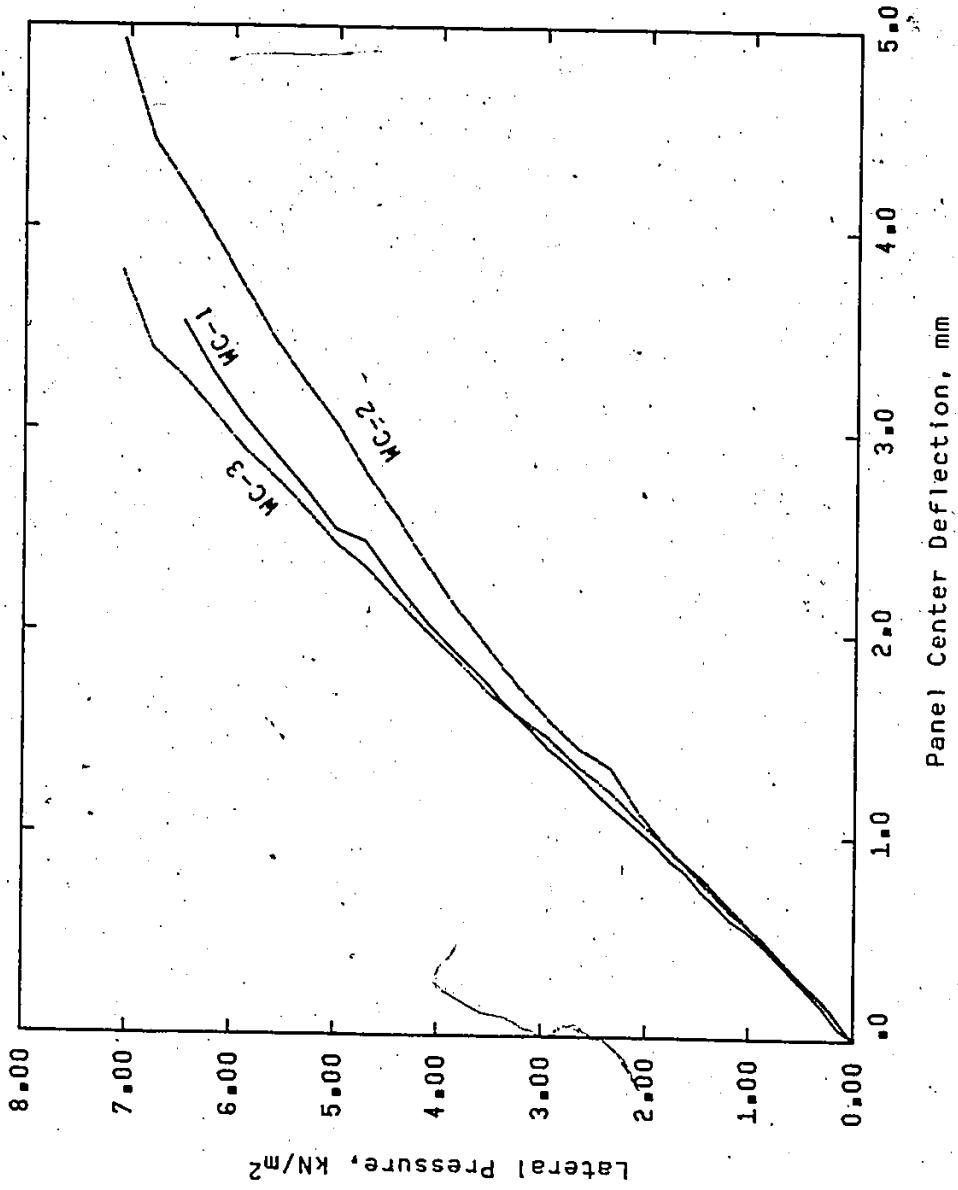
Figure 4.18   Deflection Data for Series WC Walls

Panel Center Deflection, mm

Lateral Pressure, KN/m²

joints. This in turn increases the strength in diagonal or vertical cracking when the crack passes through the bed and head joints or when this increased strength forces the crack to pass through the blocks.

The cracking pattern for Series WP walls was similar to that of Series WII walls but with a larger distance between the diagonal cracks at the center horizontal crack than for Series WII walls. This can be seen in Figure 4.19 where very few cracks other than those of the collapse mechanism were observed. This control of additional cracking is attributed to the beneficial prestressing effect of the precompression on weak bed joints.

The load deflection results for Series WP walls shown in Figure 4.20 look similar to those for Series WII as they were composed of the similar three distinct parts. First was a nearly linear part up to the development of the horizontal crack. Then, a plateau corresponded to the formation of this crack. Finally, there was a nonlinear part up to failure.

4.3.3 Comparison of Test Results For the Different Wall Series With Supports On All Four Sides

The comparison of the cracking pattern for the series having different aspect ratios indicated the presence of the horizontal crack near the panel center and the diagonal cracks for all of the tested aspect ratios. The diagonal cracks originating from the corners met at a vertical center crack in the case of the wall series with the smallest aspect ratio. However, for the other two aspect ratios, the sets of diagonal cracks met at the center horizontal crack but with a larger

131
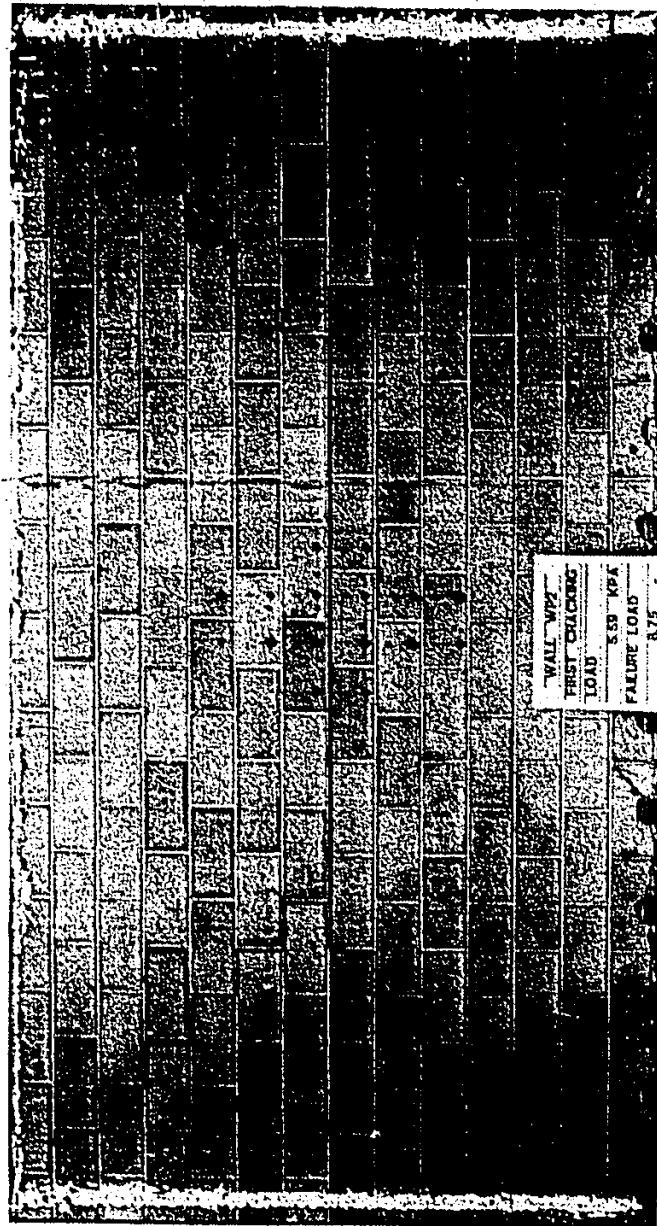
Figure 4.19   Crack Pattern for Wall WP-2
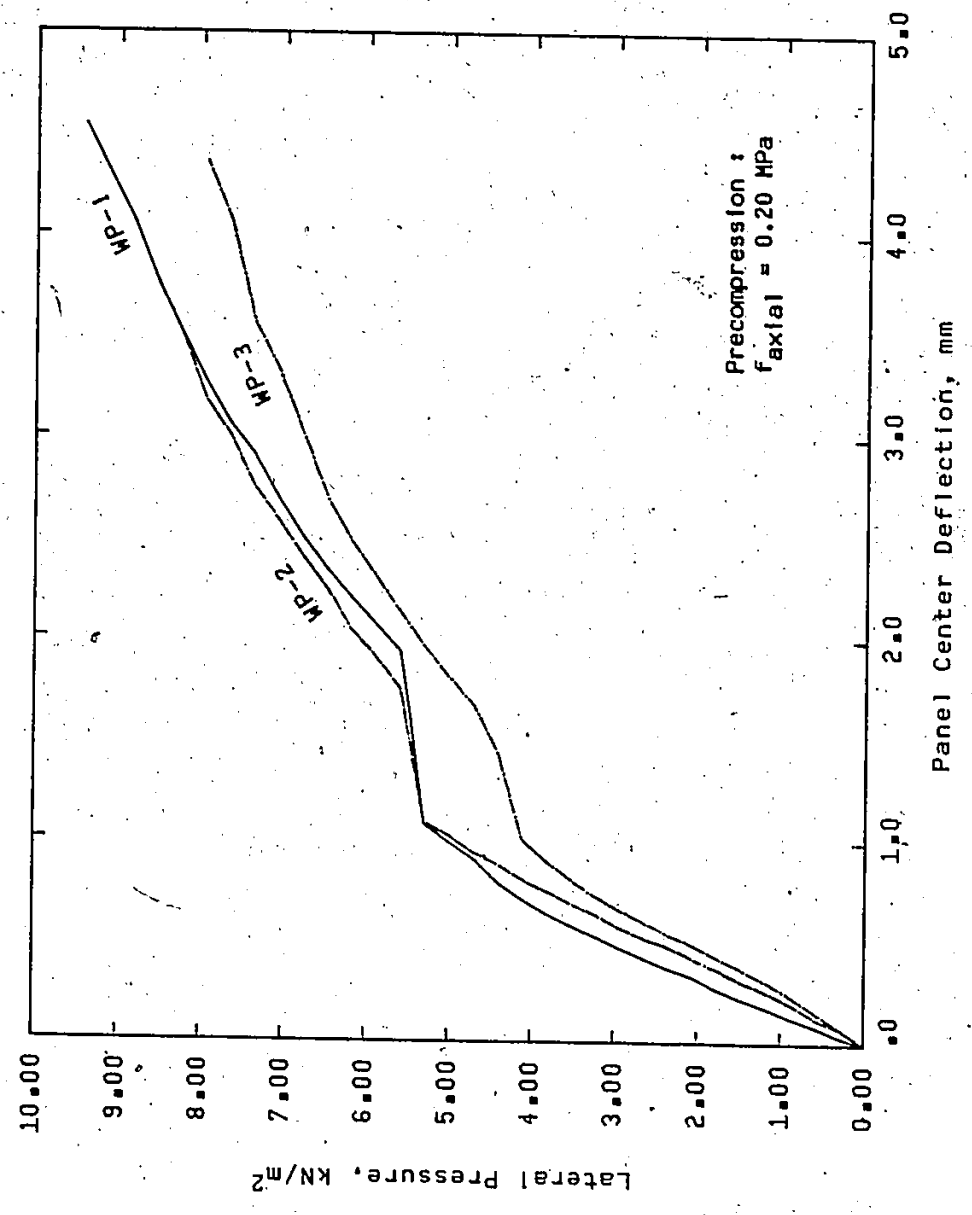
Figure 4.20   Deflection Data for Series WP Walls

distance between them for the larger aspect ratio.

The comparison of the load deflection results for three walls representing the three different aspect ratios are shown in Figure 4.21. In this figure, the increase in both the first cracking and failure loads with the decrease of the horizontal span is clearly indicated. This increase in the first cracking load for the walls with shorter horizontal spans was expected due to the increased stiffness for the horizontal direction in the statically indeterminate plate. Also, the increase in the panel capacity for the shorter walls was due to the increased moment capacity of the half walls with effectively free tops after first cracking. It should be noted that the amount of sudden deflection increase observed at formation of the horizontal crack decreased with the decrease of the horizontal span as can be seen in Figure 4.21. Moreover, for both before and after the first cracking, the increase in the stiffness for the panels with smaller aspect ratios is clearly shown in this figure.

The deflection data for one of the Series WC walls, having a precrack near the panel center, is shown in Figure 4.22 together with deflections for Wall WII-2. The failure loads for both walls were quite close and the end of the nearly linear part of the load deflection results for Wall WC-2 was reasonably close to the pressure corresponding to the formation of the horizontal crack in Wall WII-2. Finally, the initial slope of the load deflection curve for Wall WC-2 was less than that for wall WII-2. However, after the formation of the horizontal crack, the slopes of both curves were reasonably close for this nonlinear range.

134
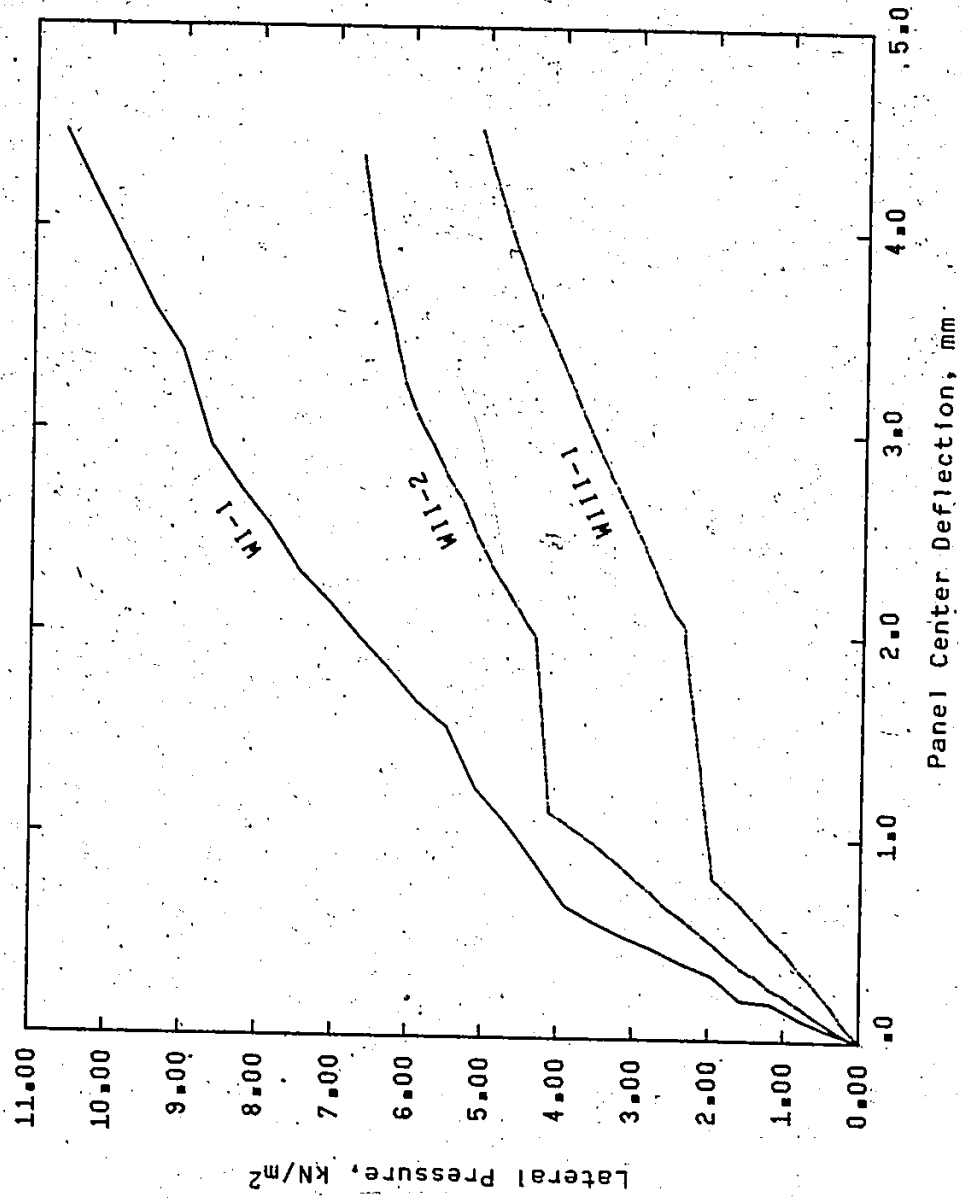
Figure 4.21 Deflection Data for Walls With Different Aspect Ratios
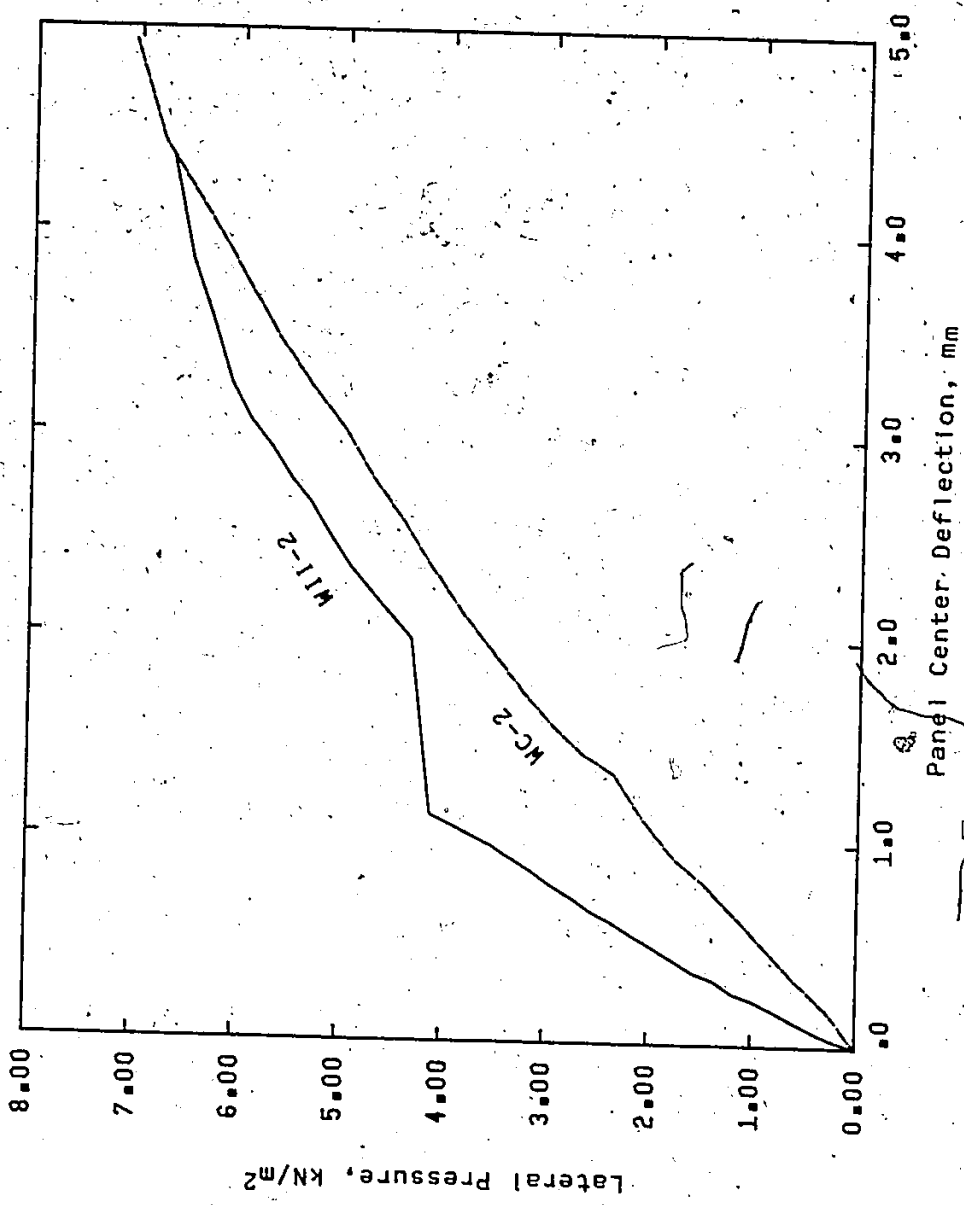
Figure 4.22   Deflection Data for Walls With Different
Initial Cracking Conditions

The comparison between Series WP walls and Series WII walls is clearly shown in Figure 4.23 where the load deflection results for a wall from each series are drawn together. A notably stiffer wall, narrower plateau and higher first cracking and failure pressures were observed for the wall with the precompression.

4.4   CONCLUDING REMARKS

The experimental results discussed above achieved the preset objectives and made it possible to reach the following conclusions :

1. The behaviour of concrete block walls when subjected to lateral (out-of-plane) loading is better understood at different stages (uncracked, cracked and failure).

2. By performing this experimental work, a body of test data on lateral loading of masonry walls with well defined support conditions is now available for North American conditions (practice and material). Having such data with well defined support conditions makes it accessible for verifying any method of analysis.

3. The considerable reduction in panel capacity with increased aspect ratio and decreased number of supported edges suggests possible approaches for design codes. These might be to limit the unsupported area of walls and to consider the possible precautions to ensure adequate support at the maximum possible number of edges.

4. The observed behaviour of wall panels in the cracked stage suggests the use of a multilayer approach for the analysis. This
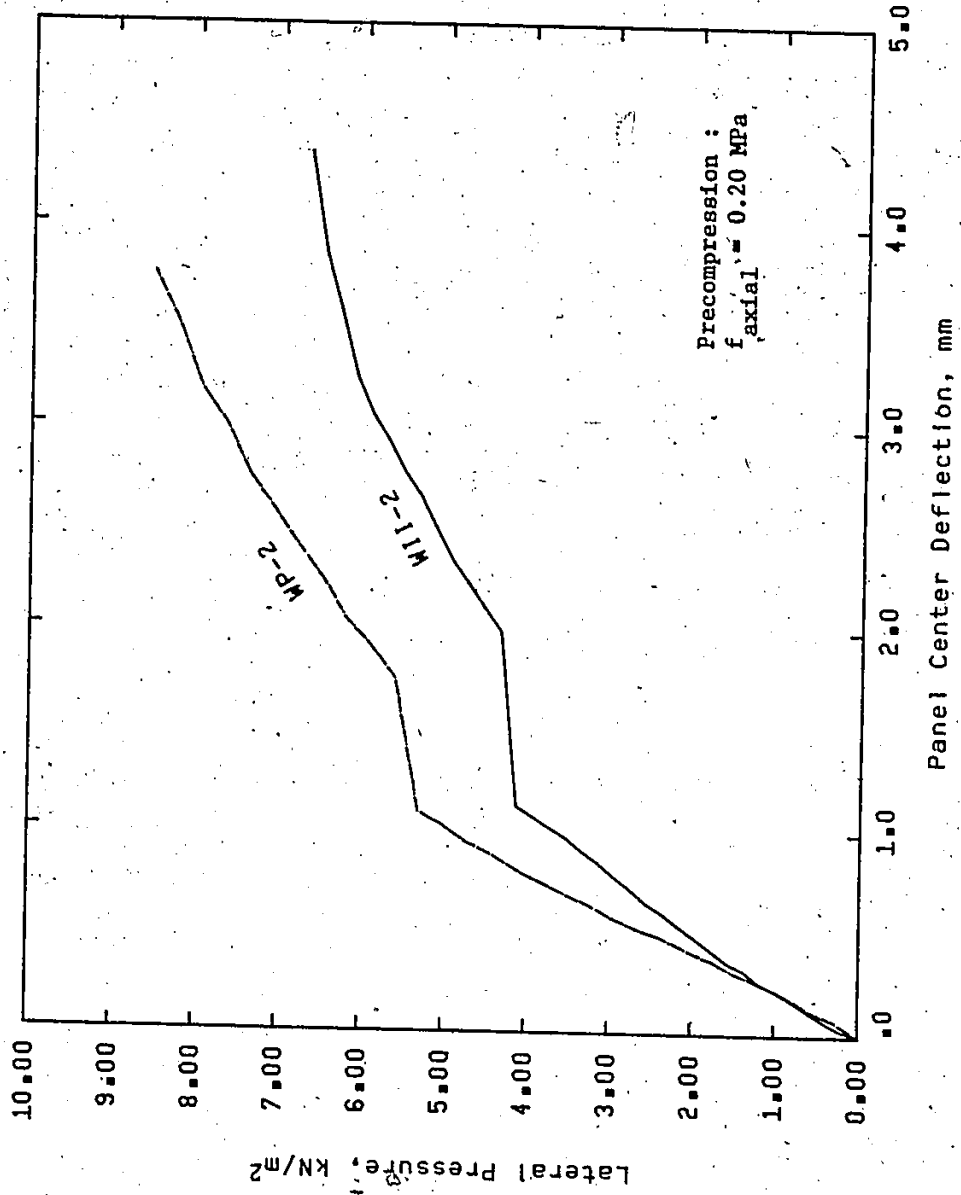
Figure 4.23   Deflection Data for Walls With Different Precompression.

is because the observed cracks were only in the tensile face of the wall and propagated through the whole thickness of the face shell of that side.

5. The experimental results of Series WC walls supports the idea of determining the ultimate capacity of walls supported on all four sides as that of its two halves after first cracking with the appropriate boundary condition at the center horizontal crack.

6. The observed behaviour of the full scale walls contradicted the yield line predictions for Series WI and WII. For Series WI walls, the yield line analysis did not predict the formation of the horizontal crack at mid-height as observed in WI walls. However, the elastic plate analysis did predict the development of this crack. It should also be noted that this horizontal crack was developed at a very small load level relative to the failure capacity. This means that such walls would exhibit serviceability failure. For Series WII walls, the observed cracking pattern was different from the X-shaped pattern predicted using the yield line analysis. Accordingly, these observations might suggest more objections for the direct use of the yield line method for the analysis of masonry walls.

7. The bond wrench test method was proven to be an acceptable method for testing masonry prisms in flexure normal and parallel to the bed joint orientation. This test is both easy to perform and economical regarding the necessary materials to produce an adequate sample size.

8. The allowable stresses in North American Codes for tension normal to bed joints are quite close to the determined strengths, especially that of the preliminary series. This information suggests that the margin of safety is not adequate. However, for tension in the direction parallel to the bed joints, the allowable stresses reported by the codes reflect a reasonable margin of safety when compared to the determined strengths.

9. The orthogonal strength ratio which is defined as the ratio of the flexural tensile strength parallel to the bed joints to that normal to the bed joints was determined from full scale wall tests and auxiliary tests. Wall tests gave an orthogonal strength ratio of 2.6 whereas the auxiliary tests yielded ratios of 3.5 and 3.3 for the preliminary and main test series, respectively. These were in all cases more than the ratio of 2.0 adopted in most codes.

10. The orthogonal rigidity ratio or the degree of orthotropy is defined as the ratio of the effective flexural rigidity in the direction parallel to the bed joints compared to that normal to the bed joints. This ratio, determined from the full scale walls tested in one-way flexure, was found to be 1.57. This indicated the orthotropic nature of concrete block masonry. The relative flexibility of the direction normal to the bed joints is thought to be due to the presence of the continuous mortar bed joints.

11. The increase in the capacity of the full scale walls including

the precompression series, Series WP, would not only be due to the prestress effect of the precompression in the direction normal to the bed joints. According to both elastic and yield line analyses, this increase would only be expected assuming that the precompression increased the amount of bending moment required to produce cracking normal and parallel to the bed joints.

12. The observed behaviour of wallettes and full scale walls supported on the two vertical sides suggests that the head joints might behave nonlinearly or in other words exhibited some plasticity after their strengths have been reached.

13. From the test results of full scale walls supported only on the top and bottom, the linear elastic behaviour up to failure may reasonably be assumed. Moreover, the relatively high variability of both strength and flexural rigidity for the direction normal to the bed joints was clearly shown. This may explain the considerable variability of the stiffness and the first cracking and failure pressures for the full scale walls supported on all four sides.

14. There was not enough evidence to identify the mechanism for crack formation. However, it is suggested that the probable failure mechanism for walls in one-way flexure might be either the partially or the fully plastic mechanism. This suggests that the blockwork may exhibit at least some load sharing similar to Baker's theory for brickwork [22].

CHAPTER 5

MACROSCOPIC BIAXIAL FAILURE CRITERION FOR

MASONRY ASSEMBLAGES

5.1   INTRODUCTION

Masonry assemblages such as shear walls, infill panels subject to wind loading, and infill panels subject to in-plane restraint or support movements are usually subject to tensile or compressive stresses parallel and normal to the bed joints plus shear stresses along these directions. This means that the assemblage is in a state of biaxial stress and sometimes a state of triaxial stress. However, strengths are determined experimentally in most cases using uniaxial states of stress. Therefore, it is necessary to establish a logical method to analyse strengths for biaxial or triaxial states of stress using the uniaxial strength information.

Failure of masonry as a brittle material follows the definition of brittle failure. This indicates that there are negligible inelastic deformations prior to such failures and that they consist of a sudden development of one or several separation surfaces within the body. Generally, brittleness is characterized by strongly differing tensile and compressive strengths, appreciable size effect and high scatter of test data [61].

Masonry researchers have been aware of the potential significance of biaxial stress conditions on strength and have proposed

failure criteria for masonry assemblages. These criteria have been based on experimental results [22,46], on finite element modelling to simulate biaxial tests [80], on isotropic material failure theories [27,111] and on composite material failure theories[51].

In general, failure theories for isotropic brittle materials such as the maximum stress theory, Coulomb's theory of internal friction and Mohr's theory of failure [75] are not applicable to masonry. This is because they are derived on the basis of the invarient state of stress concept wherein the stress orientation has no effect on the strength [51]. Masonry strength is highly sensitive to the orientation of the stresses with respect to the critical bed and head joint directions [47,50].

The available strength theories for composite lamina seem to be applicable to masonry assemblages. This is because of the inherent composite nature of masonry and the presence of continuous bed joints and blocks in layers. Also, these theories incorporate the variations in strengths with the stress orientation relative to the material principal planes which suit the anisotropic nature of masonry.

It is the objective in this chapter to propose a biaxial failure criterion for masonry. This criterion should be simple and yet provide reliable predictions of failure stresses for those combinations of stresses which can occur in the structure. To judge the reliability of the criterion, it should be confirmed by test data. In this chapter, the expected failure modes in masonry assemblages are discussed. Then, the existing failure criteria for masonry are reviewed and the

applicability to masonry of the failure theories for composite orthotropic materials are investigated. Finally, a failure criterion is proposed together with an investigation of its reliability using experimental data already available in the literature.

5.2   POSSIBLE MODES OF FAILURE IN MASONRY ASSEMBLAGES

In general, the capacity of masonry assemblages differs significantly for different modes of failure. For a masonry assemblage having specified component material strengths, the modes of failure are primarily dependent upon the relative magnitudes of the tensile or compressive and shear stresses along the critical planes normal and parallel to the bed joints. Alternatively, for a particular state of stress, the modes of failure are mainly dependent upon the relative magnitudes of the different strengths of the component materials used for this assemblage.

The possible modes of failure which can occur in masonry assemblages can be classified into two different categories. First, longitudinal modes of failure in which the failure plane propagates longitudinally in the plane of the assemblage. Secondly, transverse modes of failure in which the failure plane propagates transversely across the plane of the assemblage. In these modes the failure occurs through bed joints, head joints, masonry units (face shells in hollow concrete blockwork) or any combination of these.

The longitudinal failure modes are characterized by lateral splitting of the units in the case of solid masonry or splitting of the cross webs in the case of hollow blockwork. These modes of failure are

expected to occur primarily in uniaxial compressive states of stress with the stress applied either normal or parallel to the bed joints. Also, they are expected to occur under a biaxial stress state where both stresses normal and parallel to the bed joints are compressive. The accompanying shear stress along these planes is so small that it does not change the mode of failure.

The transverse modes of failure are characterized by debonding along the bed joints or debonding along head and bed joints around the units. These modes may also be characterized by debonding along head joints and splitting of the units in the same vertical failure plane or splitting of the units along an inclined failure plane. The different transverse failure modes are shown in Figure 5.1. These failure modes are due primarily to uniaxial tensile stress either normal or parallel to the bed joint orientation, pure shear stresses, biaxial tensile stresses or biaxial tension-compression, respectively.

In the next sections, only the transverse failure modes which are expected to occur in shear walls and infill panels with moderate levels of precompression will be considered. The longitudinal failure modes which are expected to occur in masonry bearing walls under high levels of precompression are considered to be outside the scope of this investigation.

5.3   EXISTING BIAXIAL FAILURE CRITERIA FOR MASONRY

The existing failure criteria for masonry assemblages under biaxial states of stress were proposed on various completely different bases ranging from strictly fitting of experimental data to a

Debonding Along
Bed Joint

(II) Vertically
Toothed Debonding

(I) Vertical Splitting

(II) Diagonally
Stepped Debonding

(I) Diagonal Splitting
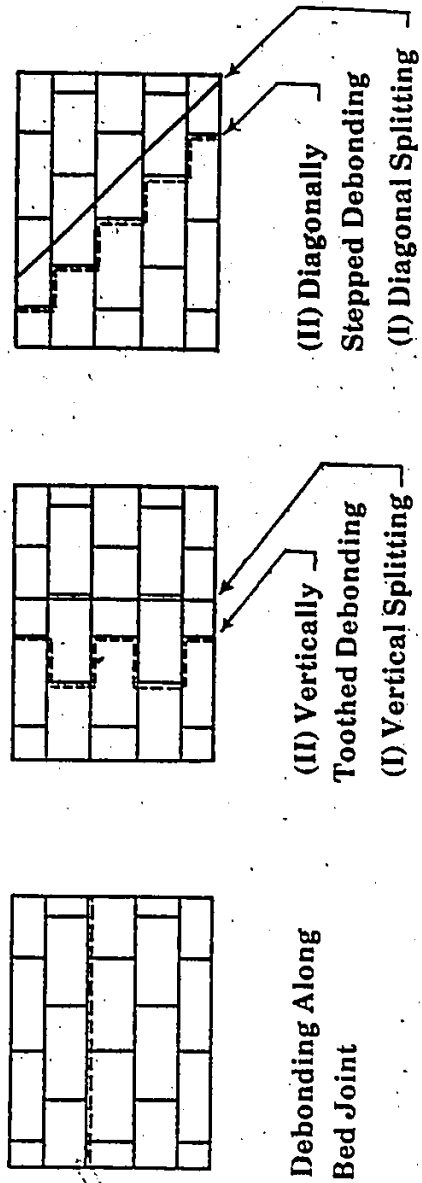
Figure 5.1   Possible Transverse Failure Modes

modification of composite material failure theories. Also, it is worth noting that the prediction of failure under certain limited stress conditions was the objective for most of these criteria.

Borchelt [27] proposed a failure hypothesis for brick assemblages subject to axial compression and in-plane shear. In his proposal, he adopted the maximum tensile stress theory for isotropic materials which assumes a constant value for the tensile strength independent of direction. However, it is suggested that this assumption is not valid for masonry due to its inherent anisotropic and composite nature.

Yokel and Fattal [111] adopted Mohr's theory of failure in order to predict the failure of brickwork assemblages subjected to combined stresses. In their approach, a straight line type of limiting curve for Mohr's failure surface was considered. The shape of this limiting curve varies considerably according to the ratio of the uniaxial compressive strength to the uniaxial tensile strength of the material [50]. Also, constant values for both splitting tensile strength and compressive strength independent of direction were used. This approach has the drawback of being based on Mohr's theory of failure which was derived on the basis of the invarient state of stress concept. It is suggested that this is not valid considering that masonry is an anisotropic material. Accordingly, the use of constant splitting tensile strength and constant compressive strength is not appropriate for masonry where the directional dependence of both tensile and compressive strengths is well known. Also, the uncertainty of the straight line assumption for the limiting curve due to the variation of the strength ratio with the

stress orientation is one of the drawbacks of this approach.

Page [80] derived a failure surface in the tension-tension range for brick masonry using a finite element model which is capable of predicting only joint failures. This failure surface was determined in terms of the two principal stresses and their orientation with respect to the bed joints. Analysis of brickwork panels with different bed joint orientations and different principal stress ratios were performed to obtain this failure surface. He stated that the shape of the failure surface depends also upon the relationship between the shear and tensile bond strengths of the joints which should be considered in the derivation of a general failure surface. This approach cannot be generalized for brickwork and blockwork for the following reasons :

1. The derived failure surface predicts only the failures in the tension-tension range which is only one quarter of the possible stress combinations.

2. It predicts only joint failures. However, failures through the units were reported even under uniaxial tensile stress parallel to the bed joints.

3. The failure surface was derived for a particular ratio of the shear bond strength to the tensile bond strength. To obtain such surfaces for other ratios, finite element simulations of biaxial tests have to be performed for these ratios. This is not practically feasible because it necessitates the availability of the model for the users of the criterion.

4. The irregularities in shape of the failure surfaces make it

difficult to represent algebraically.

Hamid and Drysdale [51] proposed a failure criterion for concrete block masonry assemblages under biaxial stresses. Their proposal rationally included the inherent anisotropic characteristics of masonry as a composite material by modifying one of the existing criterion for composite orthotropic materials. Also, they considered the necessity of not having a single criterion but a set of sub-criteria to account for the possible modes of failure. Their proposal was also based on physical interpretation rather than being strictly phenomenological. However, the assemblage capacity predictions did not compare well with the experimental data. Although they considered the interaction between the shear and normal compressive stresses, they did not consider any interaction between the shear and the tensile stresses. Moreover, they considered the different tensile failure modes as only one mode of failure to be predicted using one criterion.

Ganz and Thurlimann [45] proposed a biaxial failure criterion for highly perforated brick masonry. In this proposal, they considered the anisotropic and composite nature of masonry and presented a failure surface in the stress space of the principal material directions. Coulomb failure criterion with a zero-tension cut-off for shear on bed joints and square failure criterion for brick material were assumed. They neglected the tensile strength of bricks and the tensile bond strength of the joints. Also, in this proposal, the presence of the head joints was not considered. In this approach, five different subcriteria were suggested to represent five different failure modes. However, it is suggested that this criterion cannot be generalized for

masonry because it neglects any tensile strength and ignores the head joints.

Recently, Dhanasekar, Page and Kleeman [38] proposed failure criterion for brick masonry under biaxial stresses. In this proposal, the failure surface in the principal stress space was determined by means of biaxial tests. The continuous mortar bed joints were considered in this approach as planes of weakness. Therefore, in addition to the principal stresses at failure, their orientation with respect to the bed joint planes was considered to define the failure condition. An alternative failure surface in the stress space of the principal material directions was obtained by the transformation of biaxial test results to this stress space. In this criterion, they suggested an algebraic representation for the alternative failure surface by three intersecting elliptical cones. This algebraic representation was reasonably close to the experimentally determined surface. However, as reported by the authors, these elliptical cones of the failure surface do not correspond with distinct modes of failure. This may suggest that this criterion is phenomenological and is not based on physical interpretations. Also, the biaxial tension failure surface was not obtained experimentally but rather was based on an extrapolation of test data. Moreover, the suggested tension elliptical cone implies no interaction between stresses normal and parallel to bed joints at zero shear irrespective of the mode of failure. This contradicts the reported experimental test results for brickwork [22] and blockwork [44,46]. Finally, this criterion was based on only one

brick-mortar combination and therefore it has to be confirmed by further tests for different brick-mortar-combinations.

All the failure criteria mentioned above were for the biaxial strength of brick or block masonry assemblages for in-plane loading. However, design of tests to determine biaxial flexural strength of masonry for out-of-plane bending introduces some experimental difficulties. Of these difficulties are the large number of tests required due to the high variability of flexural strengths and the complexities of the testing apparatus. Therefore, the assumption of no interaction between the flexural tensile stresses normal and parallel to the bed joints was a simple solution. This resulted in a simple rectangular failure surface.

Baker [18,22] investigated the interaction of the flexural tensile stresses of brickwork normal and parallel to the bed joints. He proposed an elliptical failure surface to best fit the experimental data available through his investigations. To generalize his proposal, Baker also suggested an elliptical relationship between the strengths in the two principal stress directions. For the determination of the strength in the principal stress direction, he proposed an expression using the method of least squares to best fit experimental data. However, the use of these empirically based relationships for block masonry has to be confirmed by test results. It should also be noted that the logical assumption of an elliptical relationship for the principal strength criterion was used by Baker in the analysis of brick masonry walls but it was not confirmed by experimental results. Moreover, this approach did not account for the different possible failure modes.

Gazzola, Drysdale and Essawy [46] proposed a criterion based on experimental data for concrete block assemblages under off-axis bending. In their proposal, they considered the relationship between the failure criterion and the failure mode. Accordingly, they suggested interaction between the stresses normal and parallel to the bed joints only for stepped or toothed failure modes. However, they suggested that there is no significant interaction in the cases of failure by debonding along bed joints or through head joints and blocks in alternate courses. This approach rationally indicates the effect of mode of failure on the failure surface. However, it did not quantitatively evaluate the amount of the interaction, if any. It was also suggested that the controlling failure modes for different combinations of block strengths and mortar bond properties should be investigated and considered for a generalized failure criterion.

This review of the available biaxial failure criteria for masonry assemblages indicates that none can be considered to be a generalized criterion. It also reveals the required features of an acceptable generalized criterion for masonry in a biaxial state of stress which are summarized as follows :

1. To consider the anisotropic and composite nature of masonry assemblages.

2. To account for the possible modes of failure by adopting a set of sub-criteria.

3. To consider the different possible unit strengths and mortar bond properties in order to be able to define the controlling

modes of failure and consequently the failure surface.

4. To be based on physical interpretations rather than being strictly phenomenological.

5. To be able to predict both the occurrence of failure and the failure mode.

5.4   FAILURE THEORIES FOR COMPOSITE MATERIALS

Composite materials are not considered to be homogeneous and isotropic as is the case for most conventional engineering materials. However, on the macroscopic level, a non homogeneous assembly can be regarded as a homogeneous material. This equivalent homogeneous material may have different material properties in all directions (anisotropic material). However, for materials which are considered to be orthotropic, the material properties are different in three mutually perpendicular directions (principal material directions). They also have three mutually perpendicular planes of material symmetry [64].

For an isotropic material, only the algebraic values of the three principal stresses are relevant. However, for orthotropic materials, the orientation of the principal stress axes with respect to the planes of strength symmetry are also needed. Therefore, the three geometric parameters which define each orientation are added to the three stress parameters to determine the failure condition. Alternatively, and more conveniently for the case of orthotropy, the six stress components (three normal stresses and three shear stresses) with respect to the principal material directions may be used to define the state of stress. Then, the fracture condition may be represented

geometrically by a fracture surface in the six-dimensional stress-space [61].

The orthotropic failure theories which are commonly used are the maximum stress theory [64], the maximum strain theory [64], Tsai-Hill theory [64] and Hoffman theory [61]. In all of these theories, the material is considered to be homogeneous and therefore some of the microscopic failure mechanisms inherently cannot be accounted for. Also, planes of strength symmetry are assumed to be the same as those for elastic symmetry. Moreover, the cartesian coordinate system is oriented so that the coordinate planes coincide with the planes of strength symmetry.

In the maximum stress theory [64], the stresses in the principal material directions must be less than the respective strengths otherwise fracture is said to have occurred. The fracture occurs according to the failure mechanism associated with the respective strength. There is no interaction between the failure stresses in this criterion and actually it is a set of independent sub-criteria.

The maximum strain theory [64] is quite similar to the maximum stress theory but strains rather than stresses are limited. It also predicts the occurrence of the failure and the failure mechanism. However, there is some interaction between stresses due to the Poisson's ratio effect.

In the Tsai-Hill theory [64], the yield condition for anisotropic materials proposed by Hill (an extension of Von Mises isotropic yield criterion) was used by Tsai as an anisotropic strength criterion. This was considered in the spirit of both being limits of

linear elastic behaviour. In this criterion, considerable interaction between the failure stresses exists. However, because it is a single criterion, it does not account for the different modes of failure and their effect on the failure surface. Moreover, the Tsai-Hill theory assumed equal strengths in tension and compression as did Hill's original yield criterion.

The Hoffman theory [61] was proposed as a phenomenological failure or fracture condition and borrowed features of Hill's yield condition. In this theory, Hoffman added to Hill's yield condition some terms which are odd functions of the normal stresses in the three principal material directions. These odd functions were chosen to be linear as the simplest choice to account realistically for the vastly differing tensile and compressive strengths which characterize brittle behaviour. In this criterion, the interaction between the failure stresses was included. However, it does not predict or even consider the different modes of failure as it is a single phenomenological criterion.

5.5 APPLICABILITY OF FAILURE THEORIES FOR ORTHOTROPIC COMPOSITE MATERIALS TO MASONRY ASSEMBLAGES

Masonry assemblages can be regarded as composite materials because they are composed of layers of continuous bed joints and masonry units. They may also be considered to be anisotropic due to the directional dependence of the strengths. Therefore, the anisotropic composite materials failure theories were thought to be applicable for masonry assemblages. Moreover, the strength symmetry with respect to

the head and bed joint orientations simplifies the anisotropic condition to an orthotropic condition. In this orthotropic material, the three principal material directions are the parallel and the normal to the bed joint orientations in the plane of the assemblage and the perpendicular direction to this plane. Thus, the different strengths have to be evaluated in the three directions since generally there is no transverse symmetry in masonry.

The failure theories for orthotropic materials reviewed in the preceding section cannot be applied directly to masonry assemblages for the following reasons :

1. Interaction between the failure stresses is not included in the maximum stress theory [64]. However, masonry assemblages have shown some tendency to exhibit interaction between stresses under some failure modes [22,46].

2. Some interaction between the stresses is considered in the maximum strain theory [64] due to the Poisson's effect. This interaction means higher biaxial stresses than the uniaxial strength are required to cause failure in the tension-tension or compression-compression ranges compared to lower biaxial stresses for the tension-compression ranges. This type of interaction contradicts the reported tendency for stress interaction in masonry [18,22]. Moreover, no interaction is considered between the shear and any of the normal stresses in this theory. This is also not considered to be realistic.

3. The significantly differing strengths in tension and compression

of masonry cannot be accounted for in the Tsai-Hill theory [64].
Also, this theory is strictly phenomenological. Moreover, it is
a single criterion which is not logical where more than one
failure mode is expected.

4. The influence of the different modes of failure on the strength
is not considered in the Hoffman theory [61]. Also, this theory
is strictly a phenomenological theory and is not based on
physical interpretation. In addition, analysis of masonry
assemblages using the Hoffman theory showed non-realistic
interaction of stresses which contradicts the reported
behaviour of masonry [18,22].

5.6   PROPOSED FAILURE CRITERION FOR MASONRY
ASSEMBLAGES UNDER BIAXIAL STRESSES

A failure criterion for masonry assemblages i proposed herein
to account for the shortcomings which prevent the direct application of
the orthotropic failure theories discussed in Section 5.5.   It is an
attempt to satisfy the required features for an acceptable generalized
criterion for masonry as defined in Section 5.3. As will be shown, this
criterion can in fact be considered as a modified maximum stress
criterion for orthotropic materials.   The reason for choosing the
maximum stress theory to be modified is that it predicts the occurrence
of failure as well as the failure mode.   Therefore, it only needs to be
modified to rationally include the interaction of the failure stresses.

In this criterion, the masonry assemblage strengths for the
different failure modes are evaluated by the equilibrium of a free body

diagram of an isolated strip from the extreme fibers of the assemblage. Therefore, using the proposed criterion as will be shown, the biaxial strength of the assemblage can be determined for solid or hollow masonry under biaxial in-plane or out-of-plane stresses. The only difference is that the unit strength and the mortar/unit bond properties as well as the stresses acting on the assemblage have to be determined according to the materials used in the assemblage and the straining actions acting on the assemblage.

5.6.1 Joint Strength Criterion

The interaction of failure stresses in masonry assemblages is identified as being mainly due to the interaction between the shear and normal stresses acting on the mortar joints. Therefore, the prediction of biaxial strength of masonry assemblages in which the failure occurs partially or completely through mortar joints will depend on the criterion for the joint strength. Failure of mortar joints occurs by debonding at the interfaces between mortar and masonry units under either shear-compression or shear-tension stress combinations. Accordingly, there are two separate sub-criteria each concerned with one of the stress fields mentioned above.

For joint slip failure in the shear-compression stress field, it has been shown that Coulomb's theory of internal friction can reasonably predict the joint strength of masonry assemblages [25,50,79]. This, as shown in Figure 5.2, can be written as:

$$\sigma_{sbm} = \sigma_{sbmo} + \mu\sigma_{cbm}$$

<div align="right">(5.1)</div>
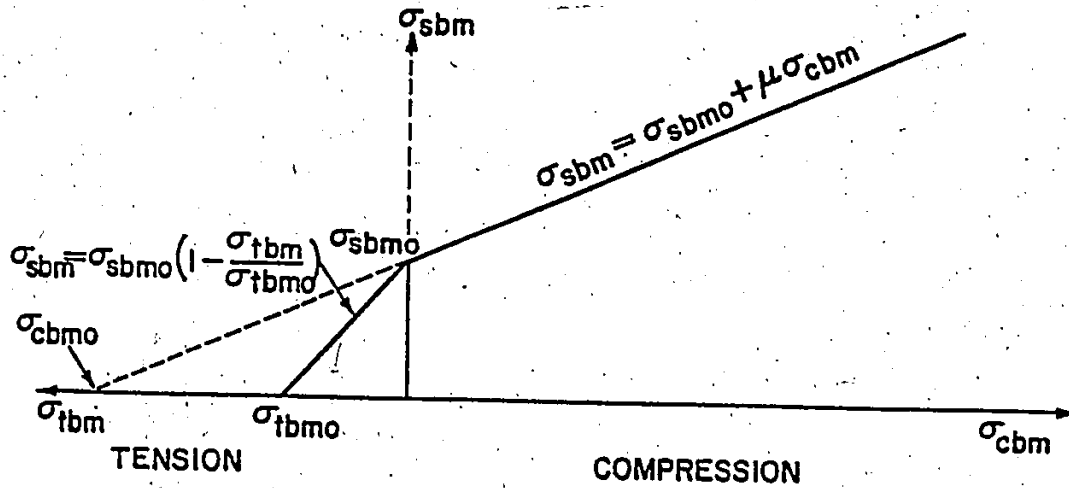
Figure 5.2   Joint Strength Criterion
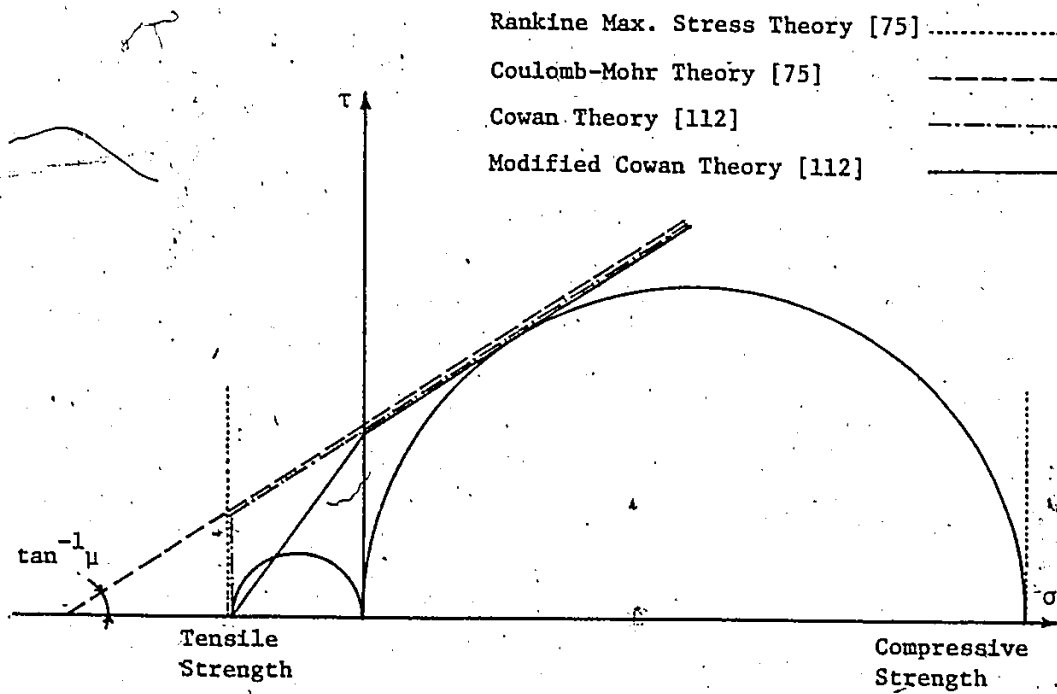
Figure 5.3   Illustration of Different Failure Theories for Brittle Materials Modified From Mohr Theory

Where,

σ_{sbmo} is the shear bond strength,

σ_{sbm} is the shear bond stress at failure,

σ_{cbm} is the normal compressive stress at failure and

μ is the coefficient of friction between mortar and masonry units.

Equation 5.1 is only valid for normal compressive stresses considerably below the compressive strength of the assemblage normal to the bed joints (Hamid [50] suggested a limiting value of 0.3 f_m'). For higher precompression, this linear relationship is no longer applicable. It should also be noted that, for precompression values approaching the uniaxial compressive strength f_m', not only does the relationship deviate from the linear expression but also the failure mode changes [50,84].

For joint bond failure under a state of shear-tension stresses, Coulomb's theory is not applicable because the interface has limited tensile strength which results in the tensile failure mode. Accordingly, the modified Cowan theory [112], which was proposed to express the failure of brittle materials in the shear-tension stress field, will be adopted for this criterion. In this theory, a linear relationship between the pure shear and tensile strengths was used as shown in Figure 5.3. Therefore, by adopting this criterion, the strength of the joint in the shear-tension region shown in Figure 5.2 is given as:

$$\frac{\sigma_{sbm}}{\sigma_{sbmo}} + \frac{\sigma_{tbm}}{\sigma_{tbmo}} = 1 \qquad (5.2)$$

Where,

σ_{tbmo} is the tensile bond strength and

σ_{tbm} is the tensile bond stress at failure.

It should be noted that this relation has been utilized previously for predicting joint strengths for both brickwork [79] and blockwork [25].

In the next section, expressions for the strengths of masonry assemblages for the different transverse failure modes shown earlier in Figure 5.1 are proposed. As will be shown, these expressions are primarily based on the shear-tension interaction relationship given in Equation 5.2. This is because it is the critical mode of failure for most assemblages and specifically for the biaxial flexure area of interest in this investigation. However, similar expressions are applicable to the shear-compression state of stress by using Equation 5.1 after reforming as follows:

$$\frac{\sigma_{sbm}}{\sigma_{sbmo}} - \mu \frac{\sigma_{cbm}}{\sigma_{sbmo}} = 1 \qquad (5.3)$$

or,

$$\frac{\sigma_{sbm}}{\sigma_{sbmo}} + \frac{\sigma_{cbm}}{\sigma_{cbmo}} = 1 \qquad (5.4)$$

Where, σ_{cbmo} is the normal stress at zero shear according to Coulomb's straight line as shown in Figure 5.2 which is determined as:

$$\sigma_{cbmo} = - \frac{\sigma_{sbmo}}{\mu} \qquad (5.5)$$

5.6.2 Biaxial Strength of Masonry Assemblages For

Different Failure Modes

5.6.2.1 Strength For Debonding Along Bed Joints

This mode of failure occurs due to either tension normal to the bed joints or shear along the bed joints or any combination of shear and tension on such joints. The assemblage is said to have failed by debonding along a bed joint if the stresses acting on this joint reach the strength value given by the shear-tension relationship for the joint. For this, Equation 5.2 may be rearranged as follows:

$$\sigma_{tbm} = \sigma_{tbmo} \left(1 - \frac{\sigma_{sbm}}{\sigma_{sbmo}} \right) \qquad (5.6)$$

For a free body taken from the extreme fibers of the assemblage under the complete biaxial stress state, as shown in Figure 5.4.a, the equilibrium equations are as follows:

$$(2a \times dt)\sigma_n = (2a \times dt)\sigma_{tbm}$$
$$\text{or, } \sigma_n = \sigma_{tbm}$$
$$(2a \times dt)\tau_{np} = (2a \times dt)\sigma_{sbm} \qquad (5.7)$$
$$\text{or, } \tau_{np} = \sigma_{sbm}$$

Where,

σ_n and τ_{np} are the tensile and shear stresses at the extreme fibers of the assemblage respectively,

2a is the nominal unit length, and

dt is the arbitrary shell thickness.

(a) Stresses on Free Body at Failure

(b) Failure Surface
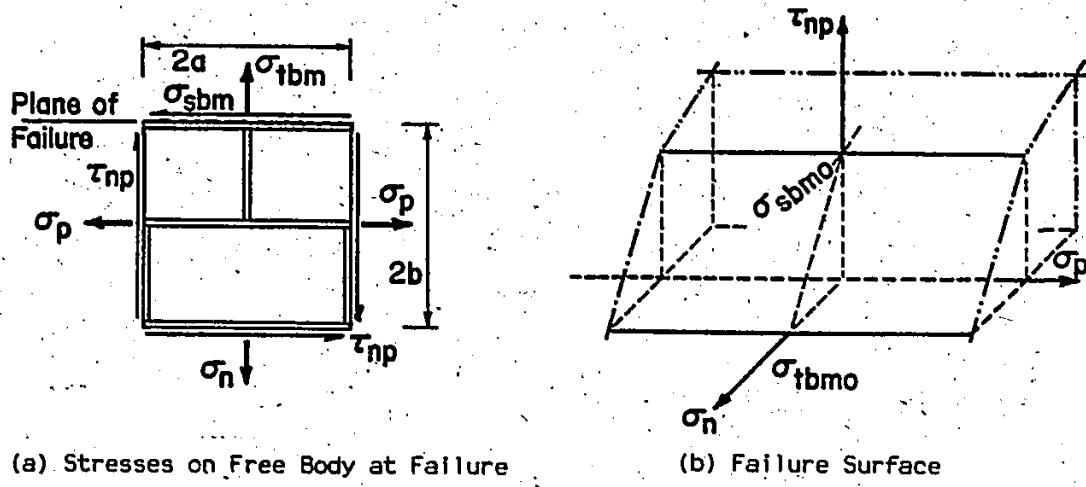
Figure 5.4   Strength of Masonry Assemblages in Debonding Along Bed Joints

(a) Stresses on Free Body at Failure
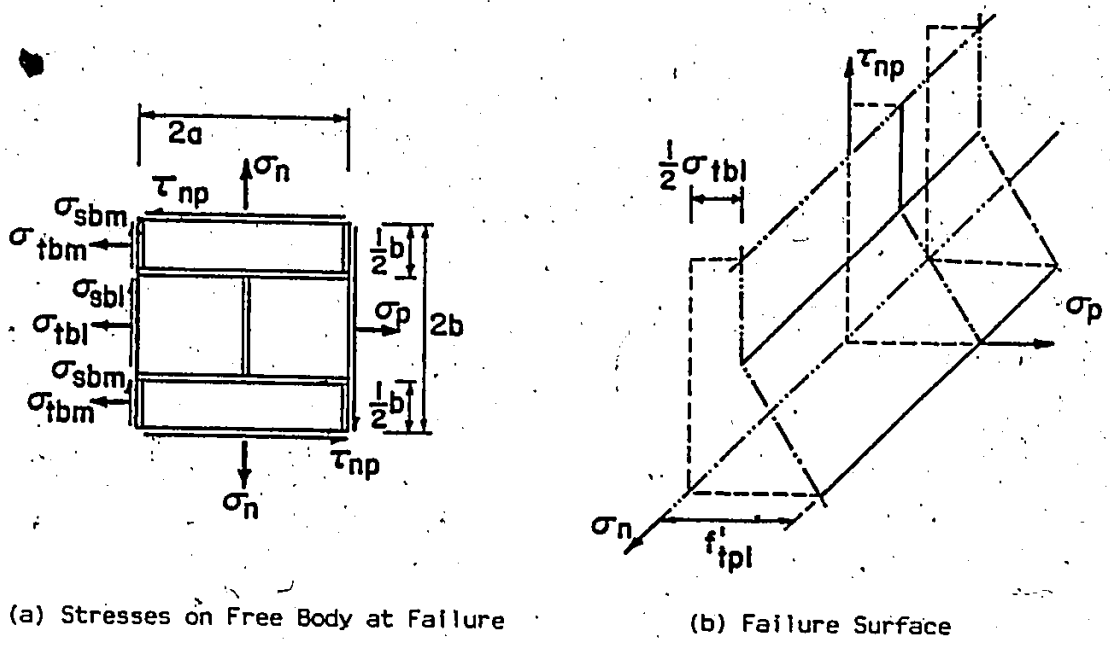
(b) Failure Surface

Figure 5.5   Strength of Masonry Assemblages in Vertical Splitting Through Head Joints and Units

By substituting Equations 5.7 in Equation 5.6, the following relation is obtained:

$$\sigma_n = \sigma_{tbmo} \left(1 - \frac{\tau_{np}}{\sigma_{sbmo}} \right) \tag{5.8}$$

This is the failure condition or failure surface in the σ_n-σ_p-τ_{np} stress space as shown in Figure 5.4.b. It can be seen in this figure that, for this failure mode, the strength is not affected by the tensile or compressive stresses parallel to the bed joints (σ_p). This observation also conforms with previous experimental results [46]. Moreover, the uniaxial tensile strength of the assemblage in this failure mode (f_{tn}') can be simply determined as follows:

$$f_{tn}' = \sigma_n \Big|_{\tau_{np}=0} = \sigma_{tbmo} \tag{5.9}$$

This is similar to the uniaxial strength expression given by Drysdale and Hamid [41] for block masonry under in-plane tension with the use of the actual cross section in strength calculations.

5.6.2.2 Strength For Debonding Along Head Joints and Splitting Through Units In Alternate Courses

The biaxial strength of an assemblage for the failure mode which involves debonding along head joints and splitting through units in alternate courses can be determined from the equilibrium of forces on a free body of the extreme fibers. The stresses at failure are shown in Figure 5.5.a. It is worth noting here that the bond strength of the head joints is considered to be the same as the bed joint strength.

Also, since this failure mode is primarily due to tension parallel to the bed joints, it can be reasonably assumed that, at failure, the masonry units attain their tensile strength. Another way of expressing this is that failure of the units obeys the original Cowan theory of failure (see Figure 5.3) while the mortar head joints exhibit the shear-tension type of failure according to the adopted joint strength criterion.

In the criterion for this failure mode, it is assumed that there will not be any premature cracking in the head joints up to the occurrence of failure through both head joints and units. This assumption is based on the observed behaviour of the mortar joints in both brickwork [30] and blockwork [44]. This is assumed to be true as long as a specific limiting value of nonlinear deformations for the head joints is not exceeded. For brickwork, this limit has been identified by a maximum ratio of assemblage tensile strength parallel to the bed joints to head joint strength of 5 [22]. In this study, the same limit is assumed to be applicable for blockwork. It should be noted that this assumption for the upper limit does not imply proportionally large nonlinear deformations to take place in the joints before failure. This is because of the dissimilar stiffnesses of the joints and units which results in uneven stress distribution in head joints and units over the assemblage height. The uneven stress distribution over the assemblage height is discussed in detail in Appendix C. It should also be noted that Baker suggested a similar mechanism for the analysis of brick masonry walls subjected to bending with tension parallel to bed joints [30] where he suggested a nonlinear behaviour for the head joints

prior to cracking.

The equations for equilibrium are as follows:

$$(2b \times dt) \, \sigma_p = (b \times dt) \, \sigma_{tbm} + (b \times dt) \, \sigma_{tbl}$$

or, $\qquad \sigma_p = \dfrac{1}{2} (\sigma_{tbm} + \sigma_{tbl})$ (5.10.a)

$$(2b \times dt) \, \tau_{np} = (b \times dt) \, \sigma_{sbm} + (b \times dt) \, \sigma_{sbl}$$

or, $\qquad \tau_{np} = \dfrac{1}{2} (\sigma_{sbm} + \sigma_{sbl})$ (5.10.b)

Where,

σ_{tbl} is the tensile strength of the masonry unit,

σ_{sbl} is the shear stresses on the masonry units, and

b is the nominal unit height.

The ratio of the shear stresses on the head joints and the masonry units depends on the relative stiffness of the head joints, bed joints and masonry units. As discussed in Appendix C, this ratio was found to be:

$$\frac{\sigma_{sbl}}{\sigma_{sbm}} = \frac{1 + 2 \dfrac{E_j}{G_j}}{1 + 2 \dfrac{E_j}{G_b}}$$

Where E_j, G_j and G_b are modulus of elasticity of mortar joints, the shear modulus of the mortar joints and the shear modulus of the masonry unit material, respectively. Accordingly, Equation 5.10.b may be rewritten in terms of only the shear stresses on the head joints as

follows:

$$\tau_{np} = \frac{1 + \dfrac{E_j}{G_j} + \dfrac{E_j}{G_b}}{1 + 2\dfrac{E_j}{G_b}} \; \sigma_{sbm} \tag{5.10.b}$$

By substituting into Equation 5.10.a for the tensile bond stress (σ_{tbm}) from the joint failure condition (Equation 5.2) and for the shear bond stress (σ_{sbm}) from Equation 5.10.b, the following expression is obtained:

$$\sigma_p = \frac{1}{2}\left[\; \sigma_{tbmo}\left(1 - \frac{1 + 2\dfrac{E_j}{G_b}}{1 + \dfrac{E_j}{G_j} + \dfrac{E_j}{G_b}} \; \frac{\tau_{np}}{\sigma_{sbmo}}\right) + \sigma_{tbl}\;\right] \tag{5.11}$$

This is the expression describing the failure surface in the σ_n-σ_p-τ_{np} stress space for this mode of failure as shown in Figure 5.5.b.

This expression for the failure condition indicates that the failure strength is independent of the tensile or compressive stresses parallel to the failure plane (normal to the bed joints in this case). This confirms the previous suggestion based on experimental results of blockwork wallettes [46]. The interaction of the shear stresses and the normal stresses parallel to the bed joints is also included in this failure condition. It should be noted here that Equation 5.11 is only valid for shear stresses up to a certain limit at which the term within the parentheses in this equation has a zero value. At this stress

level, the head joints reach their strength and thereafter a $1/2 \sigma_{tbl}$ tensile stress parallel to the bed joints is required to produce this failure mode.

As reported earlier, this failure mode is observed for assemblages under uniaxial tension parallel to the bed joint orientation. The uniaxial tensile strength in this mode of failure (f'_{tp-I}) is given by:

$$f'_{tp-I} = \sigma_{pI}\Big|_{\tau_{np}=0} = \frac{1}{2} (\sigma_{tbmo} + \sigma_{tbl})$$ (5.12)

This expression is similar to the strength condition in this mode proposed by Drysdale and Hamid [41] using the actual cross section in strength calculations.

It should also be noted that the assumption of nonlinear behaviour for the mortar head joints, as will be seen later, yielded predictions which were reasonably close to the available test data. However, another approach assuming premature cracking in the head joints was tried and found to underestimate masonry strength for available test results.

5.6.2.3 Strength For Debonding Along a Combination
of Bed and Head Joints

The failure mode involving debonding along a combination of bed and head joints includes two distinct patterns. As shown in Figure 5.1, these are vertically toothed and diagonally stepped patterns. The diagonally stepped pattern is the most likely pattern for this mode of failure for assemblages under biaxial stresses. The vertically toothed

pattern is likely to occur only under tension parallel to the bed joints with or without a low level of tensile or compressive stress normal to the bed joints. These stresses normal to the bed joints have to be so small that they only affect the bed joint failure stresses but do not change the failure pattern. However, the toothed pattern is not likely to occur under conditions of significant shear stresses and the typical diagonally stepped pattern is expected.

As was the case for the previous failure mode, it is assumed that the joint reaching its strength first (bed or head joint) will sustain that stress up to failure. The failure will occur when the stresses on the other joints within the small assemblage element shown in Figure 5.6.a reach their strength. This implies that some stress redistribution and nonlinear deformations will take place in the mortar joints prior to the debonding failure. This condition is more likely to be satisfied in most cases since, under most loading configurations, both bed and head joints are stressed. In other words, the compatibility of deformations implies that the tensile stresses on one joint is always accompanied by shear stresses on the perpendicular joint. This means that the joint controlling the failure will reach its strength level quite close to the strength level of the other joint. Moreover, for a small element such as the one shown in Figure 5.6.a, the assumption of complete sharing between the adjacent perpendicular joints within the element can be reasonably adopted. This assumption was suggested by Baker [22] for brickwork and experimental results for blockwork in this investigation and elsewhere [44] indicated similar behaviour.
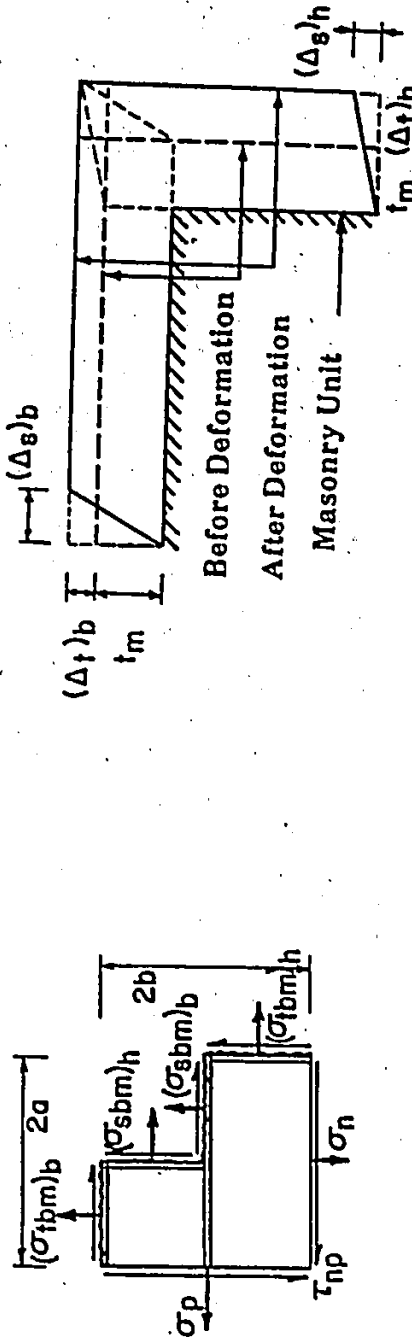
(a) Stresses on Free Body at Failure
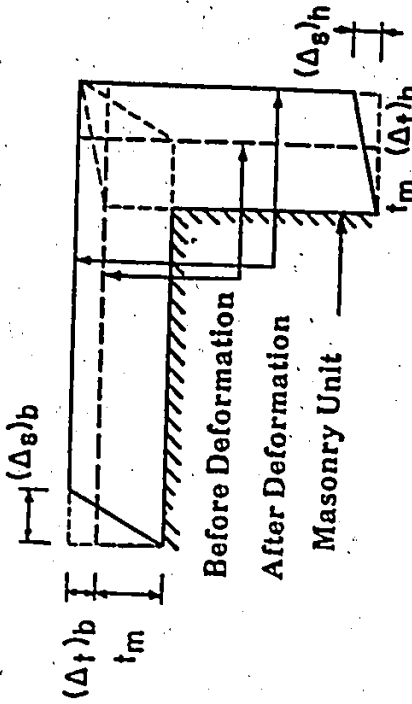
(b) Compatibility of Displacements Along Bed and Head Joints Under Shear and Tensile Stresses
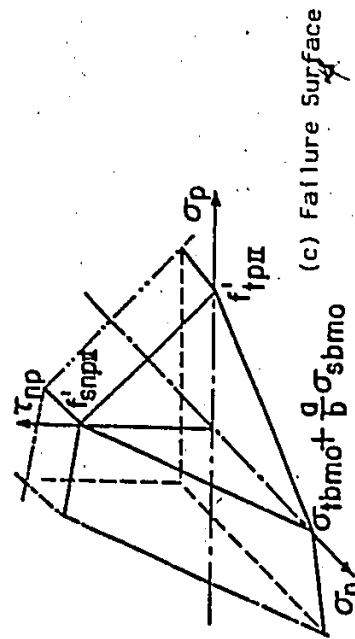
(c) Failure Surface

Figure 5.6   Strength of Masonry Assemblages in Debonding Along Bed and Head Joints

In this section, the strength sub-criterion for the diagonally stepped pattern will be derived. Here it should be noted that, the vertically toothed pattern is in fact a particular case of the general diagonally stepped pattern where the assemblage is primarily subjected to primarily tension parallel to the bed joints. The equilibrium of forces on the free body shown in Figure 5.6.a for this failure mode is given by:

$$\tau_{np} + \frac{b}{a}\sigma_p = (\sigma_{sbm})_b + \frac{b}{a}(\sigma_{tbm})_h$$

$$\tau_{np} + \frac{a}{b}\sigma_p = (\sigma_{sbm})_h + \frac{a}{b}(\sigma_{tbm})_b$$

(5.13)

Where, the subscripts b and h on the parentheses refers to the bed and head joints, respectively. At failure, both bed and head joints reach their strength level which is represented by the joint strength interaction (Equation 5.2). This equation can be rewritten for both joints as follows:

$$\frac{(\sigma_{sbm})_b}{\sigma_{sbmo}} + \frac{(\sigma_{tbm})_b}{\sigma_{tbmo}} = 1$$

(5.14.a)

$$\frac{(\sigma_{sbm})_h}{\sigma_{sbmo}} + \frac{(\sigma_{tbm})_h}{\sigma_{tbmo}} = 1$$

(5.14.b)

Equations 5.13 and 5.14 represent an indeterminate system which cannot be solved with these equations only. Then, the compatibility of deformations for both bed and head joints is needed to provide the

additional equation.

Due to loading, deformations will take place in both directions normal and parallel to bed joints as shown in Figure 5.6.b. For the deformations to be compatible, the total displacement in either direction may be considered as the displacement due to shear on a joint and simultaneously the displacement due to tension on the perpendicular joint. The compatibility equations will be derived for elastic behaviour. This is considered to be applicable up to the limit where one of the two perpendicular joints reaches its strength level. Thereafter, it is assumed that stress redistribution will take place and this joint will behave plastically. However, due to the limited nonlinearity expected, equivalent linear behaviour was assumed as an approximation with equivalent or apparent constants for stress-strain relationships other than the elastic constants.

For the compatibility of the displacements in the directions parallel and normal to the bed joints shown in Figure 5.6.b, the following relations have to be satisfied:

$$(\Delta_s)_b = (\Delta_t)_h$$
$$(\Delta_s)_h = (\Delta_t)_b \tag{5.15}$$

Where, Δ_s and Δ_t are the total displacements in shear and tension, respectively.

Under the action of uniform stresses, the displacements can be determined as follows:

$$\Delta_s = \sigma_{sbm} \frac{1}{G_m} t_m$$

$$\Delta_t = \sigma_{tbm} \frac{1}{E_m} t_m \qquad\qquad (5.16)$$

Where,

t_m is the thickness of the mortar joint and

E_m and G_m are the equivalent or apparent linear modulus of elasticity and the equivalent or apparent linear shear modulus of the mortar joints at failure, respectively.

Then, by substituting Equations 5.16 in Equations 5.15, the following relations are obtained:

$$(\sigma_{tbm})_h = \frac{(E_m)_h}{(G_m)_b} (\sigma_{sbm})_b$$

$$\qquad\qquad (5.17)$$

$$(\sigma_{tbm})_b = \frac{(E_m)_b}{(G_m)_h} (\sigma_{sbm})_h$$

The available equations are now six equations for equilibrium, strength and compatibility. However, there are only five unknowns which are the four internal stress components on the bed and head joints and the combined effect of the external stresses (σ_n, σ_p and τ_{np}). Therefore, an extra condition is required in order to have a unique solution for the above system of equations. This condition, as will be shown, implies the simultaneous failure of both bed and head joints.

By substituting for the head joint stresses from the compatibility equations (Equations 5.17) into the equilibrium equations

(Equations 5.13), these equilibrium equations can be written in terms of the bed joint stresses only as follows:

$$\tau_{np} + \frac{b}{a}\sigma_p = (\sigma_{sbm})_b \left[1 + \frac{b}{a}\frac{(E_m)_h}{(G_m)_b} \right]$$

$$\tau_{np} + \frac{a}{b}\sigma_n = (\sigma_{tbm})_b \left[\frac{(G_m)_h}{(E_m)_b} + \frac{a}{b} \right] \tag{5.18}$$

Now, By substituting for the bed joint stresses from Equations 5.18 into the failure condition for the bed joints (Equation 5.14.a), the following equation can be obtained:

$$\frac{\tau_{np} + \frac{b}{a}\sigma_p}{\sigma_{sbmo}\frac{(E_m)_h}{(G_m)_b}\left[\frac{(G_m)_b}{(E_m)_h} + \frac{b}{a}\right]} + \frac{\tau_{np} + \frac{a}{b}\sigma_n}{\sigma_{tbmo}\left[\frac{(G_m)_h}{(E_m)_b} + \frac{a}{b}\right]} = 1 \tag{5.19}$$

This is the expression which describes the strength along the bed joints for this stepped mode of failure but not necessarily along the head joints.

Alternatively, the equilibrium equations (Equations 5.13) can be written in terms of the head joint stresses by substituting for the bed joint stresses in these equations from the compatibility equations (Equations 5.17) as follows:

$$\tau_{np} + \frac{a}{b}\sigma_n = (\sigma_{sbm})_h \left[1 + \frac{a}{b}\frac{(E_m)_b}{(G_m)_h} \right] \tag{5.20.a}$$

$$\tau_{np} + \frac{b}{a} \sigma_p = (\sigma_{tbm})_h \left[\frac{(G_m)_b}{(E_m)_h} + \frac{b}{a} \right] \qquad (5.20.b)$$

By substituting Equations 5.20 into the equation for the head joint failure condition (Equation 5.14.b), the following equation can be obtained:

$$\frac{\tau_{np} + \frac{b}{a} \sigma_p}{\sigma_{tbmo} \left[\frac{(G_m)_b}{(E_m)_h} + \frac{b}{a} \right]} + \frac{\tau_{np} + \frac{a}{b} \sigma_n}{\sigma_{sbmo} \frac{(E_m)_b}{(G_m)_h} \left[\frac{(G_m)_h}{(E_m)_b} + \frac{a}{b} \right]} = 1 \qquad (5.21)$$

This is the expression which describes the strength along the head joints for this stepped mode of failure but not necessarily along the bed joints.

The condition to ensure the simultaneous failure on both bed and head joints which is also the extra condition needed to have a solution satisfying all six equations is that Equations 5.19 and 5.21 have to be identical. This means that

$$\sigma_{sbmo} \frac{(E_m)_h}{(G_m)_b} = \sigma_{tbmo}$$

or,

$$\frac{(E_m)_h}{(G_m)_b} = \frac{\sigma_{tbmo}}{\sigma_{sbmo}}$$

and

$$\frac{(E_m)_b}{(G_m)_h} = \frac{\sigma_{tbmo}}{\sigma_{sbmo}} \qquad (5.22)$$

Accordingly, the failure condition for debonding along a combination of bed and head joints is given by:

$$\frac{\tau_{np} + \frac{b}{a} \sigma_p}{\sigma_{tbmo} \left[\frac{\sigma_{sbmo}}{\sigma_{tbmo}} + \frac{b}{a} \right]} + \frac{t_{np} + \frac{a}{b} \sigma_n}{\sigma_{tbmo} \left[\frac{\sigma_{sbmo}}{\sigma_{tbmo}} + \frac{a}{b} \right]} = 1 \qquad (5.23)$$

Which can be rewritten as follows:

$$\frac{\sigma_n}{\left(\frac{b}{a} \sigma_{sbmo} + \sigma_{tbmo} \right)} + \frac{\sigma_p}{\left(\frac{a}{b} \sigma_{sbmo} + \sigma_{tbmo} \right)}$$

$$+ \tau_{np} \left[\frac{1}{\left(\sigma_{sbmo} + \frac{a}{b} \sigma_{tbmo} \right)} + \frac{1}{\left(\sigma_{sbmo} + \frac{b}{a} \sigma_{tbmo} \right)} \right] = 1 \qquad (5.24)$$

This expression represents the failure condition in the tension-tension region of normal stresses for this failure mode which involves debonding along a combination of bed and head joints.

The failure mode discussed in this section may occur also under compressive stress normal and/or parallel to the bed joints with the other stress components as long as these compressive stresses are not so high that they change the mode of failure as noted earlier in Section 5.6.1. In this case, the failure condition can be obtained by changing the bond tensile strength, σ_{tbmo}, to the normal stress at zero shear according to Coulomb's straight line, σ_{cbmo}, in the part of Equation 5.24 with σ_n or σ_p in compression. The resulting failure condition is

one of the following expressions:

for only σ_n in compression:

$$\frac{\sigma_n}{\sigma_{sbmo}\left(\dfrac{b}{a}-\dfrac{1}{\mu}\right)} + \frac{\sigma_p}{\left(\dfrac{a}{b}\,\sigma_{sbmo}+\sigma_{tbmo}\right)}$$

$$+ \tau_{np}\left[\frac{1}{\left(\sigma_{sbmo}+\dfrac{b}{a}\,\sigma_{tbmo}\right)} - \frac{1}{\sigma_{sbmo}\left(1-\dfrac{a}{b}\dfrac{1}{\mu}\right)}\right] = 1 \qquad (5.25)$$

,for only σ_p in compression:

$$\frac{\sigma_n}{\left(\dfrac{b}{a}\,\sigma_{sbmo}+\sigma_{tbmo}\right)} + \frac{\sigma_p}{\sigma_{sbmo}\left(\dfrac{a}{b}-\dfrac{1}{\mu}\right)}$$

$$+ \tau_{np}\left[\frac{-1}{\sigma_{sbmo}\left(1-\dfrac{b}{a}\dfrac{1}{\mu}\right)} + \frac{1}{\left(\sigma_{sbmo}+\dfrac{a}{b}\,\sigma_{tbmo}\right)}\right] = 1 \qquad (5.26)$$

,and for both σ_n and σ_p in compression:

$$\frac{\sigma_n}{\sigma_{tbmo}\left(\dfrac{b}{a}-\dfrac{1}{\mu}\right)} + \frac{\sigma_p}{\sigma_{sbmo}\left(\dfrac{a}{b}-\dfrac{1}{\mu}\right)}$$

$$- \tau_{np}\left[\frac{1}{\sigma_{sbmo}\left(1-\dfrac{b}{a}\dfrac{1}{\mu}\right)} + \frac{1}{\sigma_{sbmo}\left(1-\dfrac{a}{b}\dfrac{1}{\mu}\right)}\right] = 1 \qquad (5.27)$$

The failure surface for this mode is shown in Figure 5.6.c. The considerable interaction between the three stress components for this failure mode can be clearly seen in this figure particularly in the tension-tension quarter of normal stresses. It can also be seen in this figure that, where one or both normal stresses are compressive, the stresses at failure for the stepped mode increase as the level of precompression increases in either or both directions. These formulations confirm an earlier observation of increase in strength for brickwork couplets tested with precompression applied normal to the bed joints [22].

This mode of failure may also occur under uniaxial tension parallel to the bed joints or under pure shear. The uniaxial tension parallel to the bed joints results in a vertical toothed crack pattern whereas the pure shear case results in a diagonal stepped pattern. The strength of the assemblage failing in this mode by uniaxial tension parallel to the bed joints, f'_{tpII}, can be obtained from the general expression in Equation 5.24 where all but the second term are zero as follows:

$$f'_{tpII} = \sigma_{pl} \Big|_{\substack{\sigma_n=0 \\ \tau_{np}=0}} = -\frac{a}{b}\sigma_{sbmo} + \sigma_{tbmo} \qquad (5.28)$$

This is similar to the expression proposed by Drysdale and Hamid for in-plane tension [41] when the actual cross section was used in the strength calculations. Similarly, the strength for the diagonal stepped pattern due to pure shear, f'_{snpII}, is as follows:

$$f'_{snpII} = \tau_{npl}\Big|_{\substack{\sigma_n=0 \\ \sigma_p=0}}$$

$$= \frac{\left(\sigma_{sbmo} + \dfrac{a}{b}\sigma_{tbmo}\right)\left(\sigma_{sbmo} + \dfrac{b}{a}\sigma_{tbmo}\right)}{\left(\sigma_{sbmo} + \dfrac{a}{b}\sigma_{tbmo}\right)+\left(\sigma_{sbmo} + \dfrac{b}{a}\sigma_{tbmo}\right)} \qquad (5.29)$$

where all but the last term in Equation 5.24 are zero.

In this expression, the strength in pure shear or the diagonal tensile strength can be predicted as a function of the nominal block dimensions and the mortar bond characteristics. Earlier investigations empirically estimated this strength as a ratio of the square root of masonry compressive strength or semi-empirically as a ratio of the average of strengths normal and parallel to the bed joints [50]. However, as is indicated in Equation 5.29, the diagonal tensile strength for assemblages failing according to this mode is independent of the unit strength which is the controlling factor for assemblage compressive strength [50]. On the other hand, the semi-empirical approach cannot be judged as directly. In this case, the ratio of the diagonal tensile strength as in Equation 5.29 and the average of the two strengths normal and parallel to the bed joints, given in Equations 5.9 and 5.28, can be obtained as follows:

$$\frac{f'_{snpII}}{\frac{1}{2}\left(f'_{tn}+f'_{tpII}\right)}$$

$$= 2\ \frac{\dfrac{\sigma_{sbmo}}{\sigma_{tbmo}}\dfrac{b}{a}+1}{\dfrac{\sigma_{sbmo}}{\sigma_{tbmo}}+\dfrac{a}{b}+\dfrac{b}{a}+\dfrac{1}{R_{II}}\dfrac{\sigma_{sbmo}}{\sigma_{tbmo}}+\dfrac{a}{b}\dfrac{1}{R_{II}}+\dfrac{b}{a}R_{II}} \qquad (5.30)$$

Where, $R_{II}=\dfrac{f'_{tpII}}{f'_{tn}}$

As can be seen from Equation 5.30 and as is also shown in Figure 5.7, this ratio is not constant and it depends on the mortar bond properties, unit geometry and the strength ratio in the principal directions.

5.6.2.4 Strength for Splitting Through Masonry Units

In the failure mode involving splitting through masonry units, the failure plane runs through the masonry units and the mortar joints diagonally as shown in Figure 5.1. This failure plane may not be exactly a straight line because the weakest path may be that which passes through the minimum possible thickness and avoids the cross-webs in the case of hollow units. Due to the small thickness of the mortar joints relative to masonry unit dimensions (approaching 5% for concrete block units and 13% for brick units), for simplicity, the strength characteristics of the joints will be ignored and the joints will be considered part of the block. Also, since this failure can be considered to be a diagonal tension type of failure, the strength along
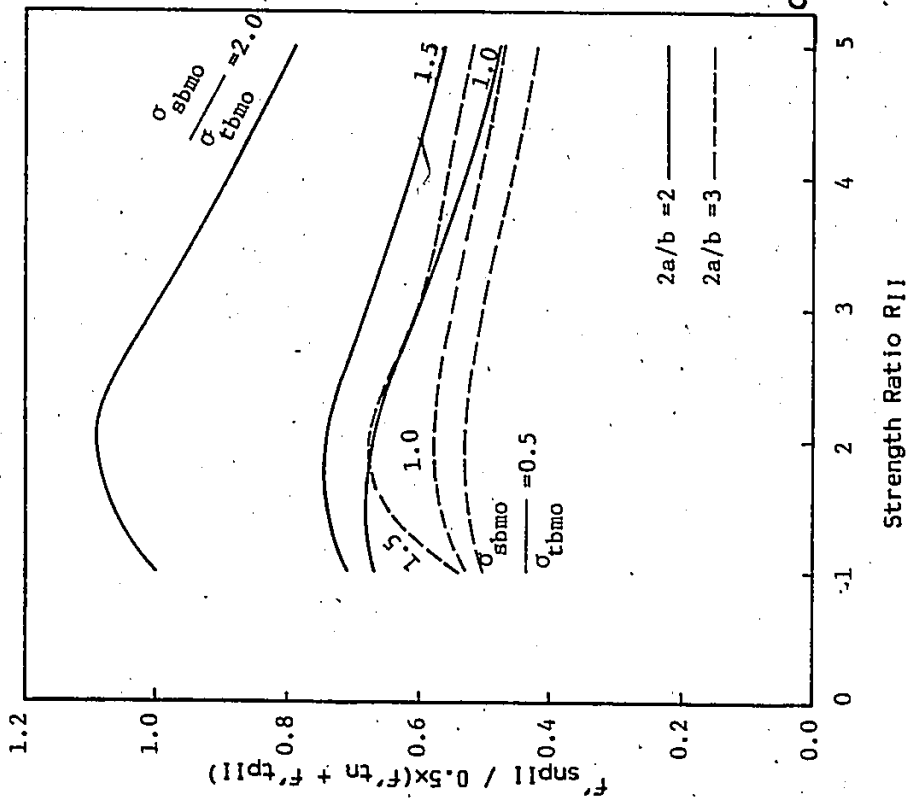
Figure 5.7   Ratio of Diagonal Tensile Strength to the Average of Tensile Strengths Normal and Parallel to the Bed Joints
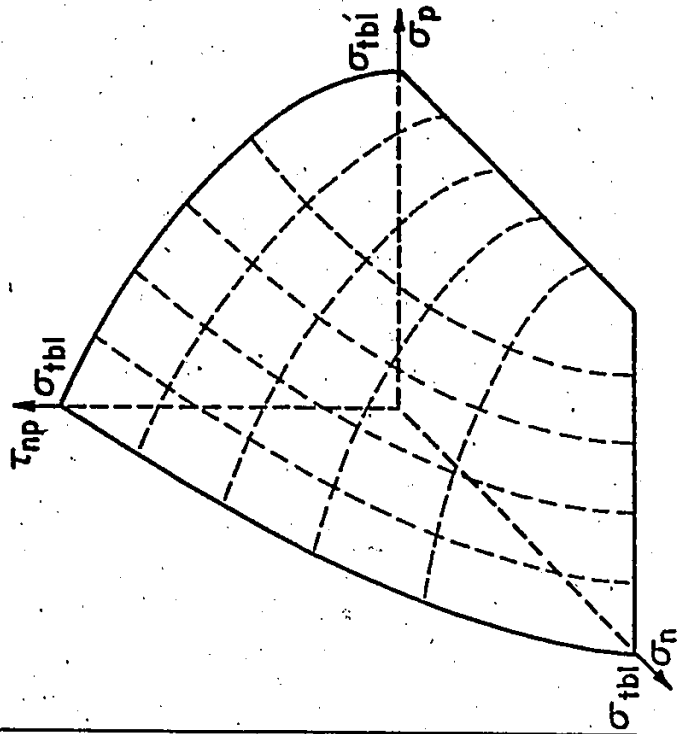
Figure 5.8   Failure Surface for the Strength of Masonry Assemblages in Diagonal Splitting Through the Units

the inclined failure plane can be assumed to be the same as the tensile strength of the masonry units, σ_{tbl}. Furthermore, it is assumed that this mode of failure occurs when the principal tensile stress reaches the prescribed tensile strength corresponding to Cowan's theory of failure adopted herein for masonry unit material.

Accordingly, for the controlling principal stress, the failure condition for an assemblage under biaxial stresses is as follows:

$$\sigma_{tbl} = \frac{\sigma_p + \sigma_n}{2} + [\; (\; \frac{\sigma_p + \sigma_n}{2} \;)^2 + \tau_{np}^2 \;]^{1/2} \qquad (5.31)$$

Isolating the square root term, squaring both sides and rearranging the above equation, the above expression may be written as follows:

$$(\; \frac{\tau_{np}}{\sigma_{tbl}} \;)^2 = (\; 1 - \frac{\sigma_n}{\sigma_{tbl}} \;)(\; 1 - \frac{\sigma_p}{\sigma_{tbl}} \;) \qquad (5.32)$$

which is the condition for diagonal splitting failure mode. The failure surface for this failure sub-criterion is shown in Figure 5.8. It should be noted here that this mode of failure is not likely to control except for the case of high shear stresses accompanied by compressive stresses parallel and/or normal to the bed joints which prestress the joints and prevent joint failures.

As can be indicated from Equation 5.32, this mode of failure may occur under uniaxial tension normal to the bed joints, uniaxial tension parallel to the bed joints or pure shear, f'_{snpl}, when the value of the respective stress reaches the unit tensile strength σ_{tbl}. However, other failure modes, in which mortar joints experience failure, yield

strength values less than σ_{tbl} for most practical ranges of masonry unit and mortar strength characteristics.

5.6.2.5 General Failure Envelope For Tension-Tension
States of Stress For Transverse Modes of Failure

A general failure criterion for masonry assemblages failing according to the different transverse failure modes can be constructed by combining the individual sub-criteria mentioned above. The general failure surface is obtained as the envelope of the controlling sub-criteria in the three dimensional stress space. This failure envelope may change significantly from one case to another depending on the strengths and the geometry of the component materials of the assemblage (i.e., σ_{tbmo}, σ_{sbmo}, σ_{tbl}, μ, $2a/b$). As an example, the failure envelope shown in Figure 5.9 was constructed using experimental data for blockwork reported by Drysdale and Hamid [41]. Upon constructing this envelope, both the strength and the respective failure mode of the assemblage can be predicted for any combination of stresses.

5.6.3   Orthogonal Strength Ratio

The ratio of the uniaxial strengths in the two principal material directions, parallel and normal to the bed joints, is known as the orthogonal strength ratio. The failure under uniaxial tension parallel to the bed joints may occur either by debonding along head joints and splitting of masonry units in alternate courses or by toothed failure through bed and head joints. Since this results in two different strengths, f'_{tpI} and f'_{tpII}, then it is necessary to have two

183
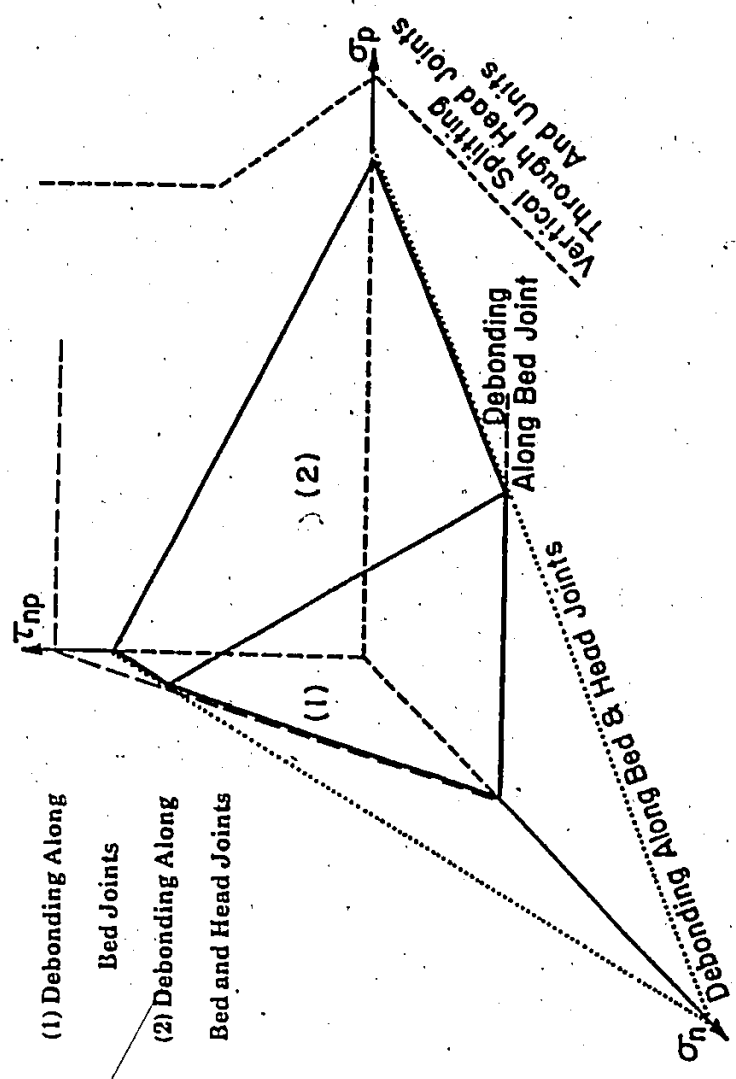
Figure 5.9   Failure Envelope in Biaxial
Tensile Stress Fields

σ_p

Vertical Splitting
Through Head Joints
And Units

Debonding
Along Bed Joint

Debonding Along Bed & Head Joints

σ_n

τ_{np}

(2)

(1)

(1) Debonding Along
Bed Joints

(2) Debonding Along
Bed and Head Joints

different strength ratios, R_I and R_{II}, according to the respective failure mode in tension parallel to the bed joints. Dividing Equations 5.12 and 5.28 by Equation 5.9, the expressions for the strength ratios are:

$$R_I = \frac{1}{2} + \frac{1}{2} \frac{\sigma_{tbl}}{f'_{tn}} \tag{5.33}$$

$$R_{II} = 1 + \frac{a}{b} \frac{\sigma_{sbmo}}{f'_{tn}} \tag{5.34}$$

which represent two families of curves for different unit strengths and different shear bond strengths.

Equation 5.33, which is the strength ratio expression for the failure through units and head joints under uniaxial tension parallel to the bed joints, is similar to that proposed by Baker [22]. It is even identical if no premature cracking takes place in the head joints up to the occurrence of failure through both head joints and units. This is consistently assumed throughout the derivation of the proposed criterion.

5.7 APPLICATION OF THE PROPOSED FAILURE CRITERION TO PREDICTING FAILURE OF MASONRY ASSEMBLAGES

In this section, the strength predictions using the proposed failure criterion for different masonry assemblages under different loading conditions are compared to the available experimental results to check the reliability of this proposal. These applications include cases of off-axis bending of blockwork wallettes, biaxial bending of brickwork joints and off-axis tension of blockwork prisms.

5.7.1 Off-Axis Bending of Concrete Blockwork Wallettes [47]

The reported [47] strengths of concrete blockwork wallettes tested in bending with the longitudinal axis at different angles from the bed joint orientation are compared in this section with the predicted strengths using the proposed criterion. Also, the adopted criterion for mortar joint strength is examined.

Even though these results were not intended to check the joint failure criterion, the measured value for shear bond strength is shown in Figure 5.10. Also shown are the stresses at failure for wallettes failing by debonding along bed joints for orientations of 90° and 75° from the longitudinal axis. Despite the relatively large variability of this data and despite having only one point on the interaction curve with combined shear and tension which is also close to the pure tension case, the decrease in the tensile stresses at failure resulting from introducing a small amount of shear is clearly indicated. This means that the assumption of no interaction (rectangular failure envelope) is unconservative. The linear or complete interaction shown seems to fit the data better.

For comparison purposes, the predicted strengths and the controlling failure modes for the tested wallettes are given in Table 5.1 together with the experimental results. Also, the failure envelope for off-axis flexural tensile strengths at different angles to the bed joint orientation is shown in Figure 5.11 along with these experimental results. Each data point in this figure represents the average of five
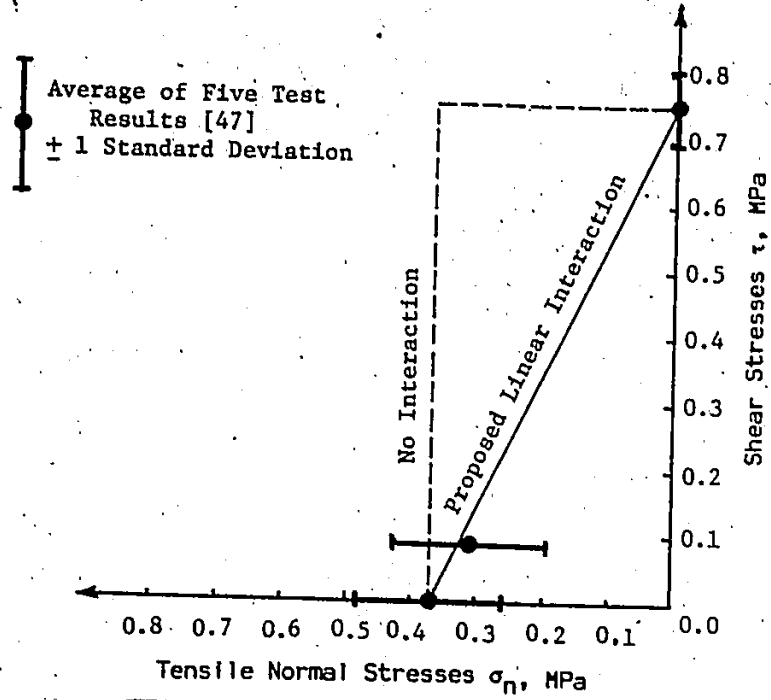
Figure 5.10   Strength of Mortar Joints in
Combined Shear and Tension

Table 5.1   Strength of Blockwork Wallettes in Off-Axis Bending

θ^o	Experimental Results		Predictions		$\dfrac{f'_{t\theta} \text{ pred.}}{f'_{t\theta} \text{ exp.}}$
	Strength MPa	Failure Mode	Strength MPa	Failure Mode	
0o	0.95	Vertical Toothed	1.07	Vertical Toothed	1.13
15o	0.78	Diagonal Stepped	0.71	Diagonal Stepped	0.91
45o	0.75	Diagonal Stepped	0.48	Bed Joint Debonding	
			0.54	Diagonal Stepped	0.71
75o	0.33	Bed Joint Debonding	0.35	Bed Joint Debonding	1.06
90o	0.37	Bed Joint Debonding	0.37	Bed Joint Debonding	1.00
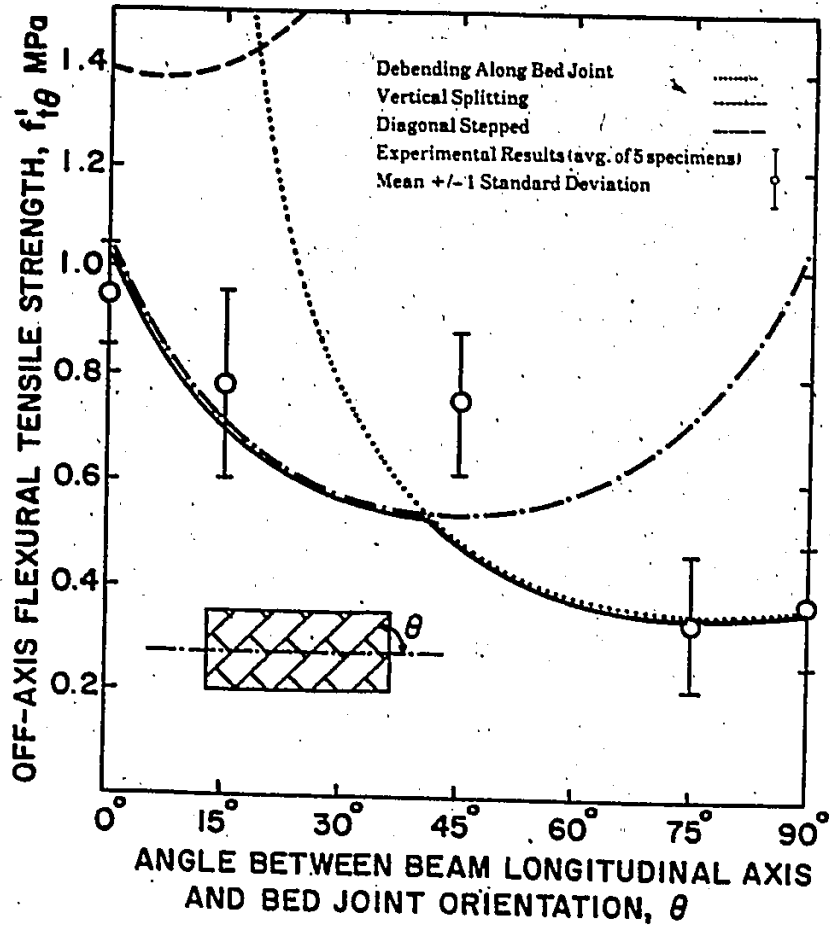
Figure 5.11   Strength Predictions of Blockwork Wallettes in Off-Axis Bending
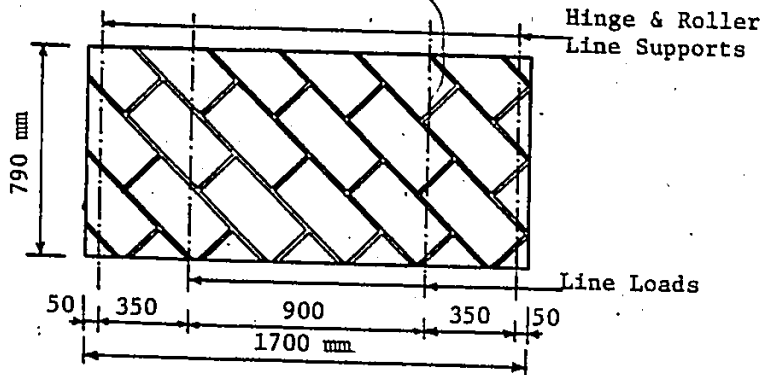
Figure 5.12   Plan View for Wallettes Having the Bed Joints Oriented at 45° From the Longitudinal Axis [47]

test results.

The comparison shown in Table 5.1 and Figure 5.11 indicated that, excluding the wallettes having 45° between the longitudinal axis and the bed joint orientation, the proposed criterion predictions for both strength and failure mode seem to agree very well with the available test results. The maximum difference is where the strength predictions is 13% higher than the test results in the strength for the vertically toothed failure pattern expected for bed joint orientation at 0° from the longitudinal axis as can be seen in Table 5.1. However, this difference between the predicted and experimental strengths can be attributed to the uneven number of bed and head joints in the wallette specimens. This is unlike the symmetric specimens considered for this investigation (see section 2.2.2.2) and the symmetric strip assumed in the criterion development. That is, for the four block wide wallettes, the flexural tension on the four blocks is resisted by flexural tensile bond on four head joints and torsional shear bond on only three bed joints. This results in 33% higher shear stresses. Accordingly, lower strength is expected for those specimens failing in the toothed pattern. To test this explanation, an analysis was performed where the shear bond stresses were increased by 33% in the proposed criterion. The strength for this mode of failure decreased to 0.9 MPa which is only 5% lower than the experimental strength reported for these wallettes.

For wallettes where the bed joints were oriented at 45° from the longitudinal axis, the proposed criterion predicts failure at 0.48 MPa by bed joint debonding as can be seen in Table 5.1 and Figure 5.11. In the reported test results, bed joint debonding was not observed in most

specimens but rather debonding along bed and head joints took place which is the next closest mode of failure to be expected. This change in mode of failure may be attributed to the specimen configuration and the loading system. According to the configuration shown in Figure 5.12, debonding along a bed joint can occur only on one bed joint within the maximum nearly constant moment zone. If this was not the weakest joint, then the mode of failure involving debonding along a bed joint cannot occur. It should be noted that, for this other mode of failure, the difference between the predicted and experimental strengths is relatively large compared to the other bed joint orientations as can be seen in Table 5.1. However, considering the inherent variability of the test results as indicated in Figure 5.11, this strength prediction may be considered to be satisfactory.

5.7.2 Orthogonal Strength Ratios For Wallette Tests [52]

Experimental test results for flexural tensile strengths normal and parallel to the bed joints were reported [52] for concrete blockwork wallettes. These wallettes were of different block sizes, different percentages of solid, different block strengths, different mortars, different grout strengths for grouted specimens and special conditions such as stack pattern, partial grouting and empty head joints. The calculated strength ratios from these experimental results are plotted in Figure 5.13 versus the flexural tensile strength normal to the bed joints. The proposed expressions for strength ratios (Equations 5.33 and 5.34) are also plotted on Figure 5.13 together with the two expressions proposed by Baker [22] for brickwork and the general
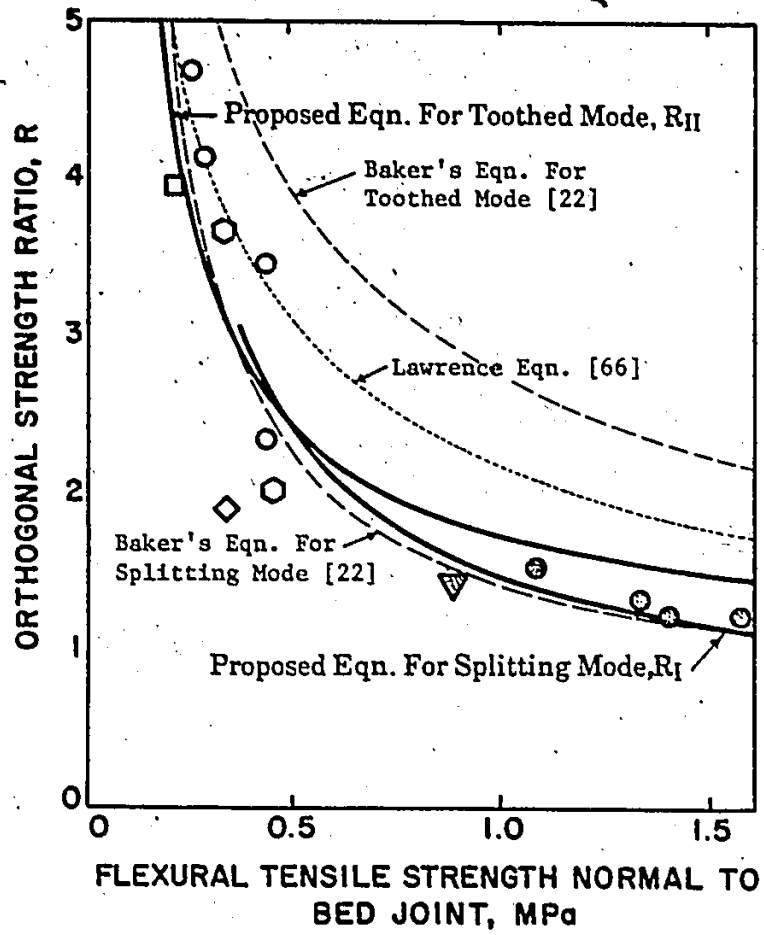
Figure 5.13   Orthogonal Strength Ratios for Blockwork Wallettes

empirical expression proposed by Lawrence [66]. In all strength ratio expressions, the available data for normal block and type S mortar were used. This is considered to be satisfactory since the strength of the normal block was approximately the average of all the reported strengths and type S mortar has been used for most specimens.

As shown in Figure 5.13, the strength ratios predicted using the proposed expressions are in reasonable agreement with the experimental results. This is true for both the splitting mode (reported for the grouted specimens) and the toothed mode (reported for the ungrouted specimens) for tension parallel to the bed joints. The strength ratios predicted according to the proposed expressions are also closer to the experimental results than those using Lawrence's empirical equation for all data and Baker's empirical equation for the toothed mode of failure.

5.7.3 Biaxial Bending of Brickwork Joints [22]

Baker [22] conducted two brickwork test series to investigate the possible interaction at failure between the flexural tensile stresses normal and parallel to the bed joints. In Figure 5.14, the test results are shown together with the elliptical relationship proposed by Baker [22] to best fit the experimental results. The fact that there are two different modes of failure was not incorporated in this relationship. Even though Baker reported these two failure modes, the empirical relationship could accommodate only one failure surface. The criterion proposed in this chapter is also included in Figure 5.14. It is also in reasonable agreement with the experimental results.
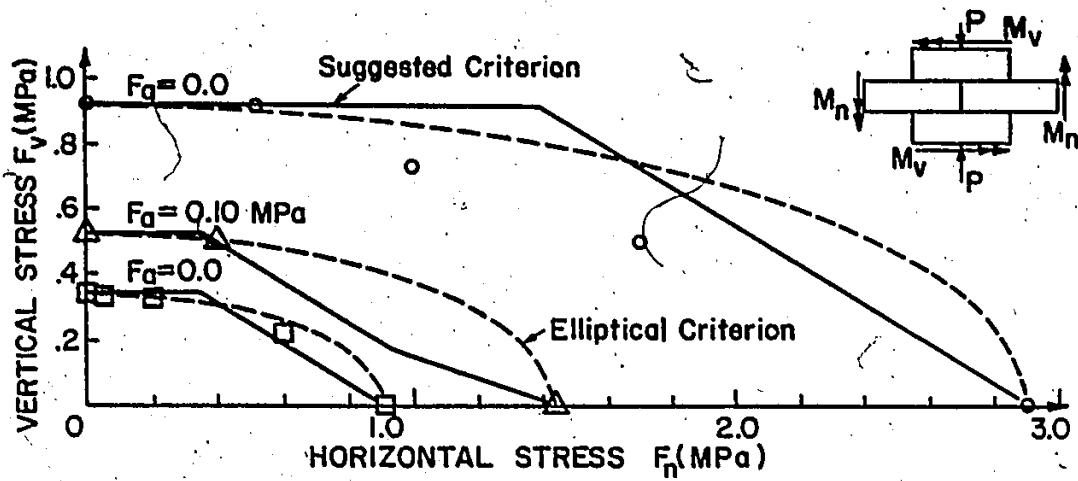
Figure 5.14   Strength of Brickwork Joints in Biaxial Bending
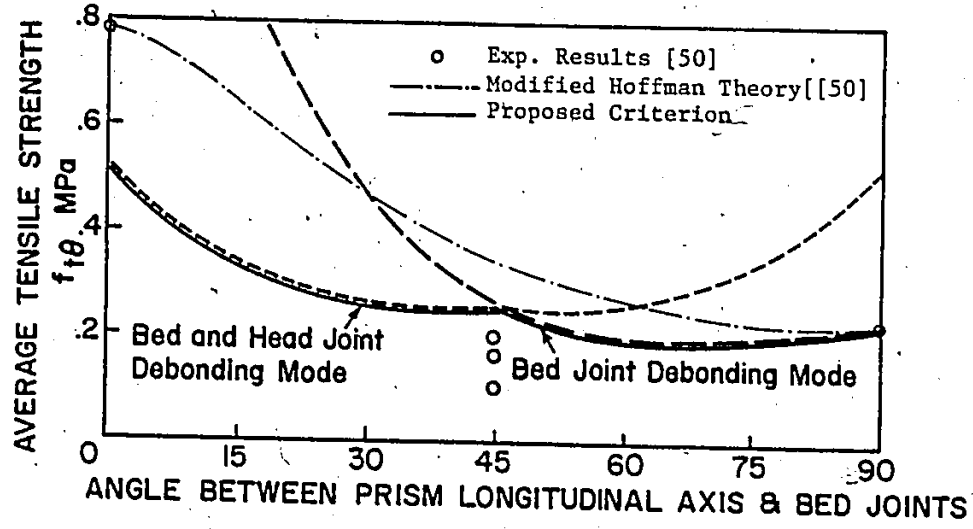
Figure 5.15   Strength of Prisms Under Off-Axis Tension

For Baker's Series IV test specimens with the 0.1 MPa precompression, the 0.18 MPa reported increase in the apparent tensile strength normal to the bed joint was thought to be due to the different stress-strain relationships for masonry assemblages in tension and compression. The failure criterion was not capable of directly accounting for such strength increases and therefore the method of stress calculation would have to incorporate this effect. However, the corresponding increases in the tensile stresses parallel to the bed joints at failure can be determined according to the failure criterion. This can be evaluated using the sub-criterion for the toothed mode of failure by introducing the 0.18 MPa as the compressive stresses normal to the bed joints on the extreme fibers at which the failure condition is reached. For this precompression case, the predicted interaction between the stresses normal and parallel to the bed joints is also shown in Figure 5.14 along with the experimental test results and the elliptical interaction relationship suggested by Baker [22]. As shown in this figure, the proposed criterion yielded reasonable predictions compared to the available experimental results

5.7.4 Off-Axis Tension of Blockwork Prisms [50]

Hamid [50] reported experimental test results for concrete blockwork prisms under direct tension with the bed joints oriented at 45° to the axis of loading. These results together with the tensile strengths normal and parallel to the bed joints as determined from splitting tests of masonry discs were replotted in Figure 5.15 to show the variation of the tensile strength with the bed joint orientation.

The modified Hoffman theory proposed by Hamid and Drysdale [51] and the criterion proposed in this investigation are also shown in Figure 5.15.

The proposed criterion prediction for the prisms having bed joints at 45° from the axis of loading, is closer to the experimental results than is the modified Hoffman theory. It also predicts the same mixed modes of failure as observed experimentally. The modified Hoffman theory passes through the points corresponding to the strengths normal and parallel to the bed joints because these points are input data for the determination of the constants and therefore are not predictions. However, as reported earlier for the proposed criterion, the assemblage strengths normal and parallel to the bed joints are not input but rather are predictions as a function of the component material strengths and geometries.

The large discrepancy shown in Figure 5.15 between the predicted and the experimental strengths parallel to the bed joints is not surprising since the experimental strength was not determined from direct tension tests but rather was from splitting tests of masonry discs. In these splitting tests, the lateral tensile stresses causing the splitting are accompanied by higher compressive stresses (at least three times the tension, according to the theory of elasticity) normal to the bed joints in this case. These compressive stresses significantly increase the shear capacity of the bed joints and hence prevent the failure from occurring in the toothed mode at the stress level predicted using the proposed criterion. Accordingly, the specimens failed, as reported experimentally, at higher stress level by debonding along head joints and splitting of blocks in alternate

courses.

For the strength normal to the bed joints, the failure occurs by debonding along a bed joint and the compressive stresses parallel to the failure plane are thought to have no effect on the strength.

5.8   CONCLUDING REMARKS

The following concluding remarks are drawn from the investigations and the discussions reported earlier in this chapter:

1. The strength of masonry assemblages differs significantly for different failure modes. These depend on the relative magnitude of the normal and shear stresses acting along the critical planes normal and parallel to the bed joints. Also, these modes of failure may differ according to the relative magnitudes of the different strengths of the component materials used for the assemblages.

2. None of the available biaxial failure criteria for masonry assemblages are appropriate as a generalized criterion for masonry because they do not include one or more of the requirements for such a generalized criterion. For instance, some of the requirements are to consider the anisotropic and composite nature of masonry, to account for the different failure modes, to include different unit strengths and geometries and mortar bond characteristics.

3. The available failure theories for orthotropic composite materials cannot be applied directly to masonry since all these theories have one or more faults. Examples of such faults are

not considering interaction between strengths, not considering interaction in a way that is consistent with observations for masonry, not considering different tensile and compressive strengths, being strictly phenomenological or overlooking of the failure modes.

4. The proposed criterion seems to be acceptable for masonry as it considers most of the preset requirements for a generalized criterion and is free of the summarized drawbacks of direct application of orthotropic failure theories to masonry.

5. In this criterion, the biaxial strengths are not determined in terms of the uniaxial assemblage strengths but rather both uniaxial and biaxial strengths are evaluated in terms of the component material strengths and geometries. This procedure generalizes the use of the criterion for any combination of unit strengths and mortar bond characteristics.

6. The predictions using the proposed criterion for the different cases of masonry assemblages considered seem to satisfactorily agree with the available experimental results.

CHAPTER 6

NONLINEAR MACROSCOPIC FINITE ELEMENT MODEL

FOR MASONRY ASSEMBLAGES

6.1   INTRODUCTION

Analyses of masonry assemblages using the finite element method
have been reported in many early investigations. In some of these
investigations, linear elastic macroscopic models were employed without
particular regard to the mortar joints. These models suffered from the
obvious inability to fully recognize the presence of mortar joints as
particular planes of weakness. The alternative of using a microscopic
models does have potential for including the specific material and
geometric properties. However, the very large number of elements needed
to separately model the component materials and their interfaces renders
this approach impractical where analyses of many wall configurations are
necessary.

It is the purpose of this chapter to describe a recently
developed macroscopic finite element model which can be used to
efficiently predict the capacity and behaviour of full scale masonry
walls and large structural elements. In this chapter, the existing
finite element models for masonry are reviewed and the developed model
is described. Then, a verification study for the model is performed and
the model predictions are compared to available solutions in the
literature for linear and nonlinear analyses. Finally, model

predictions for capacity and behaviour of full scale masonry walls are compared to test results from this investigation to judge the reliability of the model predictions for masonry walls.

6.2   EXISTING FINITE ELEMENT MODELS FOR MASONRY

Finite element modelling of large scale structural masonry assemblages originally employed standard linear elastic concepts. In these models, average properties in the context of assumed isotropic elastic behaviour greatly simplified their development. However, this form of analysis cannot fully recognize the presence of mortar joints as particular planes of weakness and it ignores the anisotropic and composite nature of masonry. Also, this simple method of analysis is only applicable up to first cracking so that any reserve of strength after first cracking is neglected. Moreover, for out-of-plane bending, the transverse shear deformations which will be shown to be significant for hollow block walls are ignored. This subject is discussed in more detail later in this chapter.

To include the presence of mortar joints as planes of weakness, a more microscopic approach was proposed [25] using different continuum elements to separately model the mortar joint and masonry unit materials. However, rather than using the properties of the mortar, the bond strengths of the mortar/unit interface were used for the shear and tensile strengths of the mortar. Since masonry usually experiences failure by debonding along mortar joints, this procedure avoided modelling the mortar/unit interface.

Another microscopic model was proposed [11] to model masonry as a discontinuous system where the discontinuities consisted of mortar joints. Besides the separate modelling of mortar and masonry unit materials (as well as grout and steel reinforcement, if present), the physical behaviour of the interfaces between different materials was added by introducing double node pairs (one on each side of each interface). The interconnection between the double nodes was specified to simulate the interface behaviour.

A third microscopic model was developed [79,80] from the analogy of the behaviour of masonry assemblages and jointed rock [48]. In this approach, the masonry units were modelled as linear elastic continuum elements and the mortar joints were modelled as linkage or joint elements.

The microscopic models mentioned above accounted for the composite nature of masonry and incorporated the inherent nonlinearity due to both mortar joint behaviour and progressive joint failure. However, application of these models for the analysis of large structural masonry elements and structures is extremely difficult due to the very large number of elements needed to separately model the component materials and their interfaces. Moreover, the development of these models was limited to in-plane loading cases. Also, the anisotropic nature of the masonry units was not incorporated into these models.

Seward [89] used a finite element package to analyse brickwork panels subjected to lateral loading without particular regard to the mortar joints in constructing the finite element mesh. In this finite

element analysis, the stiffness orthotropy and the directional dependence of the flexural tensile strength were taken into account where an elliptical transition was assumed between the two orthogonal strength values. However, no interaction between stresses in the two orthogonal directions was included in this model. The analysis was extended after the initial formation of cracks with the stiffness of the cracked element set to zero in the respective direction regardless of the crack pattern within the element. An observation is that this procedure resulted in considerable softening of the wall because of disregarding the stiffness of the element over the thickness and not only the tension zone. Also, there was no indication that the crack direction is affected by the mortar joint planes as planes of weakness. It was also assumed in this analysis that although an element loses all its bending stiffness after cracking, it still retains the ability to resist shear. However, this assumption is not realistic and, as stated by Seward, may not always be reasonable. Analyses were compared to experimental data where it yielded acceptable predictions for one case [107] and poor predictions for the other [92]. An additional negative aspect of use of this model for blockwork is that it did not account for transverse shear deformations.

Recently, Page, Kleemen and Dhanasekar [81] proposed an in-plane macroscopic finite element model for brick masonry. This model included the nonlinear deformations and progressive local failure either through joints or in modes involving both bricks and joints. The deformation relationships and failure criterion proposed in this model were derived

from biaxial test results of half scale brick masonry panels with different bed joint orientations. The presence of the mortar joints as particular planes of weakness was considered in the failure criterion adopted in this model. However, this model was limited to in-plane isotropic behaviour of one wythe solid walls.

6.3 PROPOSED FINITE ELEMENT MODEL FOR MASONRY ASSEMBLAGES

As a result of the above review, it was thought that none of the available finite element models or general purpose packages can efficiently be used for the analysis of laterally loaded masonry panels and specifically where hollow units are used. Accordingly, the proposed macroscopic finite element model was constructed to efficiently predict the capacity and the behaviour of full scale masonry walls and large structural elements. In this model, the masonry element is discretized to finite elements without particular regard to the position of the mortar joint planes. This means that some mortar joints will be included within the macro-element. However, the failure criterion adopted in this model, as reported in Chapter 5, considered not only the occurrence of failure but also the failure pattern with respect to the mortar joints.

The proposed model has been developed in a generalized form to handle both in-plane and out-of-plane loading conditions so that it can be used for analysing most masonry assemblages. This feature was achieved by incorporating both in-plane and out-of-plane degrees of freedom in the element formulation. Also, the proposed model can be used for the analysis of hollow masonry and multiwythe walls by adopting

a layered plate approach in the finite element formulation. Moreover, orthotropic properties were included for each layer to improve the acceptability of the macroscopic approach.

6.4 SIGNIFICANCE OF TRANSVERSE SHEAR DEFORMATIONS
AND LAYER ORTHOTROPY IN HOLLOW BLOCK MASONRY

A part of a hollow concrete block assemblage is shown in Figure 6.1. It clearly indicates the orthotropy of the face shells due to the different distributions of mortar joints normal and parallel to the bed joints. It also indicates the orthotropy of the core layer due to the presence and the orientation of the webs.

The longitudinal section parallel to the bed joints of a hollow concrete block wall as shown in Figure 6.1 has the appearance of a Vierendeel truss. When these walls are subjected to out-of-plane bending about the vertical axis, some significant transverse shear deformations may be experienced because of the presence of the relatively flexible webs connecting the face shells. In order to judge the significance of the shear deformations in the case of hollow concrete masonry, a longitudinal strip of a masonry wall supported along the two vertical sides was analysed using three different methods. First, it was analysed as a Vierendeel truss [74]. This was considered to represent the actual behaviour of this strip. Second, a beam theory analysis, which corresponds to the case of negligible shear deformations was done. Third, a sandwich panel analysis [7] was employed, in which the cross webs were replaced by an equivalent shear lamina.
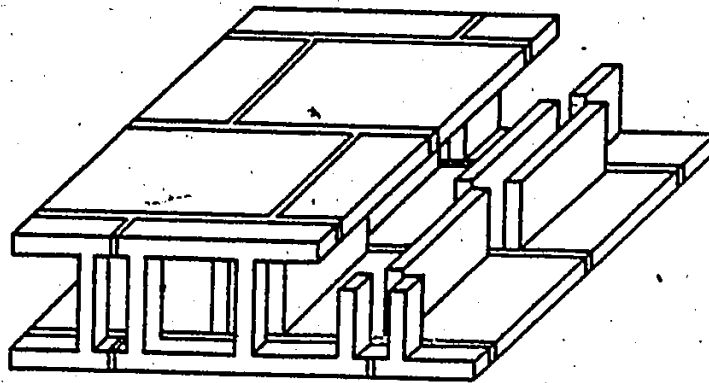
Figure 6.1   Anatomy of a Typical Hollow Concrete Block Assemblage

In all of the analyses, representative values were used for the block and mortar properties. Also, uniformly distributed loading was specified and relatively large span to depth ratios were used. Both the uniformly distributed load and the long spans tend to minimize any transverse shear effects. However, the Vierendeel truss analysis showed that neglecting the transverse shear resulted in significantly less deflections. For instance, ignoring shear deformations for a 5 m span and standard 190 mm thick hollow concrete blocks resulted in 14% less deflection. Modelling the section using the sandwich panel approach with an equivalent core layer gave slightly smaller deflections. For the above case, these were 6% less than predicted using the Vierendeel model. To confirm the above accuracy for other spans, the analyses were also performed for a 1.8 m span and the same concrete blocks. The elastic beam analysis yielded 50% less deflection than the Vierendeel analysis whereas the sandwich panel approach gave 12% less deflection compared to using the Vierendeel model. Hence, it was decided that transverse shear deformations can be significant in the case of laterally loaded hollow block masonry and that the cross webs may be replaced by an equivalent lamina or core layer with an acceptable accuracy. It should also be noted that due the discontinuity of the webs shown in Figure 6.1, shear deformations are also considered in the direction normal to the bed joints.

6.5 FINITE ELEMENT FORMULATION

Transverse shear deformations are known to have significant effects on behaviour of sandwich panels [7] and cellular plates [26]

and, as shown in the previous section, even on the horizontal bending of hollow block walls. Therefore, in the formulation of the plate type masonry element, the assumptions adopted by Mindlin [73] are used. These include that the deflections of the plate are small, stresses normal to the middle surface are negligible irrespective of the loading, and normals to the middle surface before deformation remain straight but not necessarily normal to the middle surface after deformation. As discussed elsewhere [59,60,82], the last assumption is not completely valid since some warping of the type shown in Figure 6.2 does occur as part of the shear deformation. However, a correction can be made to partially allow for the non-uniform shear distribution. Therefore, in Figure 6.2, θ_x and θ_y can be considered as the average total section rotations about the y and x axes, respectively, where

$$
\left\{ \begin{array}{c} \theta_x \\ \theta_y \end{array} \right\} = \left\{ \begin{array}{c} \dfrac{\partial w}{\partial x} + \phi_x \\ \dfrac{\partial w}{\partial y} + \phi_y \end{array} \right\}
\tag{6.1}
$$

with w as the transverse deflection in the z direction, and ϕ_x and ϕ_y are the uniform shear deformations in the x-z and y-z planes, respectively.

To accommodate both in-plane and out-of-plane loading and displacements, it was decided that the masonry finite element should include all in-plane and out-of-plane (including transverse shear) degrees of freedom. These were included by combinig the 8 degree of freedom (DOF) rectangular plane stress element, the 12 DOF non-

ACTUAL DEFORMATION

ASSUMED DEFORMATION

NORMAL TO MID-SURFACE AFTER DEFORMATION

θ_x

$\frac{\partial w}{\partial x}$

ϕ_x

MID-PLANE
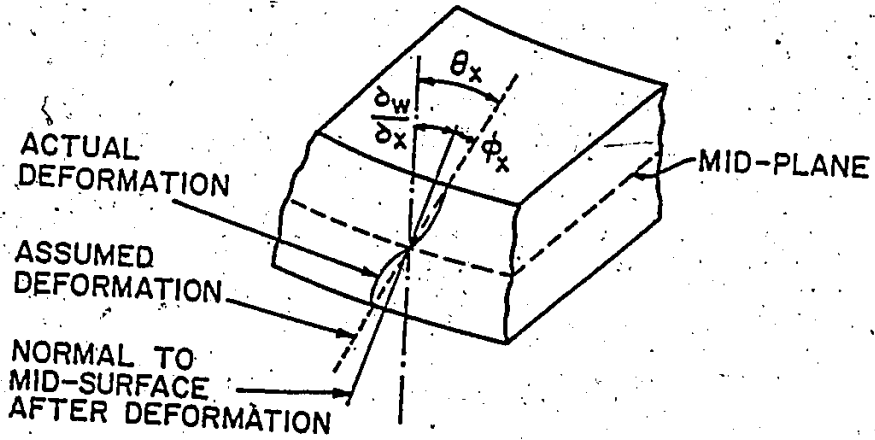
Figure 6.2   Deformation of the Cross Section of a Homogeneous Plate [60]
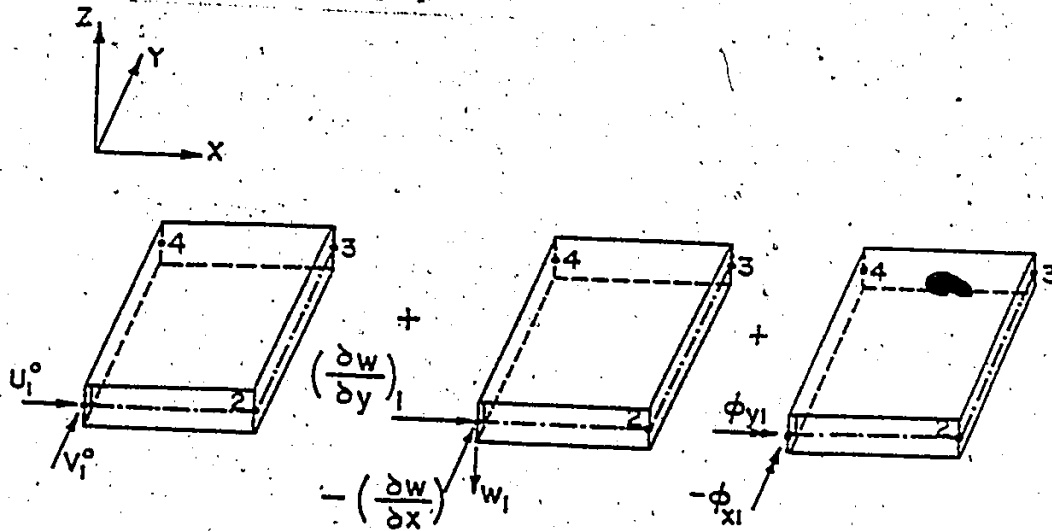
EXTENSION (8 DOF) + FLEXURE (12 DOF) + SHEAR (8 DOF)

$$w = [1,x,y,x^2,xy,y^2,x^3,$$
$$x^2y,xy^2,y^3,x^3y,xy^3][a_k]$$
$$(k = 9,20)$$

$$u^o = [1,x,y,xy][a_i]$$
$$(i = 1,4)$$

$$v^o = [1,x,y,xy][a_j]$$
$$(j = 5,8)$$

$$\theta_x = \frac{\partial w}{\partial x} + \phi_x$$

$$\theta_y = \frac{\partial w}{\partial y} + \phi_y$$

$$\phi_x = [1,x,y,xy][a_l]$$
$$(l = 21,24)$$

$$\phi_y = [1,x,y,xy][a_m]$$
$$(m = 25,28)$$

Figure 6.3   Displacement Fields for Rectangular Plate Elements (28 DOF)

conforming rectangular plate bending element and the 8 DOF rectangular transverse shear element. This resulted in the 28 DOF element shown in Figure 6.3 in which the different displacement fields of the middle surface are given. For the displacement field through the thickness of the plate, the following relations are applicable:

$$
\{ u \} = \begin{Bmatrix} u(x,y,z) \\ v(x,y,z) \\ w(x,y) \end{Bmatrix} = \begin{Bmatrix} u^{0}(x,y) - z\theta_{x}(x,y) \\ v^{0}(x,y) - z\theta_{y}(x,y) \\ w(x,y) \end{Bmatrix}
\tag{6.2}
$$

where u,v and w are the displacements in the coordinate directions x, y and z, respectively, and u^0 and v^0 are the corresponding displacements of the middle surface.

Using the displacements in Equation 6.2 and following the small displacement assumption, the strains can be written as:

$$
\{ \varepsilon \} = \begin{Bmatrix} \{\varepsilon_{ef}\} \\ \hline \{\varepsilon_{s}\} \end{Bmatrix}
$$

or

$$
\{ \varepsilon \} = \begin{Bmatrix} \varepsilon_{x}^{0} - z(\dfrac{\partial^{2}w}{\partial x^{2}} + \dfrac{\partial\phi_{x}}{\partial x}) \\[2ex] \varepsilon_{y}^{0} - z(\dfrac{\partial^{2}w}{\partial y^{2}} + \dfrac{\partial\phi_{y}}{\partial y}) \\[2ex] \gamma_{xy}^{0} - z(2\dfrac{\partial^{2}w}{\partial x \partial y} + \dfrac{\partial\phi_{x}}{\partial y} + \dfrac{\partial\phi_{y}}{\partial x}) \\[1ex] \hline - \phi_{x} \\[1ex] - \phi_{y} \end{Bmatrix}
\tag{6.3}
$$

where $\varepsilon_x{}^o$, $\varepsilon_y{}^o$ and $\gamma_{xy}{}^o$ are the middle surface strains and $\{\varepsilon_{ef}\}$ and $\{\varepsilon_s\}$ are the extension/flexure and the shear components of strain, respectively.

The curvatures $\{x\}$ including the transverse shear are then given by:

$$\{x\} = \begin{Bmatrix} x_x \\ x_y \\ x_{xy} \end{Bmatrix} = \begin{Bmatrix} -\left(\dfrac{\partial^2 w}{\partial x^2} + \dfrac{\partial \phi_x}{\partial x} \right) \\[2ex] -\left(\dfrac{\partial^2 w}{\partial y^2} + \dfrac{\partial \phi_y}{\partial y} \right) \\[2ex] -\left(2\dfrac{\partial^2 w}{\partial x\, \partial y} + \dfrac{\partial \phi_x}{\partial y} + \dfrac{\partial \phi_y}{\partial x} \right) \end{Bmatrix} \tag{6.4}$$

and lead to the following modified strain expression:

$$\{\varepsilon\} = \left\{ \frac{\{\varepsilon_{ef}\}}{\{\varepsilon_s\}} \right\} = \begin{Bmatrix} \varepsilon_x{}^o + z\, x_x \\[1ex] \varepsilon_y{}^o + z\, x_y \\[1ex] \gamma_{xy}{}^o + z\, x_{xy} \\ \hline - \phi_x \\[1ex] - \phi_y \end{Bmatrix} \tag{6.5}$$

and

$$\{\varepsilon_{ef}\} = \{\varepsilon^o\} + \{\varepsilon_f\} = \begin{Bmatrix} \varepsilon_x{}^o \\ \varepsilon_y{}^o \\ \gamma_{xy}{}^o \end{Bmatrix} + z \begin{Bmatrix} x_x \\ x_y \\ x_{xy} \end{Bmatrix} \tag{6.6}$$

Now, using the displacement fields as shown in Figure 6.3 for the rectangular plane stress, plate bending and transverse shear elements mentioned before, i.e.

$$u^o(\xi,\eta) = \sum_{i=1}^{4} N_i^o(\xi,\eta)u_i^o$$

$$v^o(\xi,\eta) = \sum_{i=1}^{4} N_i^o(\xi,\eta)v_i^o$$

$$w(\xi,\eta) = \sum_{i=1}^{12} N_i(\xi,\eta)w_i \qquad\qquad (6.7)$$

$$\phi_x(\xi,\eta) = \sum_{i=1}^{4} N_i^S(\xi,\eta)\phi_{x(i)}$$

$$\phi_y(\xi,\eta) = \sum_{i=5}^{8} N_i^S(\xi,\eta)\phi_{y(i-4)}$$

In terms of the non-dimensional ξ,η axes shown in Figure 6.4 and the different shape functions N_i^o, N_i and N_i^S, the respective strains can be easily derived via the derivatives of the shape functions as required in Equation 6.3 or 6.5. The different shape functions are listed in Appendix D. The resulting generalized strain matrix $[\bar{B}]$ then relates the nodal degrees of freedom u_i^o, v_i^o, w_i, ϕ_{xi} and ϕ_{yi} at node i to the generalized strain vector containing the middle surface in-plane strains, curvatures and shear deformations. The non-zero elements of this generalized strain matrix are also listed in Appendix D.

The derivation of the element stiffness matrix then follows the standard procedure [113,114] but with the use of the generalized constitutive relations in which the stresses represent the internal
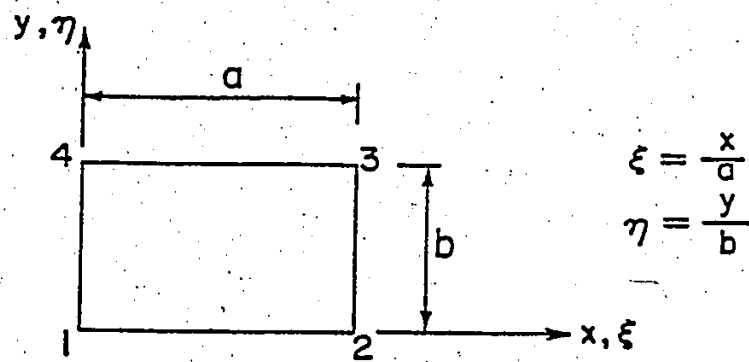
Figure 6.4   Typical Rectangular Plate Element

$\xi = \dfrac{x}{a}$

$\eta = \dfrac{y}{b}$

(a) In-Plane

(b) Out-Of-Plane
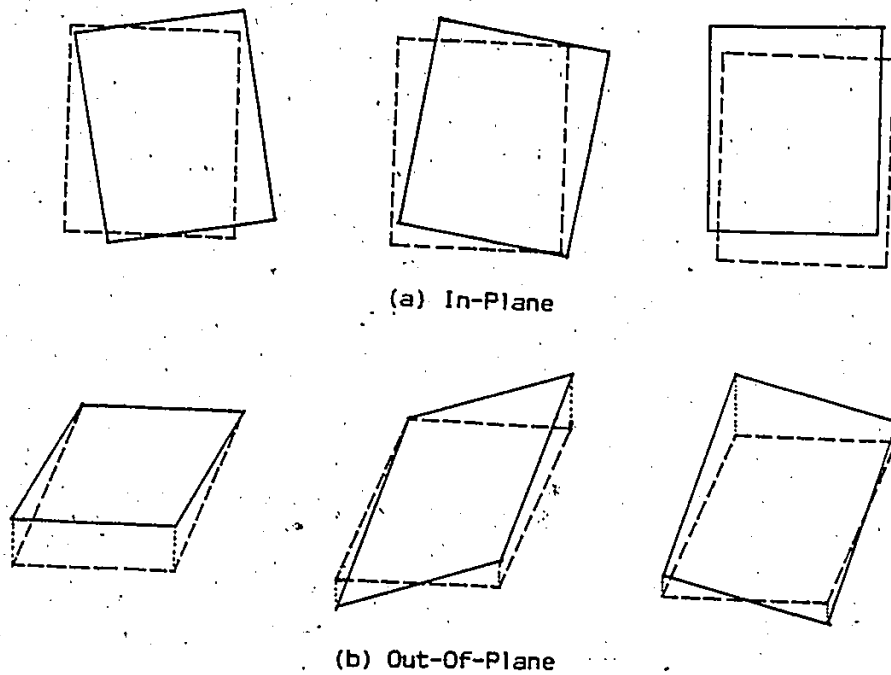
Figure 6.5   Deformation Modes Corresponding to Zero Eigenvalues
(Rigid Body Modes)

forces and the strains are caused by deformations at the middle surface. This formulation has been used previously for plate bending elements [59,113] and for laminated anisotropic plates [82,83]. Accordingly, the element stiffness matrix is given by:

$$[K_e] = \int_A [\bar{B}]^T [\bar{D}] [\bar{B}] \, dA$$
$$\text{28x28} \quad \text{28x8} \quad \text{8x8} \quad \text{8x28}$$

(6.8)

where $[\bar{B}]$ is the generalized strain matrix and $[\bar{D}]$ is the material property or the rigidity matrix. The element stiffness matrix $[K_e]$, is calculated using the three-point Gauss quadrature integration scheme along each axis. The formulation was checked by performing an eigenvalue analysis [74] of the stiffness matrix $[K_e]$. This resulted in six zero eigenvalues and the analysis of the corresponding eigenvectors as shown in Figure 6.5 indicated that these modes are the rigid body modes both in-plane and out-of-plane. Consequently, the validity of the zero strain modes was confirmed.

6.6   DEVELOPMENT OF THE RIGIDITY MATRIX

6.6.1   Formulation of the Rigidity Matrix

The rigidity matrix for masonry constructed with solid units can be developed as a single layer using equivalent properties for the masonry material based on experimental results. For cases where these properties are not available experimentally, the expressions given in Appendix C may be used. Appendix C contains derivations of some approximate expressions for the elastic constants of a masonry assemblage and the stress distributions within the assemblage. It also includes some plane stress finite element analyses to confirm the

proposed stress distributions and approximate expressions. However, for hollow block or multiwythe masonry, the rigidity matrix was developed using the concept of a layered plate. In this case, properties equivalent to the face shell and mortar combination were provided for the outer shell or wythe (either from experimental results or using the expressions given in Appendix C) and an equivalent core layer was used to replace the cross webs in the case of hollow block construction.

The concept of the layered plate, introduced here, enabled the analysis to be extended beyond the elastic or cracking limit. That is, it was only necessary to modify the stiffness of the particular layer which had reached the elastic limit or cracked condition. This approach permits modelling of observed behaviour of laterally loaded hollow block walls[42,44] where cracking was only observed on the tension side of the wall.

The rigidity matrix is derived from the constitutive relations shown below for a layer k.

$$
\begin{Bmatrix} \sigma_x \\ \sigma_y \\ \tau_{xy} \\ \tau_{xz} \\ \tau_{yz} \end{Bmatrix}^{(k)} = \begin{bmatrix} \dfrac{E_x}{(1-\nu_{xy}\nu_{yx})} & \dfrac{\nu_{xy}E_y}{(1-\nu_{xy}\nu_{yx})} & 0 & 0 & 0 \\[2ex] \dfrac{\nu_{xy}E_y}{(1-\nu_{xy}\nu_{yx})} & \dfrac{E_y}{(1-\nu_{xy}\nu_{yx})} & 0 & 0 & 0 \\[2ex] 0 & 0 & G_{xy} & 0 & 0 \\[1ex] 0 & 0 & 0 & G_{xz} & 0 \\[1ex] 0 & 0 & 0 & 0 & G_{yz} \end{bmatrix}^{(k)} \begin{Bmatrix} \varepsilon_x \\ \varepsilon_y \\ \gamma_{xy} \\ \gamma_{xz} \\ \gamma_{yz} \end{Bmatrix} \qquad (6.9)
$$

or $\{\sigma\}^k = [D]^k \{\varepsilon\} = \begin{bmatrix} [D_{ef}] & [0] \\ [0] & [D_s] \end{bmatrix} \{\varepsilon\}$

As shown above, the elasticity matrix $[D]^k$ is divisible into the uncoupled extension/flexure and shear components.

The stress resultants can be obtained by the appropriate integration of the stress components over the layer thickness. Then, summing the stress resultants for all the layers as follows:

$$\{N\} = \left\{ \begin{array}{c} N_x \\ N_y \\ N_{xy} \end{array} \right\} = \sum_{k=1}^{n} \int^k \{\sigma\}^k \, dz$$

$$= \sum_{k=1}^{n} \int^k [D_{ef}]^k \{\varepsilon\} \, dz \tag{6.10}$$

Substituting for $\{\varepsilon\}$ from Equation 6.6 gives:

$$\{N\} = [\sum_{k=1}^{n} \int^k [D_{ef}]^k \, dz]\{\varepsilon^o\} + [\sum_{k=1}^{n} \int^k [D_{ef}]^k \cdot z \, dz]\{x\}$$

or,

$$\{N\} = [\bar{D}_e]\{\varepsilon^o\} + [\bar{D}_c]\{x\} \tag{6.11}$$

where

$$[\bar{D}_e] = \sum_{k=1}^{n} \int^k [D_{ef}]^k \, dz \quad ,\text{and}$$

$$[\bar{D}_c] = \sum_{k=1}^{n} \int^k [D_{ef}]^k z \, dz \ .$$

Similar expressions can be derived for $\{M\}$ and $\{Q\}$ and the integrated or generalized constitutive equations may be written as:

$$\left\{ \begin{array}{c} \{N\} \\ \{M\} \\ \{Q\} \end{array} \right\} = \left[\begin{array}{ccc} [\bar{D}_e] & [\bar{D}_c] & 0 \\ [\bar{D}_c] & [\bar{D}_f] & 0 \\ 0 & 0 & \alpha_s[\bar{D}_s] \end{array} \right] \left\{ \begin{array}{c} \{\varepsilon^0\} \\ \{\chi\} \\ \{\phi\} \end{array} \right\} \qquad (6.12)$$

or

$$\{\bar{\sigma}\} = \qquad [\bar{D}] \qquad \{\bar{\varepsilon}\}$$

where $[\bar{D}_f] = \sum\limits_{k=1}^{n} \int^k [D_{ef}]^k z^2 \, dz$

$$\qquad (6.13)$$

$$[\bar{D}_s] = \sum\limits_{k=1}^{n} \int^k [D_s]^k \, dz$$

and α_s is the factor introduced to account for the non-uniform shear deformations or warping of the section. It has been set equal to the previously established value of 5/6 for rectangular sections [59,82].

It should be noted that the extension/flexure coupling rigidity sub-matrices $[\bar{D}_c]$ will be cancelled for a symmetric layer arrangement. However, it is presented to accommodate asymmetric arrangements.

6.6.2 Calculation of the Equivalent Elastic Constants
For Different Layers

The face shell layers or the outer wythe layers have been assumed to have identical orthotropic material properties. For these orthotropic layers, the required six elastic constants E_x, E_y, ν_{xy}, G_{xy}, G_{xz} and G_{yz} can be obtained using the available experimental data or the expressions given in Appendix C together with the component material properties. However, the cross webs, in the case of hollow block walls, are replaced by an equivalent solid layer as shown in Figure 6.6. For
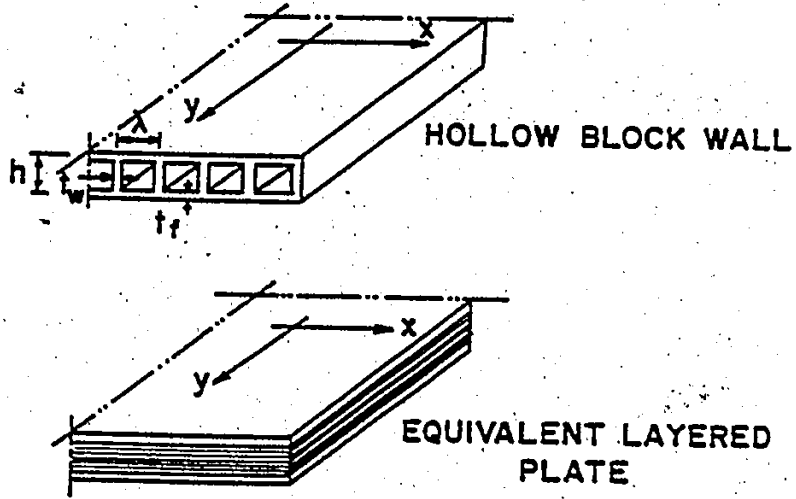
Figure 6.6   Equivalent Core Layer
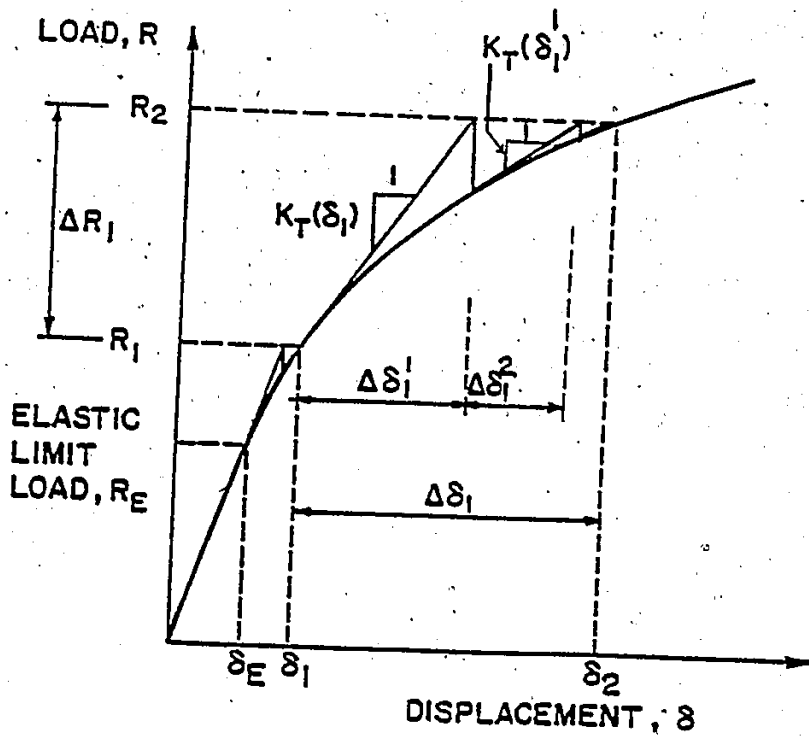
Figure 6.7   Newton-Raphson Iterative Method

cases having continuous webs, the elastic constants for this layer can be determined by separating the rigidity expressions derived by Basu and Dawson[26] for cellular plates into the contributions of the individual layers. Accordingly, the elastic constants for the web layer are as follows:

$$E_x = 0.0,$$

$$E_y = E_w \frac{t_w}{\lambda},$$

$$\nu_{yx} = \nu_w,$$

$$G_{xy} = 0.0,$$

$$G_{xz} = \frac{1}{\lambda(\frac{\lambda}{2 E_{xf} t_f^3} + \frac{h}{E_w t_w^3}) (h-t_f) (1-\nu_w^2)}, \text{ and}$$

$$G_{yz} = G_w \frac{t_w}{\lambda}$$

(6.14)

For cases of discontinuous webs such as concrete block walls, all of the above expressions for the elastic constants are applicable except those related to the y-direction (E_y and G_{yz}). Other expressions for theses two constants were obtained and found to be as follows:

$$E_y = 0.0 \text{ and}$$

$$G_{yz} = \frac{1}{\lambda(\frac{\lambda}{2 E_{yf} t_f^3} + \frac{h}{(E_w t_w/\lambda) h^3}) (h-t_f) (1-\nu_w^2)}$$

(6.15)

where, E_w, G_w and v_w are the modulus of elasticity, shear modulus and Poisson's ratio, respectively for the web material (concrete block in this case). In addition, E_{xf} and E_{yf} are the modulii of elasticity for the face shell material and all other notation refer to the transverse section dimensions shown in Figure 6.6

It should be noted that the elastic constants mentioned above also satisfy the thermodynamics constraints which lead to the positive definite condition of the elasticity matrix in Equation 6.9

6.7   MATERIAL NONLINEARITY AND INCREMENTAL ANALYSIS

In this model, the masonry material has been assumed to behave in a linear elastic manner. This is considered accurate for plain masonry where tension cracking is the controlling mode of failure. Therefore, the nonlinearity in the analysis is due to the progressive cracking of the assemblage either by debonding at mortar joints or tensile cracking of units or both.

Cracking occurs when the states of stress exceeds the preset conditions for failure according to the failure criterion suggested for masonry assemblages in biaxial state of stress as discussed in Chapter 5. Using this criterion, both the occurrence of failure and, the failure mode are predicted according to the state of stress and the component materials' geometry and properties. After the cracking limit has been exceeded in a certain layer, an incremental stress-strain relationship, similar to the generalized Hooke's law but valid beyond the elastic limit is adopted. It is given by:

$$\{d\sigma\} = [D_{cr}]\{d\varepsilon\} \qquad\qquad (6.16)$$

where $\{d\sigma\}^T = \{d\sigma_x \quad d\sigma_y \quad d\tau_{xy} \quad d\tau_{xz} \quad d\tau_{yz}\}$ is the stress increment vector, $\{d\varepsilon\}^T = \{d\varepsilon_x \quad d\varepsilon_y \quad d\gamma_{xy} \quad d\gamma_{xz} \quad d\gamma_{yz}\}$ is the total strain increment vector, and $[D_{cr}]$ is the modified elasticity matrix for the cracked layer.

6.7.1   Elasticity Matrix For Cracked Layers $[D_{cr}]$

The modification of the elasticity matrix after cracking depends upon the failure mode or cracking pattern within the cracked layer of the element and the applied state of stress. The transverse failure modes shown in Figure 5.1 and discussed in detail in the previous chapter were classified under one of three modes which are as follows:

1. Horizontal failure plane, where failure occurs by debonding along a bed joint through the element.

2. Vertical splitting or vertically toothed failure plane, where failure occurs either by debonding along head joints and splitting through masonry units in alternate courses or by debonding along head and bed joints around the units in a toothed pattern.

3. Diagonal splitting or diagonally stepped failure plane where failure occurs either by diagonal splitting through the units in an almost straight line or by debonding along bed and head joints around the units in a stepped pattern.

For cracking Modes 1 and 2, the elasticity matrix given in Equation 6.9 is modified by reducing the modulus of elasticity in the direction normal to the crack by a reduction factor, α_c, and the shear modulii by a reduction factor, β_c. However, the modulus of elasticity

and the shear modulus parallel to the failure or cracking plane are left untouched. Accordingly, considering the x and y coordinate to coincide with the parallel and normal directions to the bed-joints, respectively, the modified elasticity matrix for the first failure mode can be written as follows:

$$[D_{cr}]_1 = \begin{bmatrix} \dfrac{E_x}{(1-\nu_{xy}\nu_{yx})} & \dfrac{\nu_{xy}\alpha_c E_y}{(1-\nu_{xy}\nu_{yx})} & 0 & 0 & 0 \\[2mm] \dfrac{\nu_{xy}\alpha_c E_y}{(1-\nu_{xy}\nu_{yx})} & \dfrac{\alpha_c E_y}{(1-\nu_{xy}\nu_{yx})} & 0 & 0 & 0 \\[2mm] 0 & 0 & \beta_c G_{xy} & 0 & 0 \\[2mm] 0 & 0 & 0 & G_{xz} & 0 \\[2mm] 0 & 0 & 0 & 0 & \beta_c G_{yz} \end{bmatrix} \qquad (6.17)$$

and for the second failure modes, it is given by:

$$[D_{cr}]_2 = \begin{bmatrix} \dfrac{\alpha_c E_x}{(1-\nu_{xy}\nu_{yx})} & \dfrac{\nu_{xy}\alpha_c E_y}{(1-\nu_{xy}\nu_{yx})} & 0 & 0 & 0 \\[2mm] \dfrac{\nu_{xy}\alpha_c E_y}{(1-\nu_{xy}\nu_{yx})} & \dfrac{E_y}{(1-\nu_{xy}\nu_{yx})} & 0 & 0 & 0 \\[2mm] 0 & 0 & \beta_c G_{xy} & 0 & 0 \\[2mm] 0 & 0 & 0 & \beta_c G_{xz} & 0 \\[2mm] 0 & 0 & 0 & 0 & G_{yz} \end{bmatrix} \qquad (6.18)$$

For the third failure modes, factors α_c and β_c are applied for both elasticity modulii and all shear modulii.

The values of α_c and β_c, in the case of reinforced concrete,

vary from 0.0 to 1.0 depending upon reinforcement dowel action, aggregate interlock, and crack width [94]. However, for unreinforced masonry, these reduction factors have been assumed to depend only on the state of stress and the failure mode as follows:

1.   For the condition of cracking corresponding to the first or the second modes and tensile stress normal to the crack, α_c is set equal to zero because cracked elements cannot transmit tension normal to the crack. For compression α_c remains equal to unity because compression can be transmitted normal to the crack.

2.(a)   For the case of tensile stress normal to a crack resulting from debonding at the interface of the mortar bed joint and the units, β_c is set equal to zero. The reason is that no shear can be transmitted across these cracks because the relatively smooth surfaces will not be in contact. However, for tension cracking through the units, it is assumed that the irregular surface of the crack should be able to transfer a certain amount of shear. Accordingly a value of $\beta_c = 0.4$, as previously suggested [25] for concrete blocks, is assumed for cracking through masonry units as in the diagonal splitting mode of failure. Where cracking is partially through the units and partially along mortar joints, as in the vertical splitting pattern of modes 2, the average value of $\beta_c = 0.2$ is used.

(b)   The compression-shear bond strength before cracking can be represented by the Coulomb-Mohr failure theory [75]. After cracking by debonding, shear can only be resisted by friction. Then the shear reduction factor, β_c, can be determined by:

$$\beta_c = \frac{\mu\sigma_c}{\mu\sigma_c + \sigma_{sbmo}}$$

(6.19)

where σ_c is the applied compressive stress normal to the crack, σ_{sbmo} is the cohesion or the shear bond strength at zero precompression and μ is the coefficient of friction between mortar and units. However, if cracks run through units a value of $\beta_c = 1.0$ is used and if cracks go through both head joints and masonry units, an average value between 1.0 and the value from Equation 6.19 is assumed.

3. For the diagonally stepped pattern of the third modes, it is assumed that the crack surfaces will be irregular and consequently some shear transfer can take place across the cracked joints. Therefore, the shear reduction factor β_c for the cracked layer in this case is assumed to be 0.4. Then, since some tension can be transferred in the assemblage through shear across the cracked joints, the axial stiffness reduction factor α_c is assumed to be 0.1 for this failure pattern. These reduction factors will be discussed in detail later in this section.

There is another case where the elasticity matrix has to be modified for nonlinear response where no cracks are developed. This is the case where the head joint capacity has been exceeded. In this case, it is assumed that the head joints will behave nonlinearly and there is no premature cracking in the head joints prior to the failure through

the head joints and the masonry units in alternate courses or through a combination of head and bed joints. This assumption was suggested earlier by Baker based on experimental evidence for clay brickwork [30] and similar observed behaviour of concrete blockwork was reported in this study and elsewhere [44]. It should also be noted that the use of this assumption in predicting the assemblage strength, as mentioned in Chapter 5, consistently yielded reasonable results. However, the assumption of premature head joint cracking was tried and found to give predictions which were significantly below available experimental results [47]. Accordingly, the elasticity matrix in such cases is modified by replacing the modulus of elasticity parallel to the bed joints, E_p (represented by E_x in Equations 6.17 and 6.18) by a reduced modulus, E_p', as given in Appendix C.

6.7.2 Nonlinear Incremental Analysis

The nonlinear finite element analysis is performed in an incremental manner using an iterative scheme within each load increment. The numerical solution procedure for cracking is distinctly different from yielding because cracking necessitates redistribution of the total stress carried normal to the crack plane. This implies a different computing strategy regarding load size step, stiffness update frequency and the convergence criteria [6]. Therefore, the Newton-Raphson scheme was used for stiffness updates after each iteration within the load increment.

At the beginning of each load increment, the stiffness matrix is formulated according to the stress level at the end of the previous

increment. Then, for the present load increment, incremental displacements, strains, and stresses can be determined. The total stress at each integration point is checked against cracking. At the integration points where the cracking limit has been exceeded, the total stresses normal to the cracks and the nontransferred shears across the cracks are included in the unbalanced part of the load increment. In the next iteration, this part of the load increment is then applied to the cracked structure with the updated stiffness. These iterations will continue until convergence by reaching a stage where no more cracks develop under the unbalanced part of the load increment due to stress release at previously developed cracks. The next load increment is then applied and the same procedure repeated up to failure which is defined by excessive displacement exceeding a preset limit. A graphical representation of this incremental nonlinear analysis is shown in Figure 6.7.

6.8   CONSISTENT LOAD VECTORS AND BOUNDARY CONDITIONS

6.8.1   Consistent Load Vectors

The consistent load vector is defined as the vector containing equivalent nodal loads to produce the same potential energy as the real loading [74]. In this model, two separate consistent load vectors were generated to account for both constant and variable loads. For example, in full scale testing of masonry walls, the in-plane loads due to wall self-weight and any precompression applied along the top edge of the wall were considered as constant loads whereas the out-of-plane pressure was variable load applied in increments up to failure. Each of these

two load vectors was generated to include different loadings on the finite element such as uniformly distributed loading both in-plane and out-of-plane, distributed edge loading, concentrated nodal loading and all possible combinations of these loadings.

6.8.2 Boundary Conditions

Since this formulation includes transverse shear deformations, three out-of-plane boundary conditions have to be specified at each edge rather than the two conditions for ordinary thin plate theory. The third required boundary condition is related to the twisting of the edge and it is affected by the edge conditions as follows:

1. If there is an edge stiffener or diaphragm at the edge, then the rotation about an axis normal to that edge has to be restrained to zero (i.e., $\partial w/\partial s$ and ϕ_s are zero).

2. If no edge stiffeners or diaphragms are provided, then the twisting moment about an axis normal to that edge has to be zero. The rotations are not restrained.

Since the finite element formulation is based entirely on assumed displacement functions, only the boundary displacement conditions can be satisfied exactly according to the edge support condition and the edge stiffening conditions. For example, for an edge parallel to the y axis, the different possible boundary conditions are as follows:

(1)   For a simply supported edge

    a) with stiffeners $w = 0, \ \theta_y = 0, \ \phi_y = 0$

    b) without stiffeners $w = 0$

(ii)   For a clamped edge

a) with stiffeners $w = 0$, $\theta_x = 0$, $\phi_x = 0$,

$\theta_y = 0$, $\phi_y = 0$

b) without stiffeners $w = 0$, $\theta_x = 0$, $\phi_x = 0$

(iii) For a free edge $\phi_x = 0$

It should be noted that these boundary conditions are related to the out-of-plane degrees of freedom only. However, other boundary conditions for in-plane degrees of freedom could be added if required.

6.9   MODEL VERIFICATION USING AVAILABLE SOLUTIONS

Before using the proposed model for predicting the strength of masonry assemblages, a verification study was conducted to establish that it was fundamentally correct by checking the model predictions against available linear elastic and nonlinear solutions. Included were different cases of thin and thick simply supported plates, isotropic and orthotropic single layer plates, and a multicell bridge deck (as a layered plate having cross webs). Also, a convergence study for thin plates was performed for the proposed model. In addition, to verify the nonlinear analysis of the model, a simply supported thin plate problem for which the nonlinear analysis is available in the literature was analysed. These case studies are discussed individually below.

6.9.1   Single Layer Isotropic Plates

In order to verify the model for thick plate predictions, simply supported square plates subject to uniformly distributed load and having thickness to side length ratios of 0.01 to 0.25 were analysed using the proposed model. The results are compared in Figure 6.8 with two

$$W_{max.} = \frac{qa^4}{Eh^3}\alpha$$

$(\nu = 0.30)$

S.S.

FINITE ELEMENT WITH SHEAR DEFORM.

PRESENT MODEL

REF. [82]

REISSNER THEORY

CLASSICAL THIN PLATE THEORY

COEFFICIENT, $\alpha \times 10^2$

6.0

5.0

4.0

3.0

0

0.0   0.05   0.10   0.15   0.20   0.25

THICKNESS RATIO, h/a
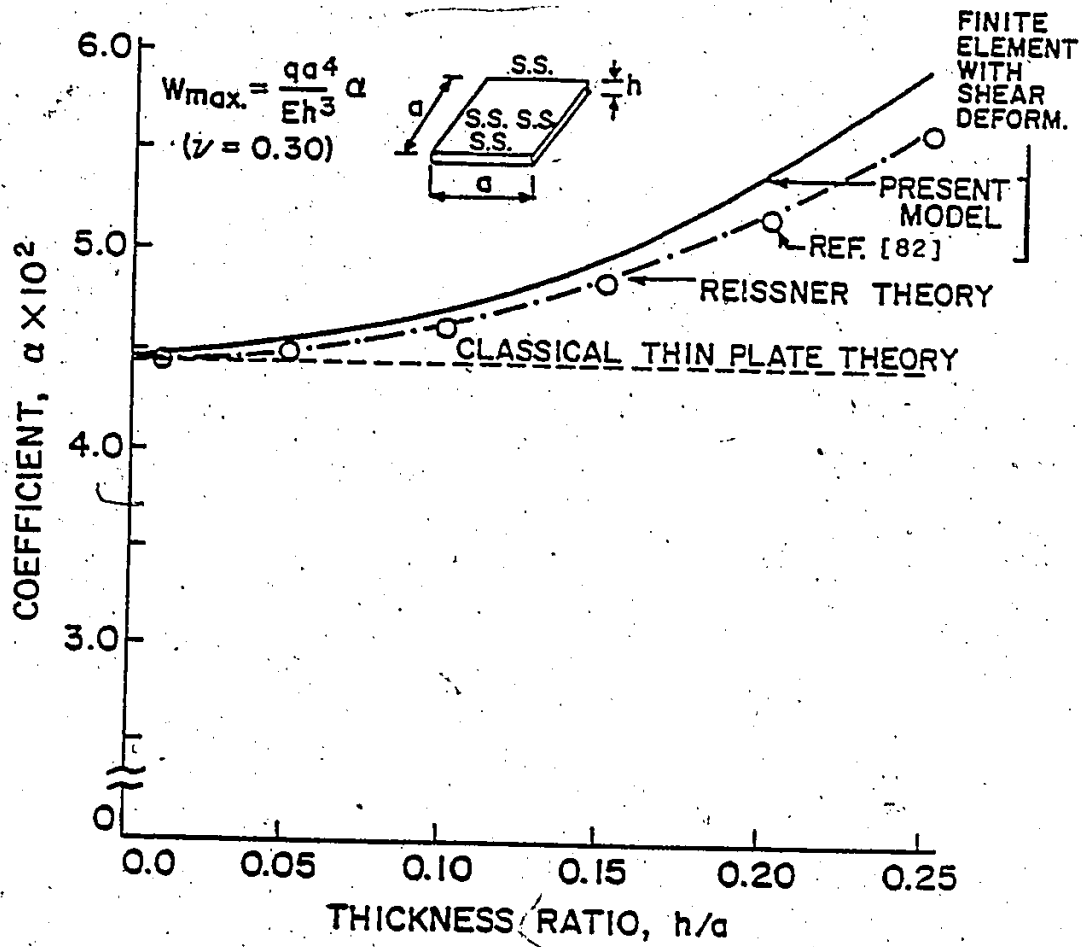
Figure 6.8   Deflections for Isotropic Single Layer Plates Under Uniformly Distributed Load

available solutions which include transverse shear deformations for thick plates [82]. This figure indicates generally good agreement with a maximum difference of 5% for the very thick plate considered.

6.9.2 Single Layer Orthotropic Thin Plates

Simply supported orthotropic thin plates having different side lengths and ratios of orthotropy were analysed and compared to the available solutions in the literature [101]. This comparison, as shown in Figure 6.9 for the center deflection, indicates very good agreement with a maximum difference of 1.4%.

6.9.3 Multicell Bridge Deck

A multicell bridge deck model simply supported at its ends, which was investigated both experimentally and analytically by Sawko and Cope [87], was analysed using the proposed model. Concentrated loads were applied at different web locations along the mid-span axis. The results of the analyses are shown in Figure 6.10 together with the experimental results and the analysis reported by Sawko and Cope [87]. The comparisons for the four different load locations (labelled A to D) show that the proposed model predictions are in good agreement with the experimental data and generally give better predictions than the other analyses.

6.9.4 Convergence Study For Thin Plates

A convergence study for a thin square plate under uniformly distributed loading was carried out for simply supported edges with shear restraint along the edges. A thickness to span ratio of 0.01 was

MAX. DEFLECTION

$$\omega_{max.} = \alpha \frac{q_o b^4}{D_y}$$

FACTOR $\alpha \times 100$

PRESENT MODEL

TIMOSHENKO [101]

ISOTROPIC

$$\frac{a}{b}\sqrt[4]{\frac{D_y}{D_x}}$$

1	1.5	1.7	2.0	2.5	
1	5.0625	8.3521	16	39.0625	$\frac{D_y}{D_x}$
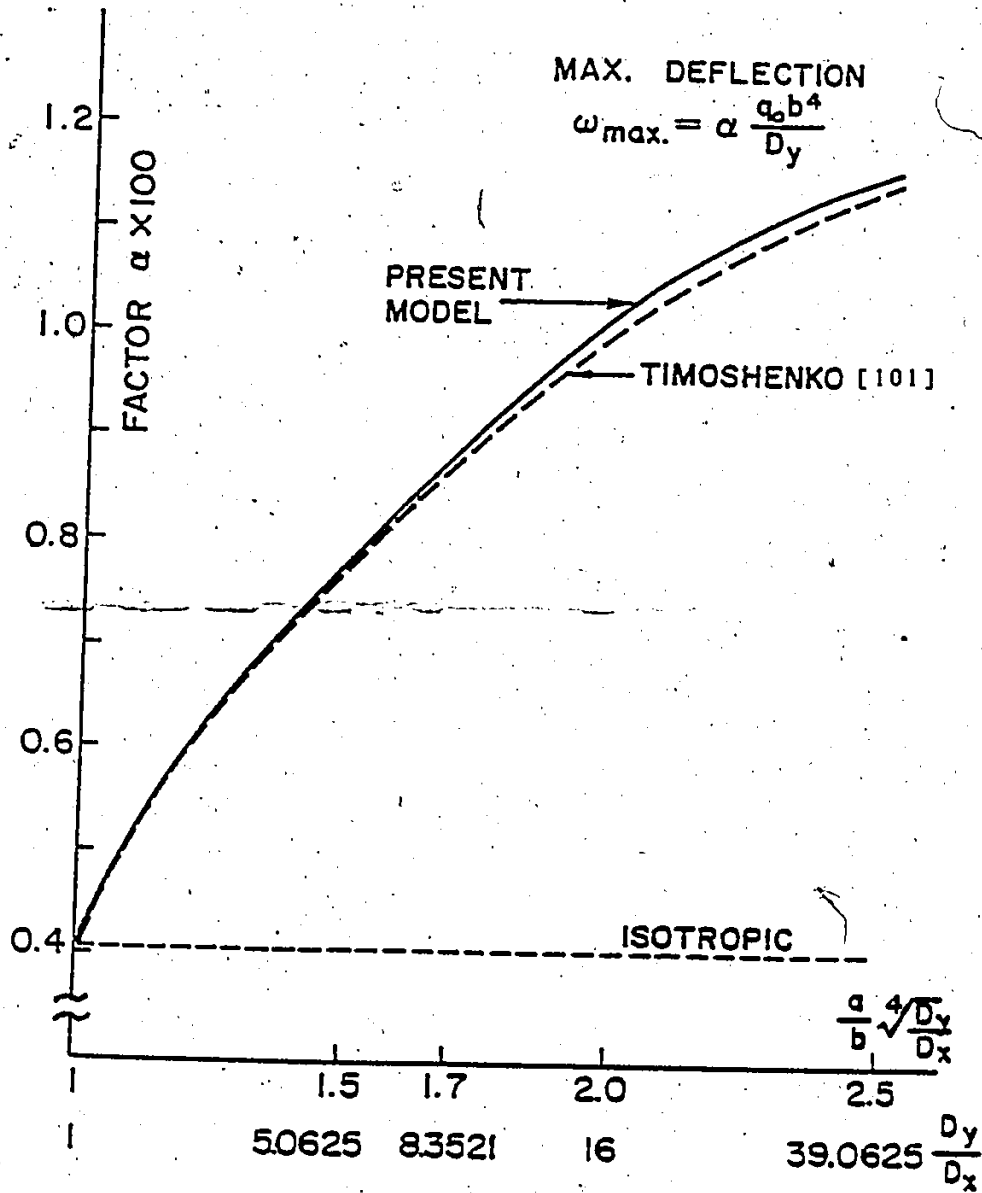
Figure 6.9   Deflections for Orthotropic Single Layer Plates Under Uniformly Distributed Load

(a) DECK MODEL

WEB NO.

(b) DEFLECTION DISTRIBUTION COEFF.

DEFLECTION DISTRIBUTION COEFFICIENTS

——— PRESENT MODEL
× EXPERIMENTAL [87]
○ PLANE STRESS
    FINITE ELEMENT [87]
△ FOLDED PLATE [87]
—— BEST FIT EXP. [87]
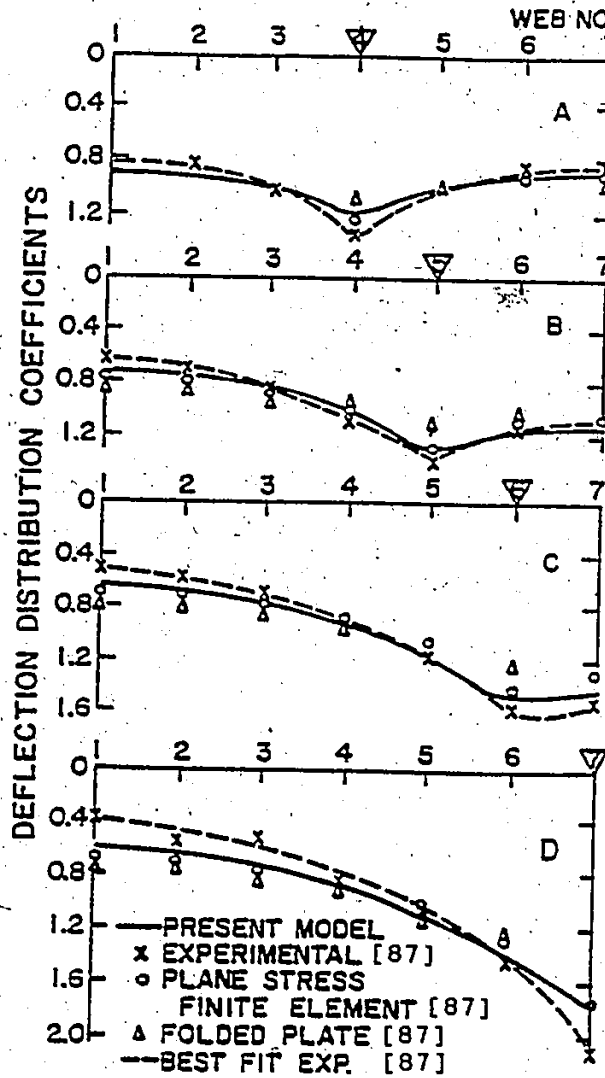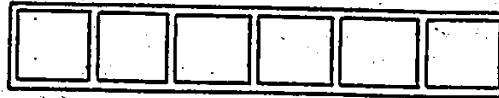
Figure 6.10   Deflections for Multicell Bridge Deck Model Under
                Point Loads at Different Web Locations

examined and deflections, bending moments, and shear forces were compared with theoretical thin plate solutions in Table 6.1 and Figure 6.11. The convergence is fairly rapid in all cases when three elements or more are used along each edge. This is also true for the shear force since the constant difference resulted from the fact that the thin plate theory does not include any shear deformations.

6.9.5 Nonlinear Analysis of a Thin Plate

A simply supported square steel plate subjected to uniformly distributed load was analysed using the proposed model both in linear and nonlinear stages. For the nonlinear incremental analysis of this plate beyond first yield, the Von Mises yield criterion and the associated flow rules which are also implemented in this model were applied. The plate dimensions, material properties and finite element mesh used for one quarter of the plate are given in Figure 6.12(a). These are the same as those available in the literature [91]. Three layers were assumed through the plate thickness to reasonably represent the three integration points through the thickness adopted in Reference 91. The load versus center deflection results from the proposed model (Analysis I) together with the reported solution are shown in Figure 6.12(b). The significant vertical shift between the two analyses is attributed to the fact that the stresses at the extreme fibers were checked for yielding in the proposed model. However, for the other analysis [91], stresses were checked at integration points located within the plate thickness. To check the validity of this argument, another analysis (Analysis II) was performed using the proposed model

TABLE 6.1 Simply Supported Square Plate Under Uniform Loading

Mesh in a Symmetric Quarter	Central Deflection $\times p \dfrac{L^4}{D}$	Central Bending Moment $\times pL^2$	Corner Twisting Moment $\times pL^2$	Mid-Edge Shear Force $\times pL$
1 × 1	0.00506	0.0546	0.0319	0.340
2 × 2	0.00433	0.0497	0.0329	0.313
3 × 3	0.00418	0.0487	0.0328	0.324
4 × 4	0.00413	0.0483	0.0327	0.326
5 × 5	0.00410	0.0481	0.0327	0.328
6 × 6	0.00409	0.0481	0.0326	0.329
Thin Plate Solution	0.00406	0.0479	0.0325	0.329
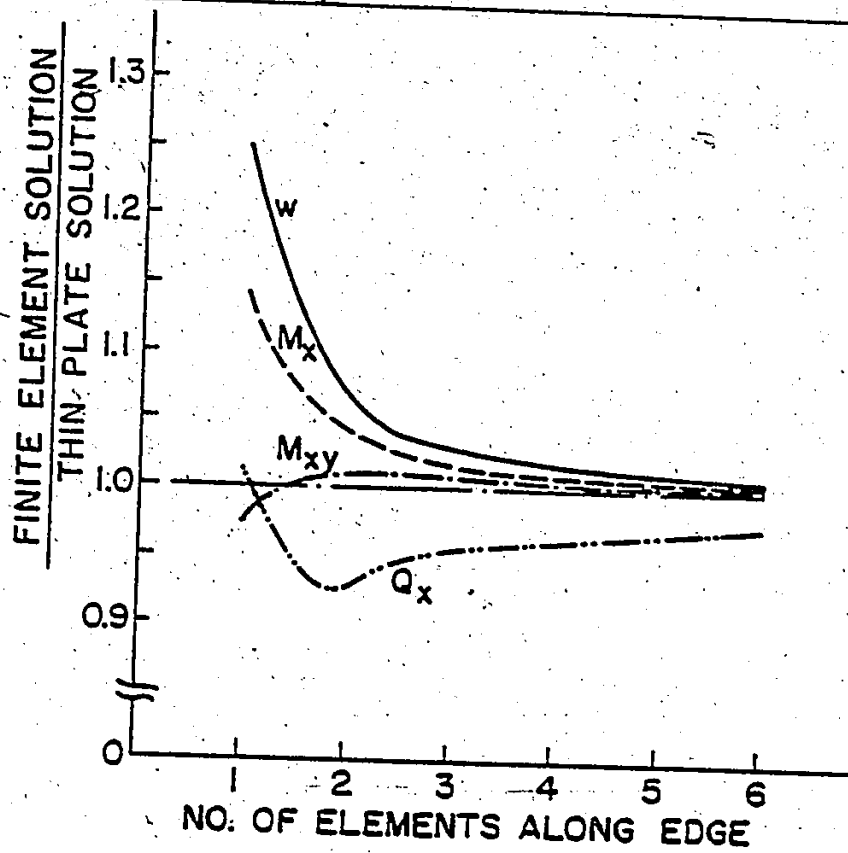
Figure 6.11   Convergence Study for Thin PLates Under Uniformly Distributed Load

(a) F.E. MESH (ONE-QUARTER)

10"×10"×0.4" PLATE
$E = 10^4$ Ksi
$E_T = 10^3$ Ksi
$\nu = 0.5$
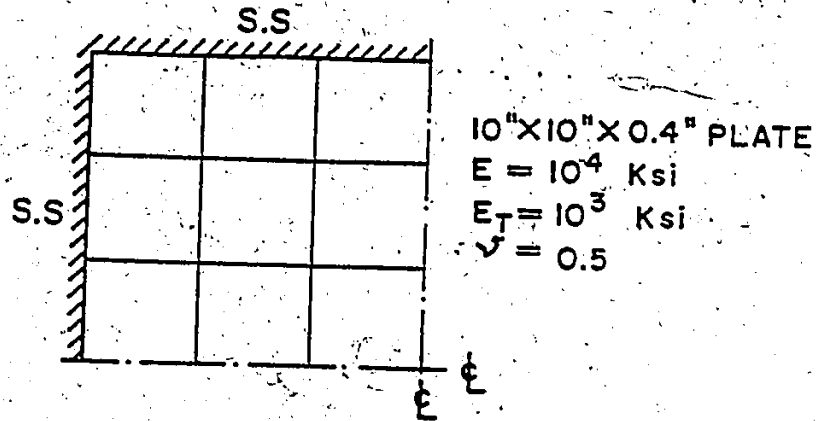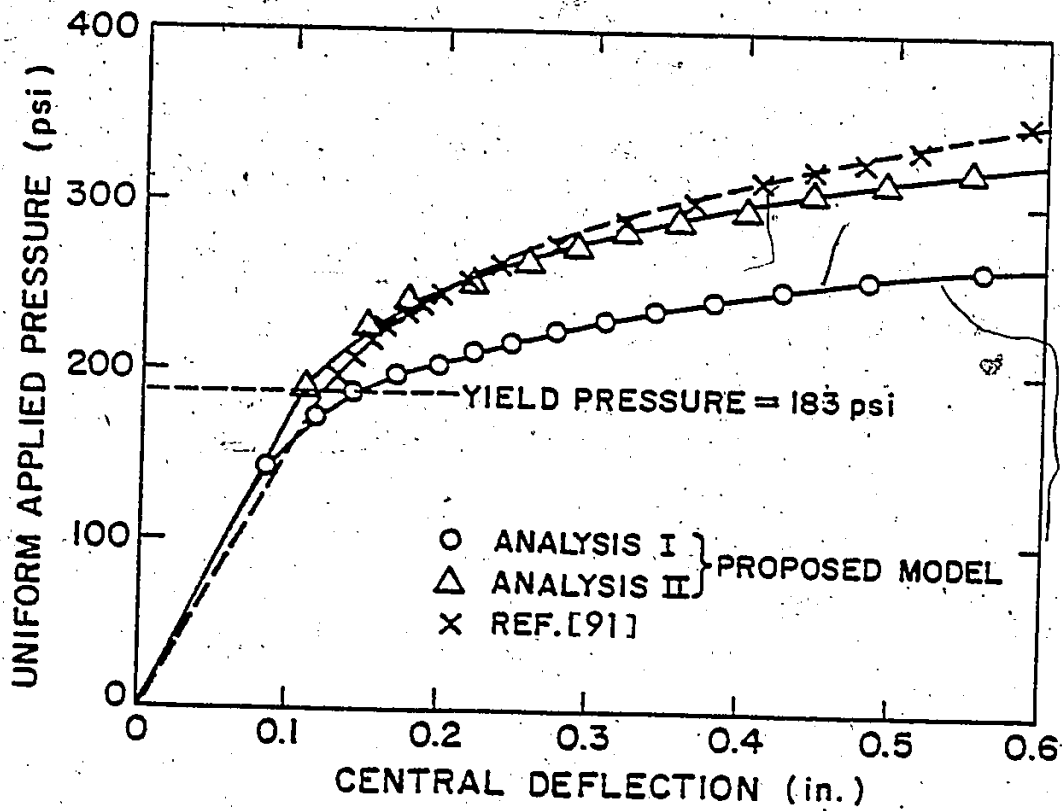
(b) LOAD-CENTRAL DEFLECTION

Figure 6.12   Nonlinear Analysis of Uniformly Loaded Simply
Supported Plate

but using stresses at the same locations as those used in Reference 91. As shown in Figure 6.12(b), these predictions confirmed the previously mentioned reasoning.

It should be noted that an analysis of this plate was also performed using a single layer and that the results were very similar to those for the three layer analysis.

6.10   APPLICATION OF THE PROPOSED MODEL TO MASONRY ASSEMBLAGES

The main objective of constructing this proposed finite element model was to extend the available knowledge of behaviour of laterally loaded full scale walls beyond the tested conditions. However, it should be noted that the model has versatility for general analysis of masonry assemblages.

In this section, the proposed model will be used to predict the behaviour and capacities of full scale walls similar to those tested experimentally and reported earlier in this investigation. These predictions will be compared to the test results to establish a measure of the reliability of the model. However, before performing these comparisons, it is necessary to evaluate the stiffness reduction factors for the cracked layers of a finite element and to determine the required finite element mesh size. These two aspects will be discussed in detail as follows.

6.10.1   Stiffness Reduction Factors α_c and β_c

The stiffness reduction factors, α_c and β_c, mentioned earlier in Section 6.7.1 were arbitrarily chosen according to the state of stress

and the failure mode. It was thought that the values of the stiffness reduction factors for all but the diagonally stepped failure mode were acceptable because of their rational development and documentation in the literature [25]. However, the case of the diagonally stepped mode was not so clear that it can be accepted without further investigation.

The axial stiffness reduction factor factor, α_c, which was considered zero for all other modes, is thought to have a non-zero value for this particular mode of failure. This is because of the irregular crack surface and the possibility of transferring some tension in the assemblage through shear across the cracked joints. Therefore, a value of 0.1 was adopted here for α_c as a non-zero yet small amount of tension to be transferred by the cracked layer.

Since this diagonally stepped mode of failure occurs in masonry assemblages under mainly shear stresses, the shear reduction factor was thought to need further investigation. Therefore, in order to investigate the effect of this arbitrarily chosen value, the basic wall test series (Series WII), which had a spans of 5.00 m long by 2.80 m high, was analysed using the proposed model with different values of the shear reduction factor β_c from 0.0 to 0.9 for this mode.The results of these analyses are shown in Figure 6.13 and Table 6.2. The increase of the failure load with the increase in the reduction factor can be seen in Figure 6.13. It was thought that the chosen value for β_c should be the one which is rationally accepted and produces reasonable predictions. The high values close to unity were rejected since they imply very small stiffness reduction after cracking which is obviously not rational. Also, a low value was not chosen since they resulted in
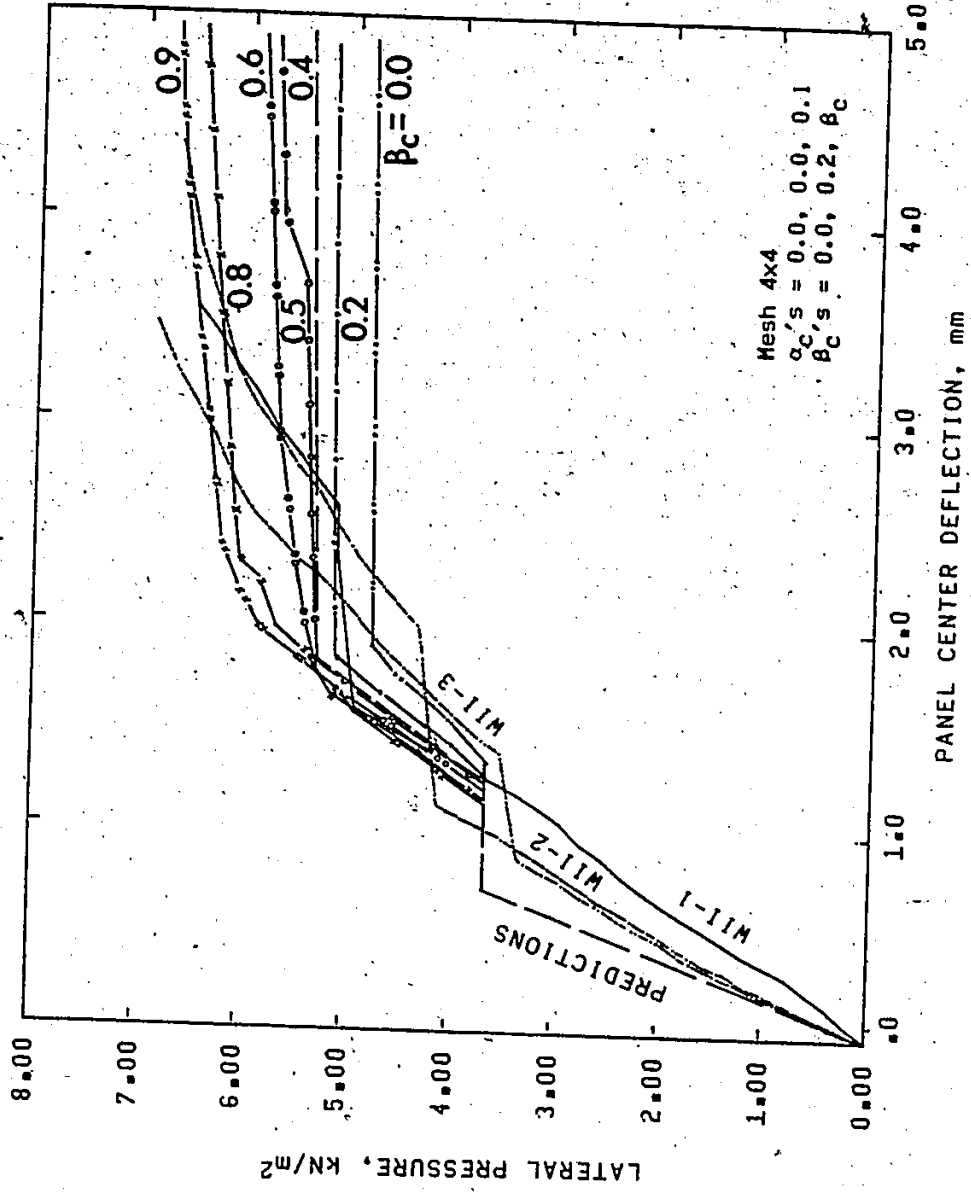
Figure 6.13   Effect of the Shear Reduction Factor on Deflections
for Series WII Walls

TABLE 6.2 Effect of Shear Reduction Factor ,β_c, for Diagonally
Stepped Failure Mode on Panel Capacity Predictions

β_c	0.0	0.2	0.4	0.5	0.6	0.8	0.9
Predicted Failure Load	4.96	5.32	5.51	5.87	6.06	6.61	6.79
Ratio of Predicted to Average Experimental Failure Load	0.73	0.78	0.81	0.86	0.89	0.97	1.00

relatively poor predictions as shown in Table 6.2. Of the intermediate values, a β_c of 0.4 was chosen for the following reasons:

1. It yielded somewhat conservative predictions.

2. High ratios of shear transfer across the cracks would result in wider band of cracks. Then, using the lower intermediate value tends to narrow the crack band which would yield better prediction of the crack pattern.

3. The value of 0.4 was used for cases of cracking through the concrete blocks. The crack surface irregularities in the mortar joint block interfaces are not expected to be as rough as the cracks through the blocks. Therefore, a value not exceeding 0.4 was also recommended for diagonally stepped cracking.

It should be noted that the values of the stiffness reduction factors for cracked layers of the elements are arbitrarily chosen and are not necessarily the correct values but rather the best in terms of acceptable predictions and a rational choice. Moreover, it is understood that these factors should not have constant values but rather continuously decrease with increase of the crack width. For non-reinforced masonry and concrete, the developed cracks are expected to be wider than those of reinforced masonry and concrete. This suggests that smaller stiffness values and higher rates of decrease in stiffness should be used for non-reinforced cracked layers of the elements. Moreover, the use of non-zero values for these factors allows the stresses at previously cracked integration points to build up again and these may again reach the cracking limit resulting in further decrease

of the stiffness. This implies the inclusion of continuously reduced values for the stiffness of the cracked elements in this model. Accordingly, the use of the arbitrary constant values is considered to be satisfactory for non-reinforced masonry.

6.10.2 Determination of the Required Finite Element Mesh Size

The choice of finite element mesh size is one of the important aspects of analyses using the finite element method since it may affect both the results and the computer costs. Therefore, the effects of choosing different finite element mesh sizes on both model predictions and computer costs were investigated in this study. This was accomplished by performing three analyses of one half of the basic wall, 'Wall WII. Use of half the wall was adequate due to the symmetry about the vertical axis at mid-length. In these analyses, the number of elements over the wall height was taken as 4, 6 or 8. The load-deflection curves resulting from these analyses are shown in Figure 6.14 together with the available test results for the three walls. These results indicated similar load-deflection curves with the prediction of the first cracking and the failure capacities increasing only 1% or 2% of the average experimentally reported values for changes in the number of elements from 4 to 6 or 8 over the wall height. However, the corresponding increase in the execution time on the CDC CYBER 170-730 Computer of McMaster University, as a measure for the computer cost, was respectively 76% or 259% more when 6 or 8 elements were used over the wall height instead of the original 4 elements.
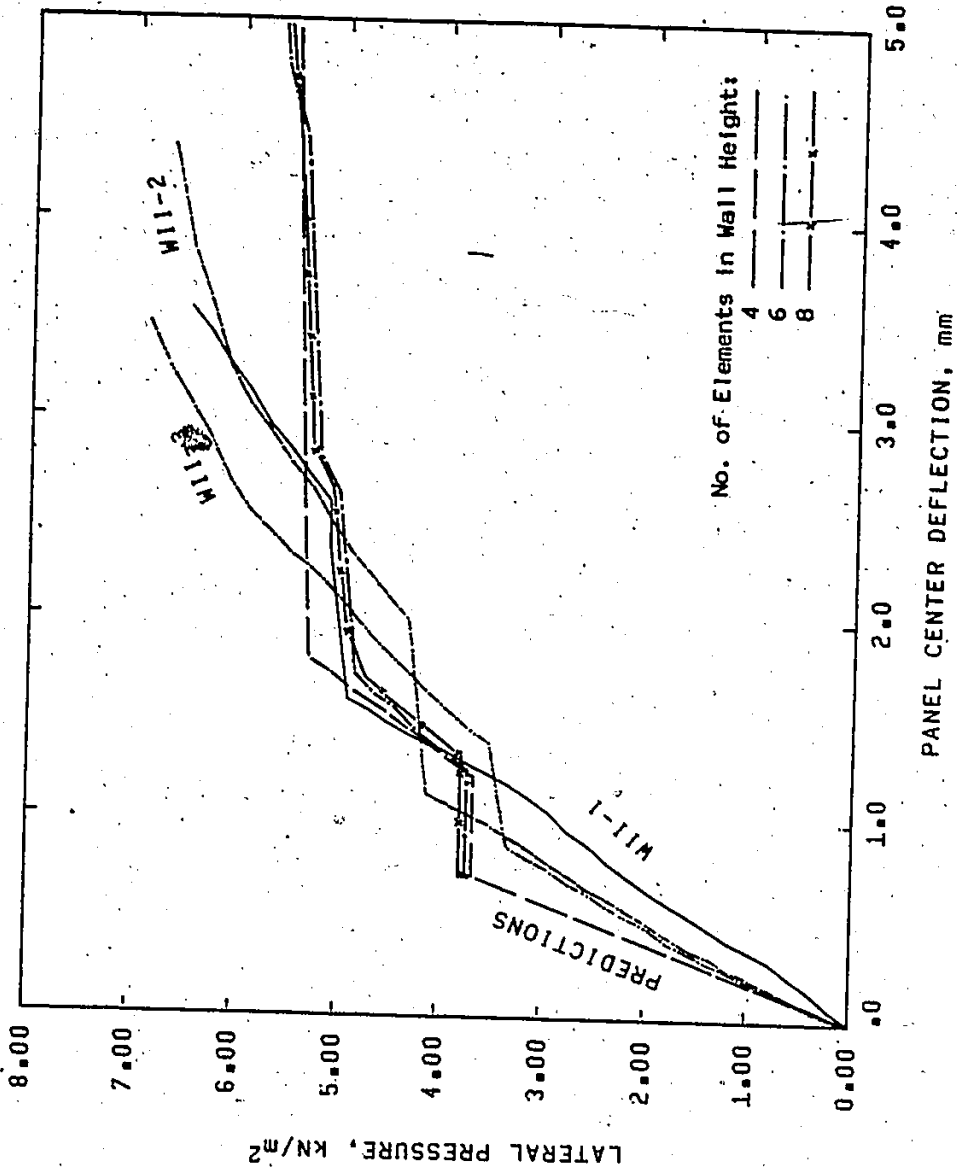
Figure 6.14   Effect of the Mesh Size on Deflections for
Series WII Walls

The predicted cracks at integration points for this wall are shown in Figures 6.15, 6.16 and 6.17 for analyses using the 4x4, 4x6 and 5x8 grids, respectively. In these figures, the cracks developed at the first cracking pressure were marked with dashed lines whereas the cracks developed at failure were marked with solid lines. The wide band of predicted cracks shown in these figures will be discussed in detail later in this section. However, the trend of the cracking pattern can be easily identified by the first crack to develop in each element (marked with a heavy line in these figures). The predicted cracks at the integration points shown in Figures 6.15, 6.16 and 6.17 indicate that there was not significant improvement in the crack distribution or the width of the crack bands for the increased number of elements.

Analyses performed for other wall series using the 4x6 mesh did not yield significant improvements in the capacity predictions and resulted in considerable increases in computer execution times. Moreover, the convergence study reported earlier for elastic square plates under uniform load indicated that, for a mesh having only 2 elements along the side of a quarter of a plate, a maximum deviation from the exact solution was only 7%. This was considered to be an acceptable accuracy when compared to the expected variability of masonry flexural strength.

As a result of this analysis, it was suggested that use of the 4x4 mesh size was reasonable for the analysis as it provided predictions which were not significantly different from the other finer meshes. Moreover, the computer time was considerably less.

4×625. = 2500. mm

4×700. = 2800. mm

— Debonding Along Bed Joint
I Debonding Along Head Joints and Splitting of Units
./ Stepped Debonding Along Bed and Head Joints
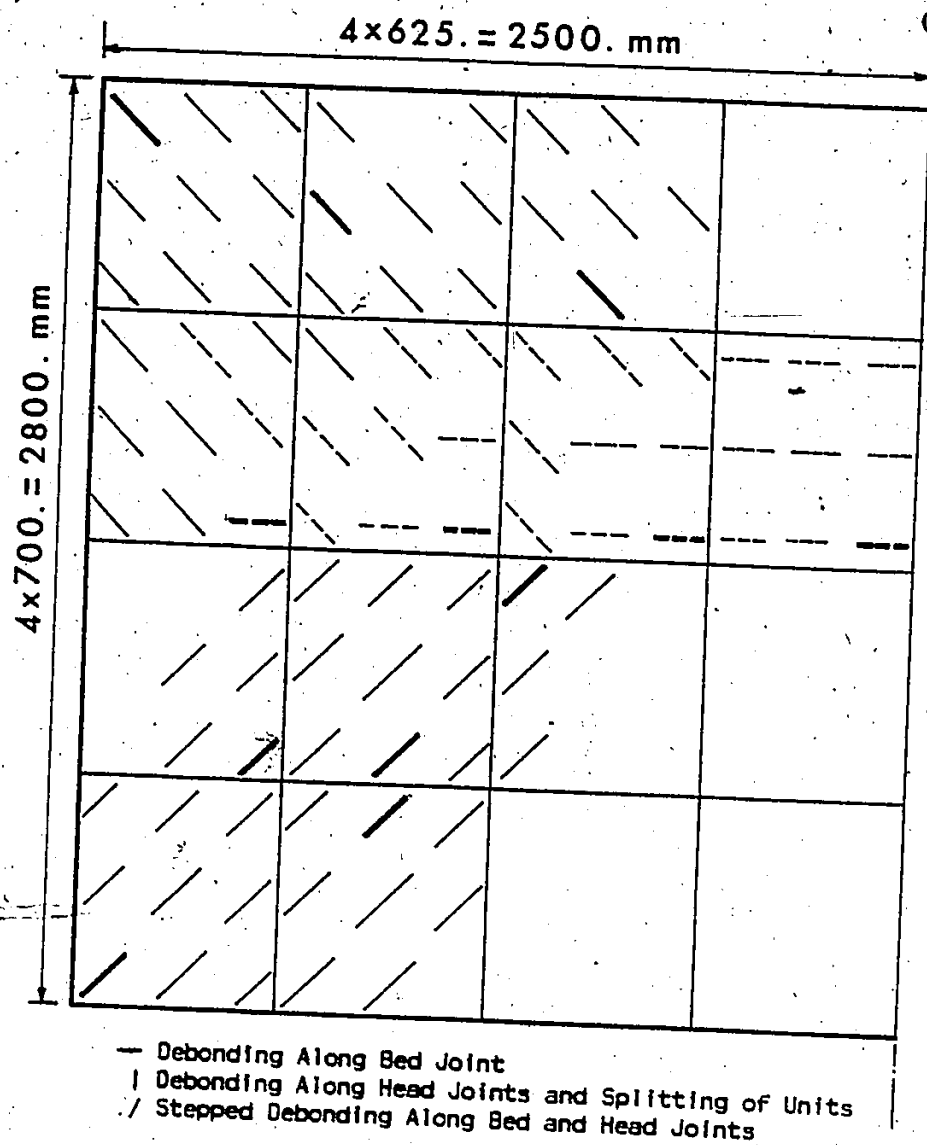
Figure 6.15   Predicted Cracks at Integration Points for Series WII
Walls Using a 4x4 Mesh

— Debonding Along Bed Joint
I Debonding Along Head Joints and Splitting of Units
/ Stepped Debonding Along Bed and Head Joints
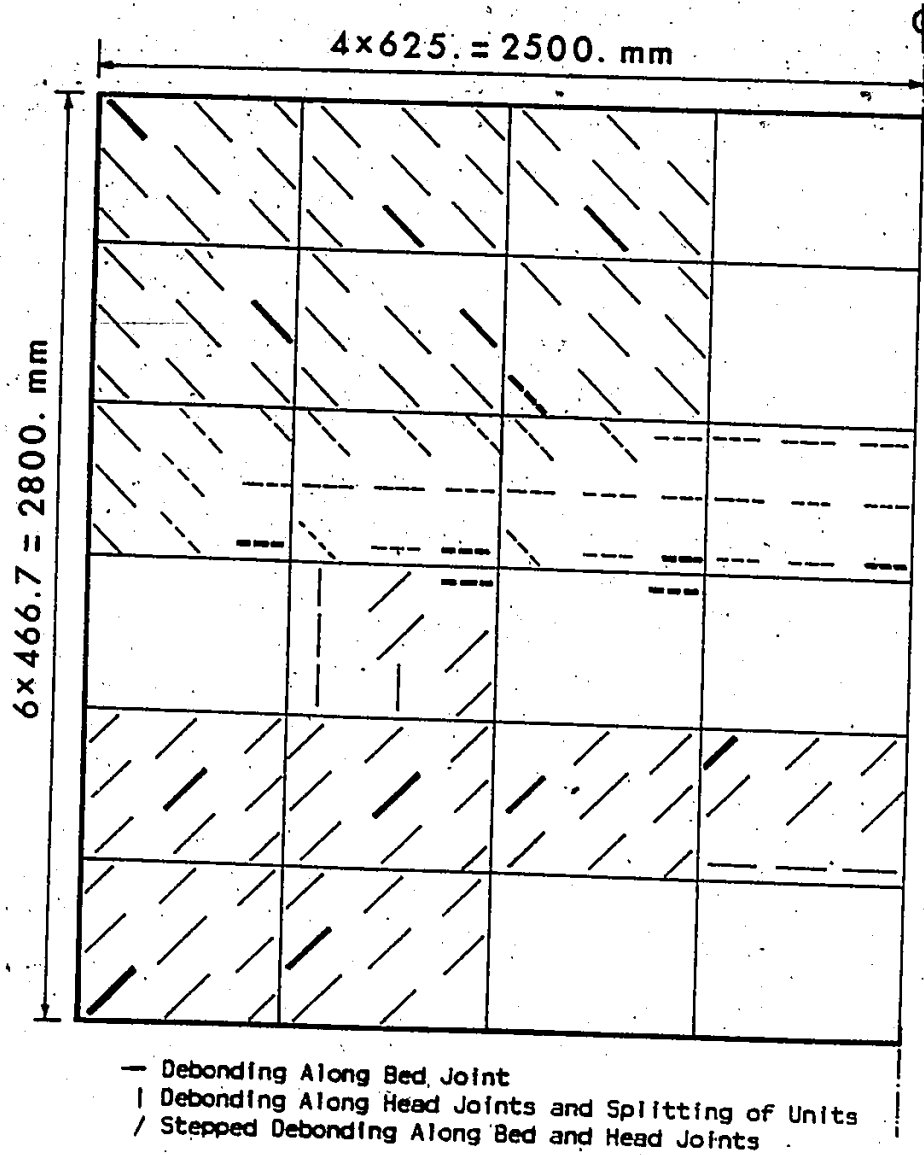
Figure 6.16   Predicted Cracks at Integration Points for Series WII
Walls Using a 4x6 Mesh

- Debonding Along Bed Joint
| Debonding Along Head Joints and Splitting of Units
/ Stepped Debonding Along Bed and Head Joints
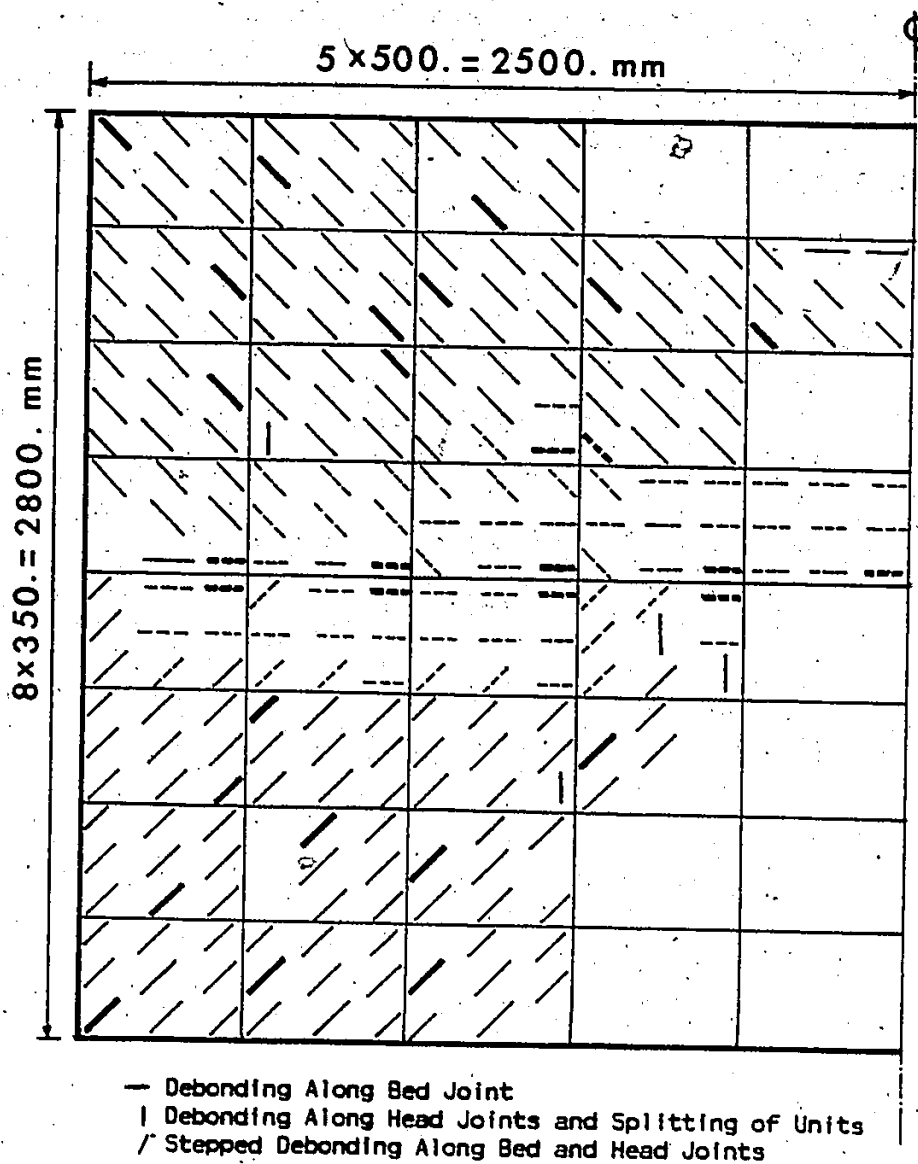
Figure 6.17   Predicted Cracks at Integration Points for Series WII
Walls Using a 5x8 Mesh

6.10.3 Finite Element Analysis of Different Full Scale Wall Series

Analyses of walls from the full scale wall test series were performed using the proposed model and considering the previously mentioned stiffness reduction factors in a 4x4 element mesh. These results are compared to the test results reported earlier in this investigation as follows:

Series WV:

The analysis for a 5.00x2.80 m wall simply supported only on the top and bottom was performed and the resulting load-deflection predictions together with the available test data for the three test walls of Series WV are shown in Figure 6.18. The linear load-deflection relationship predicted using the model is in good agreement with the available experimental data regarding both wall capacity and deflections. It should be noted that the good agreement between the observed and predicted flexural rigidity normal to the bed joints also implies reasonable predictions for the elastic constants which were determined according to the expressions given in Appendix C.

The cracks at integration points resulting from this analysis are shown in Figure 6.19. The spread of the cracks to most of the integration points within a cracked element was not surprising. This was because of the smeared cracking approach used and the assumed continuous displacements within the elements. This approach cannot allow any sharp crack or strain discontinuity to take place within the elements. However, identification of the first crack to develop within each element (marked with a heavy line in this figure) indicated a
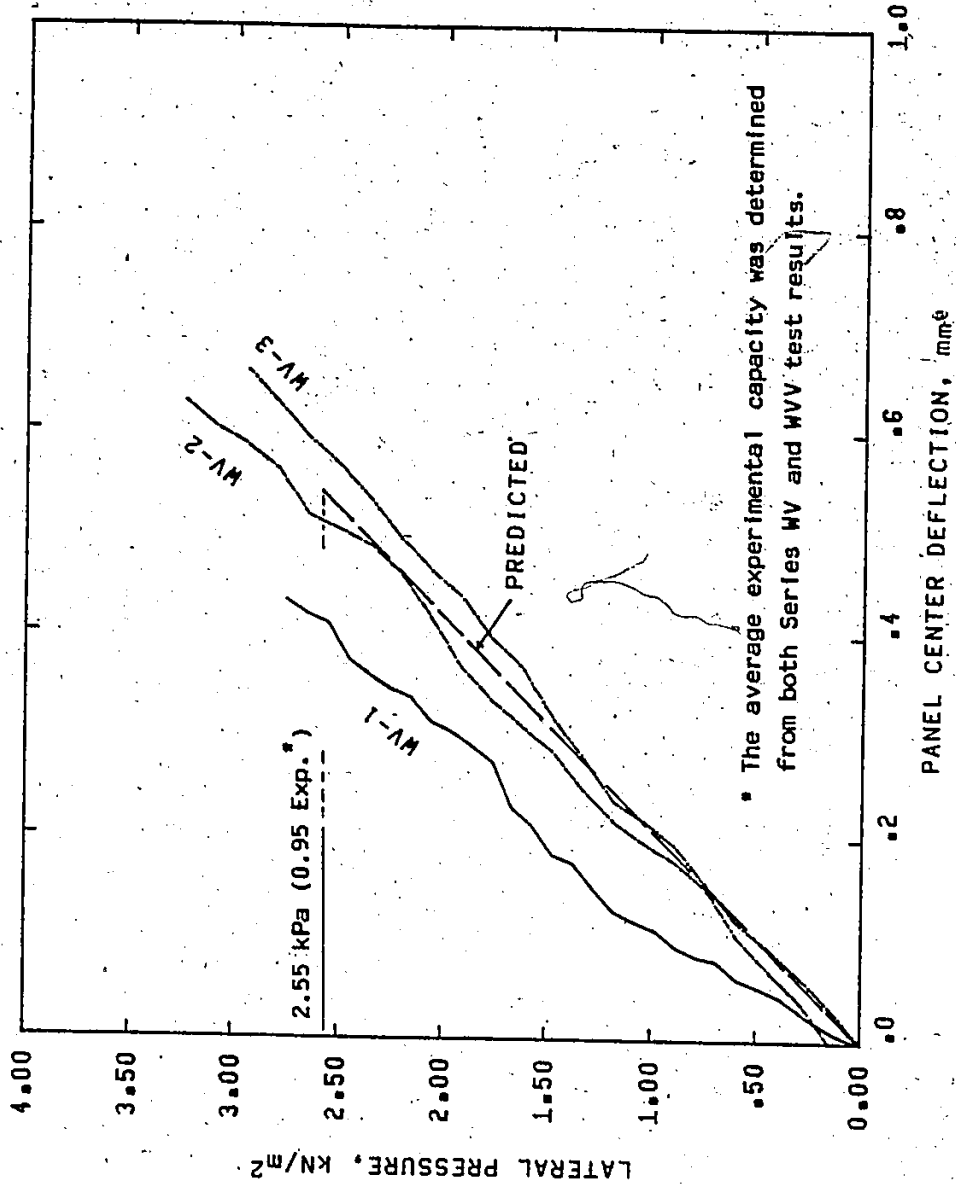
Figure 6.18   Deflections for Series WV Walls

4×625. = 2500. mm

4×700. = 2800. mm

— Debonding Along Bed Joint
| Debonding Along Head Joints and Splitting of Units
/ Stepped Debonding Along Bed and Head Joints
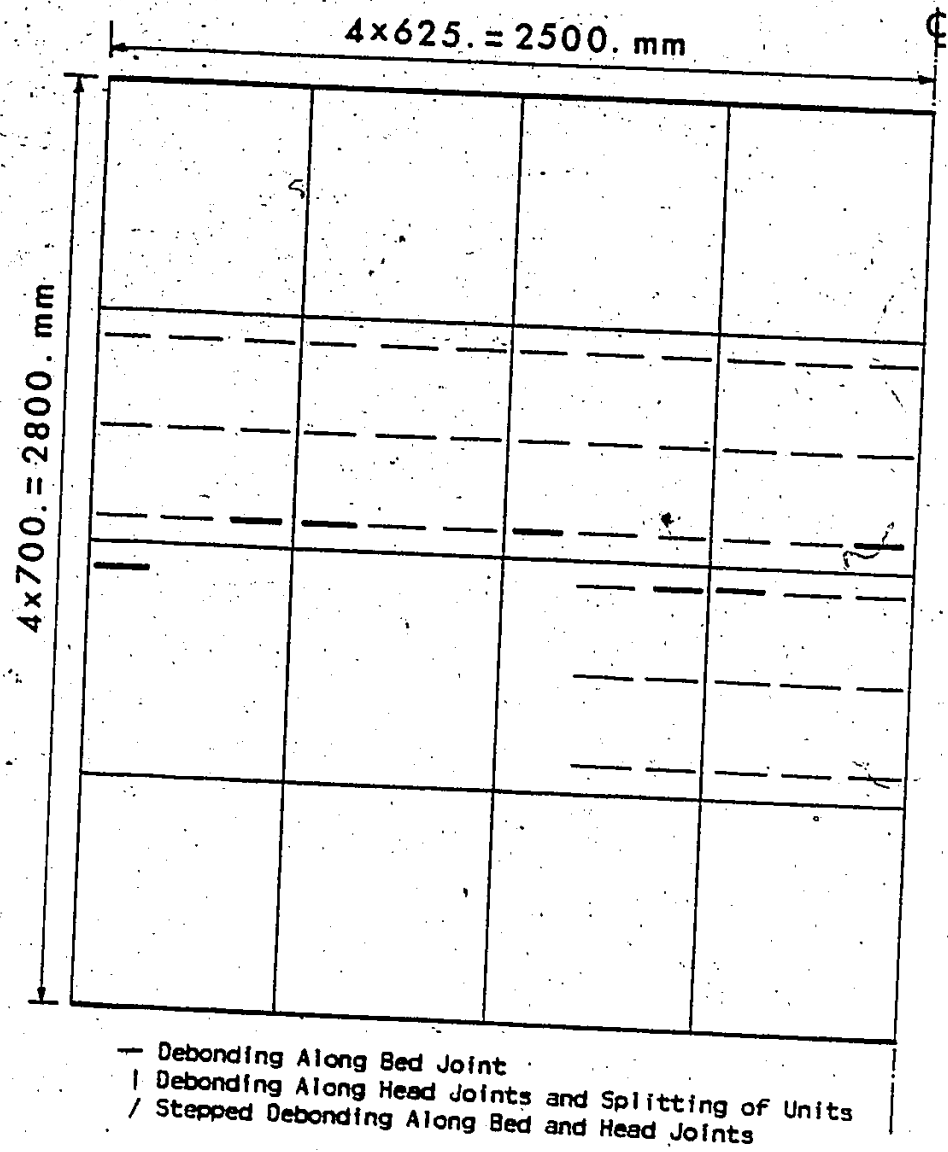
Figure 6.19   Predicted Cracks at Integration Points for Series WV Walls

central horizontal crack near the mid-height of the wall which was similar to the simple cracking pattern observed experimentally.

Series WH:

Wall Series WH, which also has dimensions of 5.00 m long by 2.8 m high but supported on the two vertical sides, was analysed using the proposed model. The results of this analysis are shown in Figures 6.20 and 6.21. The load-deflection predictions shown in Figure 6.20 together with the available experimental data again indicated good model predictions regarding both capacity and deflections. Similar to the observed behaviour, the predicted load-deflection had a nonlinear relationship. This was accomplished in the model by introducing the nonlinear behaviour of the mortar head joints which were assumed to behave plastically after their capacities had been exceeded. As shown in Figure 6.20, the load level at the predicted change in stiffness was close to the load where this stiffness change was observed. The reasonable predictions of the deflections shown in Figure 6.20 confirm the proposed expressions for the elastic constants given in Appendix C for the flexural rigidity parallel to the bed joints. It also supports the argument for having nonlinear behaviour rather than cracking in the mortar head joints where the joint capacity has been exceeded.

The spread of predicted cracks at integration points within the elements shown in Figure 6.21 is also attributed to the smeared crack approach used in this model. However, identification of the first crack to develop in each element reflects the same trend of cracking as that observed experimentally. The shift of the predicted vertical crack from
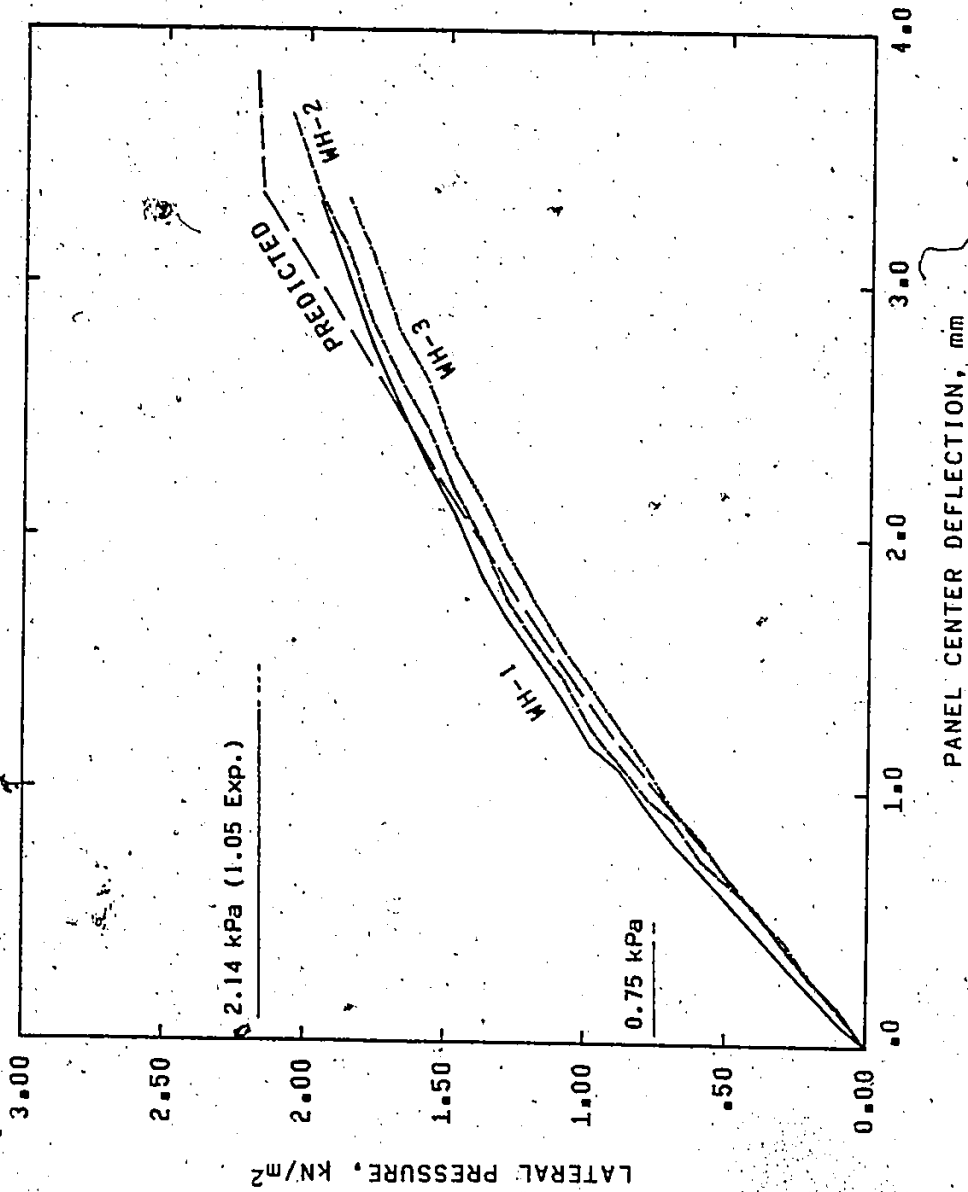
Figure 6.20   Deflections for Series WH Walls
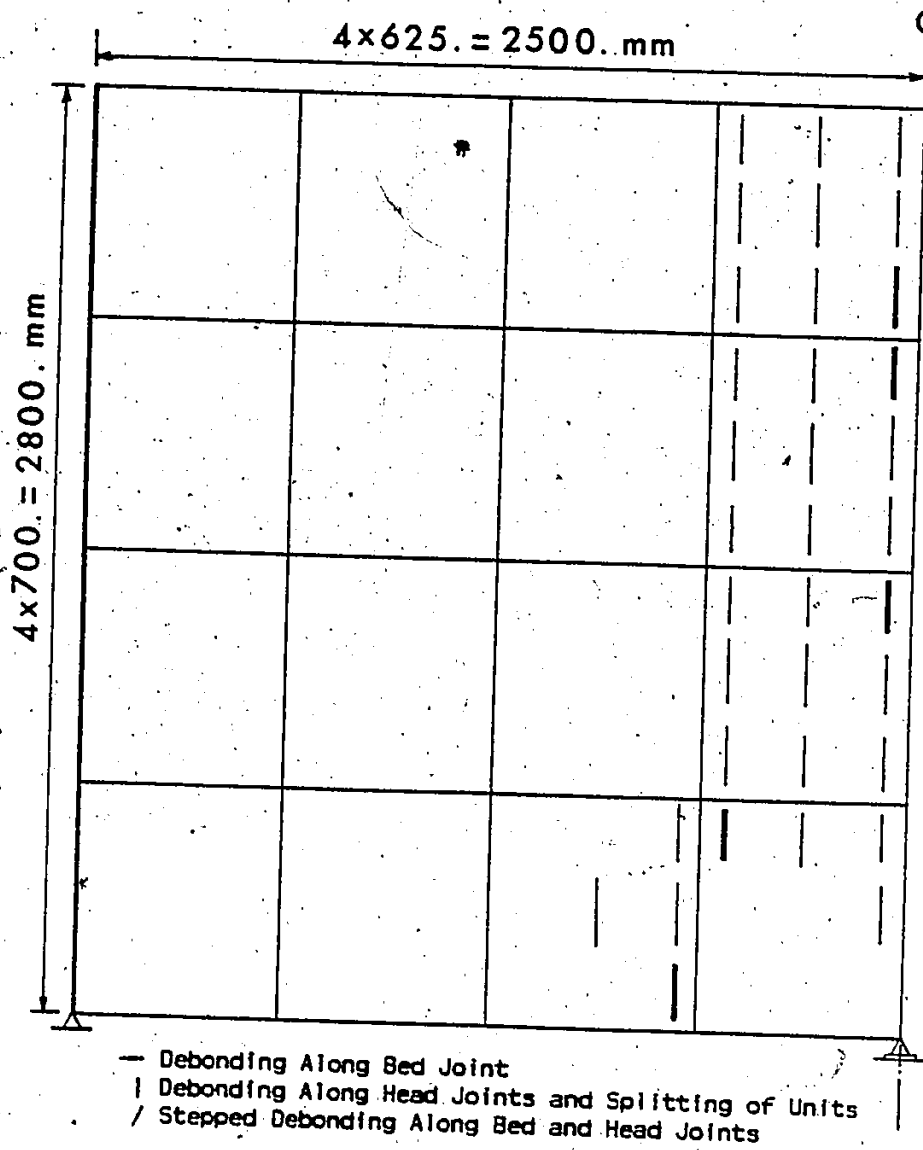
Figure 6.21   Predicted Cracks at Integration Points for Series WH Walls

- Debonding Along Bed Joint
| Debonding Along Head Joints and Splitting of Units
/ Stepped Debonding Along Bed and Head Joints

the wall center near the bottom edge may be attributed to the effect of the roller support introduced at the center to support the wall self weight. This was also observed experimentally in wall WH2 while in the two other walls the vertical crack over the full wall height was shifted half a block off the center which may also confirm this explanation.

Series WF:

For the wall series of the same 5.2 x 2.8 m dimensions as the standard wall but simply supported on three sides with the top free (Series WF), the analysis resulted in the predicted load-deflection and crack pattern shown in Figures 6.22 and 6.23, respectively. The load-deflection predictions are in reasonable agreement with the test results for both wall capacity and deflections. Although it is difficult to see, this analysis also indicates nonlinear behaviour in the early loading stages before failure. This is identified in Figure 6.22 where the experimentally observed nonlinearity is more obvious. Again, the reasonable deflection predictions combining the effects of flexural and torsional rigidities confirm both the determination of the elastic constants according to the proposed expressions in Appendix C and the suggested nonlinear behaviour of the mortar head joints. As can be seen in Figure 6.22, the predicted failure load agreed well with the experimentally recorded loads and was within 3% of the average.

The predicted cracks at integration points resulting from this analysis are shown in Figure 6.23 where it can be seen that the diagonal crack band is quite wide. As mentioned before, the smeared cracking approach is responsible for the spread of cracks within cracked

251
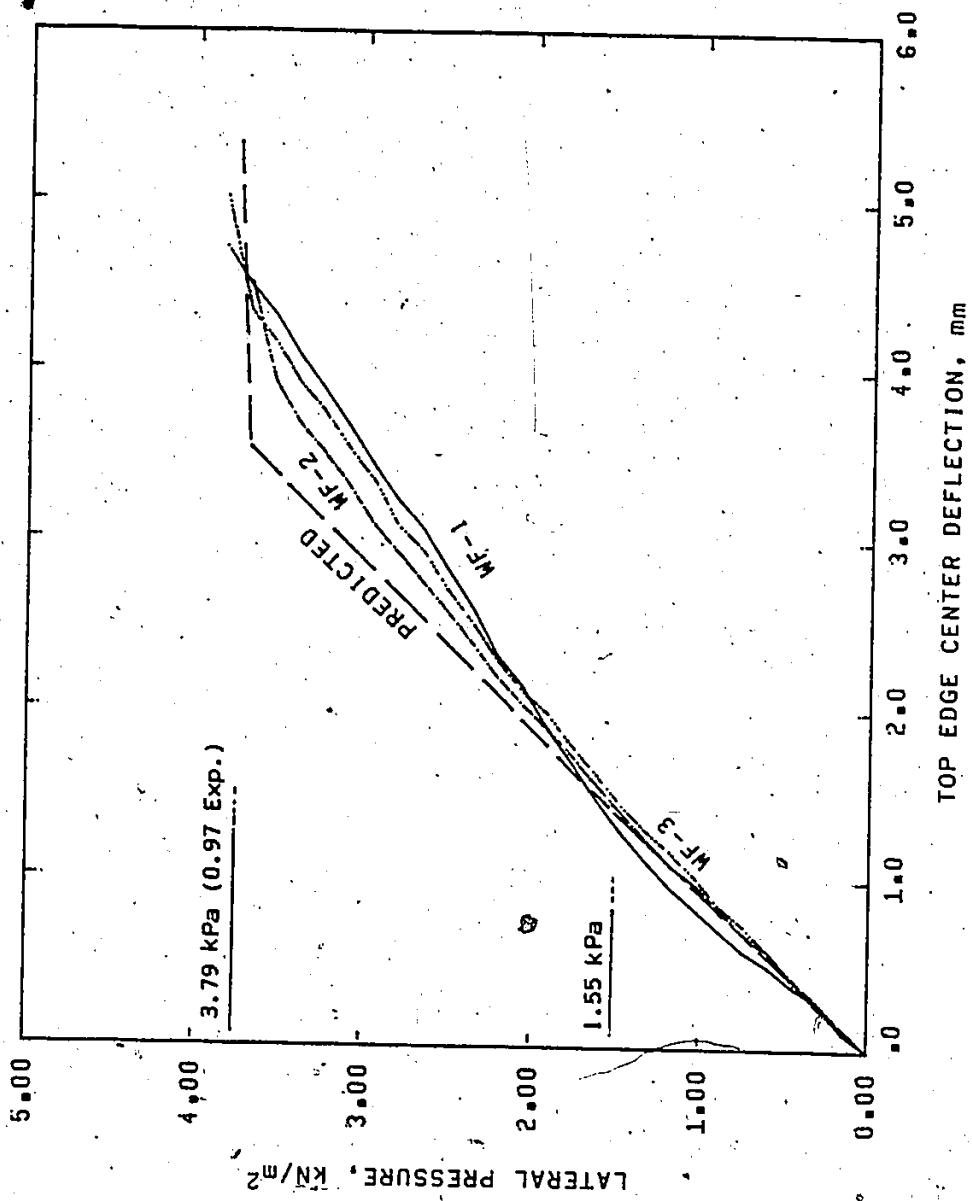
Figure 6.22   Deflections for Series WF Walls

4×625. = 2500. mm

4×700. = 2800. mm

— Debonding Along Bed Joint
| Debonding Along Head Joints and Splitting of Units
/ Stepped Debonding Along Bed and Head Joints
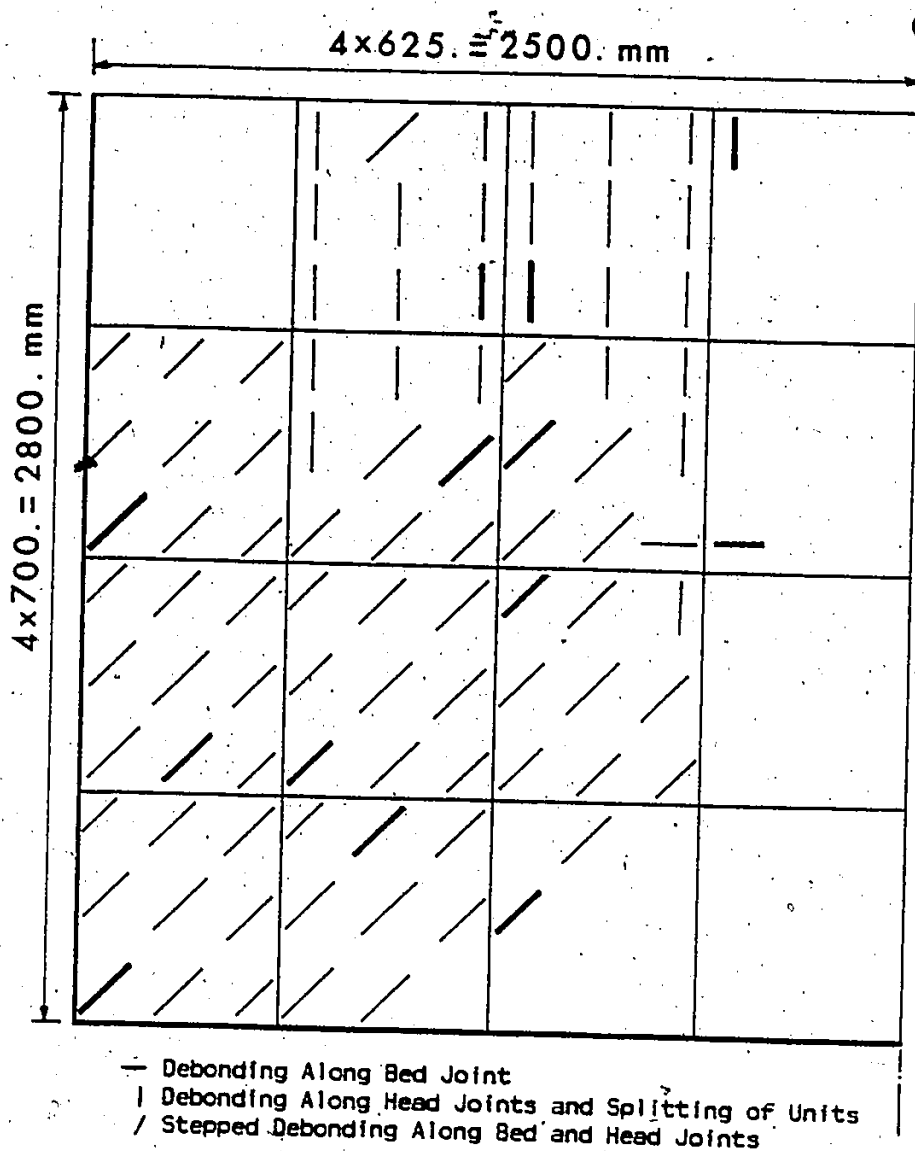
Figure 6.23 Predicted Cracks at Integration Points for Series WF Walls

elements. However, the spread of the crack band width to a large number of elements is attributed to the use of non-zero stiffness reduction factors. As mentioned in Section 6.10.1, use of non-zero values applies particularly to this diagonally stepped mode of failure. This resulted in some load transfer through the cracks which enabled the stresses to build up in other elements and reach the cracking limit. Identification of the first crack to develop in each element (marked with a heavy line in Figure 6.23) indicated the same trend of cracking as observed experimentally. Moreover, the predicted two vertical cracks near the top of the wall with the horizontal crack inbetween were also observed in two of the three walls tested.

Series WI:

For the test of the series with the smallest aspect ratio (Series WI), the analysis results are shown in Figures 6.24 and 6.25. The load deflection predictions together with the data for the three test walls are shown in Figure 6.24. It should be noted that one of these walls, Wall WI-1, was part of the preliminary series fabricated using different types of concrete blocks and mortar sand.

The analysis predicted a first cracking pressure which was considerably higher than the average experimental pressure. However, it should be noted that two of these walls had a relatively low first cracking pressure while, in the third wall, the observed first cracking pressure was reported at a level only 6% less than that predicted by the proposed model. The larger difference between the predicted and experimentally recorded first cracking pressures for the other two walls

254

PANEL CENTER DEFLECTION, mm
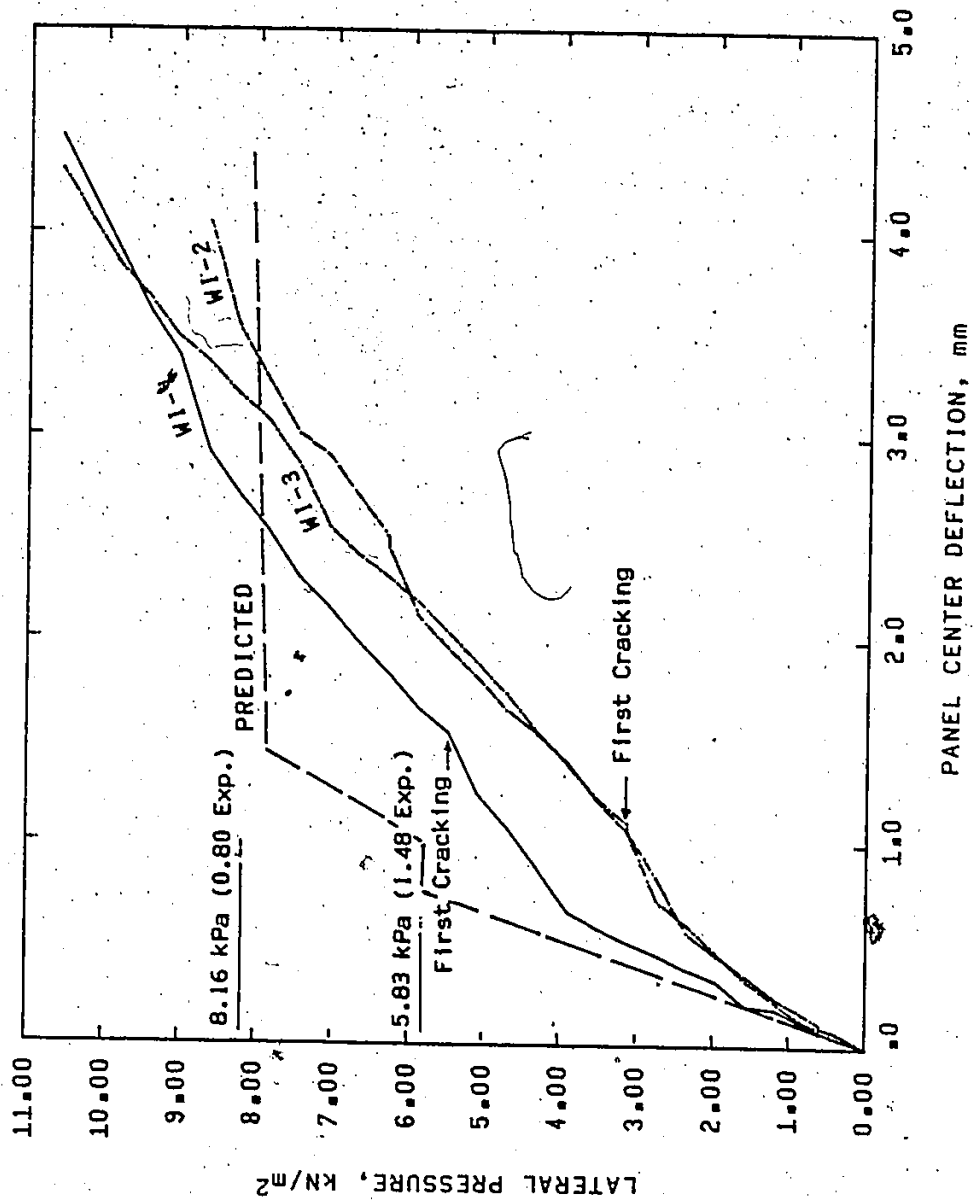
Figure 6.24   Deflections for Series WI Walls

4×425. = 1700. mm

4×700. = 2800. mm

— Debonding Along Bed Joint
| Debonding Along Head Joints and Splitting of Units
/ Stepped Debonding Along Bed and Head Joints
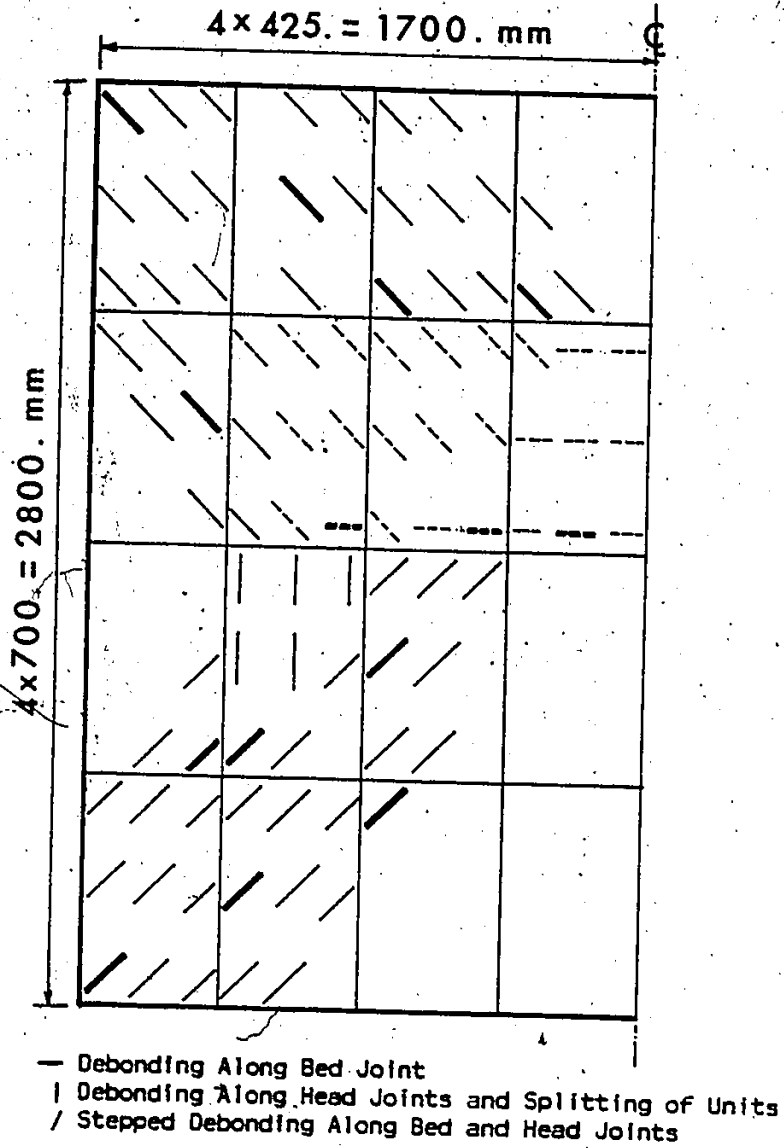
Figure 6.25   Predicted Cracks at Integration Points for Series
WI Walls

may be attributed to the variability of the flexural tensile strength normal to the bed joints and accordingly the possibility of having a critical combination of weak joints near the center of the wall. This was not incorporated in the proposed model where only the mean strengths were considered.

The model prediction for the wall capacity was 20% lower than the average experimental capacity from the three test walls. This may be attributed to the fact that, due to the smeared crack approach used in this proposed model, the analysis yielded an initial horizontal crack band which was so wide that it may have weakened the whole wall and consequently caused premature failure.

The predicted crack pattern shown in Figure 6.25 indicated the same trend of cracking as observed experimentally with the first horizontal center crack (marked as dotted lines in this figure), the diagonal cracks originating from the panel corners, and some vertical cracks near wall mid-height. This pattern can be easily recognized from Figure 6.25 by considering the first crack to develop in each element which were marked with heavy lines in this figure. The statement made earlier regarding the wide diagonal crack band is also applicable in this case.

Series WII:

The Series WII walls which were the basis for other comparisons had an intermediate aspect ratio. It was analysed using the proposed model and the predicted deflections together with the experimental data are shown in Figure 6.26. The predicted first cracking pressure was 15%
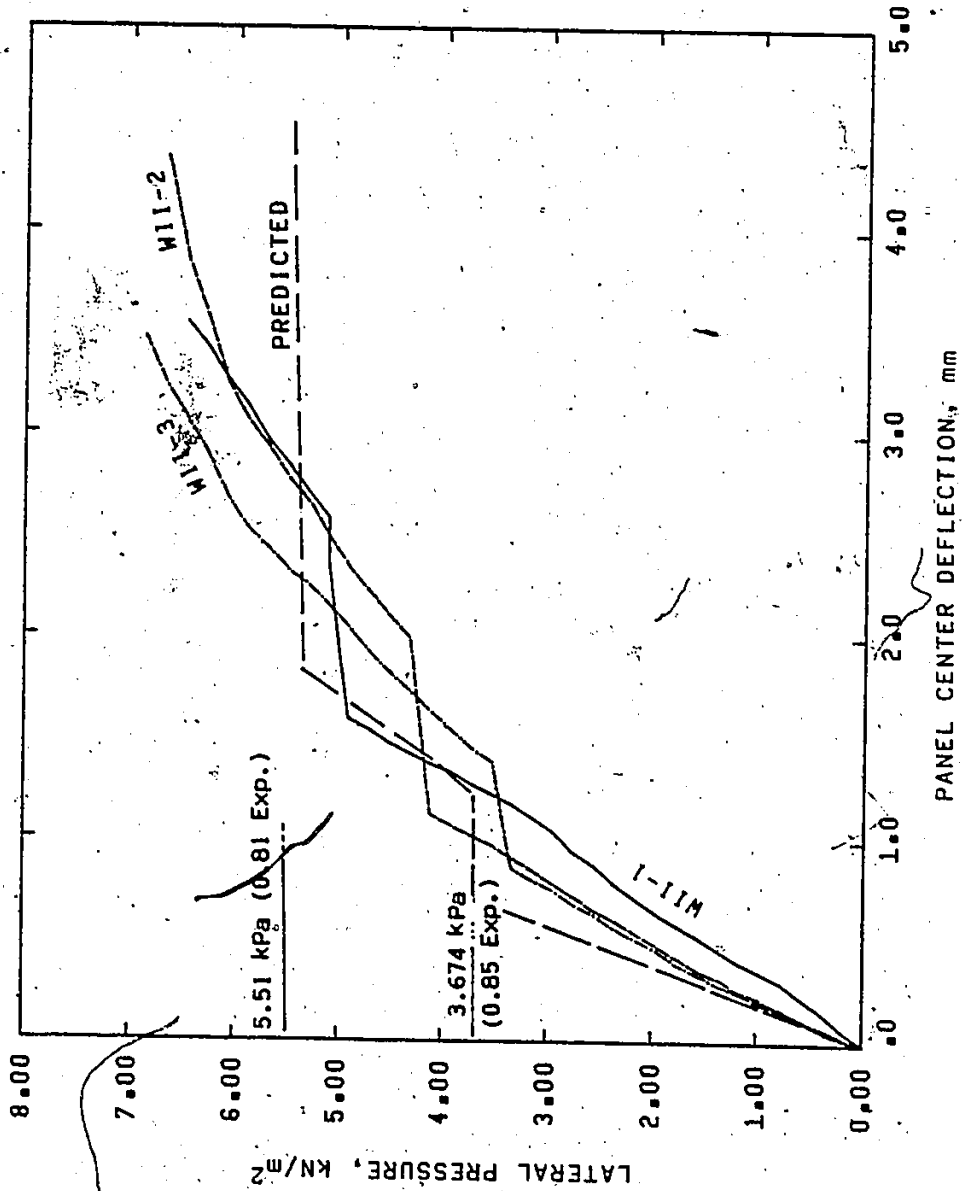
Figure 6.26 Deflections for Series WII Walls

lower than the average experimental pressure. This is considered to be acceptable compared to the known variability associated with the flexural tensile strength normal to the bed joints. The wall capacity was also predicted and found to be 19% lower than the average test capacity. This difference may be attributed to both the expected variability in masonry strength and the wide band of horizontal cracks developed prior to the final failure. However, the effect of the wide band of horizontal cracks in this case is expected to be less significant than that of Series WI. This is because, for larger horizontal spans, the diagonal cracks in Series WII meet the horizontal center crack far from the wall center where the horizontal crack band is narrower and consequently should have less effect on the capacity prediction. The sudden increase in deflection at first cracking shown in Figure 6.26 is larger than the corresponding plateau for the Series WI walls which had the smallest aspect ratio. This was observed for both the test results and the predictions which confirmed the ability of the model to predict different behaviours as observed experimentally.

The predicted cracks at the integration points for this wall, shown earlier in Figure 6.15, had the same trend of cracking pattern as observed experimentally. The two statements made earlier regarding the spread of cracks within cracked elements and the width of the band of diagonal cracks are also applicable in this case.

Series WIII:

Series WIII which had the largest aspect ratio, was also analysed using the proposed model and the results of this analysis were

plotted in Figures 6.27 and 6.28. It should also be noted that one of the three walls of this series, WIII-1, was part of the preliminary series where different types of concrete blocks and mortar sand were used. The predicted deflections together with the test data are shown in Figure 6.27. The predictions indicated a 30% increase in the first cracking pressure and a 4% decrease in the wall capacity compared to the average experimental values. However, the predicted first cracking pressure was only 11% higher than the corresponding value in one of the three walls tested. The difference between the predicted and the experimentally reported first cracking pressures may be partially attributed to the effect of the high variability in the flexural tensile strength normal to the bed joints and the associated possibility of having a critical combination of weak joints near wall mid-height. Although the effect of the width of the horizontal crack band on the failure load is still applicable, it is believed to be less significant than for the other two series mentioned earlier. This is because the diagonal cracks met the horizontal crack far from the panel center where the width of the horizontal crack band was smaller. Again, the predicted load-deflection behaviour shown in Figure 6.27 indicated a larger plateau at first cracking than the corresponding deflection increase in the other two series. This was also observed in the test data and hence confirmed the ability of the model to predict different behaviours.

In Figure 6.28, the predicted cracks at the integration points for this series, indicated the same trend of cracking as observed experimentally. However, comments regarding the influence of spread of

PANEL CENTER DEFLECTION, mm

LATERAL PRESSURE, kN/m²

PREDICTED

4.59 kPa (0.96 Exp.)

3.27 kPa (1.30 Exp.)

WIII-3

WIII-1

WIII-2
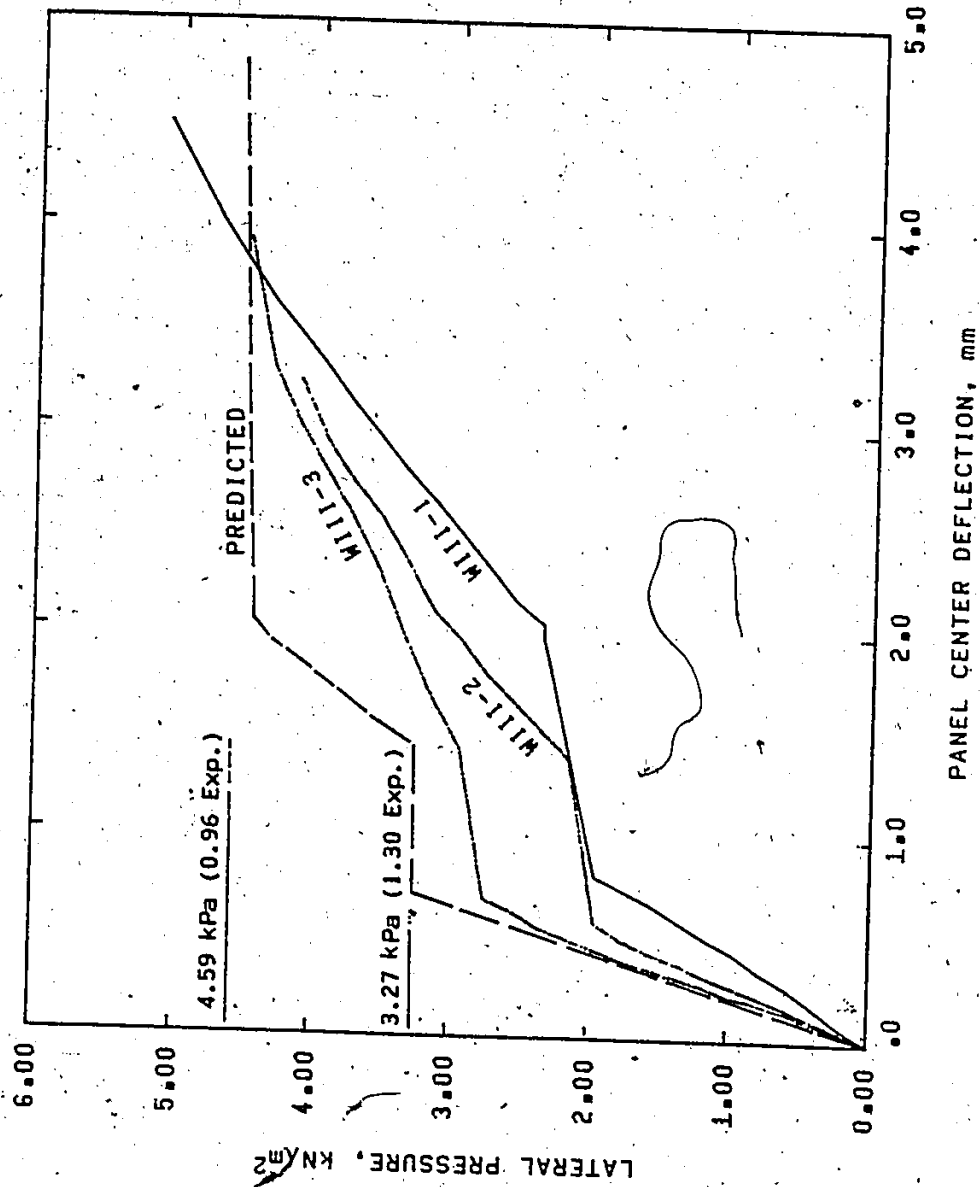
Figure 6.27   Deflections for Series WIII Walls

— Debonding Along Bed Joint
I Debonding Along Head Joints and Splitting of Units
/ Stepped Debonding Along Bed and Head Joints
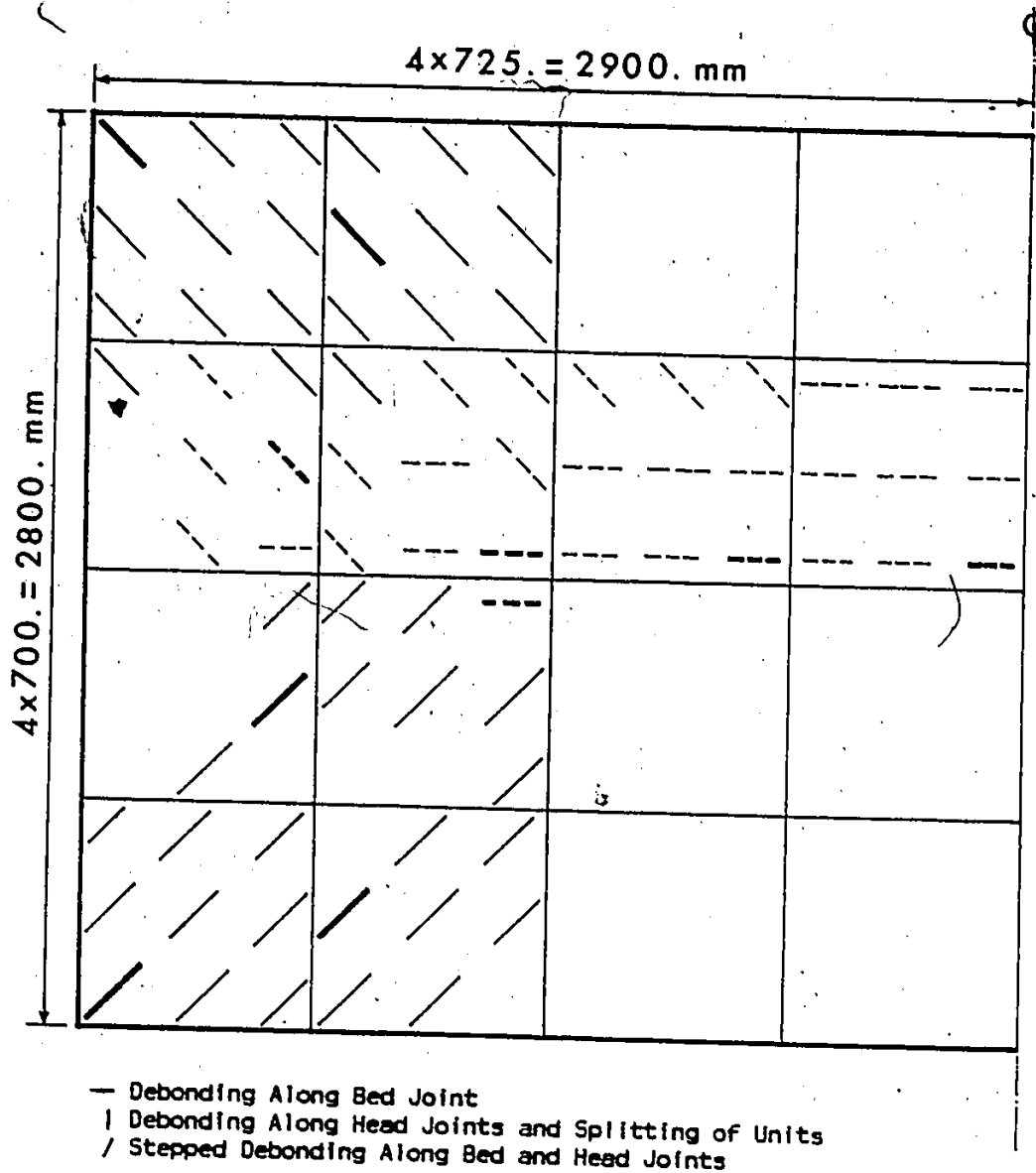
Figure 6.28   Predicted Cracks at Integration Points for Series
             WIII Walls

cracking within the elements and the width of the diagonal crack band are also applicable in this case. It should be noted that the length of the horizontal center crack between the diagonal cracks was larger than the corresponding distance predicted for the other two wall series. This is again similar to the observed results. It is suggested that this may be the reason for the larger plateau observed for this wall series for both the test results and the predictions.

Series WP:

For Wall Series WP, which had precompression applied along the top edge, the results of the analysis using the proposed model were shown in Figures 6.29 and 6.30. As can be seen in Figure 6.29, the analysis predicted a first cracking pressure and failure pressure which were respectively 5% and 20% lower than the corresponding average experimental values. Compared to Series WII, the good agreement in the first cracking pressure may be attributed to the effect of the precompression. In this regard, the additional load required to overcome the precompression stresses would lessen the relative importance of variability of flexural tensile bond and possible critical combinations of weak joints. However, for the failure pressure, the effect of the wide band of initial horizontal cracks is again thought to be a possible cause of the premature failure predicted by the model. The sudden increase in deflection at first cracking was less than the corresponding increase in Series WII where no precompression was applied. This was similar to the test results and again confirmed the ability of the model to predict different behaviours.
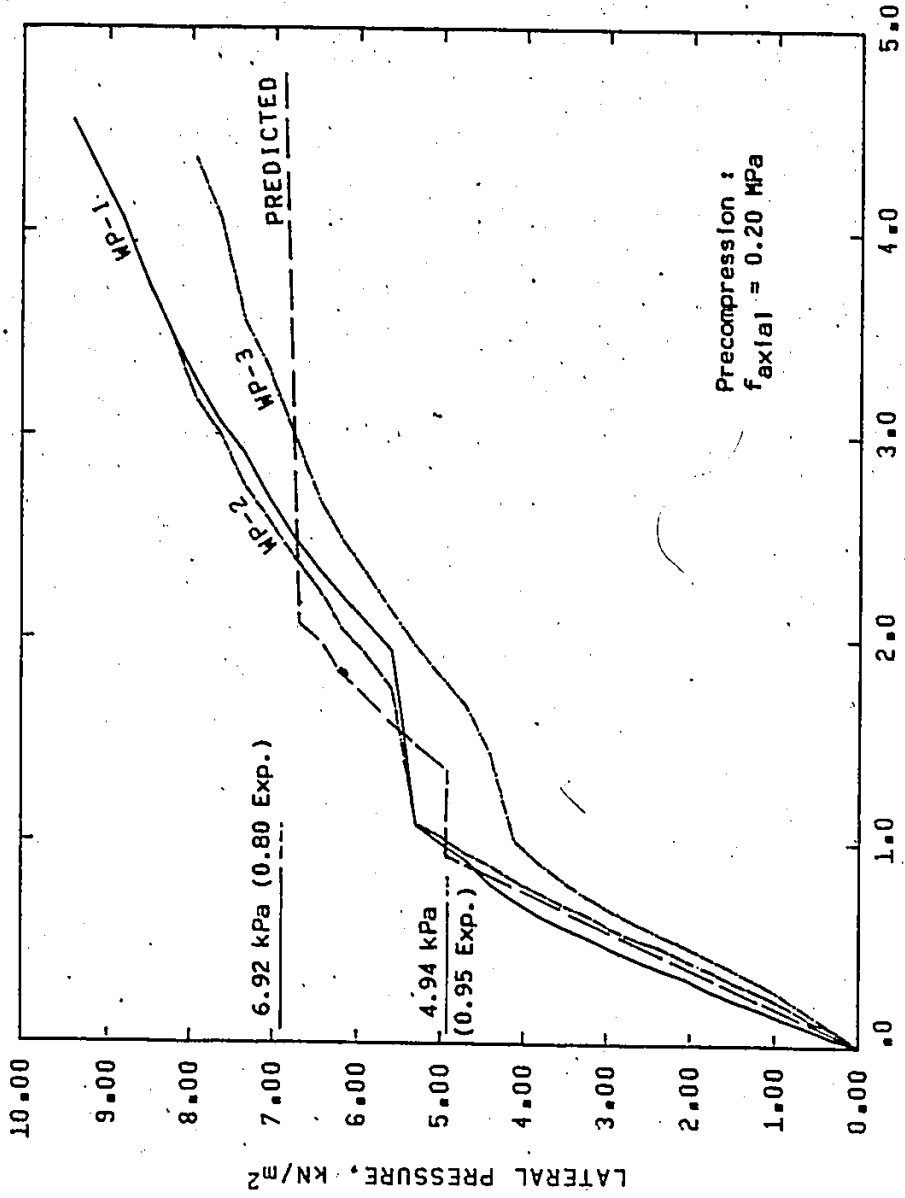
Figure 6.29 Deflections for Series WP Walls

— Debonding Along Bed Joint
| Debonding Along Head Joints and Splitting of Units
/ Stepped Debonding Along Bed and Head Joints
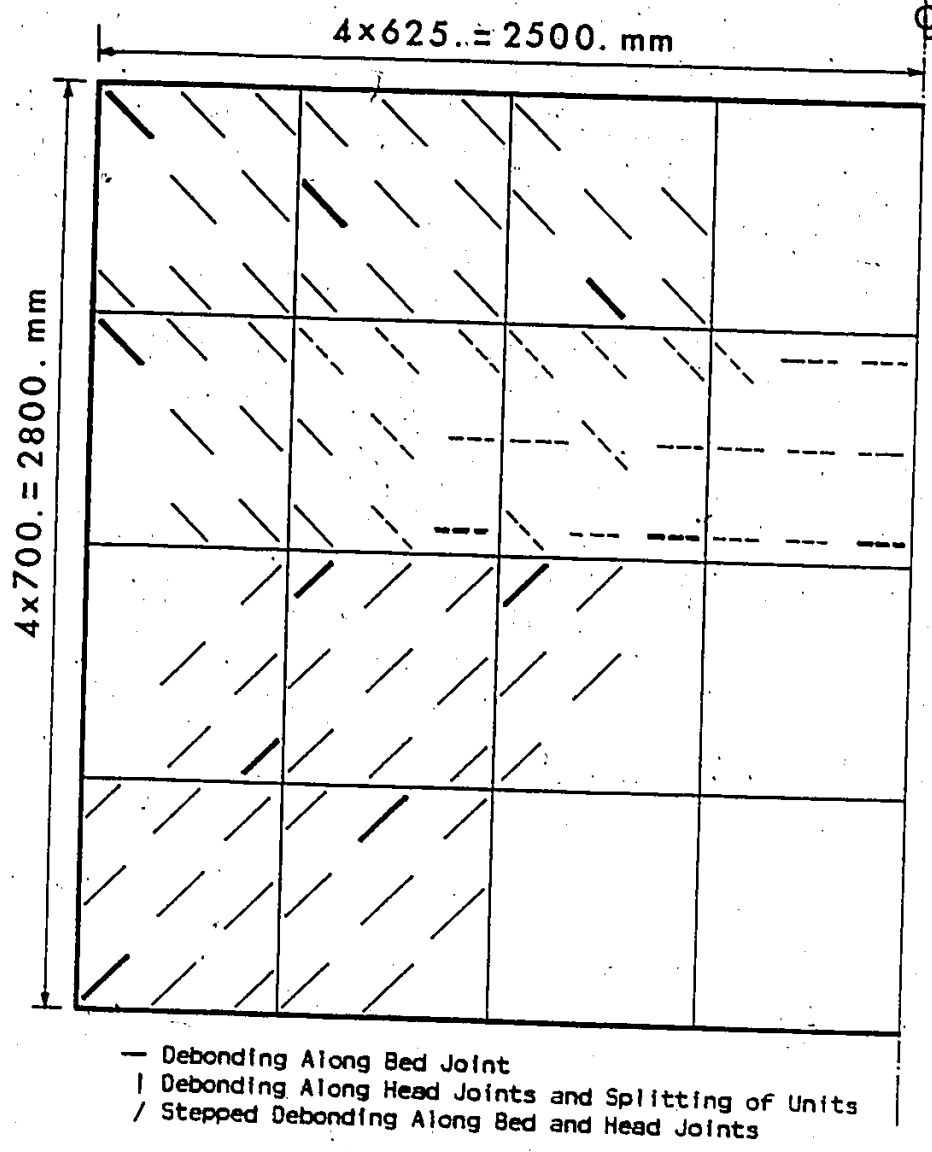
Figure 6.30   Predicted Cracks at Integration Points for Series WP Walls

The predicted cracks at integration points shown in Figure 6.30 reflect the same cracking trend as observed experimentally. This can be seen by identifying the first crack to develop in each element which was marked with a heavy line. Moreover, the previous statements regarding the influence of the spread of cracking and the wide diagonal crack band are again applicable in this case.

6.11 CONCLUDING REMARKS

The conclusions which can be drawn from the investigation reported in this chapter are as fellows:

1. The analysis of hollow block or multi-wythe masonry walls cannot be directly performed using the available finite element models for masonry particularly when out-of-plane loading is present.

2. The proposed model can be used to analyse most large masonry assemblages, structural elements and structures. This is because it has been developed in a generalized form to handle both in-plane and out-of-plane loading conditions including both constant and variable (or incremental) applications of each. Also, it can be used for multi-wythe walls by adopting a layered plate approach in the finite element formulation. Moreover, the orthotropic and composite nature of masonry was considered in the model by including the orthotropic properties for each layer and implementing the macroscopic biaxial failure criterion proposed in Chapter 5.

3. The effects of transverse shear deformations were shown to be significant in the case of laterally loaded hollow block masonry

due to the presence and the discontinuity of the cross webs. Accordingly; the transverse shear degrees of freedom were included in the proposed model to account for these significant deformations. In this case, the cross webs can be replaced by an equivalent lamina or core layer with an acceptable accuracy.

4. The concept of using layered plates enabled the analysis to be extended beyond the elastic or cracking limit by modifying the stiffness of the particular layer which had reached this limit. This permitted modelling of observed behaviour of laterally loaded hollow block walls where cracking was only observed on the tension side of the wall.

5. It is suggested that the stiffness reduction factors after cracking vary depending on the failure mode and the state of stress on the assemblage. The values chosen for these factors seem to be reasonable and are recommended for lack of other data.

6. The proposed model was verified by checking its predictions against available linear elastic and nonlinear solutions for different cases. These comparisons showed that the model predictions were in good agreement with the available solutions in all cases. Also, the convergence study performed for thin square plates under uniformly distributed load illustrated fairly rapid convergence in all cases. The comparisons with the available solutions and the convergence study established that the model was fundamentally correct before it was used to

predict behaviour of masonry assemblages.

7. The model predictions for Wall Series WV, WH, and WF established the acceptability of the model for predicting the behaviour of masonry walls for cases where no prior cracking takes place before final failure. Wall Series WI, WII, WIII, and WP are walls supported on all four sides which, as observed experimentally, experienced first cracking prior to the final failure with relatively large amount of reserve strength after first cracking. These wall series included three different aspect ratios and a series with precompression load applied along the top edge of the wall. They illustrated the ability of this finite element model to predict behaviour through various phases of cracking.

8. The comparisons of the proposed model predictions with the test data for full scale hollow block walls showed that the proposed model is capable of predicting the behaviour of full scale masonry walls with an acceptable degree of accuracy. Therefore, this model will be used to produce data for untested wall conditions and configurations and thus to extend the level of knowledge about masonry wall behaviour.

CHAPTER 7

DESIGN METHODS FOR LATERALLY LOADED MASONRY WALLS

7.1   INTRODUCTION

The available design methods for masonry walls subjected to lateral (out-of-plane) loading reviewed earlier in Chapter 1 revealed the lack of availability of a universally accepted design method. It is thought that a universally acceptable design method should be rationally developed and provide reasonably accurate predictions. Moreover, most available methods were supported by comparisons with experimental work performed primarily on brick masonry.

In this chapter, the nonlinear finite element model developed in this study will be used to extend the limited test data to cover a reasonably large range of panel sizes. This is necessary to judge the reliability of any design method. Then, strengths will be calculated using some of the available design methods in order to assess their reliability. Finally, a proposal for a rational design method for laterally loaded masonry panels will be presented.

7.2   PREDICTED BEHAVIOUR FOR MASONRY PANELS
OF DIFFERENT ASPECT RATIOS
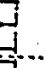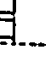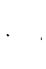
In order to be able to evaluate any design method, test data for a large range of panel sizes should be available. However, due to the considerably expense for full scale tests, only three aspect ratios for

268

walls supported on four sides and one aspect ratio for walls supported on three sides were examined experimentally. In this section, the finite element model presented in the previous chapter is used to extend the available data to cover a reasonable range of panel sizes (aspect ratios).

The range of aspect ratios included in these analyses was chosen to cover the whole range reported in the British code [28] and extended beyond it to be used for defining the approximate limits for two-way action. Therefore, a range of aspect ratios from 0.36 to 4.24 was examined and the results of these analyses for wall panels supported on four and three sides are reported in this section.

The analyses performed for walls supported on all four sides yielded the results given in Table 7.1 and shown in Figure 7.1. These results showed two distinct regions of different behaviour according to the aspect ratios. For aspect ratios up to nearly 0.5, the panels experienced nonlinear behaviour in mortar head joints after the joint strength has been exceeded. All cracks in most of these cases were developed right at failure to form a crack pattern which was characterized by a central vertical crack and diagonal cracks originating from the corners and meeting at this vertical crack. For, aspect ratios larger than 1.2, the behaviour was characterized by an initial horizontal crack extending practically the whole panel length and diagonal cracks meeting at this horizontal crack to complete the crack pattern required as a failure mechanism. After first cracking, these panels had different amounts of reserve strength which diminished

Table 7.1   Model Predictions for Walls Supported on All Four Sides

Dimensions		Aspect Ratio	Predicted Crack Pattern	Predicted Capacities kN/m²		
Wall $L_o \times H_o$ m	Frame $L \times H$ m	L/H		Head Joint Strength[a]	Initial Crack[b]	Failure
1.2 × 2.8	1.0 × 2.8	0.36		20.2	45.3[c]	56.4
1.6 × 2.8	1.4 × 2.8	0.50		12.0	28.2[c]	31.8
2.0 × 2.8	1.8 × 2.8	0.64		8.9		20.4
2.4 × 2.8	2.2 × 2.8	0.79		7.4	13.3	13.7
2.8 × 2.8	2.6 × 2.8	0.93		6.6	9.6	11.6
3.6 × 2.8	3.4 × 2.8	1.21			5.8	8.2
4.0 × 2.8	3.8 × 2.8	1.36			5.0	7.0
5.2 × 2.8	5.0 × 2.8	1.79			3.7	5.5
6.0 × 2.8	5.8 × 2.8	2.07			3.3	4.6
8.0 × 2.8	7.8 × 2.8	2.79			2.83	3.7
9.6 × 2.8	9.4 × 2.8	3.36			2.7	3.1
10.0 × 2.8	9.8 × 2.8	3.5			2.67	3.1
11.2 × 2.8	11.0 × 2.8	3.93			2.63	2.63
12.0 × 2.8	11.8 × 2.8	4.21			2.6	2.6

a. This indicates the load at which the flexural tensile strength of a head joint was reached. However, the assumption of partial plasticity prevented cracking at this stage.

b. Unless otherwise mentioned, this indicates the load at which initial horizontal crack at panel center was developed.

c. This indicates the load at which an initial crack was developed near panel corner.
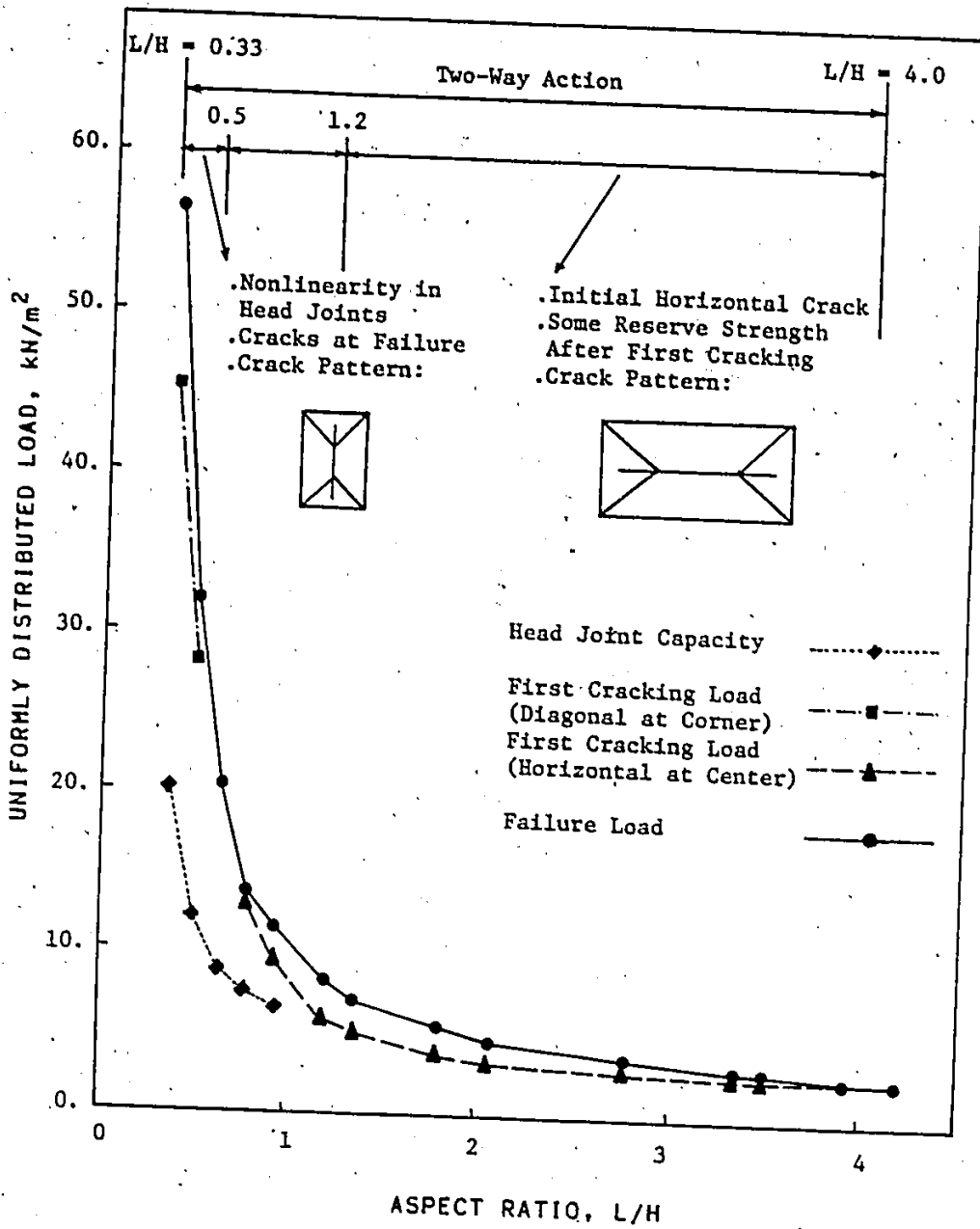
Figure 7.1   Predicted Behaviour of Walls Supported on All Four Sides

with increase in panel length or aspect ratio. The aspect ratios between 0.5 and 1.2 may be considered as a transition region between the two distinct patterns mentioned above.

The differences between the predicted capacities from the model compared to those for one-way action are shown in Figure 7.2. From this comparison, it may be concluded that for aspect ratios less than 1/3 or more than 4.0, the panel capacity may be predicted from the one way approximation with an error less than 5 or 6%, respectively. This error is conservative and considered to be acceptable.

Wall panels supported on three sides with the tops free were also analysed for the same range of aspect ratios. The results of these analyses are given in Table 7.2 and Figure 7.3. According to these analyses, all panels experienced nonlinear behaviour in the head joints after their capacity have been exceeded but prior to final collapse. These results also showed two distinct regions with two different crack patterns. For aspect ratios up to approximately 1.5, the predicted crack patterns were composed of two diagonal cracks originating from the corners and meeting at a vertical central crack which then extended to the free edge. However, for aspect ratios larger than 2.0, the crack pattern consisted of only the diagonal cracks which extended up to the free edge. The region between these two patterns may be considered as a transition zone with the intermediate pattern shown in Table 7.2.

The comparison with predictions based on one-way action showed that the panel capacity for a wall having a free top may be determined using the one-way bending approximation with an error less than 3.5% for aspect ratios less than 1/2. This error is conservative and is also
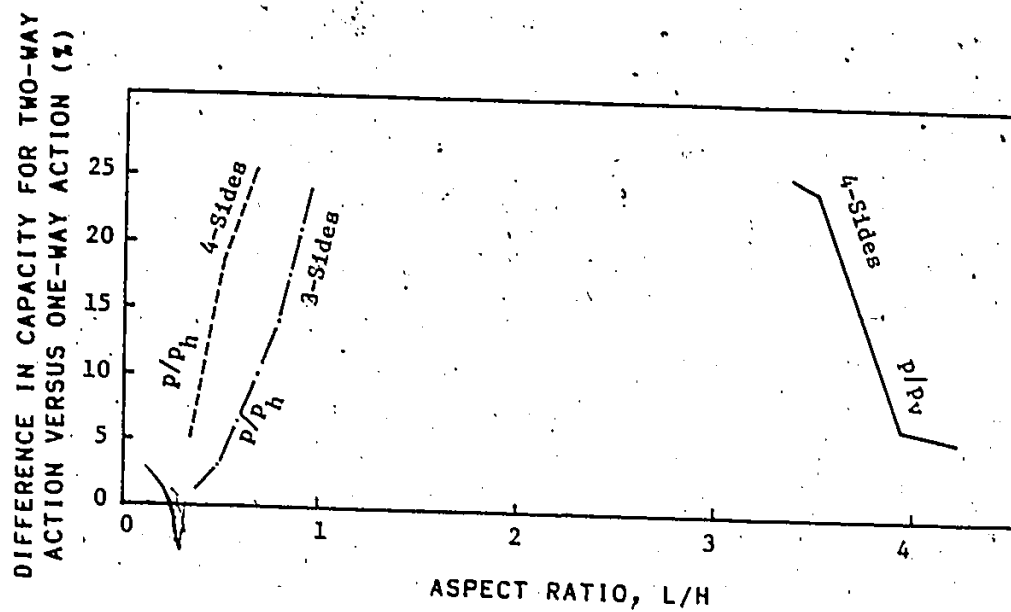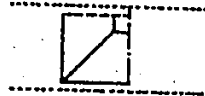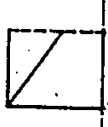
Figure 7.2   Errors in Predicted Capacity If One-Way Action
             Is Assumed

Table 7.2   Model Predictions for Walls Supported on Three Sides With the Tops Free.

Dimensions		Aspect Ratio	Predicted Crack Pattern	Predicted Capacities kN/m^2	
Wall $L_O \times H_O$ m	Frame $L \times H$ m	L/H		Head Joint Strength[*]	Failure
1.2 × 2.8	1.0 × 2.85	0.35		19.0	53.3
1.6 × 2.8	1.4 × 2.85	0.49		9.7	27.8
2.0 × 2.8	1.8 × 2.85	0.63		6.1	17.6
2.4 × 2.8	2.2 × 2.85	0.77		4.3	12.4
2.8 × 2.8	2.6 × 2.85	0.91		3.3	9.7
3.6 × 2.8	3.4 × 2.85	1.19		2.27	6.8
4.0 × 2.8	3.8 × 2.85	1.33		2.0	5.8
5.2 × 2.8	5.0 × 2.85	1.75		1.52	3.8
6.0 × 2.8	5.8 × 2.85	2.04		1.35	3.05
8.0 × 2.8	7.8 × 2.85	2.74		1.16	2.08
9.6 × 2.8	9.4 × 2.85	3.30		1.09	1.63
10.0 × 2.8	9.8 × 2.85	3.44		1.08	1.56
11.2 × 2.8	11.0 × 2.85	3.86		1.06	1.37
12.0 × 2.8	11.8 × 2.85	4.14		1.04	1.25

[*] This indicates the load at which the flexural tensile strength of a head joint was reached. However, the assumption of partial plasticity prevented cracking at this stage.
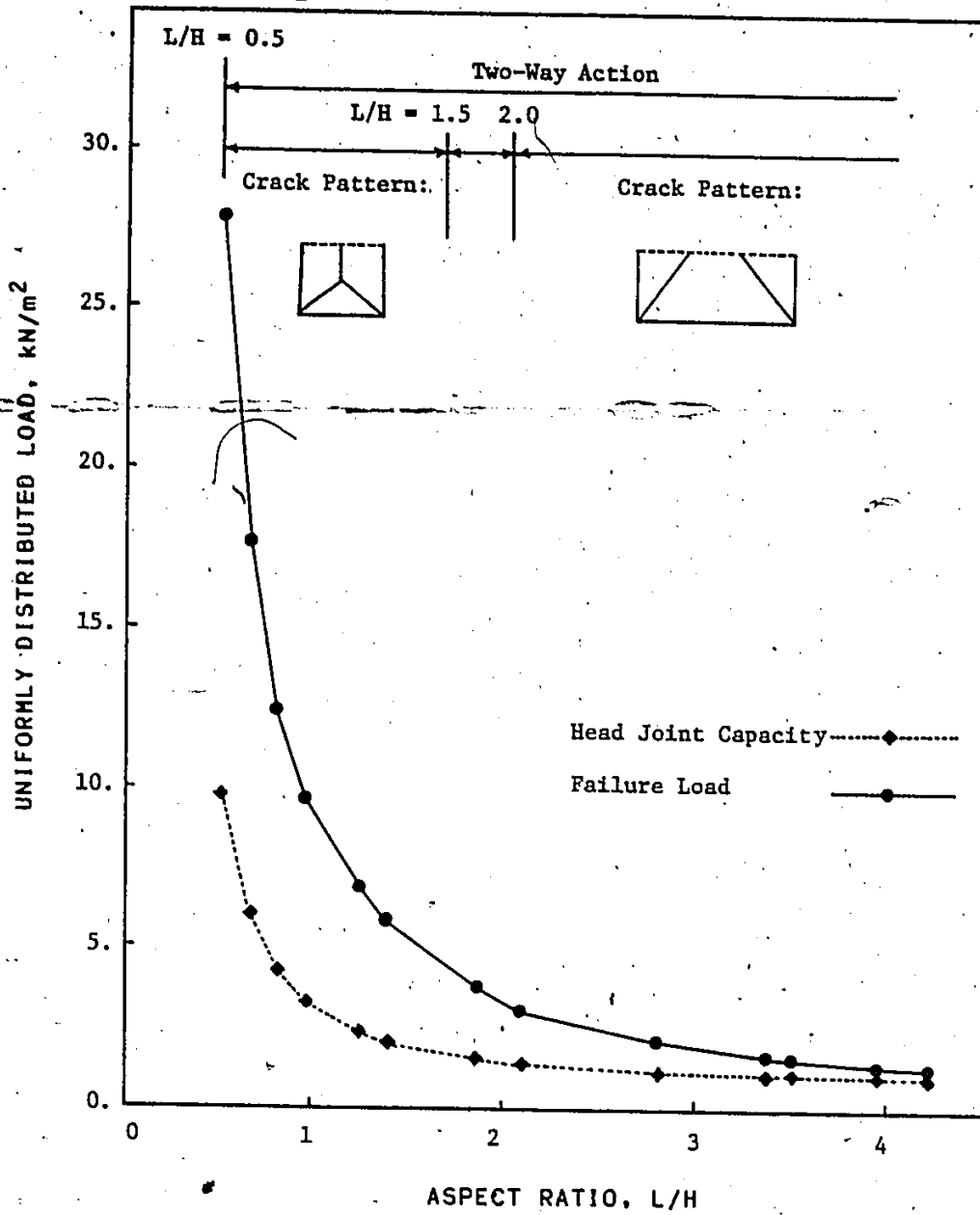
Figure 7.3   Predicted Behaviour of Walls Supported on Three
Sides With the Tops Free

considered to be acceptable.

7.3 PREDICTED WALL CAPACITIES USING AVAILABLE DESIGN METHODS

The design methods for laterally loaded masonry mentioned earlier in Chapter 1 included Lawrence's moments coefficients method [72], the empirical strip method [21,23], the conventional yield line method [30,63], British code moment coefficients [28], and Sinha's fracture line method [92]. It should be noted that there are some methods of analysis which are rationally developed but not readily available for design purposes. One of these methods is the isotropic elastic plate analysis using the principal stress criterion and considering the load sharing and joint strength variability proposed by Baker [22]. A similar elastic plate analysis using the finite element method and another principal stress criterion [46] was reported by Drysdale and Essawy [42]. Moreover, other methods of analysis for orthotropic plates which were used for masonry include the finite element model proposed by Seward [89] and the nonlinear finite element model reported in this study.

Of the available design methods, three are considered in this section where they were used to predict the capacities of panels analysed by the model described in the previous section. These methods are the empirical strip method, the conventional yield line method and the British code moment coefficients.

The wall capacities determined using the empirical strip method at first cracking and failure for panels supported on all four sides and at failure for panels supported on three sides are given in Table 7.3.

Table 7.3 Wall Capacities Predicted Using the Empirical Strip Method and Their Comparison to Finite Element Model Predictions

(a) Walls Supported on All Four Sides

Dimensions		Aspect Ratio	Initial Cracking Load[*]		Failure Load	
Wall $L_0 \times H_0$ m	Frame $L \times H$ m	L/H	P_{cr} kN/m^2	$\dfrac{P_{cr}}{P_{model}}$	P kN/m^2	$\dfrac{P}{P_{model}}$
1.2 × 2.8	1.0 × 2.8	0.36			59.9	1.06
1.6 × 2.8	1.4 × 2.8	0.50			31.9	1.00
2.0 × 2.8	1.8 × 2.8	0.64			20.3	1.00
2.4 × 2.8	2.2 × 2.8	0.79			14.5	1.06
2.8 × 2.8	2.6 × 2.8	0.93			11.1	0.96
3.6 × 2.8	3.4 × 2.8	1.21	5.3	0.90	7.6	0.93
4.0 × 2.8	3.8 × 2.8	1.36	4.6	0.92	6.7	0.95
5.2 × 2.8	5.0 × 2.8	1.79	3.5	0.96	5.0	0.90
6.0 × 2.8	5.8 × 2.8	2.07	3.1	0.95	4.4	0.95
8.0 × 2.8	7.8 × 2.8	2.79	2.7	0.95	3.6	0.99
9.6 × 2.8	9.4 × 2.8	3.36	2.7	1.00	3.3	1.08
10.0 × 2.8	9.8 × 2.8	3.5	2.7	1.00	3.3	1.07
11.2 × 2.8	11.0 × 2.8	3.93	2.7	1.02	3.15	1.20
12.0 × 2.8	11.8 × 2.8	4.21	2.7	1.03	3.1	1.18

[*] This indicates the load at which initial horizontal crack at panel center was developed.

Table 7.3   Continued

(b) Walls Supported on Three Sides With the Tops Free

Dimensions		Aspect Ratio	Failure Load	
Wall $L_o \times H_o$ m	Frame $L \times H$ m	L/H	p kN/m^2	$\dfrac{p}{p_{model}}$
1.2 × 2.8	1.0 × 2.85	0.35	57.9	1.09
1.6 × 2.8	1.4 × 2.85	0.49	29.8	1.07
2.0 × 2.8	1.8 × 2.85	0.63	18.3	1.04
2.4 × 2.8	2.2 × 2.85	0.77	12.5	1.01
2.8 × 2.8	2.6 × 2.85	0.91	9.1	0.95
3.6 × 2.8	3.4 × 2.85	1.19	5.6	0.82
4.0 × 2.8	3.8 × 2.85	1.33	4.6	0.80
5.2 × 2.8	5.0 × 2.85	1.75	2.96	0.78
6.0 × 2.8	5.8 × 2.85	2.04	2.37	0.78
8.0 × 2.8	7.8 × 2.85	2.74	1.6	0.78
9.6 × 2.8	9.4 × 2.85	3.30	1.3	0.81
10.0 × 2.8	9.8 × 2.85	3.44	1.27	0.81
11.2 × 2.8	11.0 × 2.85	3.86	1.14	0.83
12.0 × 2.8	11.8 × 2.85	4.14	1.08	0.86

The first cracking loads for panels supported on four sides determined by this method ranged from 0.9 to 1.05 of those predicted by the model. However, the panel capacities at failure showed more spread about the model predictions with ratios ranging from 0.9 to 1.20. For panels supported on three sides with the top free, the panel capacities determined by this method ranged from 0.78 to 1.09 of the model predictions and were 10 to 20% less than model predictions for most of the range of panel sizes. These comparisons indicated that the panel capacities determined by this method were in reasonable agreement with the model predictions in most cases. However, the reason for the relatively good accuracy of this method which lacks the fundamental compatibility requirements is still unexplained.

The capacities calculated by the conventional yield line method are given in Table 7.4. Two different analyses were performed for panels supported on all four sides where the critical yield line pattern included a horizontal yield line at mid-height or mid-length. The calculations differed by either assuming continuity or no continuity along the horizontal yield line. The latter was considered to account for the fact that the horizontal crack was developed at a load level considerably below the failure load in most cases.

The results given in Table 7.4(a) for panels supported on all four sides indicate distinct cracking patterns similar to those predicted by the model and which gave approximately the same limiting aspect ratios for these patterns. The transition zone between these two patterns is also indicated in Table 7.4(a) where solutions for the two

Table 7.4 Wall Capacities Predicted Using the Conventional Yield Line Method and Their Comparison to Finite Element Model Predictions

(a) Walls Supported on All Four Sides

Dimensions		Aspect Ratio	Pattern I[a]				Pattern II[a]	
			Case A[b]		Case B[b]			
Wall $L_o \times H_o$ m	Frame $L \times H$ m	L/H	p^c	$\dfrac{p}{P_{model}}$	p	$\dfrac{p}{P_{model}}$	p	$\dfrac{p}{P_{model}}$
1.2 × 2.8	1.0 × 2.8	0.36					68.3	1.21
1.6 × 2.8	1.4 × 2.8	0.50					38.6	1.21
2.0 × 2.8	1.8 × 2.8	0.64					25.9	1.27
2.4 × 2.8	2.2 × 2.8	0.79					19.2	1.40
2.8 × 2.8	2.6 × 2.8	0.93			15.7	1.35	15.2	1.31
3.6 × 2.8	3.4 × 2.8	1.21			10.5	1.29	10.8	1.32
4.0 × 2.8	3.8 × 2.8	1.36			9.1	1.30	9.5	1.35
5.2 × 2.8	5.0 × 2.8	1.79	7.1	1.30	6.4	1.15		
6.0 × 2.8	5.8 × 2.8	2.07	6.3	1.37	5.3	1.15		
8.0 × 2.8	7.8 × 2.8	2.79	5.1	1.39	3.7	1.00		
9.6 × 2.8	9.4 × 2.8	3.36	4.6	1.48	2.96	0.96		
10.0 × 2.8	9.8 × 2.8	3.5	4.5	1.46	2.8	0.92		
11.2 × 2.8	11.0 × 2.8	3.93	4.25	1.61	2.47	0.94		
12.0 × 2.8	11.8 × 2.8	4.21	4.1	1.58	2.28	0.87		

a Pattern I is that with horizontal center crack, whereas Pattern II is that with vertical center crack.

b Case A refers to the case where continuity along the initial crack was assumed, whereas the assumption of no continuity along the initail crack was considered in Case B.

c This indicates the predicted panel capacity in kN/m².

Table 7.4   Continued

(b) Walls Supported on Three Sides With the Tops Free

Dimensions		Aspect Ratio	Pattern I [*]		Pattern II [*]	
Wall $L_o \times H_o$, m	Frame $L \times H$ m	L/H	p kN/m²	$\dfrac{p}{p_{model}}$	p kN/m²	$\dfrac{p}{p_{model}}$
1.2 × 2.8	1.0 × 2.85	0.35			60.0	1.13
1.6 × 2.8	1.4 × 2.85	0.49			32.2	1.16
2.0 × 2.8	1.8 × 2.85	0.63			20.5	1.16
2.4 × 2.8	2.2 × 2.85	0.77			14.8	1.16
2.8 × 2.8	2.6 × 2.85	0.91			10.9	1.13
3.6 × 2.8	3.4 × 2.85	1.19			7.1	1.04
4.0 × 2.8	3.8 × 2.85	1.33			6.0	1.03
5.2 × 2.8	5.0 × 2.85	1.75			4.0	1.05
6.0 × 2.8	5.8 × 2.85	2.04	3.34	1.10	3.3	1.07
8.0 × 2.8	7.8 × 2.85	2.74	2.2	1.06	2.3	1.11
9.6 × 2.8	9.4 × 2.85	3.30	1.72	1.06		
10.0 × 2.8	9.8 × 2.85	3.44	1.63	1.05		
11.2 × 2.8	11.0 × 2.85	3.86	1.41⁻	1.03		
12.0 × 2.8	11.8 × 2.85	4.14	1.29	1.03		

[*] Pattern I is that with diagonal cracks extended to the free edge, whereas Pattern II is that with diagonal cracks meeting at center vertical crack.

patterns were available. The conventional yield line method as given in this table overestimated the panel capacity for panels supported on all four sides by 20 to 60% compared to the model predictions. However, introducing no continuity along the horizontal yield line produced capacities closer to model predictions (normally within 15%).

For panels supported on three sides with tops free, the results given in Table 7.4(b) also indicate the two distinct crack patterns and the transition region but with higher limiting aspect ratios. The conventional yield line predictions in this case were in better agreement with the model predictions than was the case for panels supported on four sides.

Table 7.5 contains the predicted results using the British Code moment coefficients and comparisons with finite element predictions. The British code moment coefficients yielded capacities similar to those for the yield line method except for larger aspect ratios over 3.5 where considerably lower capacities were obtained for panels supported on three or four sides. This agreement was expected because the British code coefficients were based mainly on yield line analysis with some modifications to satisfy available experimental data.

Even though the results obtained by the conventional yield line method and using the British code coefficients were reasonably accurate for some cases, this does not change the fact that this method is not rationally justified for use in masonry design. This is because the brittle nature or the very limited nonlinearity of masonry assemblages cannot always provide the plastic behaviour necessary for the yield line method. Also, the crack lines in a plate made of such brittle material

Table 7.5   Wall Capacities Predicted Using the British Code Coefficients and Their Comparison to Finite Element Model Predictions

Dimensions		Aspect Ratio	Walls Supported on All 4 Sides		Walls Supported on Three Sides With the Tops Free	
Wall $L_o \times H_o$ m	Frame $L \times H$ m	L/H	p kN/m^2	$\frac{p}{P_{model}}$	p kN/m^2	$\frac{p}{P_{model}}$
1.2 × 2.8	1.0 × 2.8	0.36	77.1	1.37	64.3	1.21
1.6 × 2.8	1.4 × 2.8	0.50	39.4	1.24	32.8	1.18
2.0 × 2.8	1.8 × 2.8	0.64	25.0	1.23	20.3	1.15
2.4 × 2.8	2.2 × 2.8	0.79	18.5	1.35	14.6	1.16
2.8 × 2.8	2.6 × 2.8	0.93	15.0	1.29	10.8	1.12
3.6 × 2.8	3.4 × 2.8	1.21	10.4	1.27	6.9	1.02
4.0 × 2.8	3.8 × 2.8	1.36	9.1	1.29	5.8	1.01
5.2 × 2.8	5.0 × 2.8	1.79	6.9	1.25	3.94	1.04
6.0 × 2.8	5.8 × 2.8	2.07	6.0	1.32	3.2	1.05
8.0 × 2.8	7.8 × 2.8	2.79	4.8	1.30	2.17	1.04
9.6 × 2.8	9.4 × 2.8	3.36	4.2	1.36	1.68	1.03
10.0 × 2.8	9.8 × 2.8	3.5	3.9	1.26	1.55	0.99
11.2 × 2.8	11.0 × 2.8	3.93	3.07	1.17	1.23	0.89
12.0 × 2.8	11.8 × 2.8	4.21	2.67	1.02	1.07	0.85

are not necessarily yield lines of constant moment capacity simultaneously attained along these lines but rather progressive cracking lines. These progressive cracking lines were initiated at a critical location and then propagated due to the release of stresses at this location. Moreover, the yield line method was applied to masonry as a way of getting capacity predictions which were reasonably accurate for some cases but it was never claimed to represent the real behaviour of the material.

The panel capacities calculated according to the these methods are shown in Figures 7.4 and 7.5 for walls supported on four and three sides, respectively. In these figures, it is clearly indicated that in general the empirical strip method yielded capacities lower than those of the conventional yield line and the British code.

It should be noted that the model predictions of failure load for panels supported on four sides were approximately 20% lower than the reported experimental results for aspect ratios less than 2.0. This was attributed to the effect of the smeared cracking approach incorporated in the model which affects the failure load for these aspect ratios. Even though, the good agreement between the capacities calculated by the empirical strip method and those predicted by the model does not necessarily prove the accuracy of this method, it indicates roughly the same reasonably acceptable accuracy as the model. However, both the conventional yield line method and British code coefficients overestimate the capacities of the panels.

For wall panels supported on three sides, for most cases, the
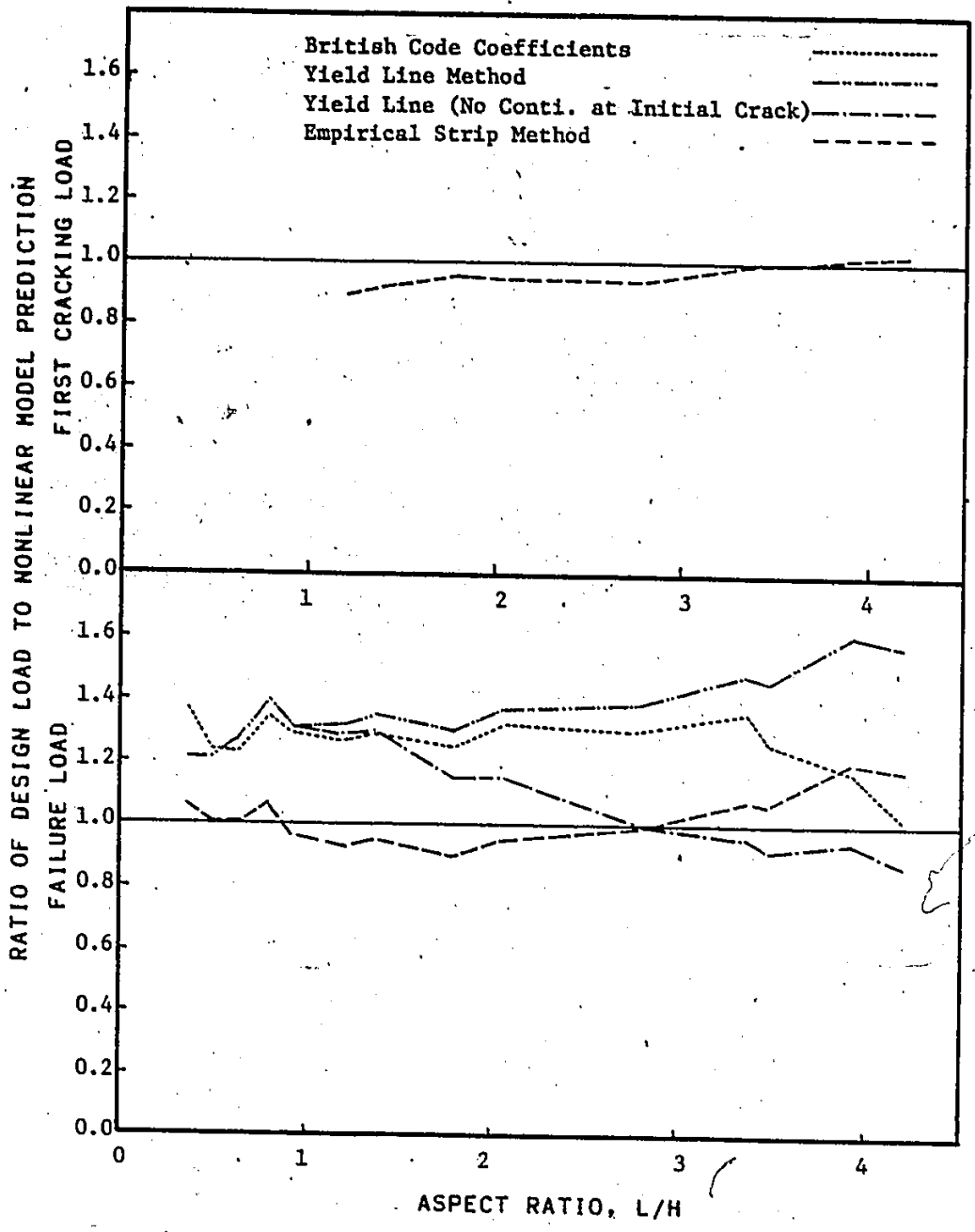
Figure 7.4   Capacity Predictions for Walls Supported on All Four Sides Using the Available Design Methods
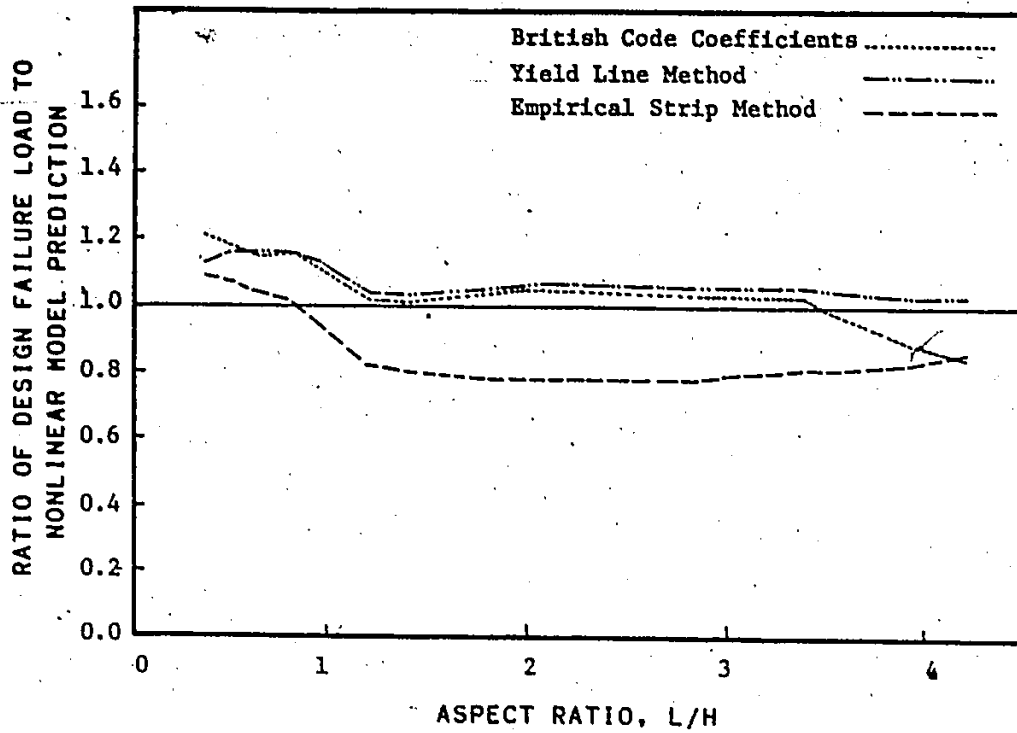
Figure 7.5   Capacity Predictions for Walls Supported on Three Sides
              With the Tops Free Using the Available Design Methods

comparison shown in Figure 7.5 indicated reasonably good predictions, using the yield line method and the British code coefficients for most cases. It also indicated an underestimation of approximately 20% using the empirical strip method predictions.

The above comparisons indicated that the accuracy of the panel capacities calculated by these methods may be acceptable in some cases but not for the whole range of aspect ratios and boundary conditions. Moreover, these methods are still not rationally developed or at least not sufficiently rationally justified to be a universally acceptable design method for laterally loaded masonry walls.

7.4   PROPOSED DESIGN METHOD BASED ON ELASTIC PLATE THEORY

Early trials for the use of elastic plate theory as a design method for laterally loaded masonry walls were limited to first cracking load predictions of panels supported on all four sides. It was thought that it could not be used to predict the failure load for these panels due to the presence of the initial crack at panel center in most cases. Also, the solutions presented in textbooks [100,101] for panels supported on three sides with tops free were limited to the moment components acting at the panel centers and at the centers of free edges. These two locations are not necessarily the critical locations for panel capacity determination. This is due to the anisotropic and composite nature of masonry which implies the directional dependence of assemblage strength.

The critical location for determining panel capacity is not necessarily the location of the highest principal moment but rather the

location of largest ratio of principal moment to the moment of resistance in the principal moment orientation. Accordingly, the correct solution needs the determination of principal moments or stresses and their directions at different locations within the panel plus a logical method for strength determination for different orientations. Then, the panel capacity can be determined by examining the acting stress and strength values at different locations throughout the panel. Therefore, the explicit solution of the plate problem is needed to determine the moment components at different locations throughout the plate.

The need to consider the orientation of principal moments was recognized and taken into account in the different methods of analysis reported by Baker [22], Drysdale and Essawy [42], Seward [89] and the finite element model presented in this study. However, all of these are not yet in a form suitable for a generalized design method.

In the remainder of this section, the above mentioned approach will be presented in a suitable form for practical design where some assumptions and approximations were adopted to simplify the development and use of this method. Also, a method for determination of the assemblage strength for different orientations is presented. Finally, the proposed method is discussed in detail.

7.4.1 Main Assumptions and Approximations

In order to simplify and generalize the application of this method to laterally loaded masonry panels, some assumptions and approximations adopted are as follows:

1. The assemblage masonry material is assumed to be isotropic. According to this assumption, the degree of orthotropy observed and determined in this study as well as that reported in the literature is neglected. The justification of this assumption will be discussed later.

2. No interaction is considered between orthogonal stresses at failure. This assumption is only introduced for simple calculations and for the general application of the method. However, any suitable criterion for the interaction can easily be incorporated in the design process using this method. It should be noted that the amount of interaction varies according to the mode of failure as discussed earlier in Chapter 5. For example, for debonding along bed joints which was observed at the centers of most panels supported on four sides, it is suggested that there is no interaction between the stresses normal and parallel to the bed joints at this location of zero shear stresses. Also, for panels experiencing vertical central cracking through head joints and units at alternate courses, it is suggested that there is no interaction between stresses normal and parallel to the bed joints. Moreover, for diagonal cracks where the two principal stresses are of different signs, Baker [22] suggested no interaction and considered only the tensile principal stress to cause the failure. Accordingly, it is thought that for a large number of cases, the assumption of no interaction may be reasonably accepted.

3. Panels are assumed to be simply supported along all four sides or three sides with tops free. This assumption was chosen to match the

boundary conditions of the available test data through this study. It also provides a conservative approximation of practical boundary conditions. However, the method can be easily extended to include other boundary conditions.

4. For panels supported on all four sides and having aspect ratios less than or equal to 1/3 or more than or equal to 4, the panel may be analysed assuming one way action in the horizontal or vertical directions, respectively, without introducing any significant error in the calculations. For panels supported on three sides with free tops, the one way approximations may be used for panels of aspect ratios up to 1/2 without introducing any significant error in the calculations.

5. The simplified elastic plate analysis in the form of a modified crossed strips method was adopted for the determination of the first cracking load for panels supported on all four sides. For panels with vertical initial cracks, the failure capacities are assumed to coincide with the first cracking load. However, for a panel with a horizontal initial crack, some reserve of strength after first cracking is assumed.

6. For a panel supported on all four sides with a horizontal initial crack, it is assumed that the panel will be divided by this crack into two sub-panels supported on three sides with free edges at the crack. It is also assumed that no shear transfer will take place across this crack due to symmetry at the panel center and the only force to be transferred through this crack is the in-plane

compressive loads due to the self weight or any surcharge applied along the top of the panel. Therefore, the panel capacity in this case may be estimated as the capacity of a panel supported on three sides and having an aspect ratio equal to double the ratio of the original panel. It should be noted that this assumption was previously suggested and confirmed experimentally by Baker [22] and in the experimental work of this study. Also, Baker [22] and Drysdale and Essawy [42] obtained reasonably good results using this assumption.

7.4.2 Determination of First Cracking Load For Walls Supported On All Four Sides

The first cracking load for walls supported on all four sides may be determined by theory of plates solutions available in textbooks [100,101]. However, for simplicity and to be able to easily obtain solutions for different boundary conditions, a modified crossed strips approach initially developed by Marcus [100] is proposed. In this approach, the plate is replaced by two equivalent strips in the two orthogonal directions as shown in Figure 7.6(a). Assuming isotropic properties, the compatibility of the center deflection of both strips yielded the following expressions for the strip loads expressed as functions of the panel load:

$$Pv = \frac{r^4}{1 + r^4} P$$

$$Ph = \frac{1}{1 + r^4} P \tag{7.1}$$

$P_h = \beta p$
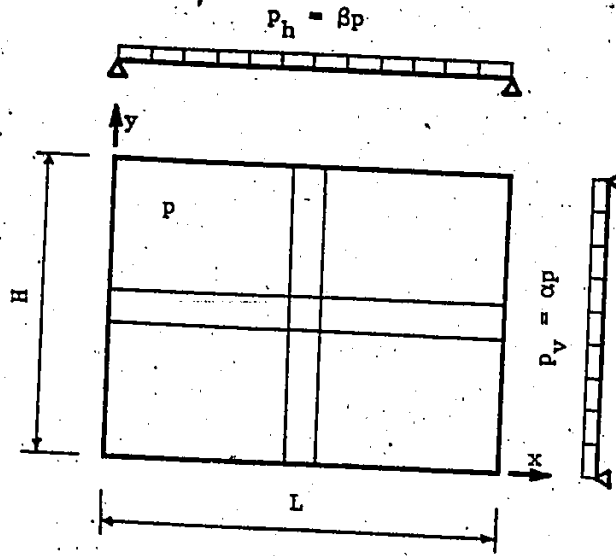
Figure 7.6(a) Equivalent Plate Strips
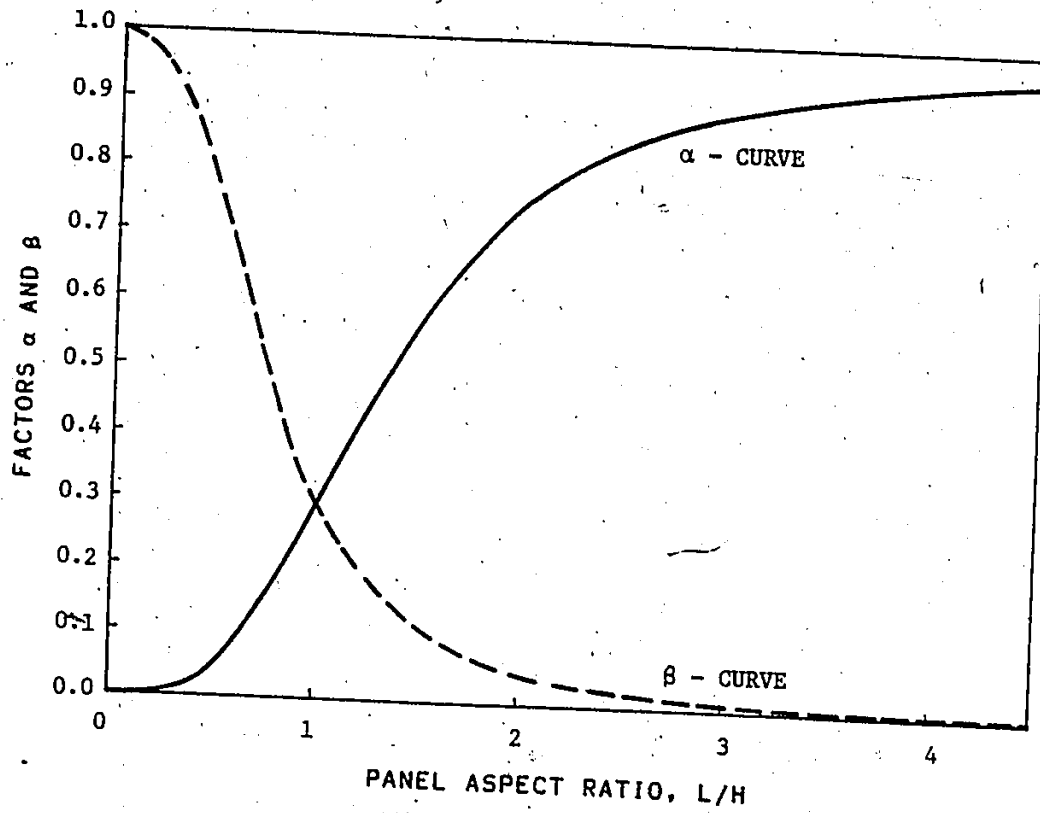
Figure 7.6(b) Coefficients for Loads on Equivalent Plate Strips

Where,

Pᵥ and Pₕ are the loads on the vertical and horizontal strips, respectively,

p is the uniformly distributed load on the panel, and

r is the panel length to height or aspect ratio.

Accordingly, the maximum deflections and bending moments for the equivalent strips can be easily determined. However, the torsional resistance of the plate, which reduces deflections and consequently moments of the equivalent strips, has to be taken into consideration. In the case of uniformly distributed load, Marcus proposed the following expressions for maximum moments [100]:

$$M_x = M_h \left[1 - \frac{5}{6} \left(\frac{L}{H} \right)^2 \frac{M_h}{M_{xo}} \right] = \beta \frac{pL^2}{8}$$

$$M_y = M_v \left[1 - \frac{5}{6} \left(\frac{H}{L} \right)^2 \frac{M_v}{M_{yo}} \right] = \alpha \frac{pH^2}{8}$$

(7.2)

Where,

L and H are the panel length and height, respectively,

M_x and M_y are the equivalent plate maximum moments in the horizontal and vertical directions, respectively,

M_v and M_h are the maximum moments of the vertical and the horizontal strips due to uniform loads of P_v and P_h, respectively and

M_{xo} and M_{yo} are the maximum moments of simply supported beams subjected to the total load p in the horizontal and vertical

directions, respectively.

Substituting for M_v, M_h, M_{xo} and M_{yo} respectively as $p_vH^2/8$, $p_hL^2/8$, $pL^2/8$ and $pH^2/8$ in the above expressions, the coefficients α and β were evaluated. These coefficients which define the ratios of load on the vertical and horizontal equivalent strips to determine the moments at plate center were found to be:

$$\alpha = \frac{r^4}{1 + r^4} \left[1 - \frac{5}{6} \left(\frac{1}{r} \right)^2 \frac{r^4}{1 + r^4} \right]$$

$$\beta = \frac{1}{1 + r^4} \left[1 - \frac{5}{6} (r)^2 \frac{1}{1 + r^4} \right] \tag{7.3}$$

The values of these coefficients are given in Table 7.6 and are also shown in Figure 7.6(b) for different aspect ratios up to 4.

To determine the first cracking load for a masonry panel, the loads on the equivalent plate strips can be determined according to the panel's aspect ratio. Then, to determine the critical panel load, the values of the maximum acting moments in the vertical and horizontal strips can be compared to the internal moment capacities normal and parallel to the bed joints, respectively. For cases where the load on the horizontal strip is critical, a center vertical crack is expected to occur. This vertical crack together with the diagonal cracks required to form the collapse mechanism are assumed to develop simultaneously at the cracking load level. Therefore, the panel capacity in this case is considered to coincide with the first cracking load. On the other hand, for cases where the load on the vertical strip is critical, an initial

Table 7.6   Values of α and β Factors for Load Intensities
on the Two Orthogonal Strips

Aspect Ratio L/H	Factor α	Factor β	(α + β)
0.25	0.004	0.944	0.948
0.33	0.011	0.900	0.948
0.50	0.047	0.757	0.804
0.75	0.155	0.489	0.644
1.00	0.292	0.292	0.584
1.25	0.441	0.181	0.622
1.50	0.577	0.114	0.691
1.75	0.681	0.073	0.754
2.00	0.757	0.047	0.804
2.25	0.81	0.032	0.842
2.50	0.848	0.022	0.870
2.75	0.876	0.015	0.892
3.00	0.897	0.011	0.908
3.50	0.926	0.006	0.932
4.00	0.944	0.004	0.948

horizontal crack is expected to develop at this load level. Some reserve of strength after first cracking is expected for such panels. The panel capacity in these cases is determined as two sub-panels supported on three sides with free edges at the initial crack.

7.4.3 Determination of Panel Capacity For Walls Supported On Three Sides With Tops Free

For walls supported on three sides with tops free, the panel capacities will be determined according to the elastic theory of plates. As mentioned earlier, the available solutions in textbooks [100,101] are expressed as the moment components only at two locations (namely, the plate center and the center of the free edge). These solutions are not always suitable for direct application to masonry walls due to the directional dependence of the strength and consequently the need to explicitly determine the strength at any location within the wall panel. Therefore, the explicit solution for plates simply supported on three sides with the fourth side free is presented in this section. Then, the determination of masonry strength for different orientations of bending moment with respect to the bed joints is discussed and finally the solution is presented in a suitable form for design purposes.

7.4.3.1 The Explicit Solution For a Laterally Loaded Plate Simply Supported On Three Sides With the Fourth Side Free

The general solution for a laterally loaded isotropic plate simply supported on three sides with the top free was given by Timoshenko [101]. Considering the x-axis to be parallel to the free edge

(horizontal direction), the y-axis in the vertical direction, and the origin to be located at the bottom left corner, the plate transverse deflection was defined as follows:

$$W = W_1 + W_2 \tag{7.4}$$

Where,

$$W_1 = \frac{4pL^4}{\pi^5 D} \sum_{m=1,3,5}^{\infty} \frac{1}{m^5} \sin \frac{m\pi x}{L}, \tag{7.5}$$

$$W_2 = \sum_{m=1,3,5}^{\infty} Y_m \sin \frac{m\pi x}{L}, \tag{7.6}$$

$$Y_m = \frac{pL^4}{D} [A_m \cosh \beta_m \frac{y}{H} + B_m \beta_m \frac{y}{H} \sinh \beta_m \frac{y}{H}$$

$$+ C_m \sinh \beta_m \frac{y}{H} + D_m \beta_m \frac{y}{H} \cosh \beta_m \frac{y}{H}], \tag{7.7}$$

$$\beta_m = \frac{m\pi H}{L} \text{ and}$$

D is the flexural rigidity of the plate.

However, for this case, the explicit evaluation of the constants A_m, B_m, C_m and D_m was not given. Therefore, these constants were evaluated to satisfy the boundary conditions at the bottom support and the top free edge and found to be:

$$A_m = - \frac{4}{\pi^5 m^5} \tag{7.8}$$

$$B_m = \frac{2}{\pi^5 m^5} \tag{7.9}$$

$$C_m = \frac{2}{\pi^5 m^5} \frac{2\nu(1+\nu)(1-\cosh \beta_m)\cosh \beta_m - 2\nu(1-\nu)\beta_m \sinh \beta_m}{\begin{array}{c}(3+\nu)(1-\nu)\sinh \beta_m \cosh \beta_m + (1-\nu)^2 \beta_m \\ +2(3-\nu)\sinh^2 \beta_m - (1-\nu)^2\beta_m^2\end{array}}$$

(7.10)

$$D_m = \frac{2}{\pi^5 m^5} \frac{2\nu \cosh \beta_m - 3 \sinh^2 \beta_m - \nu(\cosh^2 \beta_m + 1)}{(3+\nu)\sinh \beta_m \cosh \beta_m + (1-\nu)\beta_m}$$

(7.11)

The bending moments M_x and M_y and the torsional moment M_{xy} are given by:

$$M_x = -D \left(\frac{\partial^2 w}{\partial x^2} + \nu \frac{\partial^2 w}{\partial y^2} \right)$$

$$M_y = -D \left(\frac{\partial^2 w}{\partial y^2} + \nu \frac{\partial^2 w}{\partial x^2} \right)$$

(7.12)

$$M_{xy} = D(1-\nu) \frac{\partial^2 w}{\partial x \partial y}$$

Substituting Equation 7.4 in Equation 7.12, the above expressions may be rewritten as follows:

$$\frac{M_x}{pL^2} = \sum_{m=1,3,5}^{\infty} \frac{1}{m^3\pi^3} \sin \frac{m\pi x}{L} \left(4 + \pi^5 m^5 Y_m \right)$$

$$-\nu \sum_{m=1,3,5}^{\infty} \pi^2 m^2 \sin \frac{m\pi x}{L} \left[A_m \cosh \beta_m\frac{y}{H} + B_m \left(2 \cosh \beta_m\frac{y}{H} \right.\right.$$

$$\left. + \beta_m\frac{y}{H} \sinh \beta_m\frac{y}{H} \right) + C_m \sinh \beta_m\frac{y}{H} + D_m \left(2 \sinh \beta_m\frac{y}{H} \right.$$

$$\left.\left. + \beta_m\frac{y}{H} \cosh \beta_m\frac{y}{H} \right) \right]$$

(7.13)

$$\frac{M_y}{pL^2} = \nu \sum_{m=1,3,5}^{\infty} \frac{1}{m^3\pi^3} \sin \frac{m\pi x}{L} (4 + \pi^5 m^5 Y_m)$$

$$- \sum_{m=1,3,5}^{\infty} \pi^2 m^2 \sin \frac{m\pi x}{L} [A_m \cosh \beta_m \frac{y}{H} + B_m (2 \cosh \beta_m \frac{y}{H}$$

$$+ \beta_m \frac{y}{H} \sinh \beta_m \frac{y}{H}) + C_m \sinh \beta_m \frac{y}{H} + D_m (2 \sinh \beta_m \frac{y}{H}$$

$$+ \beta_m \frac{y}{H} \cosh \beta_m \frac{y}{H})] \qquad\qquad (7.14)$$

$$\frac{M_{xy}}{pL^2} = (1-\nu) \sum_{m=1,3,5}^{\infty} \pi^2 m^2 \cos \frac{m\pi x}{L} [A_m \sinh \beta_m \frac{y}{H} + B_m (\sinh \beta_m \frac{y}{H}$$

$$+ \beta_m \frac{y}{H} \cosh \beta_m \frac{y}{H}) + C_m \cosh \beta_m \frac{y}{H} + D_m (\cosh \beta_m \frac{y}{H}$$

$$+ \beta_m \frac{y}{H} \sinh \beta_m \frac{y}{H})] \qquad\qquad (7.15)$$

Now, the deflections and moments can be evaluated at any point within the plate for a specific aspect ratio and Poisson's ratio. A value of Poisson's ratio of 0.20 was assumed for masonry and the deflection and moment coefficients were evaluated for different aspect ratios up to 8. For each aspect ratio, these coefficients were determined for x/L and y/H values at 0.1 increments up to o.5 and 1.0, respectively. A sample of these values for the aspect ratio of 2.0 are given in Table 7.7.

Table 7.7   Deflection and Moment Coefficients For Plate Simply
Supported on Three Sides With the Top Free (L/H = 2)

x/L	y/H	$w =$ Coeff. $\times pL^4/D$	$M_x =$ Coeff. $\times pL^2$	$M_y =$ Coeff. $\times pL^2$	$M_{xy} =$ Coeff. $\times pL^2$
0.0	0.0	0.00000	0.00000	0.00000	0.04185
0.0	0.1	0.00000	0.00000	0.00000	0.04104
0.0	0.2	0.00000	0.00000	0.00000	0.03925
0.0	0.3	0.00000	0.00000	0.00000	0.03703
0.0	0.4	0.00000	0.00000	0.00000	0.03468
0.0	0.5	0.00000	0.00000	0.00000	0.03242
0.0	0.6	0.00000	0.00000	0.00000	0.03046
0.0	0.7	0.00000	0.00000	0.00000	0.02896
0.0	0.8	0.00000	0.00000	0.00000	0.02815
0.0	0.9	0.00000	0.00000	0.00000	0.02827
0.0	1.0	0.00000	0.00000	0.00000	0.02969
0.1	0.0	0.00000	0.00000	0.00000	0.03842
0.1	0.1	0.00025	0.00444	0.00392	0.03787
0.1	0.2	0.00050	0.00822	0.00624	0.03650
0.1	0.3	0.00073	0.01141	0.00757	0.03465
0.1	0.4	0.00095	0.01411	0.00820	0.03260
0.1	0.5	0.00116	0.01641	0.00825	0.03058
0.1	0.6	0.00135	0.01837	0.00778	0.02879
0.1	0.7	0.00153	0.02007	0.00680	0.02741
0.1	0.8	0.00170	0.02157	0.00527	0.02664
0.1	0.9	0.00188	0.02294	0.00307	0.02668
0.1	1.0	0.00205	0.02432	0.00000	0.02777
0.2	0.0	0.00000	0.00000	0.00000	0.03076
0.2	0.1	0.00047	0.00639	0.00613	0.03049
0.2	0.2	0.00093	0.01221	0.01026	0.02968
0.2	0.3	0.00136	0.01742	0.01282	0.02845
0.2	0.4	0.00178	0.02202	0.01410	0.02699
0.2	0.5	0.00216	0.02606	0.01429	0.02549
0.2	0.6	0.00253	0.02959	0.01350	0.02411
0.2	0.7	0.00287	0.03269	0.01175	0.02302
0.2	0.8	0.00320	0.03544	0.00899	0.02237
0.2	0.9	0.00353	0.03793	0.00513	0.02231
0.2	1.0	0.00386	0.04029	0.00000	0.02295
0.3	0.0	0.00000	0.00000	0.00000	0.02131
0.3	0.1	0.00063	0.00747	0.00743	0.02116
0.3	0.2	0.00125	0.01440	0.01271	0.02070
0.3	0.3	0.00184	0.02075	0.01613	0.01997
0.3	0.4	0.00240	0.02650	0.01794	0.01907
0.3	0.5	0.00293	0.03164	0.01831	0.01811
0.3	0.6	0.00343	0.03622	0.01734	0.01722
0.3	0.7	0.00390	0.04028	0.01508	0.01649
0.3	0.8	0.00435	0.04391	0.01150	0.01603

Table 7.7 Continued

0.3	0.9	0.00480	0.04718	0.00652	0.01593
0.3	1.0	0.00526	0.05020	0.00000	0.01628
0.4	0.0	0.00000	0.00000	0.00000	0.01091
0.4	0.1	0.00073	0.00803	0.00812	0.01084
0.4	0.2	0.00145	0.01554	0.01403	0.01062
0.4	0.3	0.00214	0.02247	0.01795	0.01027
0.4	0.4	0.00279	0.02881	0.02008	0.00984
0.4	0.5	0.00341	0.03455	0.02057	0.00937
0.4	0.6	0.00399	0.03971	0.01953	0.00893
0.4	0.7	0.00454	0.04430	0.01699	0.00856
0.4	0.8	0.00508	0.04844	0.01295	0.00834
0.4	0.9	0.00560	0.05217	0.00732	0.00828
0.4	1.0	0.00613	0.05558	0.00000	0.00844
0.5	0.0	0.00000	0.00000	0.00000	0.00000
0.5	0.1	0.00077	0.00819	0.00834	0.00000
0.5	0.2	0.00152	0.01588	0.01446	0.00000
0.5	0.3	0.00224	0.02301	0.01854	0.00000
0.5	0.4	0.00293	0.02954	0.02077	0.00000
0.5	0.5	0.00357	0.03547	0.02131	0.00000
0.5	0.6	0.00418	0.04080	0.02024	0.00000
0.5	0.7	0.00476	0.04559	0.01761	0.00000
0.5	0.8	0.00532	0.04988	0.01342	0.00000
0.5	0.9	0.00587	0.05375	0.00758	0.00000
0.5	1.0	0.00643	0.05729	0.00000	0.00000

7.4.3.2 Flexural Strength of Masonry Assemblages with Bending At Different Orientations to the Bed Joints

Strength of masonry assemblages is known to vary with the stress orientation due to the composite and anisotropic nature of such material. Most codes specify strength values normal and parallel to the bed joints. Therefore, it is thought that, for design purposes, it is more convenient to express the strength at different orientations as a function of these two values instead of using the rigorous criterion presented in Chapter 5. This criterion is more suitable for detailed analysis than a simplified design process.

There are some available test data for brickwork [30,86] and blockwork [47,56] strengths at orientations other than the two principal directions normal and parallel to the bed joints. However, there is not yet a universally acceptable logical method to determine the strength at a particular orientation. Baker [22] proposed an empirical expression for the strength as a function of the two orthogonal strengths and the orientation. Even though this expression seems to reasonably fit most available data as shown in Figure 7.7, it lacks the basic requirement of zero slopes at θ equal to 0° and 90° due to symmetry. This means that the strength at θ equal to -15° should be the same as that for θ equal to 15° and similarly the strengths at θ values of 80° and 100° should be the same. Losberg and Johansson, as reported by Cajdert [30], used vectorial addition in the usual way to express the moment capacity at any orientation as a function of the moment capacities in the normal and parallel directions and proposed the following expression:
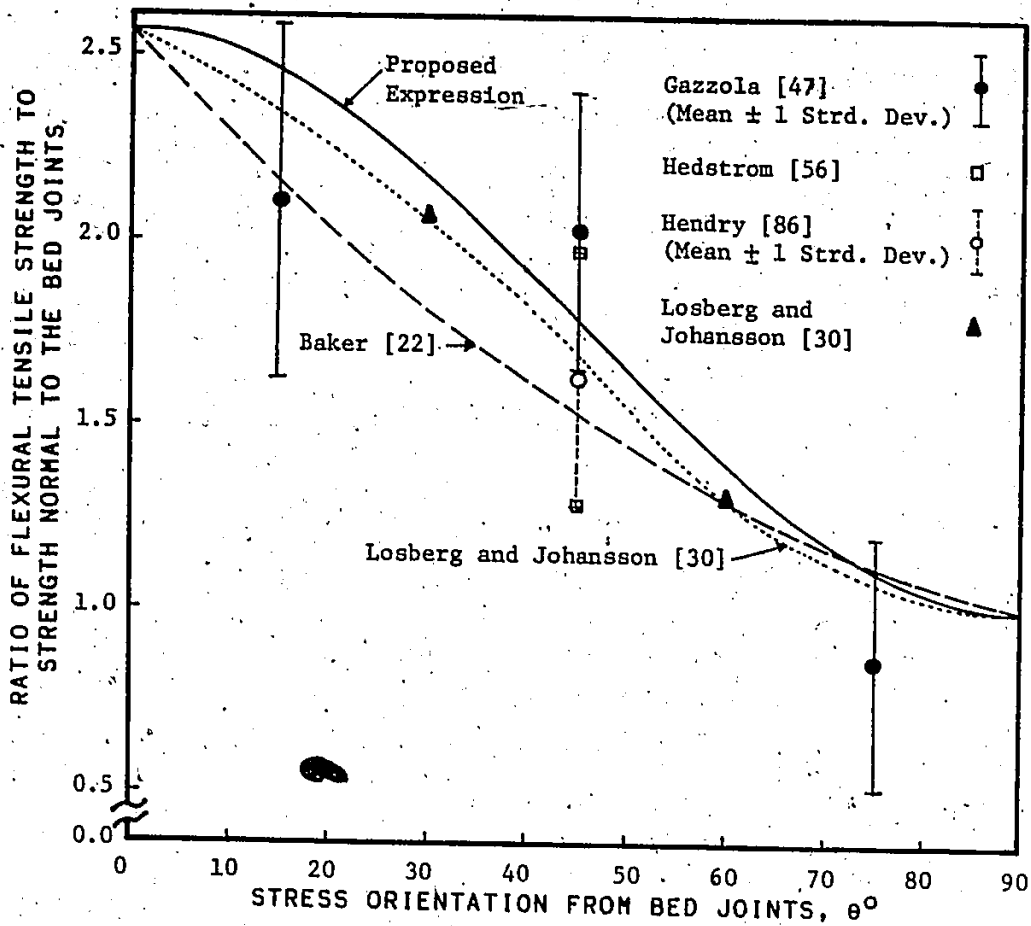
Figure 7.7   Masonry Strength at Different Oreintations With Respect
to the Bed Joints
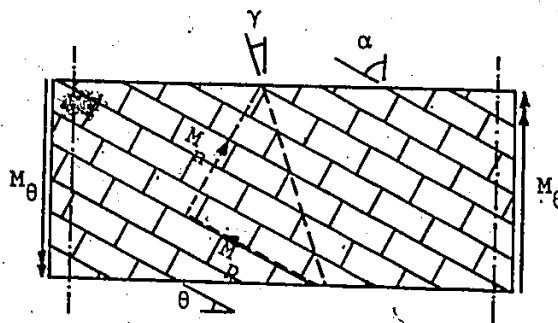
Figure 7.8   Off-Axis Bending of Masonry in Running Bond Pattern

$$M_\theta = M_p \cos^2\alpha + M_n \sin^2\alpha - (M_n - M_p) \sin\alpha \cos\alpha \tan\gamma \qquad (7.16)$$

Where, M_n, M_p, M_θ are the bending moment capacity vectors per unit length normal, parallel and at an angle θ with respect to the bed joints. Angles α, γ and θ are defined as shown in Figure 7.8.

In this section, the Losberg and Johansson relation will be simplified further to be suitable for use in a practical design process. The angle γ between the failure plane and the vertical axis shown in Figure 7.8 depends on the mode of failure which is therefore difficult to determine. For example, it is the same as α for debonding along bed joint. Similarly, for vertically toothed or vertical splitting failure modes, γ equals $(90^\circ - \alpha)$. However, for diagonally stepped or diagonal splitting modes, it is given by:

$$\gamma = \alpha - \tan^{-1} \frac{2b}{2a} \qquad (7.17)$$

Where, 2a and b are the masonry unit length and height, respectively. Accordingly, γ equals zero and the whole third term in Equation 7.16 becomes zero for cases of α equals 0°, 90° and also 45° where failure is according to the diagonally stepped or diagonal splitting modes. Moreover, neglecting the third term of Equation 7.16 resulted in increases of strengths of less than 5% which is considered to be negligible. Therefore, Equation 7.16 is rewritten as follows:

$$M_\theta = M_p \cos^2\alpha + M_n \sin^2\alpha \qquad (7.18)$$

Substituting in the above expression for $\theta = 90^\circ - \alpha$ and for the moment

capacities in terms of the section modulus and the appropriate strength value, the following expression was obtained:

$$f'_{t\theta} = f'_{tn} \sin^2\theta + f'_{tp} \cos^2\theta \tag{7.19}$$

Where, f'_{tn}, f'_{tp}, and $f'_{t\theta}$ are respectively the flexural tensile strength values normal, parallel, and at θ with respect to the bed joints. Expressing the strength parallel to the bed joints in terms of the strength normal to the bed joints by the orthogonal strength ratio, R, Equation 7.19 may be rewritten as follows:

$$f'_{t\theta} = f'_{tn} [1 + (R-1) \cos^2\theta] \tag{7.20}$$

Equation 7.20 is represented graphically in Figure 7.7 where it indicates reasonable fitting of available data and a relatively small vertical shift from Losberg and Johansson's proposal [30]. As discussed earlier, it also satisfies the logical requirement of zero slopes at θ equal to zero and 90° due to symmetry.

7.4.3.3 Critical Locations of Moments and Panel Capacities
For Different Orthogonal Strength Ratios

The capacities of panels simply supported on three sides with tops free are dependent on both the panel aspect ratio and the orthogonal strength ratio. The panel aspect ratio affects the bending and torsional moment values at any location within the panel whereas the orthogonal strength ratio determines the critical location for capacity determination. Accordingly, different analyses were performed using the explicit solution obtained for elastic isotropic plates simply supported

strengths at different orientations. In these analyses, orthogonal strength ratios from 1 to 5, which cover most of the range of reported values in the literature, and panel aspect ratios up to approximately 8 were considered. However, all other data were kept the same as those considered earlier in this chapter. These analyses yielded the results given in Table 7.8 where both the panel capacity and the critical location are given for each orthogonal strength and aspect ratios. As can be seen in this table, the critical location and consequently the panel capacity for a specific aspect ratio are significantly affected by the value of the orthogonal strength ratio.

7.4.3.4 Design Tables For Panel Capacity Determination

The critical locations for capacity determination given in Table 7.8 are summarized again in Table 7.9 for different orthogonal strength ratios and ranges of aspect ratios. Table 7.9 is considered to be the master table for the determination of the critical moment coefficients for different panel aspect ratios and orthogonal strength ratios. The critical moment coefficients for a particular orthogonal strength ratio may be obtained by consulting Table 7.9 to define the critical locations for different aspect ratios. Then, the moment coefficients at these locations may be obtained from the explicit solution tables such as Table 7.7 for an aspect ratio of 2. The above procedure was used to obtain the critical moment coefficients for the different orthogonal strength ratios given in Table 7.10. This table may be used as a design table for determination of the capacities of panels supported on three sides with tops free. The complete table is given for an orthogonal

Table 7.8 Elastic Capacities for Walls Supported on Three Sides With the Tops Free and Having Different Orthogonal Strength Ratios

Wall $L_0 \times H_0$ a	Frame $L \times H$ a	Aspect Ratio L/H	R = 1 Predicted Capacity kN/m²	R = 1 Critical Location x/L y/H	R = 2 Predicted Capacity kN/m²	R = 2 Critical Location x/L y/H	R = 3 Predicted Capacity kN/m²	R = 3 Critical Location x/L y/H	R = 4 Predicted Capacity kN/m²	R = 4 Critical Location x/L y/H	R = 5 Predicted Capacity kN/m²	R = 5 Critical Location x/L y/H
1.2 x 2.8	1.0 x 2.85	0.35	19.1	0.5 1.0	35.4	0.0 0.0	46.8	0.0 0.0	58.1	0.0 0.0	59.9	0.5 0.2
1.6 x 2.8	1.4 x 2.85	0.49	9.8	0.5 1.0	19.7	0.5 1.0	29.6	0.5 1.0	33.4	0.5 0.4	33.4	0.5 0.4
2.0 x 2.8	1.8 x 2.85	0.63	6.2	0.5 1.0	12.4	0.5 1.0	18.6	0.5 1.0	20.5	0.5 0.4	20.5	0.5 0.4
2.4 x 2.8	2.2 x 2.85	0.77	4.4	0.5 1.0	8.8	0.5 1.0	13.3	0.5 1.0	14.5	0.5 0.4	14.5	0.5 0.4
2.8 x 2.8	2.6 x 2.85	0.91	3.4	0.5 1.0	6.8	0.5 1.0	10.2	0.5 1.0	11.2	0.5 0.4	11.2	0.5 0.4
3.6 x 2.8	3.4 x 2.85	1.19	2.4	0.5 1.0	4.86	0.5 1.0	7.3	0.5 1.0	7.7	0.5 0.5	7.7	0.5 0.5
4.0 x 2.8	3.8 x 2.85	1.33	2.14	0.5 1.0	4.3	0.5 1.0	6.3	0.1 0.3	6.7	0.5 0.5	6.7	0.5 0.5
6.0 x 2.8	5.8 x 2.85	2.04	1.46	0.3 0.7	2.4	0.1 0.3	3.2	0.1 0.3	4.04	0.1 0.3	4.8	0.5 0.5
8.0 x 2.8	7.8 x 2.85	2.74	1.04	0.1 0.7	1.62	0.1 0.3	2.16	0.1 0.3	2.7	0.1 0.3	3.2	0.0 0.0
9.6 x 2.8	9.4 x 2.85	3.30	0.83	0.1 0.7	1.28	0.1 0.3	1.7	0.1 0.3	2.12	0.1 0.3	2.53	0.0 0.0
10.0 x 2.8	9.8 x 2.85	3.44	0.80	0.1 0.7	1.22	0.1 0.3	1.62	0.1 0.3	2.01	0.1 0.3	2.4	0.0 0.0
11.2 x 2.8	11.0 x 2.85	3.86	0.71	0.1 0.5	1.08	0.1 0.3	1.43	0.1 0.3	1.78	0.0 0.0	2.13	0.0 0.0
12.0 x 2.8	11.8 x 2.85	4.14	0.64	0.1 0.5	0.97	0.1 0.3	1.29	0.0 0.0	1.60	0.0 0.0	1.91	0.0 0.0
14.0 x 2.8	13.8 x 2.85	4.84	0.68	0.1 0.3	1.01	0.1 0.3	1.34	0.0 0.0	1.67	0.0 0.0	1.99	0.0 0.0
22.4 x 2.8	22.2 x 2.85	7.79	0.32	0.0 0.2	0.58	0.0 0.2	0.77	0.0 0.2	0.96	0.0 0.2	1.14	0.0 0.2

Table 7.9   Critical Locations (x/L,y/H) for Elastic Capacity of Panels Supported on Three Sides With the Top Free and Having Different Orthogonal Strength Ratios

Aspect Ratio L/H	Orthogonal Strength Ratio				
	R = 1	R = 2	R = 3	R = 4	R = 5
< 1.0				(0.5 , 0.4)	
		(0.5 , 1.0)			
< 1.5				(0.5 , 0.5)	
< 2.5	(0.3 , 0.7)				(0.5 , 0.5)
			(0.1 , 0.3)		
< 4.0	(0.1-, 0.7)				
< 6.0		(0.1 , 0.3)	(0.0 , 0.0)		(0.0 , 0.0)
> 6.0			(0.0 , 0.0)		

Table 7.10 Critical Moment Coefficients for Different Strength Ratios (ν = 0.2)

Aspect Ratio L/H	Orthogonal Strength Ratio													
	R = 1			R = 2			R = 3			R = 4			R = 5		
	$\frac{M_x}{pL^2}$	$\frac{M_y}{pL^2}$	$\frac{M_{xy}}{pL^2}$	$\frac{M_x}{pL^2}$	$\frac{M_y}{pL^2}$	$\frac{M_{xy}}{pL^2}$	$\frac{M_x}{pL^2}$	$\frac{M_y}{pL^2}$	$\frac{M_{xy}}{pL^2}$	$\frac{M_x}{pL^2}$	$\frac{M_y}{pL^2}$	$\frac{M_{xy}}{pL^2}$	$\frac{M_x}{pL^2}$	$\frac{M_y}{pL^2}$	$\frac{M_{xy}}{pL^2}$
0.33				0.12516	0.	0.				0.11734	0.02889	0.			
0.50				0.12971	0.	0.				0.10349	0.03337	0.			
0.75	See Table for R = 2			0.12213	0.	0.	See Table for R = 2			0.08323	0.03566	0.	See Table for R = 4		
1.00	R = 2			0.10916	0.	0.				0.06687	0.03422	0.	R = 4		
1.25				0.09441	0.	0.				0.06346	0.03103	0.			
1.50				0.08028	0.	0.				0.05200	0.02782	0.			
1.75	0.04766	0.01708	0.01643	0.01329	0.00851	0.03617	See Table for R = 2			See Table for R = 2			0.04280	0.02446	0.
2.00	0.04028	0.01508	0.01649	0.01141	0.00757	0.03465							0.03547	0.02131	0.
2.25	0.03426	0.01327	0.01617	0.00989	0.00676	0.03293							0.02964	0.01849	0.
2.50	0.02934	0.01167	0.01565	0.00867	0.00606	0.03120							0.02498	0.01606	0.
3.00	0.01251	0.00453	0.02473	0.00682	0.00493	0.02792							0.	0.	0.03239
3.50	0.01027	0.00379	0.02283	0.00552	0.00410	0.02507							0.	0.	0.02887
4.00	0.00861	0.00322	0.02102	0.00457	0.00346	0.02265							0.	0.	0.02598
4.50	See Table for R = 2			0.00386	0.00297	0.02060	0.	0.	0.02359	See Table for R = 3			See Table for R = 3		
5.00				0.00330	0.00258	0.01886	0.	0.	0.02158	R = 3					
5.50				0.00286	0.00227	0.01737	0.	0.	0.01988						
6.00	See Table for R = 2			0.00250	0.00201	0.01608	0.	0.	0.01842	See Table for R = 2			See Table for R = 2		
6.50	R = 2			0.	0.	0.01716	See Table for R = 2			R = 2			R = 2		
7.00				0.	0.	0.01605	R = 2								
7.50				0.	0.	0.01508									
8.00				0.	0.	0.01421									

strength ratio of 2 because of its common use in most codes. However, for other orthogonal strength ratios, the coefficients for the incomplete portions were referred to the other appropriate parts of the table. It is suggested that, for aspect ratios and orthogonal strength ratios not given in this table, linear interpolation may be used. As mentioned earlier, this table can also be used for determining the capacity of a panel supported on all four sides with an initial horizontal crack at the panel center.

7.5 PANEL CAPACITY PREDICTIONS USING THE PROPOSED METHOD FOR DIFFERENT ASPECT RATIOS

The method proposed in Section 7.4 was used to predict first cracking loads and panel capacities for walls supported on all four sides and panel capacities for walls supported on three sides with tops free. The results of these analyses are given in Table 7.11 and shown in Figures 7.9 and 7.10. The capacity predictions for panels supported on three sides as presented in Table 7.11(b) and Figure 7.9 ranged from 0.86 to 1.08 of the nonlinear model predictions and were within 10% of the model predictions for most of the range of aspect ratios examined in these analyses. This accuracy is considered to be acceptable for this relatively simple method. For panels supported on all four sides, the first cracking loads predictions using the proposed method were in very good agreement with the model predictions and were within 6% as shown in Figure 7.10. However, the panel capacities predicted by this method indicate greater discrepancy from the model predictions.

Table 7.11 Wall Capacities Predicted Using the Proposed Method

(a) Walls Supported on All Four Sides

Dimensions		Aspect Ratio	Initial Cracking Load*		Failure Load	
Wall $L_o \times H_o$ m	Frame $L \times H$ m	L/H	P_{cr} kN/m²	$\dfrac{P_{cr}}{P_{model}}$	P kN/m²	$\dfrac{P}{P_{model}}$
1.2 × 2.8	1.0 × 2.8	0.36			58.9	1.04
1.6 × 2.8	1.4 × 2.8	0.50			35.5	1.12
2.0 × 2.8	1.8 × 2.8	0.64			24.3	1.19
2.4 × 2.8	2.2 × 2.8	0.79	14.1	1.06	16.9	1.24
2.8 × 2.8	2.6 × 2.8	0.93	9.8	1.02	15.2	1.31
3.6 × 2.8	3.4 × 2.8	1.21	5.9	1.01	10.3	1.26
4.0 × 2.8	3.8 × 2.8	1.36	4.9	0.98	8.9	1.26
5.2 × 2.8	5.0 × 2.8	1.79	3.5	0.97	6.3	1.15
6.0 × 2.8	5.8 × 2.8	2.07	3.2	0.97	5.3	1.16
8.0 × 2.8	7.8 × 2.8	2.79	2.8	0.99	3.85	1.05
9.6 × 2.8	9.4 × 2.8	3.36	2.68	1.00	3.13	1.01
10.0 × 2.8	9.8 × 2.8	3.5	2.66	1.00	3.0	0.97
11.2 × 2.8	11.0 × 2.8	3.93	2.62	0.99	2.63	1.00
12.0 × 2.8	11.8 × 2.8	4.21	2.60	0.99	2.60	0.99

* This indicates the load at which initial horizontal crack at panel center was developed.

Table 7.11 Continued

(b) Walls Supported on Three Sides With the Tops Free

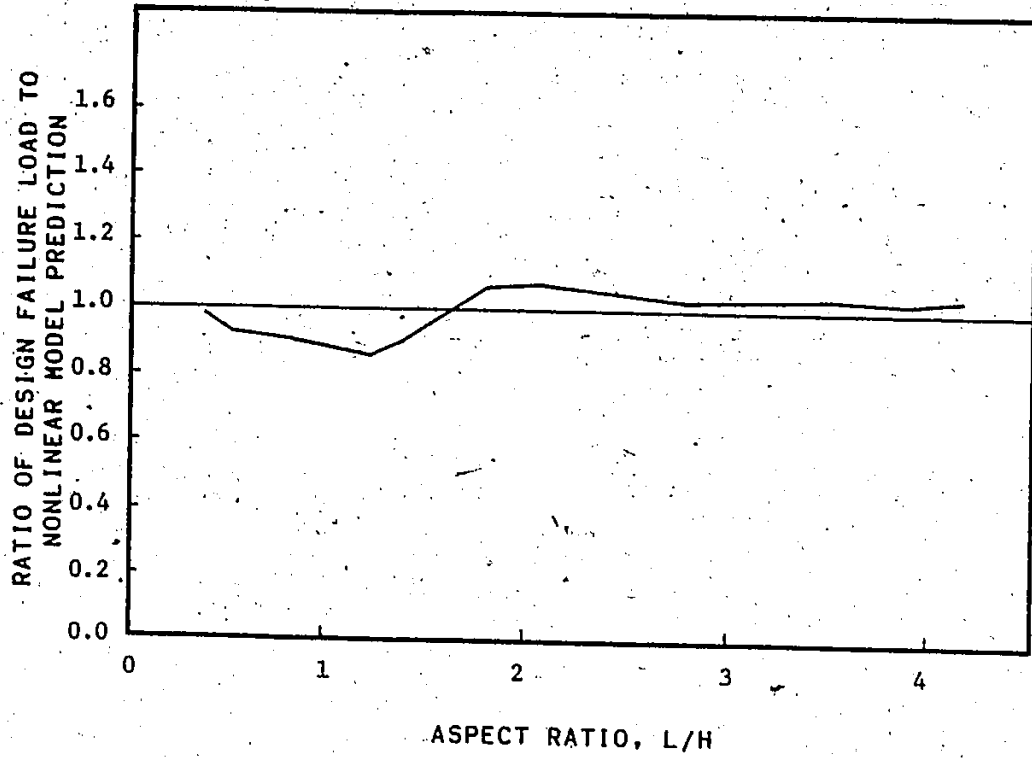| Dimensions		Aspect Ratio	Failure Load	
Wall $L_o \times H_o$ m	Frame $L \times H$ m	L/H	P kN/m^2	$\dfrac{P}{P_{model}}$
1.2 × 2.8	1.0 × 2.85	0.35	52.2	0.98
1.6 × 2.8	1.4 × 2.85	0.49	25.9	0.93
2.0 × 2.8	1.8 × 2.85	0.63	16.2	0.92
2.4 × 2.8	2.2 × 2.85	0.77	11.3	0.91
2.8 × 2.8	2.6 × 2.85	0.91	8.6	0.89
3.6 × 2.8	3.4 × 2.85	1.19	5.9	0.86
4.0 × 2.8	3.8 × 2.85	1.33	5.2	0.90
5.2 × 2.8	5.0 × 2.85	1.75	4.05	1.07
6.0 × 2.8	5.8 × 2.85	2.04	3.3	1.08
8.0 × 2.8	7.8 × 2.85	2.74	2.14	1.03
9.6 × 2.8	9.4 × 2.85	3.30	1.7	1.04
10.0 × 2.8	9.8 × 2.85	3.44	1.62	1.04
11.2 × 2.8	11.0 × 2.85	3.86	1.42	1.03
12.0 × 2.8	11.8 × 2.85	4.14	1.31	1.05

Figure 7.9   Capacity Predictions for Walls Supported on Three Sides
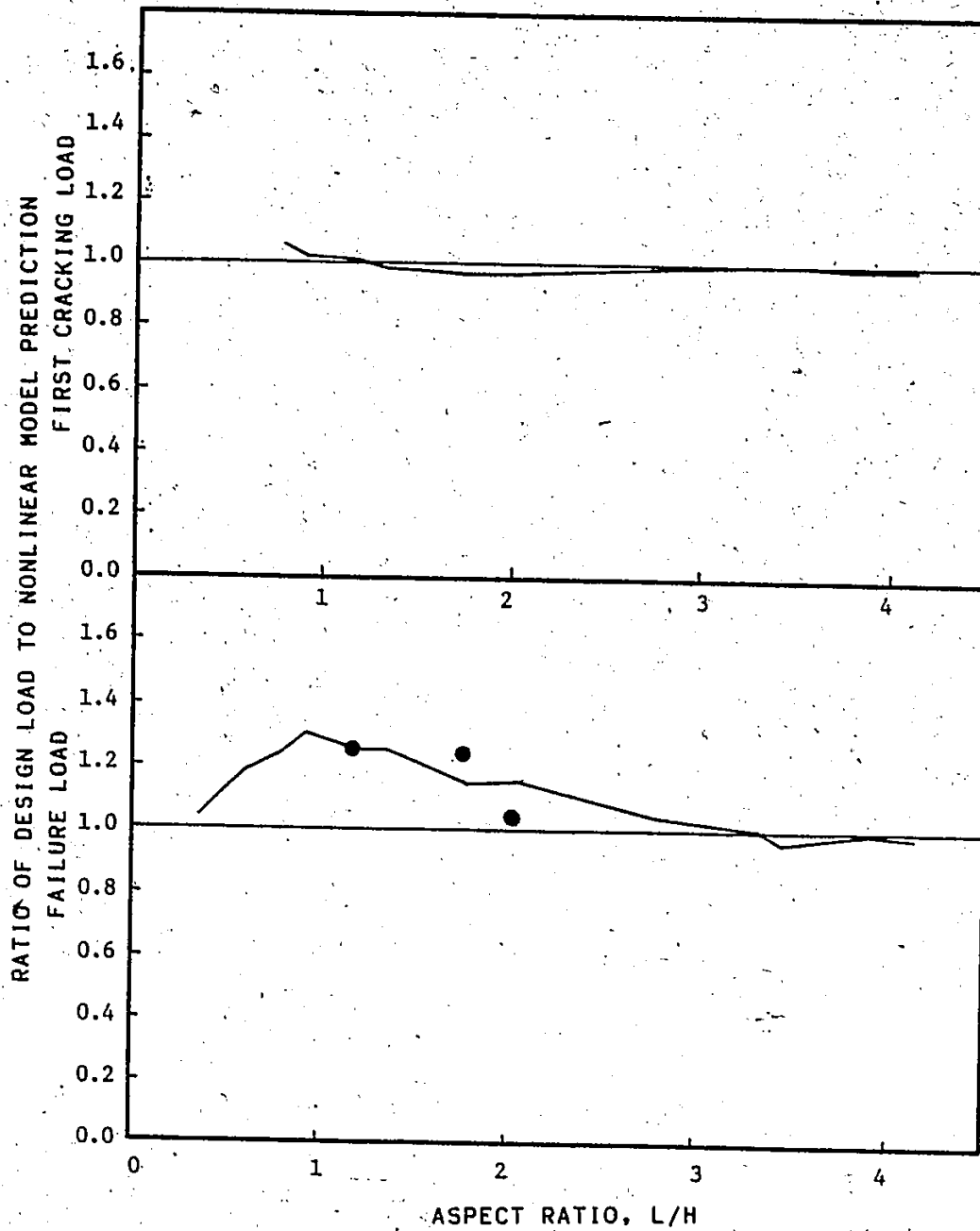With the Tops Free Using the Proposed Design Method

Figure 7.10   Capacity Predictions for Walls Supported on All Four Sides Using the Proposed Design Method

It should be noted here again that the model predictions for aspect ratios less than 2.0 underestimated the failure capacities for walls supported on all four sides by about 20% which is attributed to the smeared cracking approach used in the model. Therefore, the non conservative discrepancy for the proposed method will be much closer to actual behaviour when this factor is taken into account. This was confirmed by comparing predictions from the proposed method directly to the available test results which, as shown in Figure 7.10, indicated a reasonable accuracy.

It is suggested that the discrepancy of failure loads determined by this method for panels supported on three or four sides is not related to the assumed isotropic behaviour (see section 7.4.1). This assumption was justified for use in the panels supported on three sides by performing two elastic analyses for different aspect ratios with different degrees of orthotropy. In one of these analyses, isotropic behaviour was assumed. The other used a ratio of orthotropy of 1.40 similar to that obtained from the finite element model and similar to results reported in the literature [92]. As shown in Figure 7.11, both analyses yielded similar results with differences within 5% which is considered to be acceptable. This confirms an early conclusion by Baker [22] regarding the effect of orthotropy.

Since the solution for panels supported on three sides are also used for panels supported on all four sides with initial horizontal cracking, a similar statement for the relatively negligible effect of orthotropy is also applicable. However, for other panels supported on all four sides with vertical center cracks, both the analyses using the
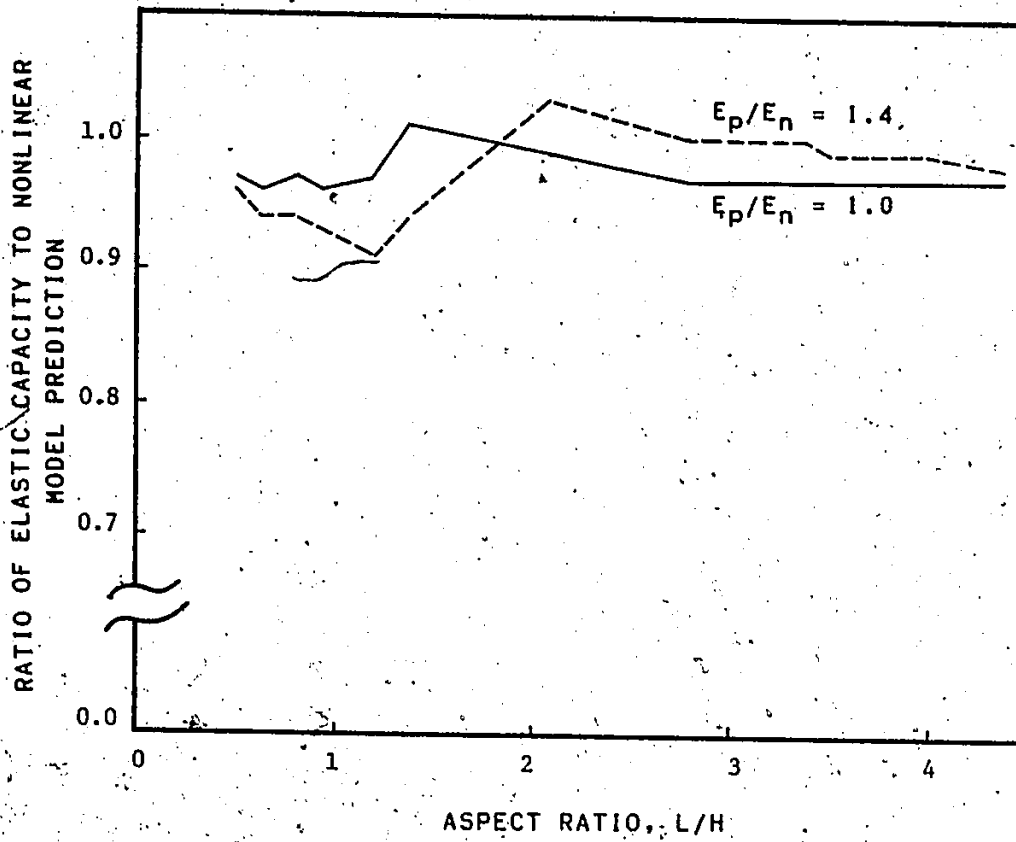
Figure 7.11 Elastic Capacities for Walls Supported on Three Sides With the Tops Free and With Different Ratios of Orthotropy

model and the observed behaviours indicated nonlinear behaviour in the mortar head joints after their strengths have been exceeded. This results in a gradual decrease in the stiffness in the direction parallel to the bed joints and consequently reduces the degree of orthotropy. Therefore, the assumption of isotropic behaviour in these cases is also considered to be acceptable.

The relative accuracies of the different design methods including the one proposed in this study were examined using failure load ratios plotted in Figures 7.12 and 7.13. For panels supported on three sides, the relative capacities shown in Figure 7.12 indicated similar and for some cases identical results obtained by the proposed elastic method and the yield line method for aspect ratios over 1.5. However, for aspect ratios less than 1.5, much higher capacities were obtained by the yield line method. For most of the examined range of aspect ratios, the empirical strip method predictions were significantly lower than those predicted by the proposed method.

For panels supported on all four sides, both the proposed method and the empirical strip method yielded very similar results for the first cracking loads as shown in Figure 7.13. However, for panel capacities, reasonable agreement between the proposed method predictions and those of the yield line assuming no continuity along the initial horizontal crack is clearly indicated in Figure 7.13 for aspect ratios larger than 1. For aspect ratios less than 1, slightly higher capacities were obtained by the yield line method.

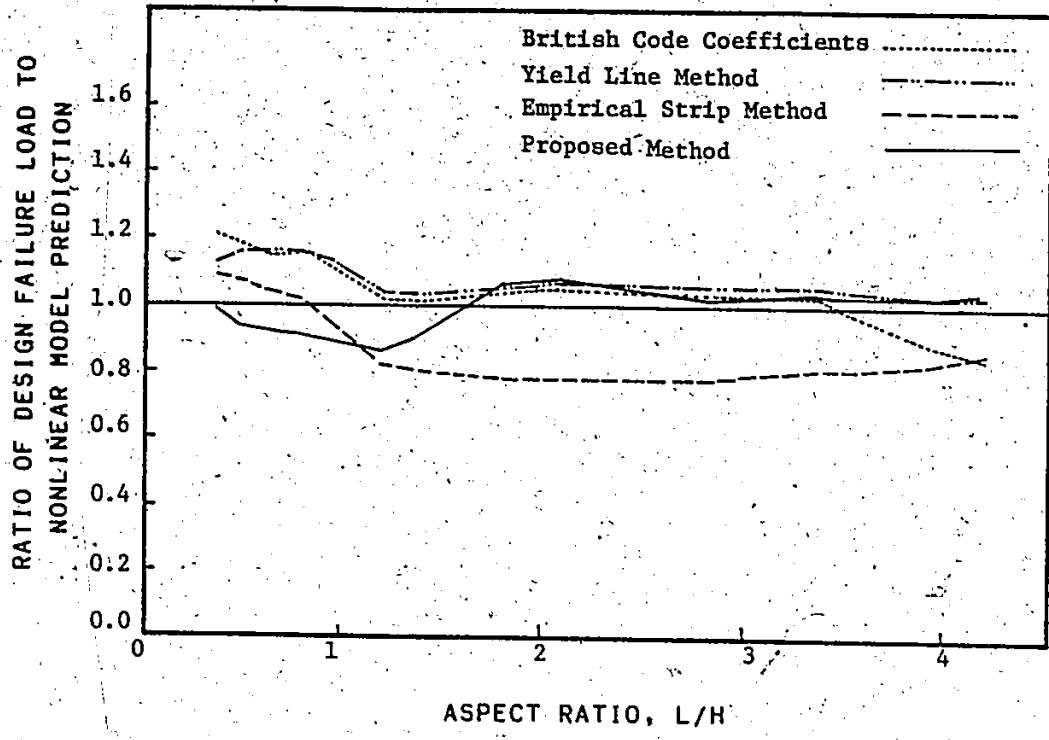The above comparisons for walls supported on three and four

Figure 7.12   Capacity Predictions for Walls Supported on Three Sides
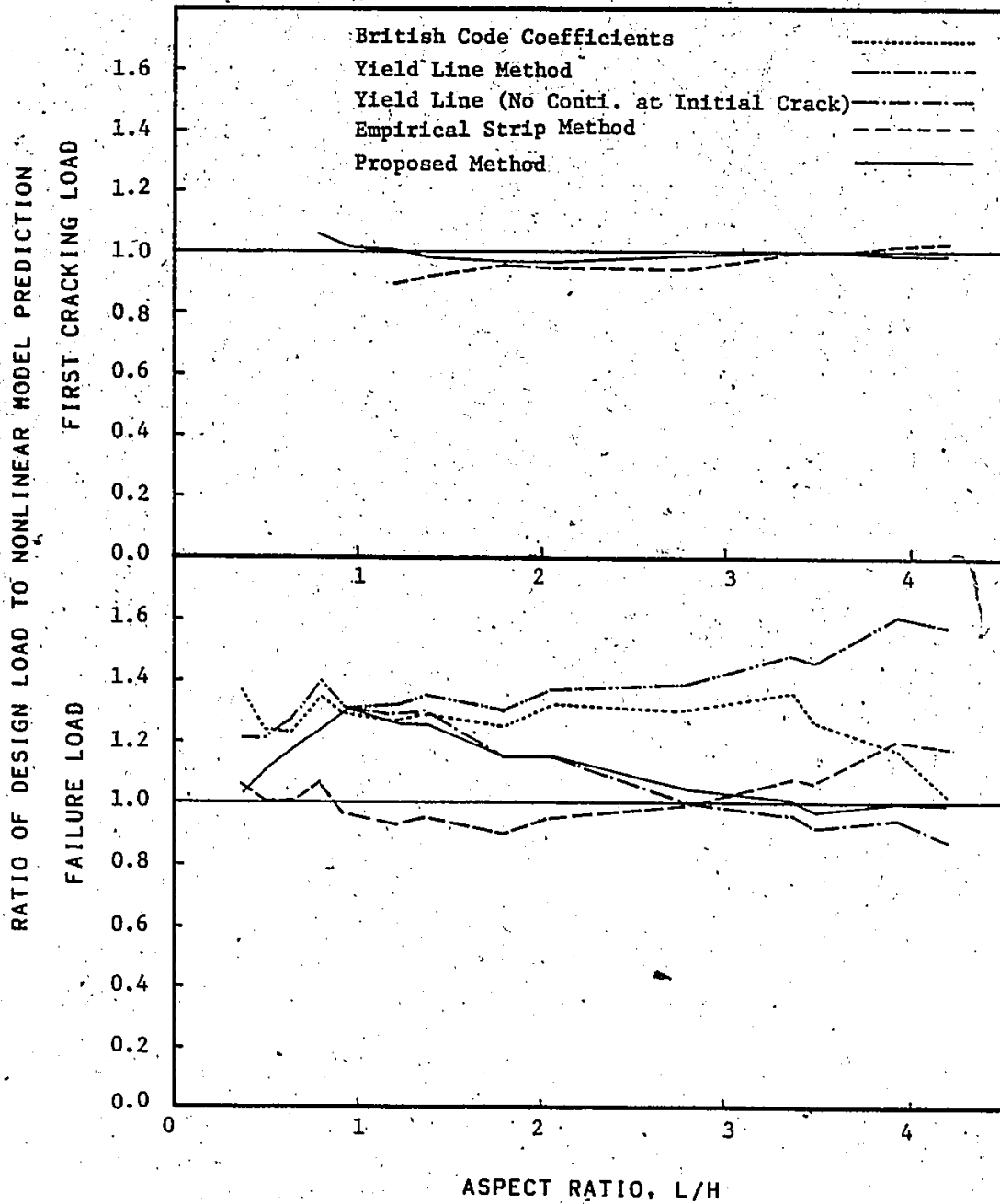With the Tops Free Using Different Design Methods

Figure 7.13   Capacity Predictions for Walls Supported on All
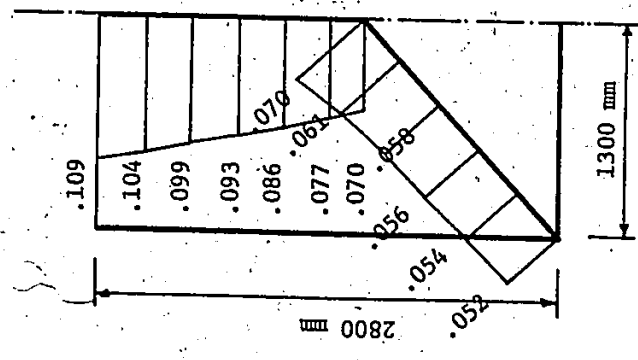Four Sides Using Different Design Methods

sides indicated that for some cases both the yield line method and the proposed elastic method yielded similar results. This result may have revealed the reason for the good predictions using the yield line method. The reason is that for similar boundary conditions and aspect ratios, the stress distribution from the elastic analysis is almost uniform along the so called yield line. To further confirm this argument, the stress distributions along the expected yield lines are shown in Figure 7.14 for two panels with different aspect ratios. For the panel with a 0.93 aspect ratio, the stress distribution is non-uniform and the capacity determined using the yield line method was much higher than that using the proposed elastic method. On the other hand, for the panel with a 2.07 aspect ratio, the stress distribution is almost uniform and both methods yielded similar results. It is worth noting that most tests and analyses have been done for panels with aspect ratios greater than 1.5.

7.6   CONCLUDING REMARKS

The conclusions which can be drawn from the study reported in this chapter are as follows:

1. According to results of the analyses performed using the developed nonlinear finite element model, one way approximations may be used for determining panel capacities for aspect ratios less than 1/3 and higher than 4 for panels supported on all four sides. However, for panels supported on three sides, one way approximations may be applied only for cases with aspect ratios less than 1/2.

321

(b) Panel Aspect Ratio = 0.93

$M = \text{coeff.} \times p\ L^2$

(a) Panel Aspect Ratio = 2.07

$M = \text{coeff.} \times p\ L^2$

Figure 7.14 Elastic Distributions of Moments Along the Expected
Yield Lines for Panels Simply Supported on Three
Sides With the Tops Free

2. The accuracy of the panel capacities calculated by the empirical strip method, the conventional yield line method and the British code coefficients may be acceptable for some cases but not for the whole range of aspect ratios and boundary conditions.

3. The proposed expression for strength determination for bending at different orientations to the bed joints yielded results which were reasonably close to the available experimental data. It also satisfies the requirements for strength symmetry relative to directions normal and parallel to the bed joints.

4. The proposed design method for laterally loaded masonry walls was rationally developed and is a simplified elastic plate analysis which is acceptable for representing the behaviour of such brittle material having very limited nonlinearity.

5. The proposed method yielded predictions for capacities of masonry panels which are in reasonable agreement with the available test data from this study and the extended data obtained from the proposed nonlinear finite element model.

6. The detailed review of the analyses confirmed that, in some cases, the reason for good predictions being obtained using the yield line method is the reasonably uniform elastic stress distributions along the expected yield lines for uniformly loaded panels with certain aspect ratios and support conditions. For panels supported on all four sides with initial horizontal cracks, the above reasoning is applicable for the expected diagonal yield lines where no continuity is assumed along the initial crack.

7. It is suggested that the proposed method has potential for being included as a design method in masonry codes. This is because of its rational development, simplicity and because it uses techniques familiar to practicing engineers.

CHAPTER 8

SUMMARY, CONCLUSIONS AND RECOMMENDATIONS

8.1   SUMMARY

The available literature on laterally loaded masonry walls was reviewed and it revealed the need for further research on the behaviour of laterally loaded hollow concrete block masonry. Therefore, this study was initiated to investigate the flexural behaviour of hollow concrete block masonry and to assess the design methods for laterally loaded masonry walls.

The experimental program for this study included 30 full scale wall tests representing different support conditions and aspect ratios. In addition, 29 one block wide stack bonded prisms and 34 wallettes served as assemblage control specimens. The full scale tests were performed using a test facility especially constructed for this study. This test facility was designed to accommodate tests of masonry panels up to 6.00 m long by 3.60 m high and to provide well defined support conditions. The component materials used in fabricating the test specimens were the standard 190 mm hollow concrete blocks, type S mortar and standard truss type joint reinforcement.

The test specimens were fabricated in two series (preliminary and main series). The concrete blocks for these two series were cured differently and, therefore, tension and compression test results were presented for both types. The observed behaviours of the walls were

324

compared to other walls of the same series and to other tests to investigate the effects of variability and of any changes made in the different series.

Even including the large number of full scale tests reported in this investigation, there is not enough data for an assessment of design methods. Therefore, it was necessary to extend the knowledge of masonry wall behaviour to include untested conditions and configurations by means of an analytical model capable of reproducing the observed behaviour of the walls. The existing models were reviewed and a nonlinear finite element model was constructed to closely predict the behaviour of masonry panels. In this model, the anisotropic nature of masonry, the nonlinearity due to cracking and the effects of the transverse shear deformations due to the presence and the discontinuity of the core webs were taken into consideration. This model was fundamentally verified using linear elastic and nonlinear solutions available in the literature and it was also compared to tested masonry panels to verify its use for predicting the behaviour of masonry walls. Also, the existing biaxial failure criteria were reviewed and a proposed macroscopic biaxial failure criterion was incorporated in the finite element model to predict the strength and the mode of failure of masonry assemblages. This criterion accounted for the anisotropic and composite nature of masonry and was based on physical interpretations rather than being strictly a phenomenological criterion.

Finally, the available design methods were compared using the extended data from the analytical model. Then, a design method based on

elastic plate theory was proposed. This method was rationally developed to predict first cracking and failure capacities for masonry panels simply supported on three or four sides for a wide range of aspect ratios.

8.2   CONCLUSIONS

The conclusions concerning the experimental results, the biaxial failure criteria, the finite element models and the design methods were presented at the end of Chapters 4, 5, 6 and 7, respectively. However, general conclusions are also presented below to help gain an overall understanding of the behaviour of laterally loaded masonry panels and consequently the design of these panels. These conclusions are as follows:

1. By performing the experimental work, the behaviour of concrete block walls when subjected to lateral (out-of-plane) loading is better understood at different stages (uncracked, cracked and failure). Also, a body of test data on lateral loading of masonry walls with well defined support conditions is available for North American conditions (practice and material) and is accessible for verifying any method of analysis.

2. The experimental results of the full scale walls indicated the possibility of determining the ultimate capacity of walls supported on all four sides as that for its two halves after first cracking with the appropriate boundary condition at the center horizontal crack.

3. The full scale wall and assemblage test results confirmed the

relatively high variability of both strength and flexural rigidity for bending normal to the bed joints. This explains the considerable variability of the stiffness and the first cracking and failure pressures of the full scale walls supported on all four sides.

4. The observed behaviour of the full scale walls contradicted the yield line predictions for some panels. This may suggest more objections to the direct use of the yield line method for the analysis of masonry walls. Also, detailed analyses indicated that a reason for the good predictions obtained using the yield line method in some cases is the reasonably uniform elastic stress distribution along the expected yield line for certain aspect ratios and support conditions.

5. The allowable stresses in North American Codes for flexure normal to bed joints are quite close to the determined strength, especially that of the preliminary series.) This evidence leads to the conclusion that the margin of safety is not adequate. However, for the direction parallel to the bed joints, the allowable stresses in the codes reflect a reasonable margin of safety when compared to the determined strength. Also, wall tests gave an orthogonal strength ratio of 2.6 whereas the auxiliary tests yielded ratios of 3.5 and 3.3 for the preliminary and main test series, respectively. These were in all cases more than the ratio of 2.0 specified in most design codes.

6. The strengths of masonry assemblages differ significantly for

different failure modes. These depend on the relative magnitudes of the normal and shear stresses acting along the critical planes normal and parallel to the bed joints. Also, these modes of failure may differ according to the relative magnitudes of the different strengths of the component materials used for the assemblages.

7. The proposed failure criterion seems to be acceptable for masonry. It has most of the required features for a generalized criterion and is free of the drawbacks of direct application of orthotropic failure theories to masonry. In this criterion, the biaxial strengths are not determined in terms of the uniaxial assemblage strengths but rather both uniaxial and biaxial strengths are evaluated in terms of the component material strengths and geometries. This procedure generalizes the use of the criterion for any combination of unit strengths and mortar bond characteristics. Also, the predictions using the proposed criterion for the different cases of masonry assemblages seem to agree satisfactorily with the available experimental results in all cases.

8. The proposed nonlinear macroscopic finite element model can be used to analyse most large masonry assemblages, structural elements and structures. This is because it has been developed in a generalized form to handle both in-plane and out-of-plane loading conditions including both constant and variable (or incremental) loading histories. Also, by adopting a layered

plate approach in the finite element-formulation, the analysis was extended beyond the elastic or cracking limit by modifying the stiffness of the particular layer which had reached this limit. Thus an added feature is that the model can also be used for the analysis of multi-wythe walls. Moreover, the orthotropic and composite nature of masonry was considered in the model by including the orthotropic properties for each layer and implementing the macroscopic biaxial failure criterion proposed in Chapter 5. Furthermore, the transverse shear degrees of freedom were included in the proposed model to account for the transverse shear deformations which were shown to be significant in the case of laterally loaded hollow block masonry.

9. The verification of the proposed model using available linear elastic and nonlinear solutions and the convergence study indicated good model predictions and fairly rapid convergence in all cases. Also, the comparisons of the proposed model predictions with the test data for full scale hollow block walls showed that the proposed model is capable of predicting the behaviour of full scale masonry walls with an acceptable degree of accuracy. Accordingly, it was used to produce data for other untested wall conditions and configurations and thus provided additional knowledge about masonry wall behaviour.

10. The proposed design method for laterally loaded masonry walls was rationally developed using a simplified elastic plate analysis. In this method, according to the results of the

analyses using the nonlinear finite element model, the approximation of one way bending may be used to determine panel capacities for aspect ratios less than 1/3 and higher than 4 for panels supported on all four sides. However, for panels supported on three sides, this approximation may be applied only for cases with aspect ratios less than 1/2.

11. The proposed design method yielded predictions for capacities of masonry panels which are in reasonable agreement with the available test data from this study and the extended data obtained using the finite element model which was developed. It is suggested that this method has potential for being included as a design method in masonry codes. This is because of its rational development and simplicity and because it uses techniques familiar to practicing engineers.

8.3   RECOMMENDATIONS FOR FUTURE RESEARCH

During the course of completing this study, some related areas requiring further research have become apparent. The following are recommended: -

1. An experimental study should be undertaken to investigate the behaviour of hollow concrete block masonry walls having boundary conditions other than simple supports. Also, the effect of arching action on the behaviour and particularly on the capacity of such panels would be a relevant investigation.

2. The lateral load behaviour of partially or fully grouted reinforced concrete block walls should be included.

3. An experimental and analytical study is needed to investigate the behaviour of the mortar joints and particularly the head joints under both in-plane and flexural tension. This would help to verify or modify the assumption of nonlinear behaviour adopted in the present study.

4. The interaction of flexural tensile and torsional shear stresses acting on mortar joints should be tested. Appropriate data would help to verify or modify the linear interaction relationship assumed in the present study.

5. Extending the proposed biaxial-failure criterion to include the longitudinal failure mode (characterized by splitting of the cross webs in the case of hollow masonry) would be worthwhile. This would generalize this criterion to predict the strength and failure modes of masonry assemblages for the different regions of biaxial stresses normal and parallel to the bed joints.

6. Development of a detailed microscopic numerical model for predicting the behaviour of small masonry assemblages would be valuable for verifying and calibrating the macroscopic model proposed in this study. It would also be useful to provide reasonable values for the stiffness reduction factors needed for the nonlinear macroscopic model.

7. Extending the proposed design method to incorporate boundary conditions other than the simple supports would result in greater versatility and efficiency for this method. Also, provision of some design aids for panels having window or door openings would be a desirable feature for the design method.

APPENDIX A

TEST RESULTS FOR PROPERTIES OF THE BUBBLE CURED BLOCKS

A.1   INTRODUCTION

The interpretation or prediction of the capacity and behaviour
of full-scale walls or masonry assemblages generally requires knowledge
of the behaviour characteristics of masonry components. In this
Appendix, the experimental tests performed to document the behavioural
characteristics of bubble cured blocks are described and the results are
reported. These results have been referred to earlier in this thesis
where the discussion, interpretation, and use of particular results were
appropriate. These tests were conducted by the author in collaboration
with two other graduate students at McMaster University who were using
the same type of block in their masonry research [47,89].

The tests were performed on blocks chosen randomly from the
shipments of blocks used for the main assemblage specimens. They were
tested at representative ages comparable to that of the main
assemblages.

A.2   TESTS OF BLOCKS IN COMPRESSION

These tests were performed in order to evaluate the compressive
strength of the blocks and their deformational characteristics under
compressive loading. Due to the absence of a universally accepted
consistent test method for determining block compressive strength, it

332

was decided to perform the following five different compression tests:

1. Full blocks tested flatwise in accordance with the quality control of blocks described in A.S.T.M. Standard C140-75.

2. Similar tests of fully capped half blocks which are thought to differ from 1 in that more uniform axial deformation can be achieved and that there should be somewhat less effect of end platten restraint because of the higher height to thickness ratio in one direction.

3. Tests of half blocks similar to 2 but with only face shell capping, since this condition represents the real load application on blocks in walls.

4. Tests of prisms made by gluing together four face shells of blocks. This was an attempt to exclude the influence of block shape and to get material properties which were less influenced by geometry of the test specimens.

5. Full blocks tested endwise to provide information for compression applied parallel to the bed joints in blockwork.

It should be noted here that all half blocks were cut from the flat end of splitter block units so that symmetry was maintained. Also, only hard capping was used. The hard capping material was gypsum cement which is commercially known as Hydrostone.

The details and results for the 5 above mentioned types of compression tests follow.

A.2.1 Compression of Full Blocks Tested Flatwise (Test Cl)

Ten stretcher blocks were tested in a hydraulic Tinius Olsen

test machine with the compressive loading applied normal to the bed joint plane. Hydrostone capping was placed over the entire cross-section of the unit (face shells and cross webs) and capped onto 75mm thick steel plates top and bottom. These thick steel plates were used to ensure the uniformity of the loading over the entire block, since the circular loading head only had a diameter of 200mm. The failure loads were recorded and the compressive stresses at failure for the individual specimens are given in Table A.1 together with the mean compressive strength and the coefficient of variation. No strain measurements were taken since the significant effects of end platten restraint would obscure the actual stress-strain properties of the block material. The failure stresses were calculated using the minimum net area of a block unit being 51% of the gross cross-sectional area (i.e. 0.51*190*390= 37791 mm^2).

A.2.2 Compression of Fully Capped Half Blocks (Test C2)

Ten half hollow block specimens were tested flatwise with capping material covering the overall cross-sectional area. These half block specimens were prepared by cutting the full splitter units with a diamond blade saw. All ten specimens were tested to failure. Mechanical strain gauge points (using a 100mm gauge length) were mounted on the two face shells of five specimens as shown in Figure A.1 a), so that the deformation in the vertical and horizontal directions could be measured. The deformations between the gauge points were measured at each load increment by means of a Huggenberger mechanical strain indicator having a resolution of 0.001mm. This resolution, together with the 100mm gauge

TABLE A.1

SUMMARY OF CONCRETE BLOCK COMPRESSION TESTS

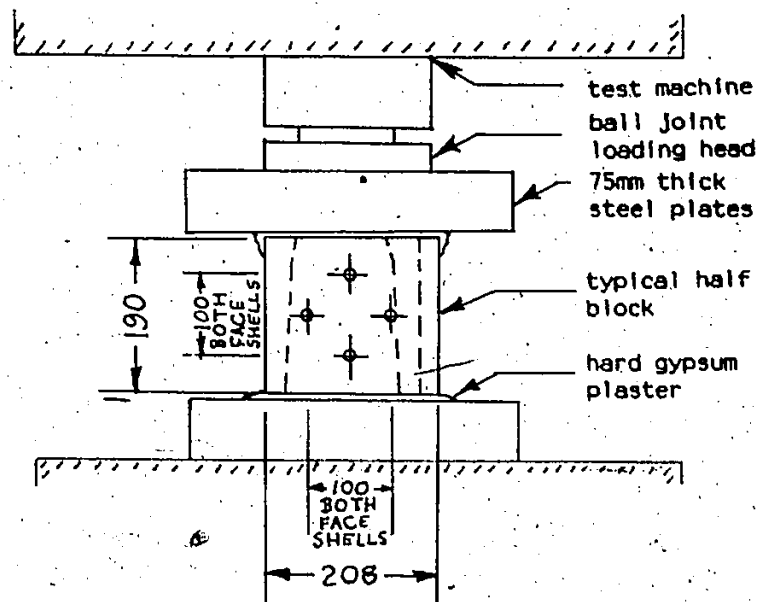| SPECIMEN	FAILURE STRESS (MPa)* FOR TEST				
	C1	C2	C3	C4	C5
1	24.3	21.9	27.7	16.7	19.6
2	21.5	21.7	26.9	17.7	20.8
3	23.9	20.4	27.4	17.6	17.9
4	24.0	20.3	27.7	17.9	23.8
5	21.8	20.0	26.4	20.0	15.2
6	23.7	20.1	25.3	18.3	20.1
7	20.8	23.4	28.7	19.1	15.8
8	22.5	24.4	25.0	18.6	17.2
9	23.3	25.3	27.2	20.4	19.0
10	22.0	23.4	25.7	18.7	17.5
Mean (MPa)	22.8	22.1	26.8	18.5	18.7
COV (%)	5.4	8.7	4.4	6.1	13.6

* stresses based on minimum net cross-sectional area.

Figure A.1 a)STRAIN GAUGE POINT PLACEMENT FOR THE HALF BLOCK
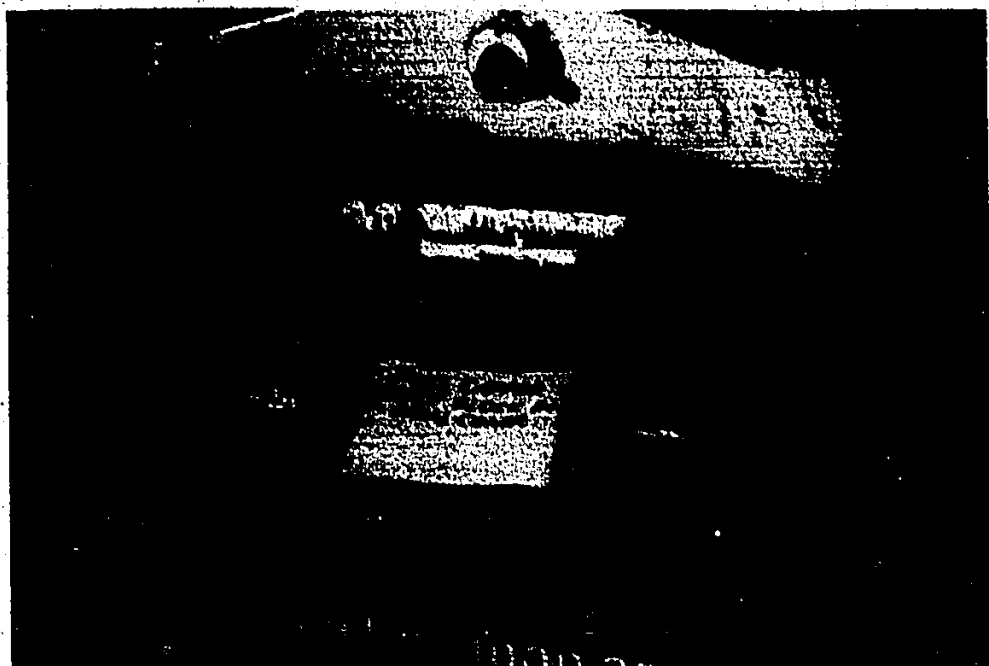COMPRESSION SPECIMENS (Tests C2 and C3)

Figure A.1 b)TEST SET-UP AND CONICAL FAILURE FOR FULLY CAPPED HALF
BLOCK SPECIMENS (Test C2)

length used, provided a precision of 10 micro-strain for the calculated strains.

The compressive strengths of the 10 specimens as well as the mean strength and coefficient of variation are shown as Test C2 in Table A.1. These stresses were calculated on the basis of the minimum net area of 19612 mm^2 at the bottom of the block. This is about 54% of the gross area of the half block specimens. The typical conical failure pattern can be seen in Figure A.1 b).

The stress-strain results for the fully capped half block specimens are shown in Figure A.2, where at each load level, the average of the strains from both face shells was plotted for each specimen. The non-linear behaviour of the concrete block under high axial compression is quite evident. A fourth order polynomial was used to obtain the regression equation to best fit the data shown in Figure A.2. Expressing stress, σ (MPa), in terms of the strain, ε, resulted in Equation A.1.

$$\sigma = 24908\varepsilon - 13356\varepsilon^2 + 4.17 \times 10^9\varepsilon^3 - 5.57 \times 10^{11}\varepsilon^4 \tag{A.1}$$

It should be noted that the regression analysis performed, used the mean strain of each specimen at a stress level normalized in such a way that the failure load of each specimen equalled the mean failure load.

Two different values for the Modulus of Elasticity of concrete blocks in compression were determined from the stress-strain curve in Figure A.2 as expressed in Equation A.1. The first was the initial Tangential Modulus of Elasticity and was found to be 24.9X10^3 MPa. The second was the Secant Modulus of Elasticity at a stress of one half the strength, which had a value of 18.2X10^3 MPa.
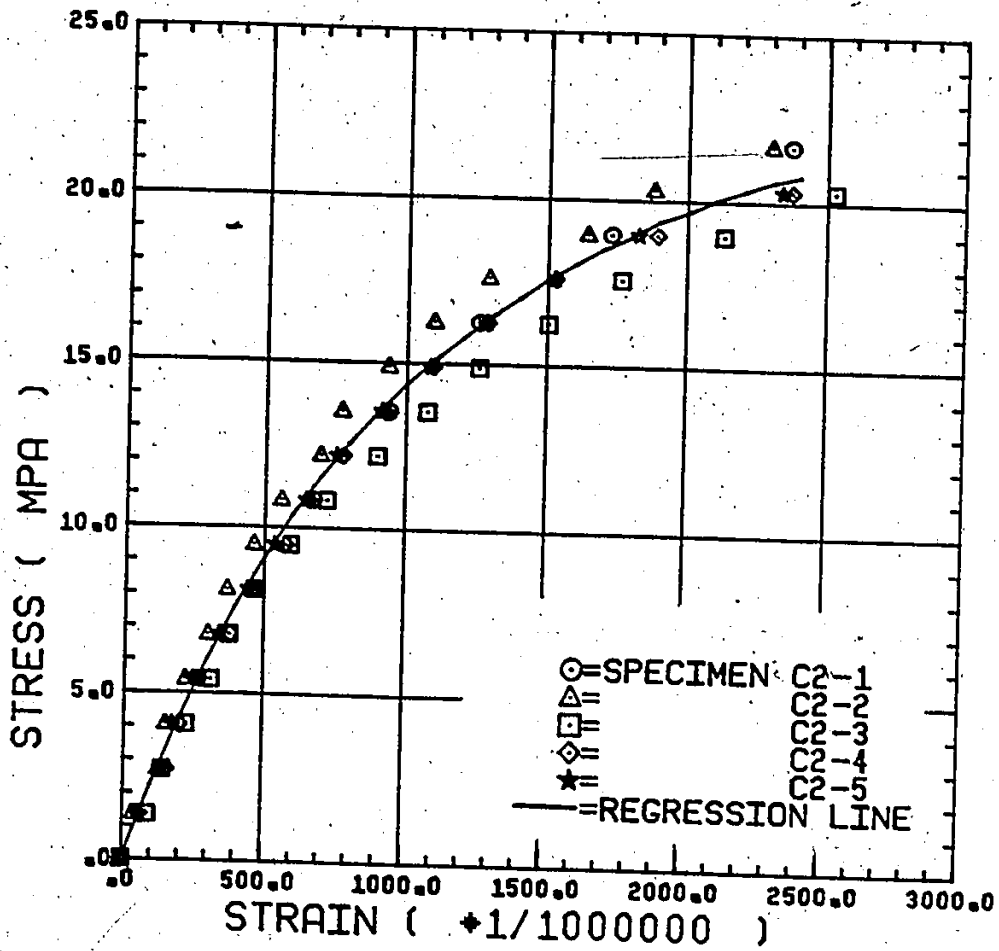
Figure A.2   STRESS-STRAIN RELATIONSHIP FOR FULLY CAPPED HALF BLOCKS
             1N COMPRESSION (Test C2)

The Poisson's Ratios were determined for these blocks from the measured transverse deformations. These are shown in Figure A.3 versus the axial (longitudinal) stress. Again, each point represents the average of two readings from the two sides of each specimen. The transverse strains at stress levels below 5 MPa were not shown due to the inaccuracy of the Huggenberger instrument with such small deformations. A large scatter of results occurs at this low stress level with errors in the strain readings of as much as 40%. The regression line shown in Figure A.3 helps to show the increase in Poisson's Ratio at higher stress levels as the specimens approach failure. These higher values are attributed to the non-linearity in the behaviour owing to the extensive development of micro-cracks within concrete at stresses near failure [77]. Of course, the apparent high values for Poisson's Ratio and the suggested explanation for these values both contradict the normal definition of this value. Accordingly, an estimate for the Poisson's Ratio was obtained by a linear regression analysis performed on a plot of the lateral versus the horizontal strain, considering only the strain values at stress levels above and including the 5 MPa level (corresponding approximately to 200 micro-strain) and below and including the 1000 micro-strain level (corresponding approximately to 15 MPa). This yielded a Poisson's Ratio of 0.33 for the stress range below levels where extensive microcracking would be expected.

A.2.3   Compression of Half Blocks With Only Face Shell Capping (Test C3)

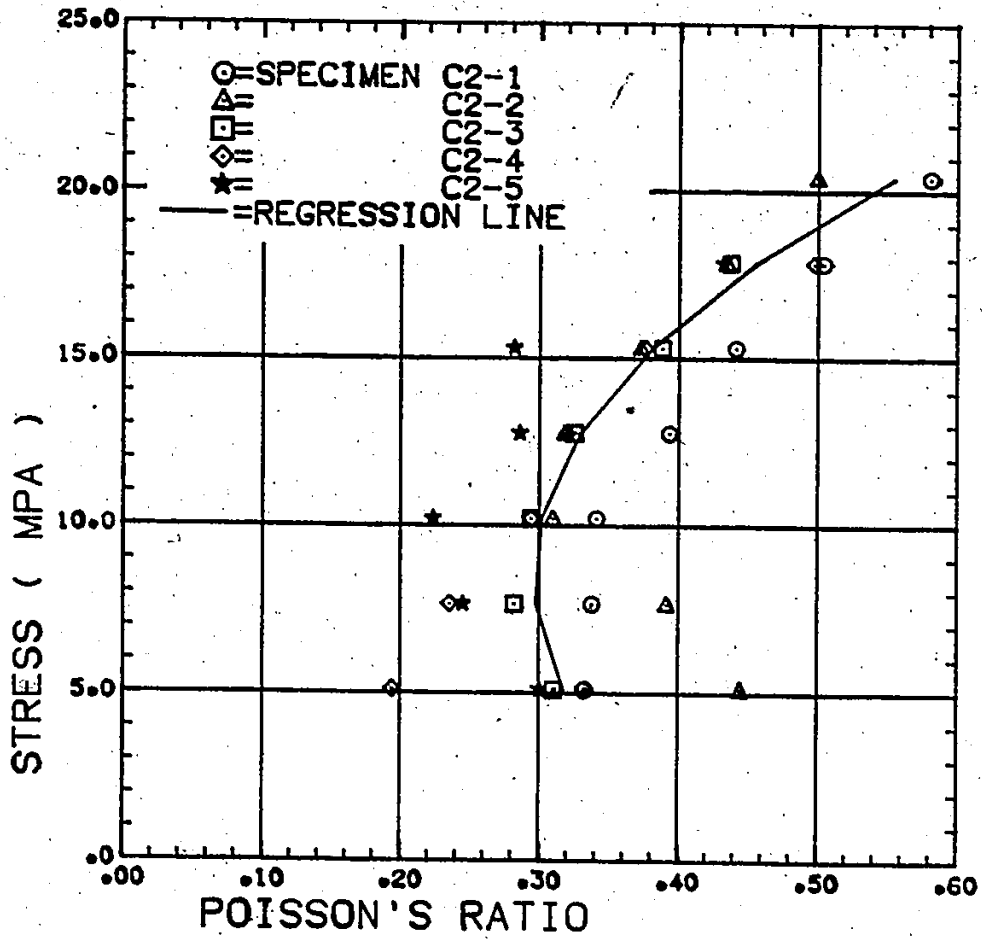Ten half block specimens saw cut from the splitter units were

Figure A.3   STRESS-POISSON'S RATIO RELATIONSHIP FOR FULLY CAPPED
HALF BLOCKS IN COMPRESSION (Test C2)

tested flatwise with the only difference from Test C2 being that they were capped only on the face shells. The minimum face shell capping area was assured by covering the cross webs with cardboard during capping. In this test, gauge points were mounted on the face shells of five specimens for axial and transverse strain measurements. The same Huggenberger instrument as in Test C2 using a 100mm gauge length to measure deformation was used.

The strengths of the 10 specimens were calculated using a net cross-sectional area of 12,800 mm^2 based on a minimum face shell thickness of 32mm and are listed in Table A.1 under Test C3. The mean strength and the coefficient of variation are also listed. The observed failure mode was a conical failure similar to that shown in Figure A.1 b) for Test C2, but was primarily in the face shells with some web cracking.

The stress-strain data from Test C3 is shown in Figure A.4 where each point represents the average of two face shell readings. A regression analysis was used to find the best fit curve where the stress was normalized to the average strength. This yielded the following expression with stress, σ (MPa), expressed in terms of strain, ε:

$$\sigma = 20236\varepsilon - 62571\varepsilon^2 + 9.1 \times 10^6 \varepsilon^3 - 4.23 \times 10^{10}\varepsilon^4 \qquad (A.2)$$

The calculated initial Tangential Modulus of Elasticity was found to be 20.2X10^3 MPa and the Secant Modulus of Elasticity at a stress level of one half the strength was found to be 15.5X10^3 MPa.

The axial or longitudinal stress versus Poisson's Ratio is shown in Figure A.5. Poisson's Ratio was determined from the measured
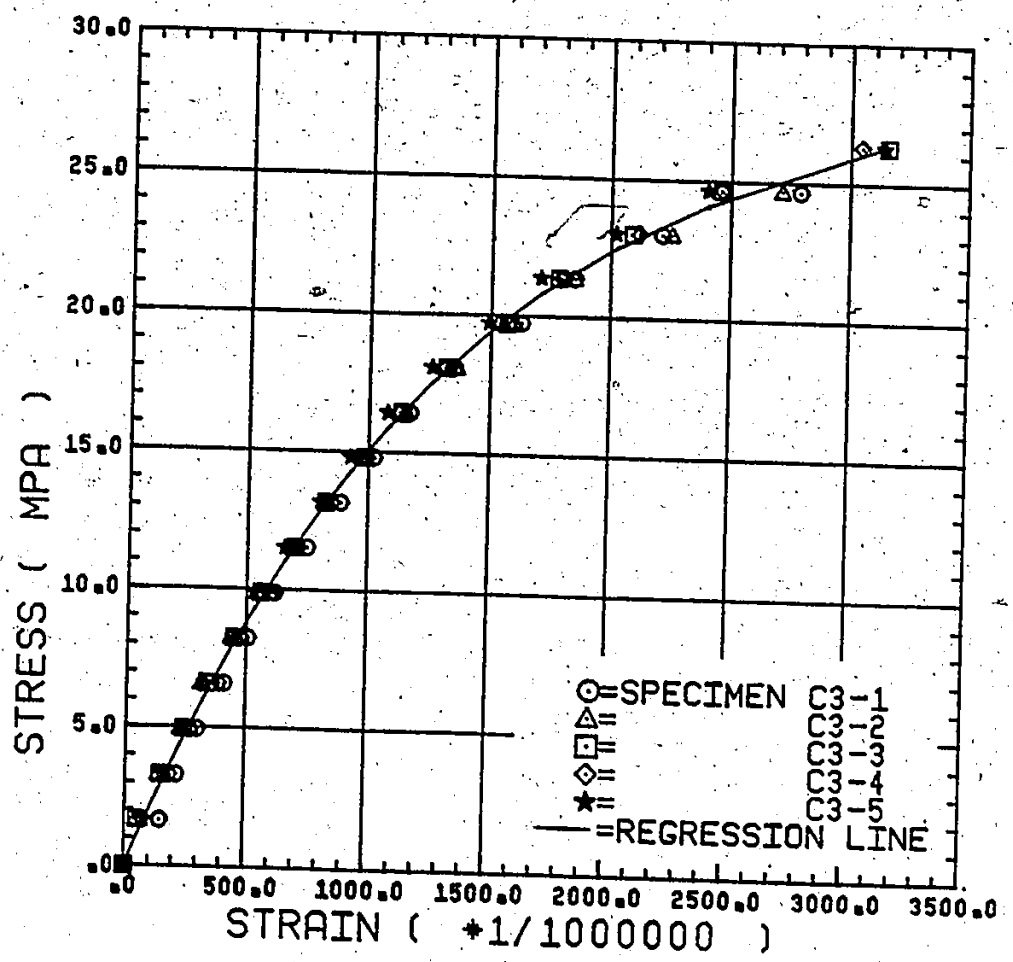
Figure A.4   STRESS-STRAIN RELATIONSHIP FOR FACESHELL CAPPED
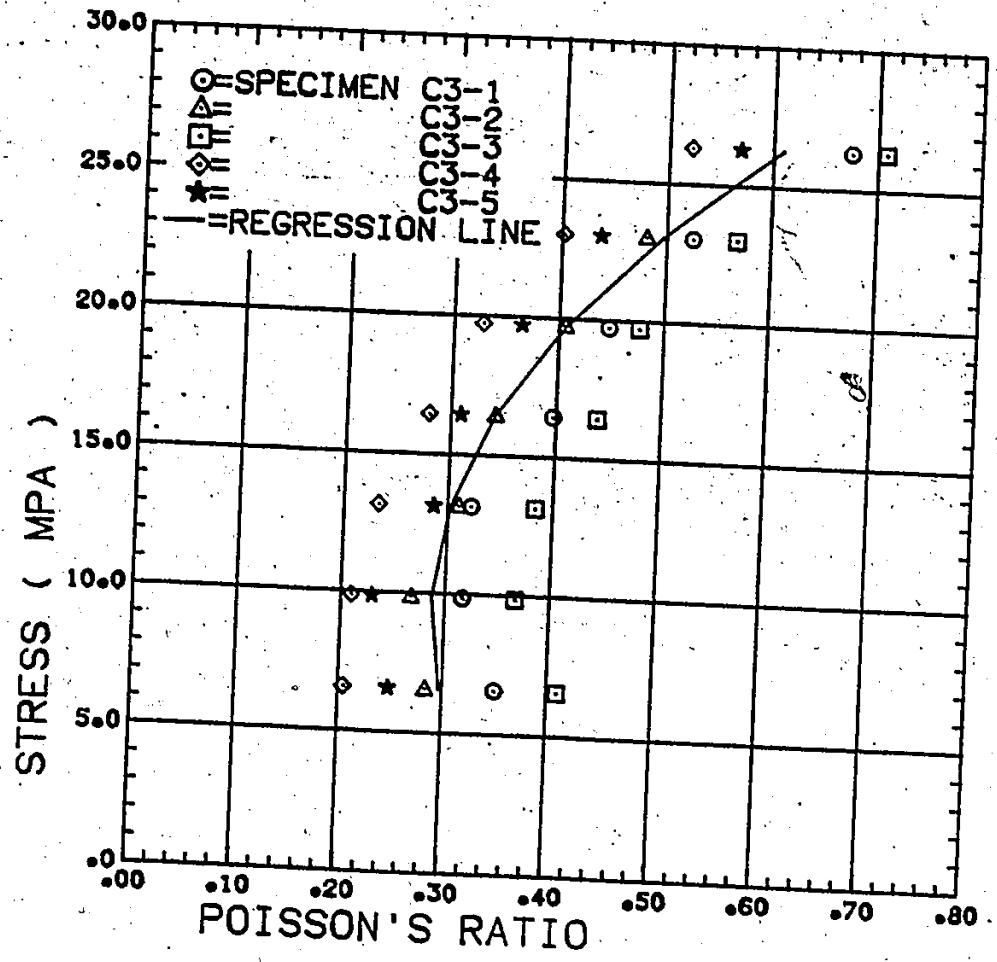HALF BLOCKS IN COMPRESSION (Test C3)

Figure A.5   STRESS-POISSON'S RATIO RELATIONSHIP FOR FACESHELL CAPPED
HALF BLOCKS IN COMPRESSION (Test C3)

The axial or longitudinal stress versus Poisson's Ratio is shown in Figure A.5. Poisson's Ratio was determined from the measured transverse deformations and the longitudinal deformations. The discussion of similar results shown in Figure A.3 are applicable here and using the same procedure, the value for the Poisson's Ratio for Test C3 was found to be 0.30.

A.2.4 Compression of Glued Face Shells (Test C4)

Four separate face shells were cut from full stretcher units. They were sawn so that the tapers were removed in order that the thickness was uniform through the face shell height. Then, to avoid having a slender specimen, these four face shells were spot-glued together with thinly applied two component epoxy resin cement commercially known as Sikadur 31, Hi-Mod Gel. This type of specimen was tested to try to obtain information on the concrete block material properties from a specimen which would be relatively free of the geometric effects associated with the shape of blocks.

Ten specimens were prepared and hard capped with the gypsum cement compound, "Hydrostone". The failure loads were recorded for all specimens and axial and transverse strain readings were taken on five specimens by means of electrical resistance strain gauges and strain transducers newly developed by a graduate student working on masonry research at McMaster University [110]. Both strain measuring devices were used to document the accuracy of these newly developed strain transducers.

The individual strengths as well as the mean strength and the

coefficient of variation are listed in Table A.1 for Test C4. These stresses were based on the actual measured cross-sectional area of the four face shells contained in each specimen. One of the five specimens used for strain measurements is shown during testing in Figure A.6 a) while Figure A.6 b) shows the failure pattern of this specimen which was reasonably typical for all specimens.

The stress-strain data for the glued face shell specimens is shown in Figure A.7 where the average of the strains measured on all four sides of the specimen at each load level is represented by a point in the figure. The non-linear behaviour of the concrete material under compression at high load levels is readily apparent. The equation for the regression line to best fit the experimental data as shown in Figure A.7 for the stress, σ (MPa), expressed in terms of strain, ε, is as follows:

$$\sigma = 24655\varepsilon - 11660\varepsilon^2 + 2.287 \times 10^9 \varepsilon^3 - 1.937 \times 10^{11}\varepsilon^4 \qquad (A.3)$$

It was derived using normalized stresses as described earlier. Accordingly, the initial Tangential Modulus of Elasticity and the Secant Modulus at half the failure load are 24.7×10^3 MPa and 19.7×10^3 MPa, respectively.

The axial or longitudinal stress versus Poisson's Ratio is shown in Figure A.8. Poisson's Ratio was determined from the measured transverse deformations on both faces of the specimens and the longitudinal deformations. The noticeably large increases in the Poisson's Ratios at high stress levels may be attributed, as reported earlier, to the extensive development of micro-cracks at these high
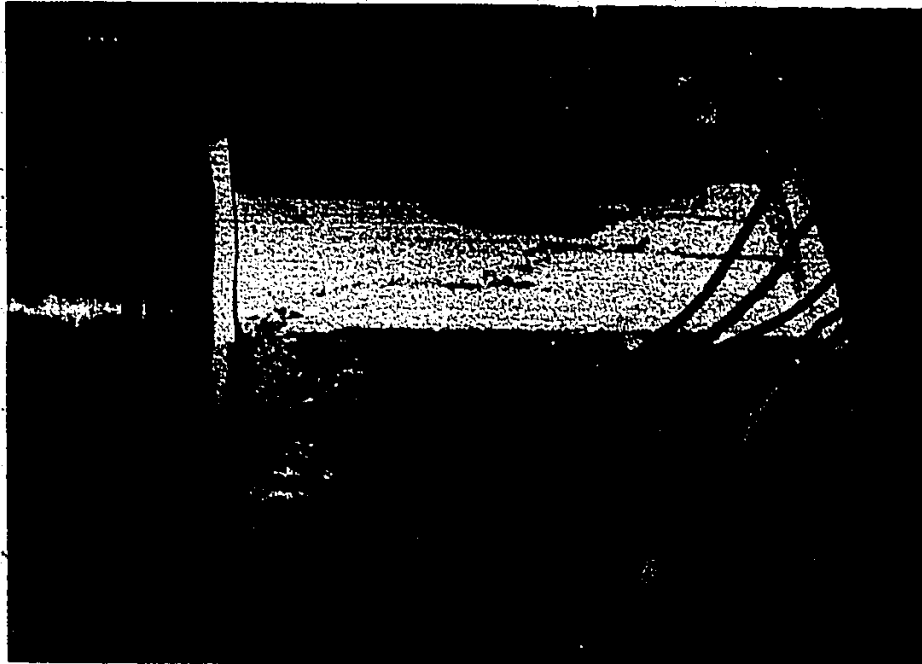
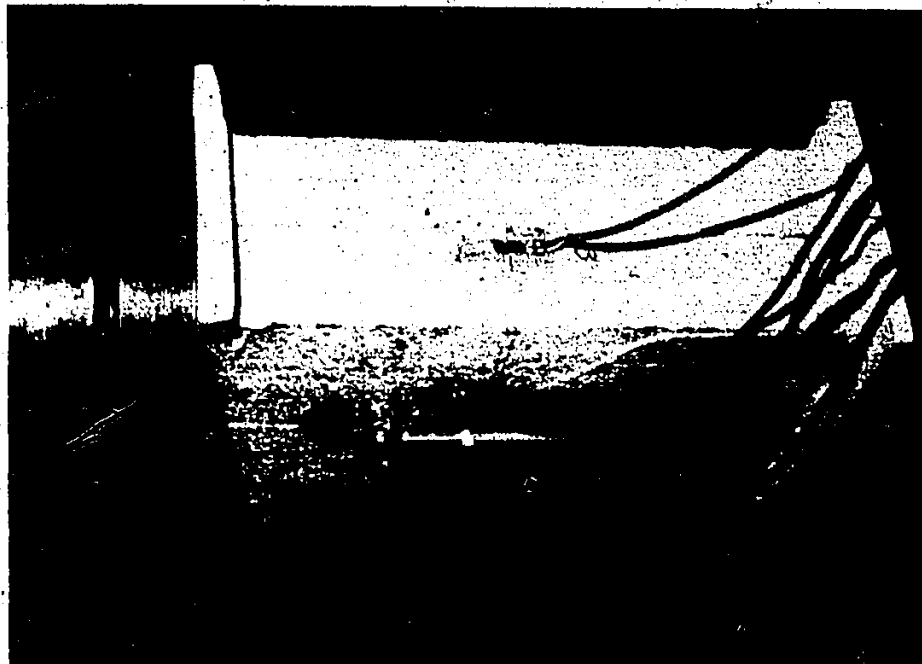Figure A.6 b) FAILURE OF A TYPICAL GLUED FACESHELL SPECIMEN

Figure A.6 a) STRAIN GAUGE PLACEMENT FOR THE GLUED FACESHELL SPECIMENS IN COMPRESSION (Test C4)
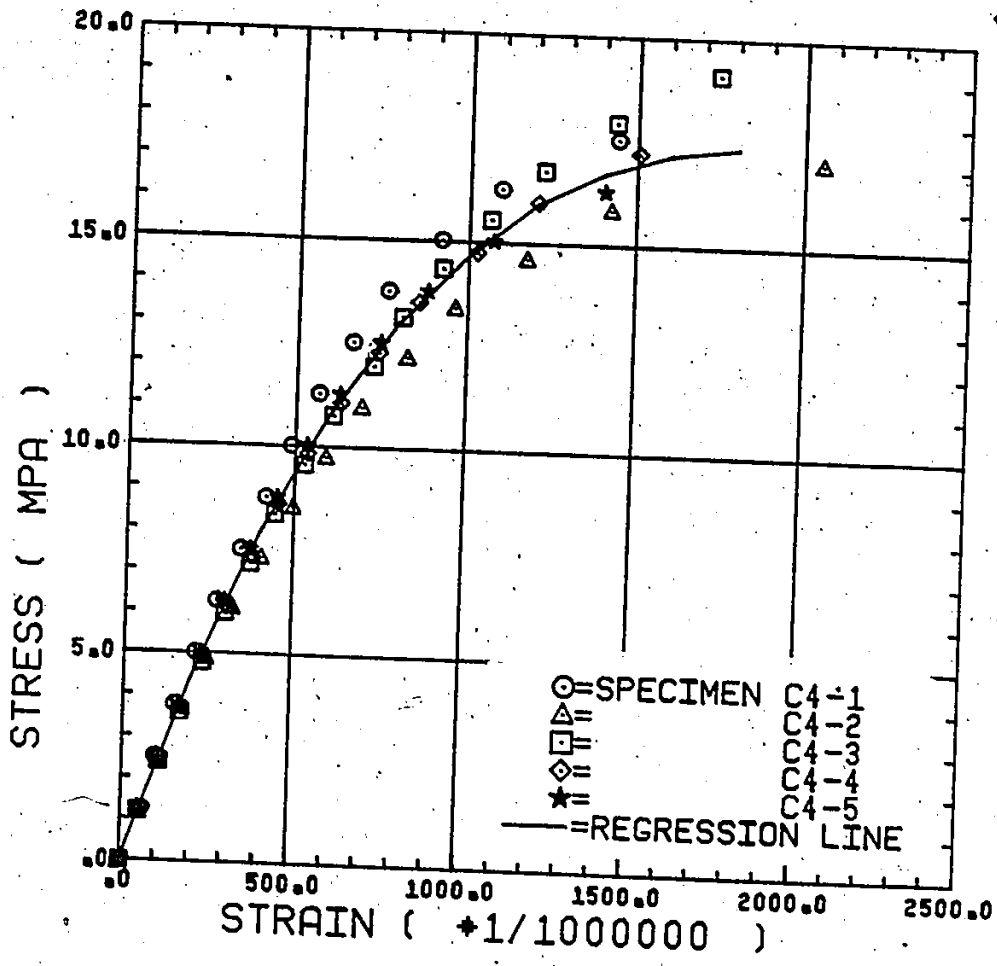
Figure A.7   STRESS-STRAIN RELATIONSHIP FOR THE GLUED
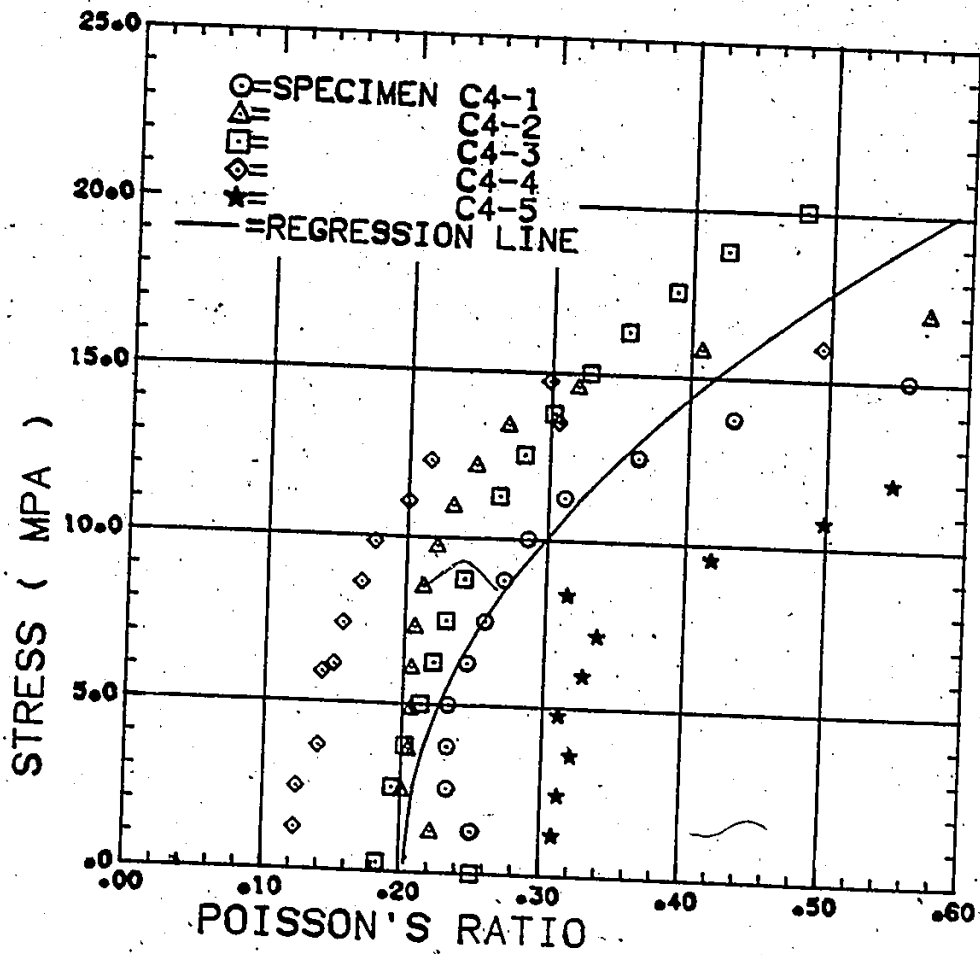FACESHELL SPECIMEN IN COMPRESSION (Test C4)

Figure A.8   STRESS-POISSON'S RATIO RELATIONSHIP FOR THE GLUED
FACESHELL SPECIMEN IN COMPRESSION (Test C4)

stress levels [77]. For this test series, the more accurate measurement of lateral strains made it possible to include data at stress levels below the 5 MPa restriction of previous tests. Thus, the estimate for the Poisson's Ratio was obtained by performing a regression analysis on a plot of lateral versus horizontal strains considering only strain values below and including 1000 micro-strain. This yielded a value for the Poisson's Ratio of 0.34.

A.2.5 Compression of Full Blocks Tested Endwise (Test C5)

Ten full hollow stretcher units were capped on the head joint ends of the face shells and were tested under compressive load acting parallel to the bed joint plane. As these specimens had an aspect ratio larger than that of the full blocks and half block specimens tested flatwise, it is thought that the results would be affected both by the different influence of the orientation of the webs and the reduced effect of end platten restraint.

These specimens were tested up to failure and the strengths are shown in Table A.1 as Test C5 along with the mean and coefficient of variation. The net area used in the stress calculations (13000 mm^2) was based on an effective thickness of 34mm which is equivalent to the average cross-sectional thickness. The typical failure of these specimens was characterized by a diagonal failure plane joining the opposite corners of the face shells as shown in Figure A.9.

Mechanical strain gauge points were mounted on five specimens to measure axial and transverse strains as shown in Figure A.9. The Huggenberger mechanical strain indicator described earlier was used to
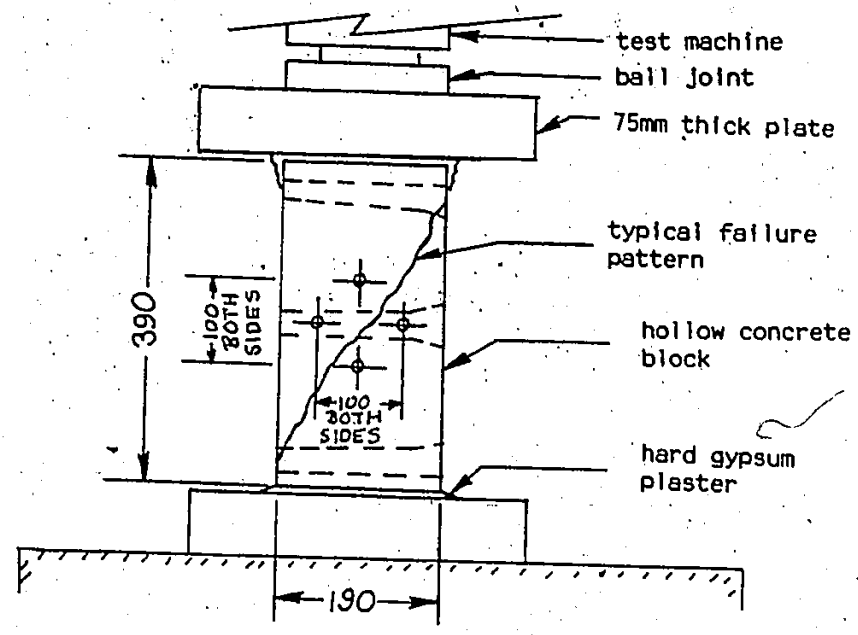
Figure A.9   COMPRESSION TEST SET-UP AND FAILURE MODE FOR THE FULL
BLOCKS TESTED ENDWISE (Test C5)

measure deformations between the gauge points. The resulting stress-strain data are shown in Figure A.10 where each point represents the average of 6 readings for axial strain in each specimen. Using a regression analysis, the curve to best fit the data, where stresses were normalized to the mean strength, is shown in Figure A.10. This curve is represented by the following equation:

$$\sigma = 20022\varepsilon - 86614\varepsilon^2 + 2.52 \times 10^9 \varepsilon^3 - 4.55 \times 10^{11}\varepsilon^4 \qquad (A.4)$$

where σ is stress in MPa and ε is strain. The corresponding initial Tangential Modulus of Elasticity and Secant Modulus of Elasticity at half the failure stress are 20.0×10^3 MPa and 15.6×10^3 MPa, respectively.

The axial or longitudinal stress versus Poisson's Ratio is shown in Figure A.11. The increase in Poisson's Ratio at high stress levels is similar to the earlier tests. The values corresponding to stresses below the 5 MPa level were not included due to the considerably large scatter in the results from the limitations in accuracy of the Huggenberger instrument at low stress levels. A Poisson's Ratio of 0.19 was obtained from a regression analysis performed on lateral versus horizontal strains up to a longitudinal strain of 1000 micro-strain.

A.3   TESTS OF BLOCKS IN TENSION

Three different tension tests for hollow concrete block units were performed. Two of these tests measured the splitting tensile strength, which was shown in earlier research at McMaster University [50] to be a good measure for the axial tensile strength of block material. This splitting tension test is a relatively simple test to
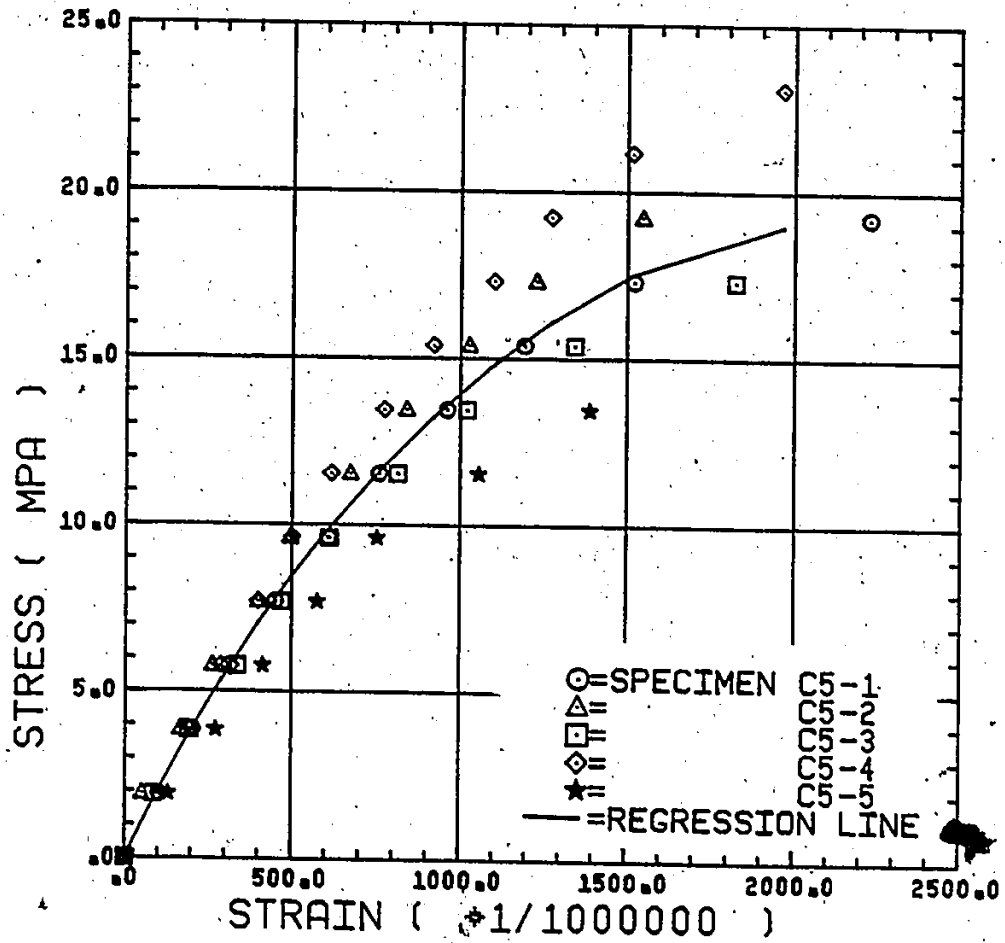
Figure A.10   STRESS-STRAIN RELATIONSHIP FOR THE COMPRESSION OF FULL
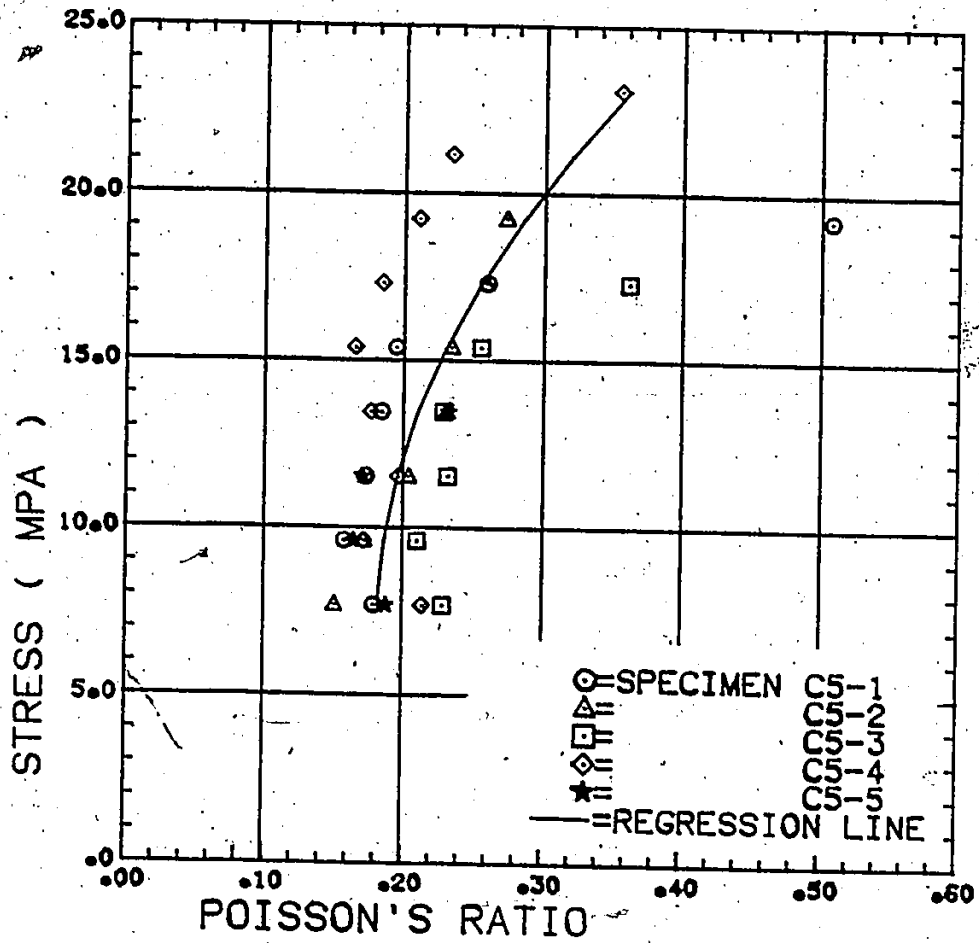BLOCKS TESTED ENDWISE (Test C5)

Figure A.11   STRESS-POISSON'S RATIO RELATIONSHIP FOR THE
COMPRESSION OF FULL BLOCKS TESTED ENDWISE (Test C5)

perform as compared to a direct tension test. The third tension test that was performed was a flexural tensile strength test on the unit.

In Test T1, the splitting strength of the face shells was determined. This is thought to represent the axial tensile strength of the blocks in the plane of the wall. The splitting strength of the webs was evaluated in Test Series T2. This strength is thought to be applicable to the typical splitting failure pattern observed for axial load tests of most face shell bedded prisms and walls. The last test, Test Series T3, was used to determine the out-of-plane bending strength of the block. It has been shown previously [50] that the apparent tensile strength of concrete blocks is very sensitive to the type of test. Therefore this test was necessary in order to provide data for out-of-plane tests of walls.

In the following sections the different test results are reported.

A.3.1   Splitting of Face Shells in Half Block Specimens (Test T1)

Ten half block specimens saw cut from hollow splitter units were tested under compressive line loads crossing the face shells as shown in Figure A.12 a). Ten millimeter diameter steel bars were used for the load application. However, the stress concentration expected at the bar-specimen contact line was avoided by means of 5mm thick plywood strips inserted between the steel bars and the half block specimen.

The failure loads were recorded for each specimen and the splitting strengths were calculated using an effective face shell thickness of 34mm based on the average cross-sectional thickness and the
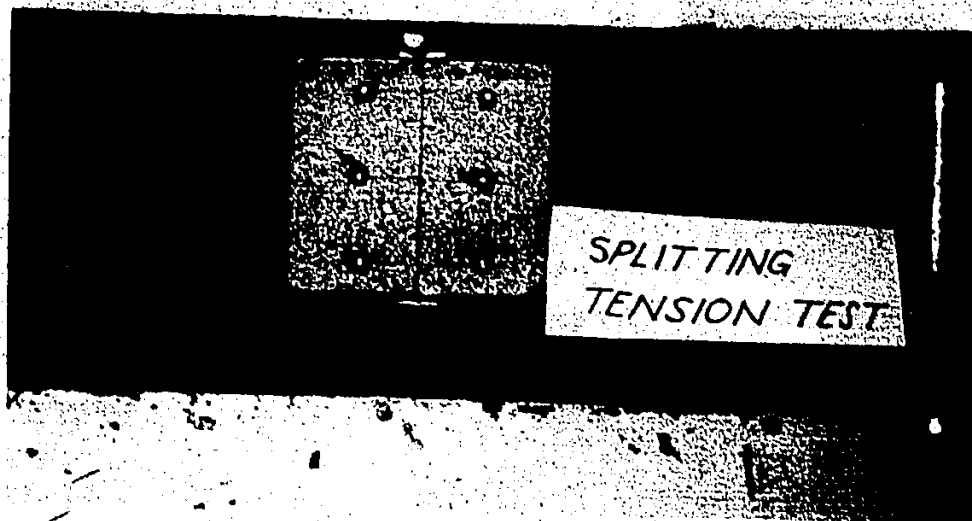
Figure A.12 a)SPLITTING TENSION TEST SET-UP (Tests TI and T2)

Figure A.12 b)TYPICAL FAILURE OF A SPLITTING TENSION SPECIMEN

following relationship (67):

$$\sigma_t = 2P/(\pi th)$$

where P is the splitting load, h is the specimen height and t is the thickness of the splitting plane.

The strengths of individual specimens are given in Table A.2 together with the mean and coefficient of variation. Figure A.12 b) is a photograph of the typical failure pattern for this test which is characterized by a splitting of the vertical plane of loading. Measurement of transverse strain was attempted using the Huggenberger instrument used for the compression tests. However the results proved inadequate due to the very small deformations obtained relative to the accuracy of the measuring device.

A.3.2   Splitting of Cross Webs in Half Block Specimens (Test T2)

Ten specimens were tested in a similar manner to Test Series T1 with the only difference being that the line loads crossed the webs instead of the face shells. The splitting strengths obtained from these tests are shown as Test T2 in Table A.2 and the observed failure mode in the webs was similar to that reported for Test T1.

A.3.3   Out-of-Plane Bending of Full Block Specimens (Test T3)

The out-of-plane bending was first attempted on a beam constructed of two blocks glued end to end using the Sikadur epoxy resin glue mentioned earlier. In these tests, premature failure tended to occur in the shear span due to bending of the block's cross webs as they acted similar to

TABLE A.2

SUMMARY OF CONCRETE BLOCK TENSION TESTS

SPECIMEN	FAILURE STRESS (MPa) FOR TEST		
	T1	T2	T3
1	1.51	1.15	2.40
2	1.54	1.45	2.43
3	1.41	1.07	2.21
4	1.81	0.86	2.42
5	1.41	1.55	2.23
6	1.98	1.25	2.73
7	1.69	1.56	2.45
8	1.48	1.16	----
9	1.53	1.42	----
10	1.61	1.50	----
Mean (MPa)	1.60	1.30	2.41
COV (%)	11.4	18.1	7.1

the verticals of a Vierendeel truss type of specimen. To overcome this problem, the projecting frogged ends of individual blocks were cut away with a diamond saw blade so that the flush faces could be glued to 25mm thick steel plates. These steel plates had been welded to 200mm square hollow steel sections. Bending tests were performed using two of these steel sections with a block glued between them to form a span of 1640mm with a two point loading system located at 500mm from each support. This resulted in a nearly constant moment over the length of the block. Figure A.13 a) is a photograph of this test set-up. Strains were measured on the outer surfaces of the two face shells by means of the newly developed strain transducers mentioned in Section A.2.4. Two such transducers were attached to each face shell as shown in Figure A.13 b) and the strains were directly recorded using a data acquisition system.

The flexural tensile strengths for the seven test specimens are shown in Table A.2 as Test T3 with the mean and coefficient of variation. These stresses were calculated using the coupled face shell section properties based on a minimum face shell thickness of 32mm. In all cases, the failure occurred through the thin part of the face shells as seen in Figure A.13 c).

The measured strains on both face shells were utilized to calculate the curvatures which are shown in Figure A.14 versus the corresponding bending moments. The curvature axis was shifted up by an amount equal to the moment due to the weight of the equipment (200000 N-mm) before the regression analysis was performed. The regression analysis yielded the following fourth order polynomial relationship between the moment, M and the curvature x:
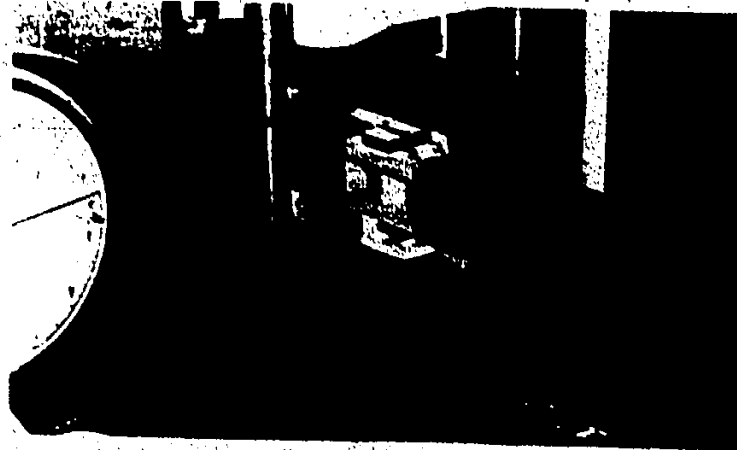
Figure A.13 a)OUT-OF-PLANE BENDING TEST SET-UP (Test T3)

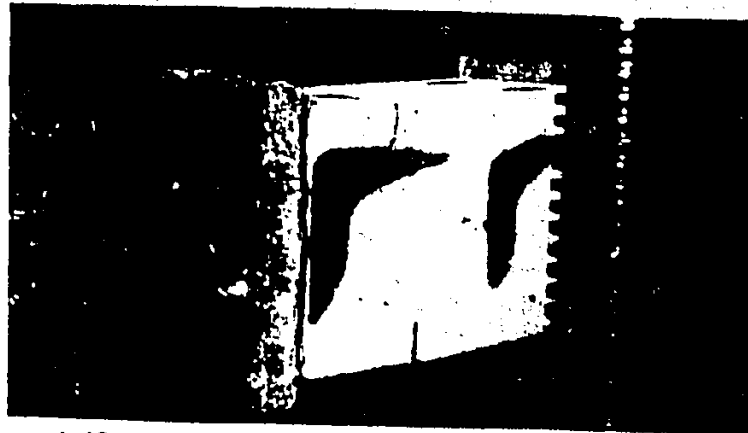Figure A.13 b)STRAIN TRANSDUCER PLACEMENT FOR BLOCK BENDING TESTS

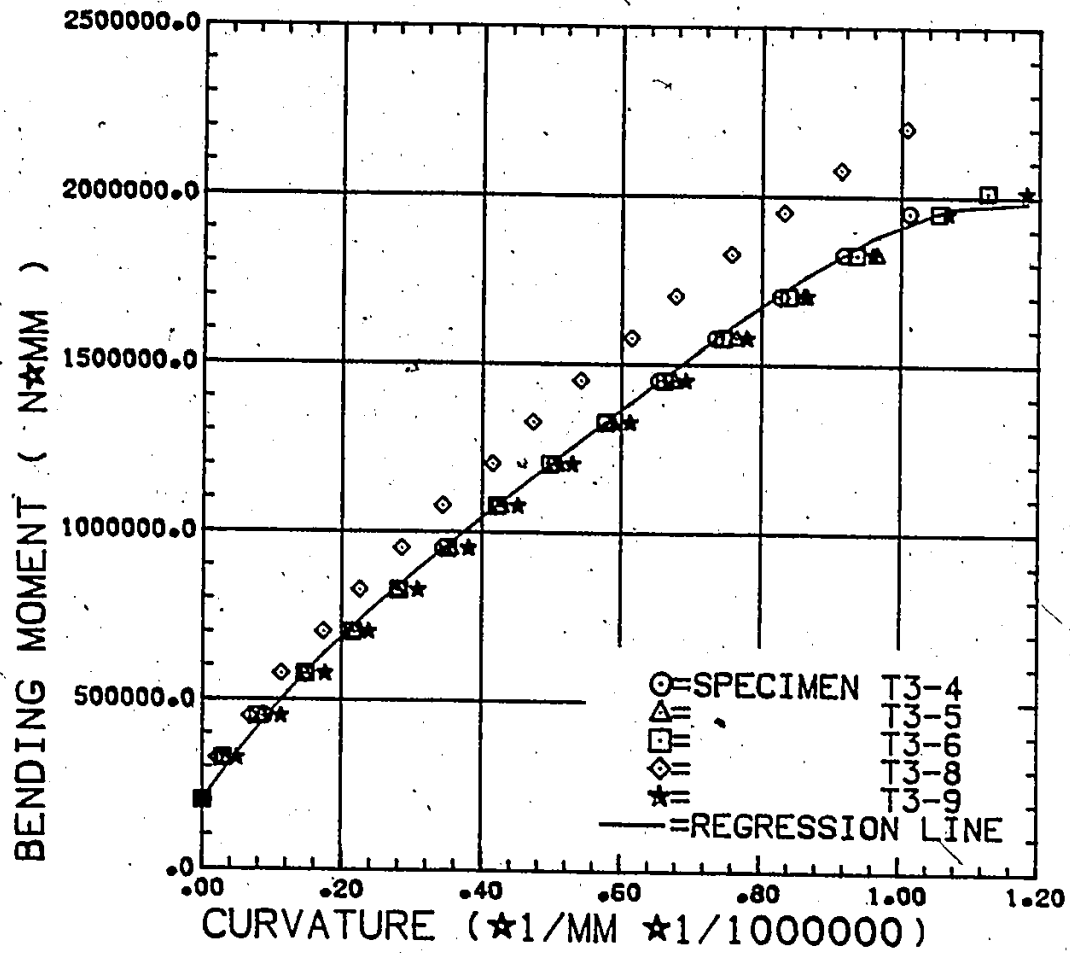Figure A.13 c)TYPICAL FAILURE OF BLOCK IN OUT-OF-PLANE BENDING

Figure A.14 MOMENT-CURVATURE RELATIONSHIP FOR THE OUT-OF-PLANE
BENDING OF CONCRETE BLOCKS (Test T3)

$$M = 3.00 \times 10^{12} x - 3.59 \times 10^{18} x^2 + 4.15 \times 10^{24} x^3 - 1.84 \times 10^{30} x^4 \quad \text{(A.6)}$$

However, assuming a linear relationship, the analysis yielded the following expression:

$$M = 1.82 \times 10^{12} x \quad \text{(A.7)}$$

This linear relationship is equivalent to stating that the Flexural Rigidity of the standard 190mm hollow concrete block is 1.82×10^{12} MPa.

APPENDIX B

CRACKING PATTERNS OF FULL SCALE WALLS

B.1 INTRODUCTION

The typical failure patterns for each group of full scale wall tests were given earlier in Chapter 4 during reporting and discussion of the test results. However, in Chapter 4 only the failure pattern of one wall in each series was shown except where the discussion necessitated otherwise. Therefore, the cracking patterns for the other walls not reported in Chapter 4 are provided in this Appendix. The reason for this is to provide a complete record of these full scale wall tests since the crack patterns within each group were not identical.

Figure B.1   Crack Pattern for Wall WH-[

Figure B.2   Crack Pattern for Wall WH-2
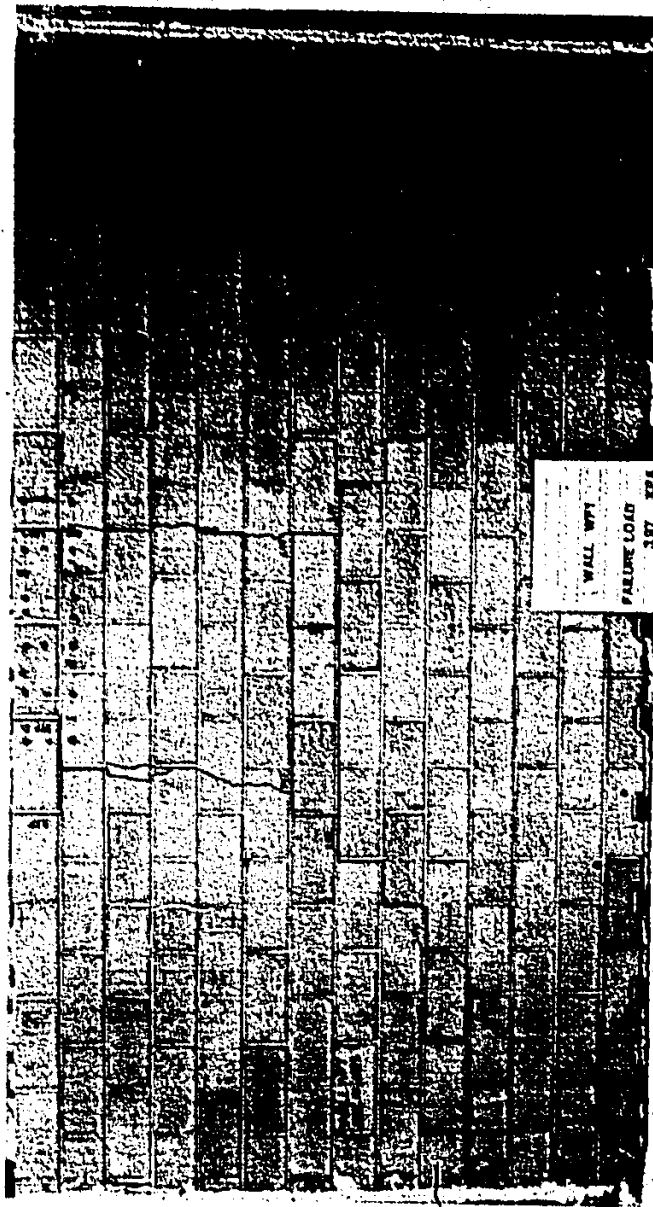
Figure B.3   Crack Pattern for Wall WF-1

Figure B.4   Crack Pattern for Wall WF-2
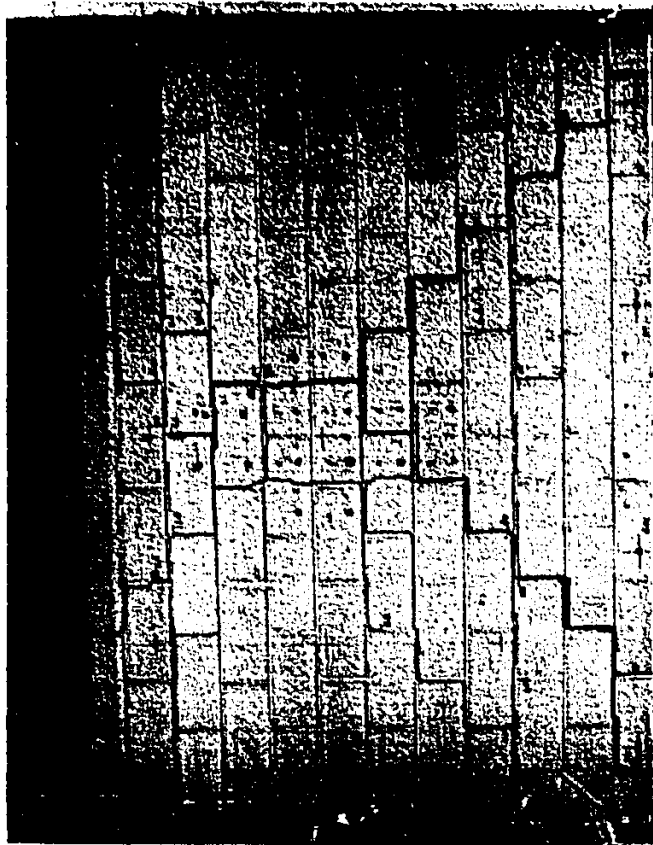
Figure B.5   Crack Pattern for Wall W1-1

WALL W13
FIRST CRACKING
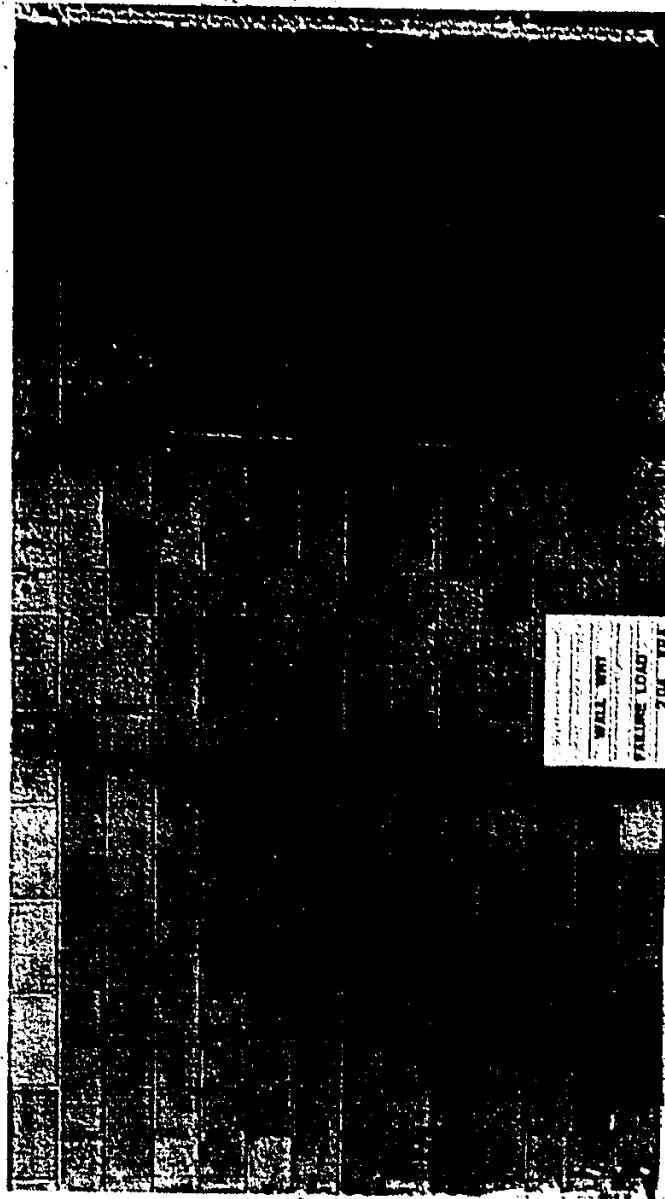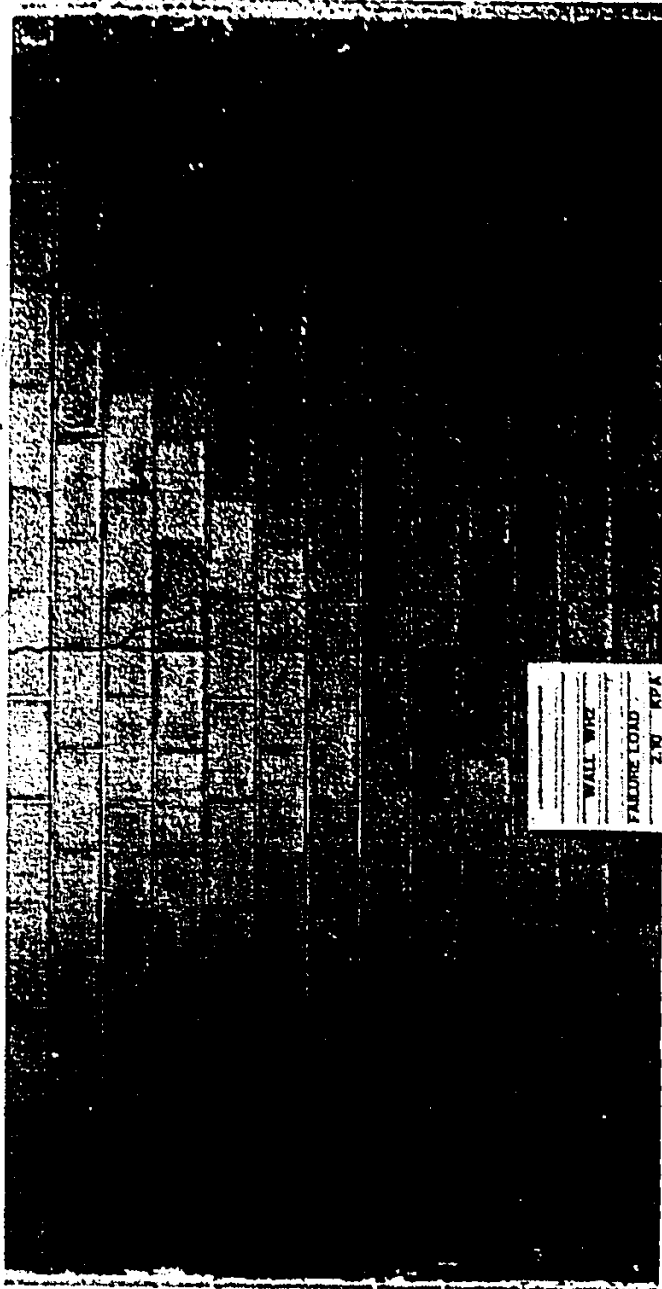LOAD   2.14   KPA
FAILURE LOAD 10.50
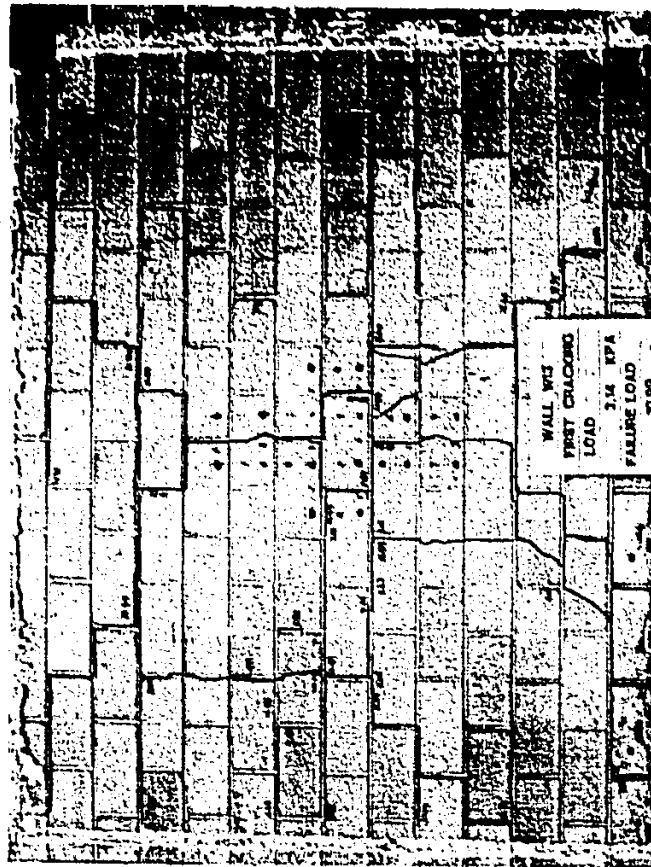
Figure B.6   Crack Pattern for Wall W1-3

Figure B.7   Crack Pattern for Wall WII-1
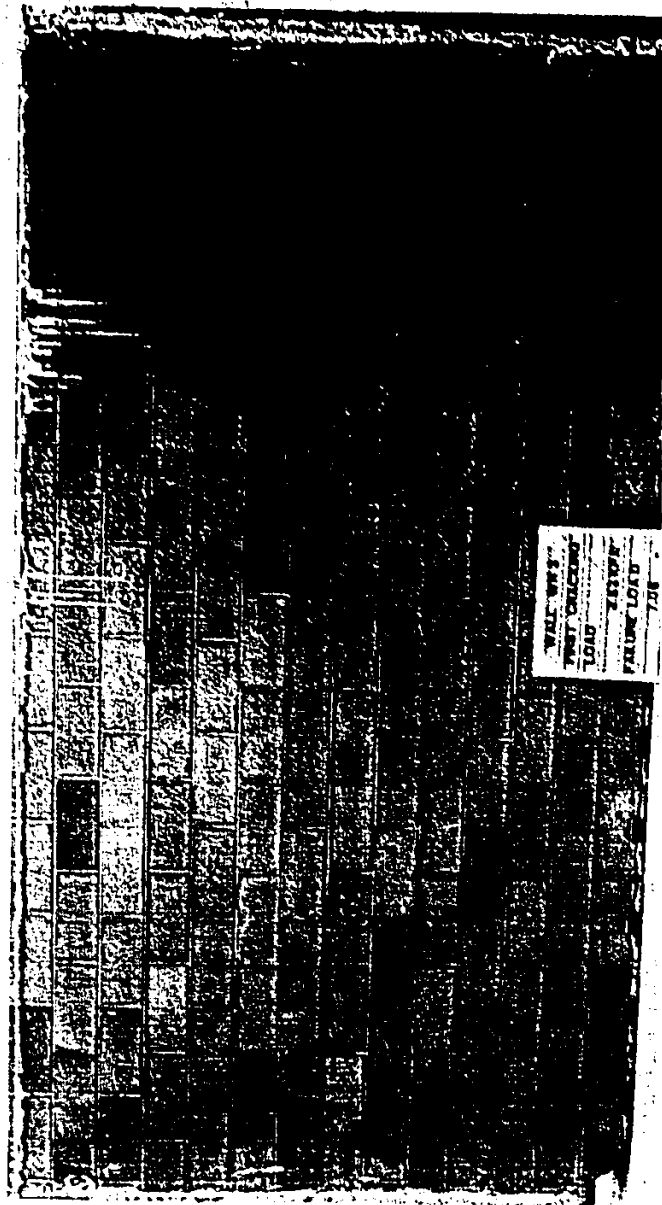
Figure B.8   Crack Pattern for Wall WII-3

371
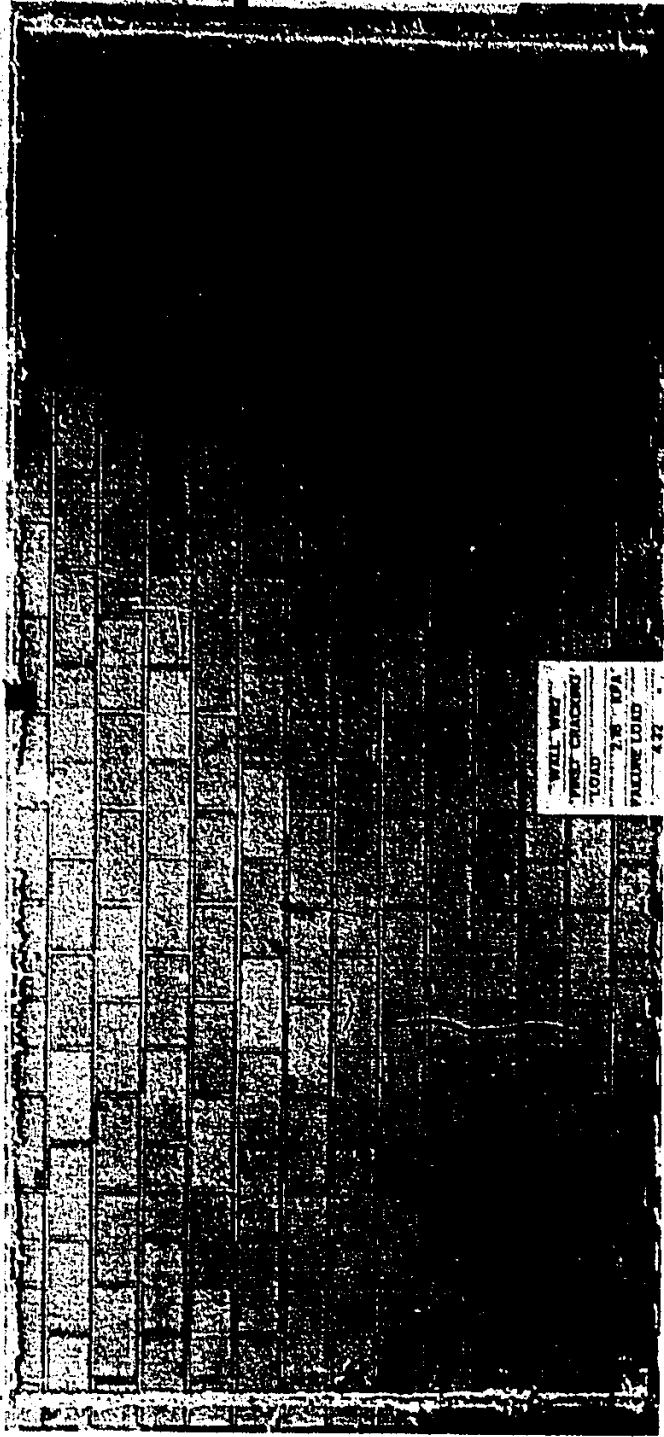
Figure B.9   Crack Pattern for Wall WI11-2

WALL WC1
FAILURE LOAD
721 kPa
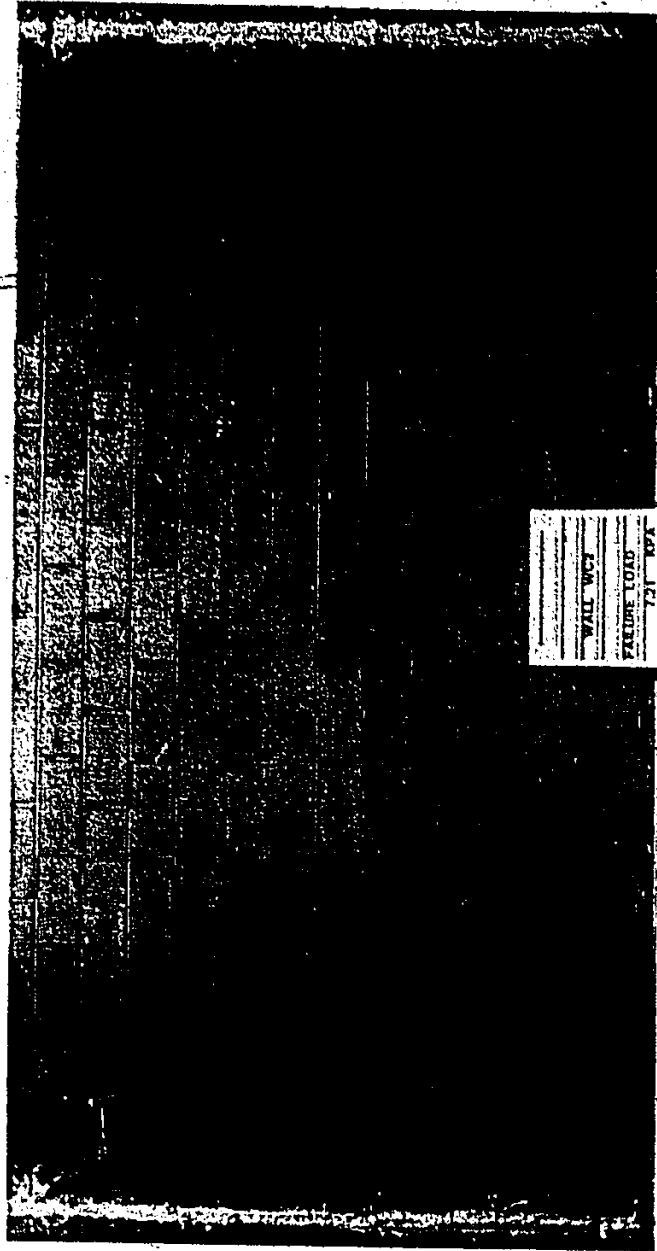
Figure B.10   Crack Pattern for Wall WC-2
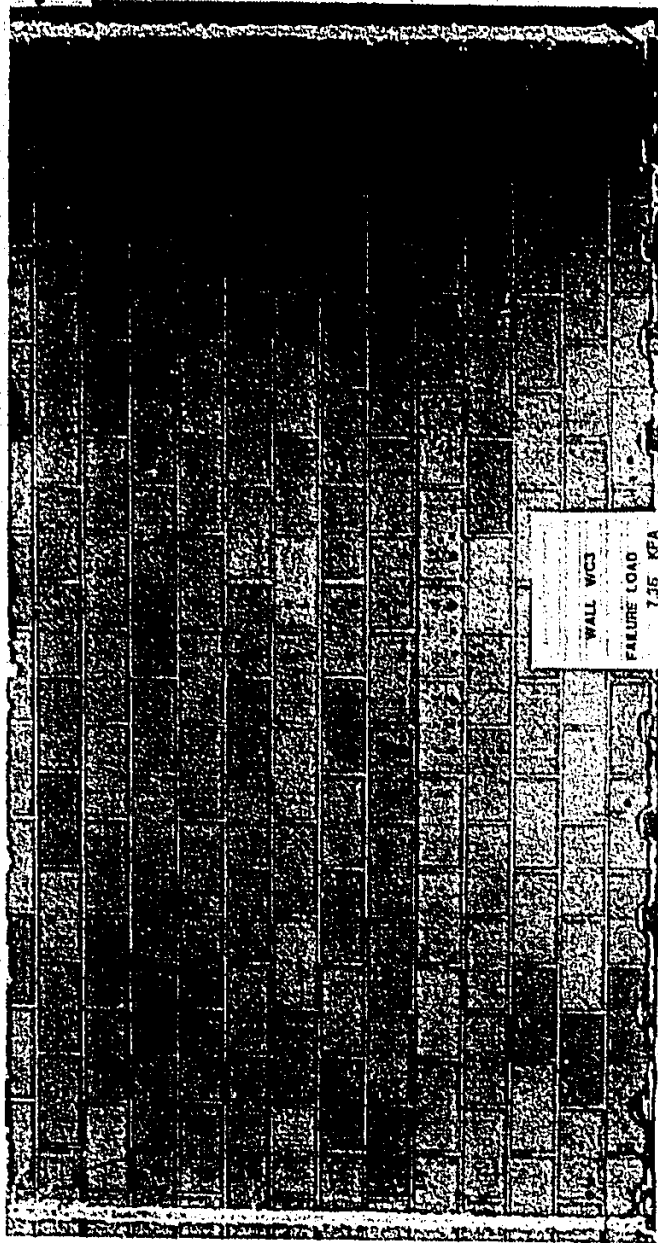
Figure B.11   Crack Pattern for Wall WC-3

WALL	WP-1
FIRST CRACKING LOAD	5.59 KPA
FAILURE LOAD	9.42
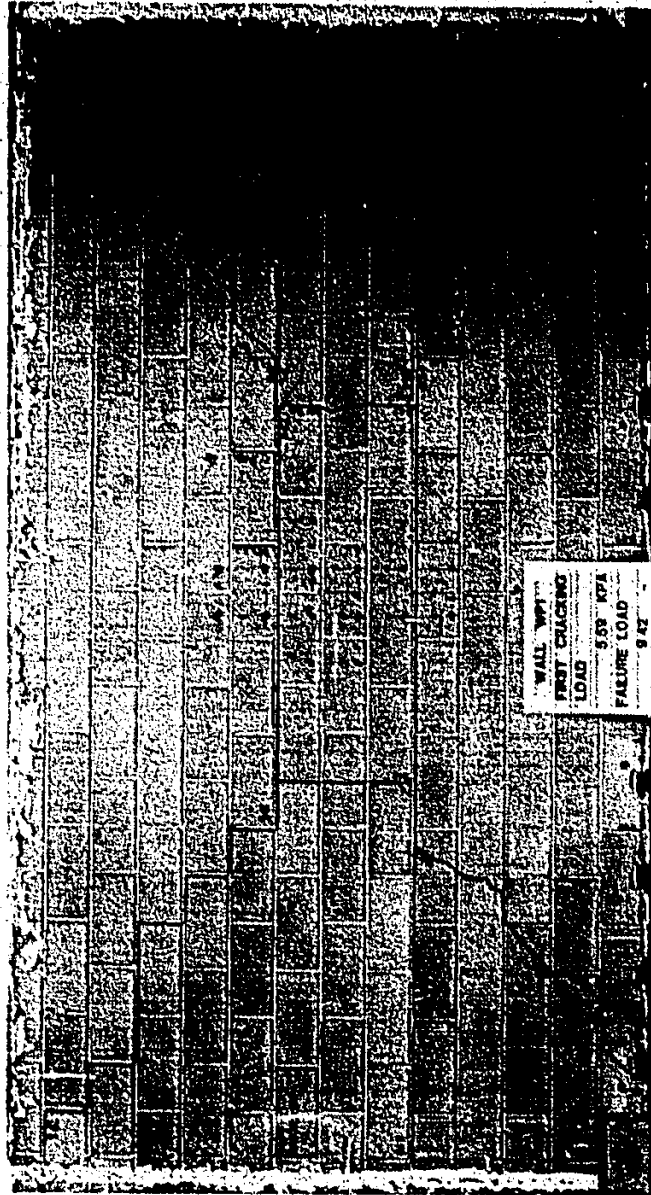
Figure B.12   Crack Pattern for Wall WP-1

WALL WP3	
FIRST CRACKING	
LOAD	44.1 KIP
FAILURE LOAD	
	82.4
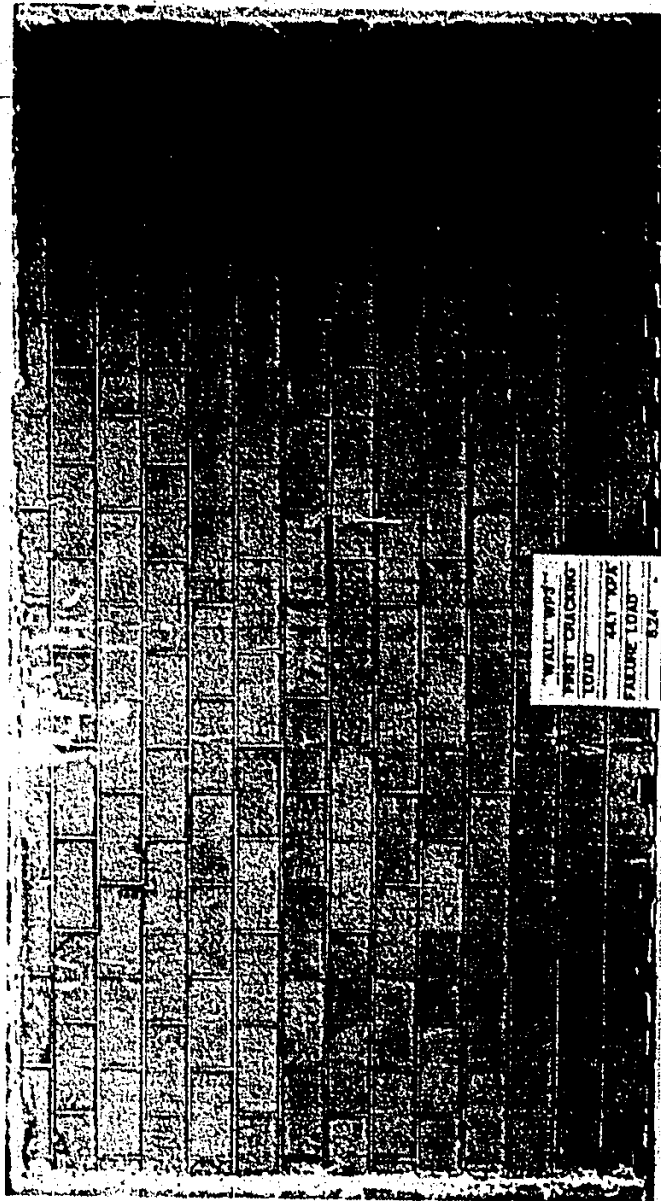
Figure B.13   Crack Pattern for Wall WP-3

APPENDIX C

STRESS DISTRIBUTIONS AND EQUIVALENT ELASTIC CONSTANTS
FOR MASONRY ASSEMBLAGES IN RUNNING BOND

C.1   INTRODUCTION

Masonry assemblages are composite materials of masonry units and mortar joints. Composite action takes place only in mortared face shells of the hollow units and across the wall thickness for solid units. For assemblages manufactured in running bond pattern, the mortar joints and the masonry units act together to give stronger and stiffer assemblage for stresses parallel to the bed joints. The distribution of the stresses within the assemblage even under some uniaxial stress states is not well understood. This stress distribution needs to be understood to justify some assumptions in the derivation of the proposed failure criterion. Moreover, the equivalent elastic constants for the composite masonry material composed of units (or, face shell in hollow units) and mortar joints have to be evaluated. These elastic constants are needed as input data for the finite element model developed in this study.

In this appendix, an approximate analysis for the determination of the stress distributions for some uniaxial stress fields is reported. Also, some expressions for the determination of the equivalent elastic constants are given in terms of the component materials (mortar joints and units) elastic constants and geometries. Finally, a finite element

376

analysis is performed to check the suggested mechanism for load transfer
and the approximate expressions obtained for both the stress
distributions and the elastic constants.

C.2   ELASTIC CONSTANTS FOR THE COMPONENT MATERIALS

C.2.1   Masonry Units

Elastic constants for the material of the masonry units have to
be determined experimentally for the type of units used in the
assemblage. Previous investigations considered concrete block and brick
materials to be isotropic [11,79]. An investigation reported in Chapter
3 and Appendix A of this study showed that the material of the concrete
blocks may be considered isotropic. The results also suggest that the
observed anisotropy in hollow blocks may be due to the geometric
configuration of these blocks.

For an isotropic masonry unit material, only two elastic
constants have to be determined. These are the modulus of elasticity
and the Poisson's ratio. These constants were commonly determined from
tests of masonry units under compressive stresses and were assumed to be
also applicable under tensile stresses. This is due to the brittle
nature of masonry and its constituent materials and the associated
difficulties in measuring deformations under tensile stresses. Examples
of these constants for concrete blocks are reported in Chapter 3 are as
follows:

E_b = 19660 MPa

v_b = 0.3

For clay bricks, Page [79] reported the following values:

$$E_b = 6740 \text{ MPa}$$

$$v_b = 0.167$$

C.2.2 Mortar Joints

The properties of the mortar joints including joint/unit interfaces have been investigated previously for both concrete block [50] and clay brick assemblages [79]. In these investigations, the deformations of the joints were calculated from the measured deformations between centers of the units across the joints and the deformations within the units. Again here, although these constants were evaluated for compression and shear loadings, they will be also considered to be applicable for cases of tension and shear loadings. According to these investigations, examples of the modulus of elasticity of the mortar joints and the shear modulus across the mortar joints were as follows:

For concrete blockwork [50],

$$E_m = 1190 \text{ MPa}$$

$$G_m = 488 \text{ MPa}$$

For clay brickwork [79],

$$E_m = 1400 \text{ MPa}$$

$$G_m = 463 \text{ MPa}$$

It has to be noted that the values mentioned above for the elastic constants of the mortar joints are only examples of reported values as a result of experimental tests performed on assemblages of certain types of units and mortars. These values may be considered as a rough estimates only for cases where no experimental data is available.

However, since similar concrete blocks and the same mortar composition as those reported above for blockwork [50] were used in this investigation, the above mentioned elastic constants for mortar joints were considered to be applicable for this study.

C.3 STRESS DISTRIBUTIONS AND EQUIVALENT ELASTIC CONSTANTS FOR ASSEMBLAGES

The equivalent masonry material composed of solid units or face shells of hollow units and mortar joints may be considered to be orthotropic material because of the uneven distribution of the mortar joints in the plane of the assemblage. Therefore, six equivalent elastic constants need to be evaluated. These include two modulii of elasticity in the two principal material directions, three shear modulii and Poisson's ratio. These equivalent elastic constants and the stress distributions under some loading conditions are discussd and determined in this section as a function of the component material characteristics and geometries. The obtained expressions were based on summing the unit and joint deformations. This procedure has been utilized before by Hamid [50] and Page [79] to calculate the deformation characteristics of the mortar joints.

C.3.1 Modulus of Elasticity Normal to the Bed Joints, E_n, and Poisson's Ratio, v_{np}

For an element, such as that shown in Figure C.1, subjected to uniform tension normal to the bed joints, σ_n, the total displacement Δ_t may be given by:

$$\Delta_t = \Delta_b + \Delta_m \tag{C.1}$$

Where, Δ_b and Δ_m are the total displacements occurring in the units and mortar joints, respectively. Substituting the appropriate modulus of elasticity and height in this expression for the displacements in terms of the stress, Equation C.1 can be rewritten as :

$$\frac{\sigma_n}{E_n} h_t = \frac{\sigma_n}{E_b} \frac{t_m}{t_b} h_b + \frac{\sigma_n}{E_m} h_m \tag{C.2}$$

Where,

E_b; E_m; and E_n are the modulii of elasticity for masonry units; mortar joints; and equivalent masonry material, respectively,

h_b; h_m; and h_t are the unit height; joint thickness; and total height, respectively and

t_b and t_m are the average unit and joint thicknesses perpendicular to the plane of the assemblage shown in Figure C.1. These thicknesses are usually the same except for variable face shell thickness in hollow concrete blockwork. For this case, an analysis performed to evaluate the total deformations in the face shells by integration over masonry unit height showed that an equivalent constant thickness, to give the same cross sectional area, may be used as given in the above expression.

Equation C.2 can be rearranged as:

$$E_n = \frac{1}{\dfrac{h_b}{h_t} \dfrac{t_m}{t_b} + \dfrac{E_b}{E_m} \dfrac{h_m}{h_t}} E_b \tag{C.3}$$
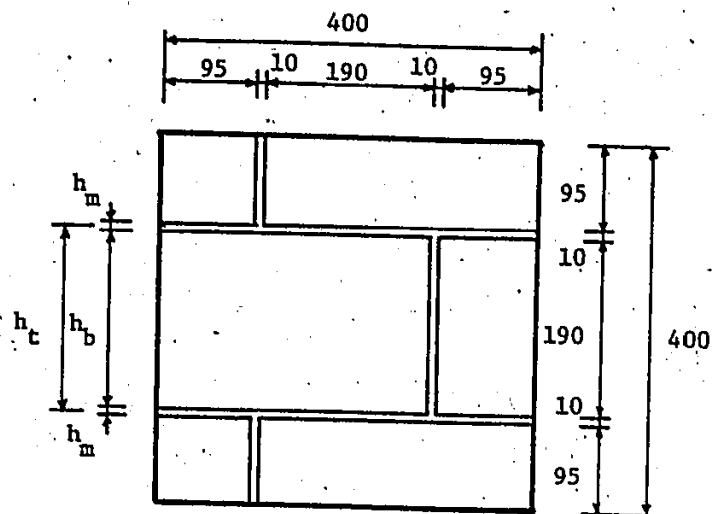
Figure C.1.   Masonry Assemblage Element

This is the expression for the equivalent modulus of elasticity normal to the bed joints for masonry material in terms of the unit and joint elastic and geometric characteristics.

For the component materials used in this investigation, considering the dimensions shown in Figure C.1 and the data given in the previous section, the equivalent modulus of elasticity normal to the bed joints is given by:

$$E_n = 0.59 \, E_b = 11600 \text{ MPa}$$

The lateral deformations (parallel to the bed joints) are not only due to the Poisson's ratio effect but also due to the confining forces at bed joint levels to satisfy the compatibility of the deformations of relatively rigid masonry units and comparably flexible mortar joints [50]. Therefore, the Poisson's ratio, v_{np}, cannot easily be evaluated by a similar approximate analysis and instead it will be estimated from the results of the finite element analysis reported later in this appendix.

C.3.2 Stress Distribution and Modulus of Elasticity
Parallel to the Bed Joints, E_p

For a masonry assemblage loaded in uniform tension parallel to the bed joints, the staggered distribution of the head joints in a running bond pattern affects the stress distribution along this direction parallel to the bed joints. It is thought that, due to the flexibility of the mortar joints relative to the units, shear stresses exist on the bed joints as shown in Figure C.2(a). These shear stresses result in more tensile stresses in the units to increase their

(a) Deformations of Isolated Components

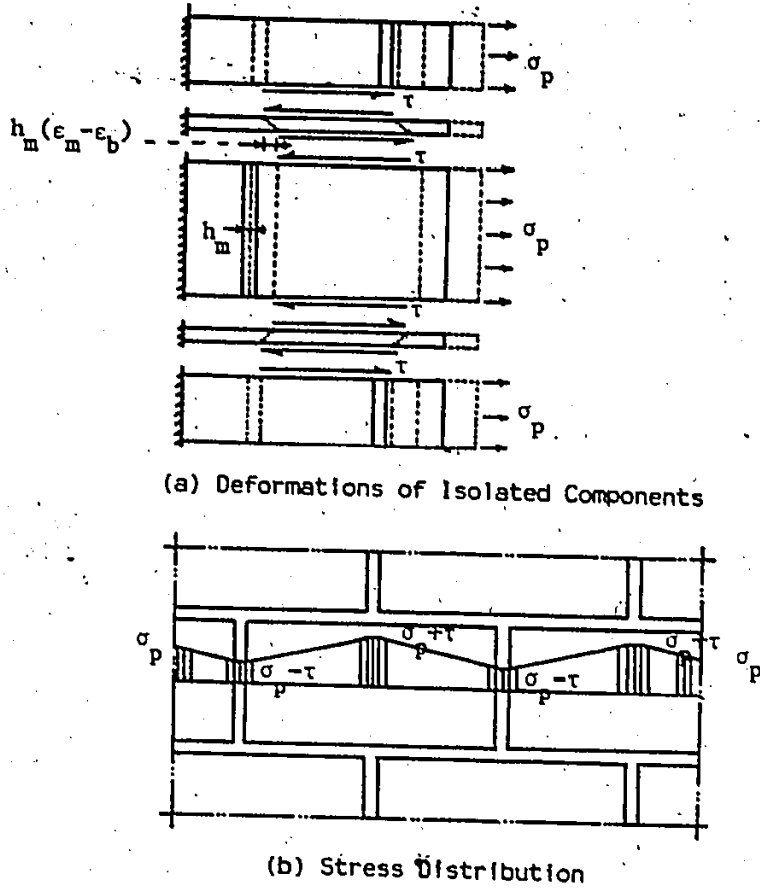(b) Stress Distribution

Figure C.2   Masonry Assemblage Under Tension Parallel to
the Bed Joints
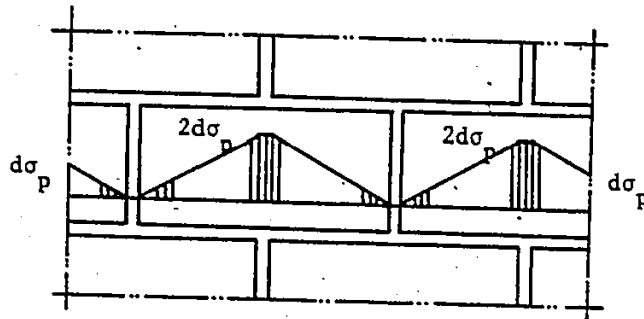
Figure C.3   Uneven Stress Distribution for Loading Beyond
the Head Joint Strength Limit

deformations and compressive stresses (less tension) in the head joints to decrease their deformations in order to attain compatibility of unit and joint deformations as shown in Figure C.2(a). Assuming uniform shear stresses along the bed joints, the resulting uneven tensile stress distribution is shown schematically in Figure C.2(b).

According to Figure C.2(a), the shear stresses on the bed joints may be determined as follows:

$$\tau = G_m \, \gamma_m = G_m \, \frac{(\epsilon_m - \epsilon_b) \, h_m}{h_m} \qquad (C.4)$$

Where,

τ is the uniform shear stress on the mortar bed joints,

G_m is the shear modulus of the mortar bed joints,

γ_m is the shear strain in the mortar bed joints and

ϵ_m and ϵ_b are the longitudinal tensile strains in the mortar head joints and the units, respectively.

Substituting for tensile strains in Equation C.4 in terms of stresses and elastic modulii, this equation can be rewritten as:

$$\tau = G_m \left(\frac{\sigma_p - \tau}{E_m} - \frac{\sigma_p + \tau}{E_b} \right) \qquad (C.5)$$

or,

$$\tau = \sigma_p \left(\frac{\dfrac{G_m}{E_m} - \dfrac{G_m}{E_b}}{1 + \dfrac{G_m}{E_m} + \dfrac{G_m}{E_b}} \right) \qquad (C.6)$$

In this expression, the shear stress in bed joints is determined as a function of the tensile stress parallel to the bed joints and the elastic properties of both mortar joints and masonry units. Accordingly, the uneven stress distribution shown in Figure C.2(b) can be described by a reduced tension at head joints of

$$\sigma_p - \tau = \sigma_p \left(\frac{1 + 2\dfrac{G_m}{E_b}}{1 + \dfrac{G_m}{E_m} + \dfrac{G_m}{E_b}} \right) \qquad \text{(C.7)}$$

and an increased tension at the centers of masonry units of

$$\sigma_p + \tau = \sigma_p \left(\frac{1 + 2\dfrac{G_m}{E_m}}{1 + \dfrac{G_m}{E_m} + \dfrac{G_m}{E_b}} \right) \qquad \text{(C.8)}$$

It should be noted that the average stress across the assemblage remains as the applied uniform tension σ_p. For the component materials used in this investigation, Equation C.6 yields a shear in bed joints of $0.27 \cdot \sigma_p$. This results in a tensile stress in head joints of $0.73 \sigma_p$ and maximum stress in concrete blocks of $1.27 \sigma_p$.

The equivalent modulus of elasticity parallel to the bed joints also can be determined by superposition of the deformations and by using the equivalent constant masonry unit thickness (for the same cross sectional area) where variable face shell thickness is present.

or $\quad \Delta_t = \Delta_b + \Delta_m$

$$\frac{\sigma_p}{E_p} \frac{l_t}{t_m} = \frac{\sigma_p}{E_b} \frac{l_b}{t_b} + \frac{(\sigma_p - \tau)}{E_m} \frac{h_m}{t_m} \qquad (C.9)$$

Where, l_t and l_b are the assemblage and masonry unit lengths respectively. Substituting for $(\sigma_p - \tau)$ from Equation C.7, Equation C.9 can be rearranged as follows:

$$E_p = \left(\frac{1}{\dfrac{l_b}{l_t} \dfrac{t_m}{t_b} + \dfrac{h_m}{l_t} \dfrac{E_b}{E_m} \dfrac{1 + 2\dfrac{G_m}{E_b}}{1 + \dfrac{G_m}{E_m} + \dfrac{G_m}{E_b}}} \right) E_b \qquad (C.10)$$

This is the expression for the equivalent modulus of elasticity parallel to the bed joints in terms of the geometric and elastic properties of the mortar joints and the masonry units.

For the component materials used in this investigation, using the previously mentioned geometric and elastic data, the equivalent modulus of elasticity parallel to the bed joints is

$$E_p = 0.84 \, E_b = 16510 \text{ MPa}$$

This yields a degree of orthotropy of

$$\frac{E_p}{E_n} = 1.42$$

Experimental results for walls or wallettes in horizontal bending in this investigation and others [44,70] indicated sudden

changes in stiffness. These stiffness changes were observed at tensile stresses parallel to the bed joints close to the tensile strengths of the head joints. Therefore, it is thought that the mortar joints and specifically the head joints have nonlinear stress strain properties near the failure stress. Some supporting evidence for this assumption can be found in reported nonlinear behaviour of mortar joints [30,50,79]. Also, it is thought that for a crack in a head joint to open, it would necessitate more deformations to take place in bed joints and/or the masonry units. Therefore, it is assumed that after the head joint strength has been reached, the head joints will behave in a plastic fashion with zero stiffness up to failure. Failure is assumed to occur either when the bed joints reach their shear capacity and the assemblage fails by debonding along both bed and head joints or when the units reach their tensile strength which results in splitting failure through units and head joints.

As mentioned earlier in Chapter 5, the plastic behaviour in the head joints was limited to cases where the assemblage flexural tensile strength parallel to the bed joints is less than 5 times the tensile strength of the head joints. For cases of assemblage flexural tensile strength exceeding this limit, plastic behaviour is no longer applicable and it is assumed that premature cracking will develop in the head joints before failure. However, most available data for masonry units and mortars indicated assemblage flexural tensile strength to head joint strength ratios less than 5.

For the load increments above that corresponding to the head

Joint strength, the uneven stress distribution can be obtained by introducing E_m equal to zero in Equation C.5. This yields an incremental bed joint shear stress of the same magnitude as the increment of applied tensile stress ($d\tau = d\sigma_p$) as shown in Figure C.3.

The equivalent constant of proportionality between stress and strain increments after the head joint strength limit has been reached may be considered as a reduced modulus of elasticity. This reduced modulus, E'_p, may be also determined by superposition of the incremental deformations. The longitudinal deformations parallel to the bed joints may be considered to consist of the tensile deformations of the masonry units and the shear deformations of the bed joints. Accordingly, the equivalent reduced modulus of elasticity may be obtained as follows:

$$\Delta_t = \Delta_b + (\Delta_m)_b \qquad (C.11)$$

Where the subscript b on the parenthesis refers to the bed joints. Or,

$$\frac{\sigma_p}{E'_p} \frac{l_t}{t_m} = \frac{\sigma_p}{E_b} \frac{l_b}{t_b} + \frac{\sigma_p}{G_m} \frac{h_m}{t_m} \qquad (C.12)$$

Which can be rearranged as:

$$E'_p = (\frac{1}{\frac{l_b}{l_t} \frac{t_m}{t_b} + \frac{h_m}{l_t} \frac{E_b}{G_m}}) E_b \qquad (C.13)$$

This is the expression for the reduced elastic constant in terms of the geometric and elastic characteristics of the component materials. Substituting the data for the masonry units and mortar joints for this

investigation, yields the following:

$$E'_p = 0.527 \ E_b \quad \text{and}$$

$$\frac{E'_p}{E_p} = 0.627$$

C.3.3   In-Plane Shear Modulus and Stress Distribution

The in-plane shear modulus for the equivalent masonry material may be determined from the analysis of an assemblage subjected to pure shear stress as shown in Figure C.4(a). However, due to the complicated nature of the problem and to be able to obtain simple expressions for hand calculations, a simple approximate procedure is suggested. In this procedure, the stress distribution and the deformations will be evaluated from separate analyses for shear stresses parallel and normal to the bed joints. Then, an average of the equivalent shear modulus will be obtained. It should be noted that these analyses are not proper but rather are approximate analyses because using individual shear stresses does not satisfy equilibrium and equilibrium is only satisfied where both the shear stresses normal and parallel to the bed joints act.

This procedure is performed as follows:

(1) Due to only the shear parallel to the bed joints as shown in Figure C.4(b), the compatibility of the total displacement yields:

$$\Delta_t = \Delta_b + \Delta_m \ \text{,or}$$

$$\gamma_t h_t = \gamma_b h_b + \gamma_m h_m \tag{C.14}$$

Where, γ_b, γ_m and γ_t are the masonry unit, mortar joint and total
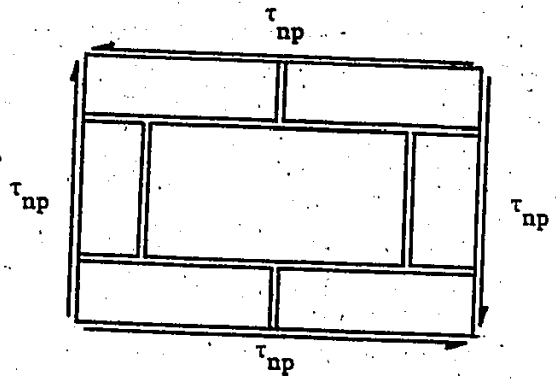
(a) Masonry Assemblage Under In-Plane Pure Shear
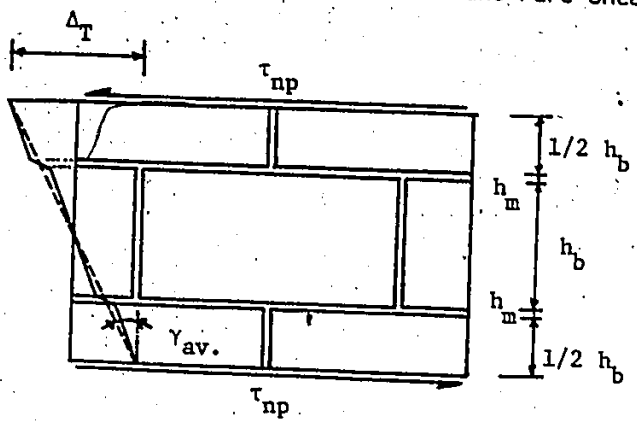
(b) Deformations Under Shear Parallel to the Bed Joints

(c) Deformations and Stress Distributions
Under Shear Normal to the Bed Joints

Figure C.4   Masonry Assemblage Under In-Plane Shear

shear strains, respectively. Equation C.14 can be rewritten in terms of the stresses and the elastic modulii as follows:

$$\frac{\tau_{np}}{(G_{np})_1} \frac{h_t}{t_m} = \frac{\tau_{np}}{G_b} \frac{h_b}{t_b} + \frac{\tau_{np}}{G_m} \frac{h_m}{t_m} \qquad (C.15)$$

Where,

G_b and G_m are the shear modulii of the masonry units and the mortar joints, respectively.
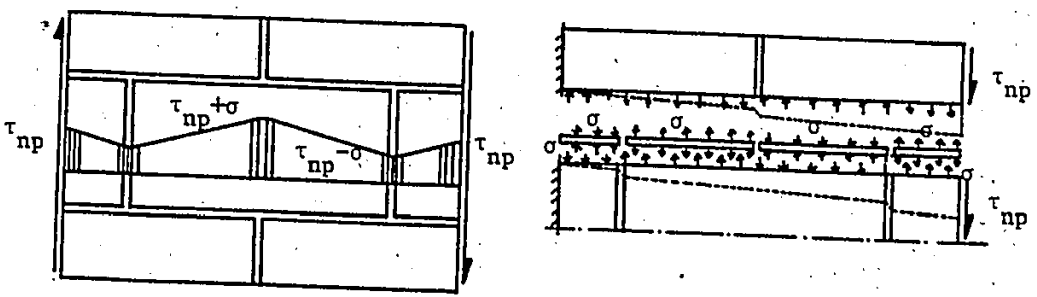
τ_{np} is the acting shear stress on the assemblage and

$(G_{np})_1$ is the apparent equivalent shear modulus as determined from Equation C.15 which is given by:

$$(G_{np})_1 = (\frac{1}{\dfrac{h_b}{h_t} \dfrac{t_m}{t_b} + \dfrac{G_b}{G_m} \dfrac{h_m}{h_t}}) G_b \qquad (C.16)$$

(ii) Due to only the shear normal to the bed joints, the expected uneven shear stress distribution isshowninFigure C.4(c). This stress distributionissuggestedon a similar basis as that for tension parallel to the bed joints. The normal stress, σ, on the bed joints due to the relative shear deformations at head joint locations is given by:

$$\sigma = E_m (\frac{\tau_{np} - \sigma}{G_m} - \frac{\tau_{np} + \sigma}{G_b}) \qquad (C.17)$$

This yields an expression for the normal stress, σ, as follows:

$$\sigma = \left(\frac{\dfrac{E_m}{G_m} - \dfrac{E_m}{G_b}}{1 + \dfrac{E_m}{G_m} + \dfrac{E_m}{G_b}} \right) \tau_{np} \tag{C.18}$$

Accordingly, the head joints are subjected to a reduced shear stress of

$$\tau_{np} - \sigma = \left(\frac{1 + 2\dfrac{E_m}{G_b}}{1 + \dfrac{E_m}{G_m} + \dfrac{E_m}{G_b}} \right) \tau_{np} \tag{C.19}$$

whereas the masonry units are subjected to a maximum shear stress of

$$\tau_{np} + \sigma = \left(\frac{1 + 2\dfrac{E_m}{G_m}}{1 + \dfrac{E_m}{G_m} + \dfrac{E_m}{G_b}} \right) \tau_{np} \tag{C.20}$$

Again, the average shear stress on the assemblage along either horizontal or vertical line across the assemblage is still the applied stress, τ_{np}. This is clearly indicated in the shear stress distributions shown in Figure C.4(c).

For the component materials used in this investigation, Equation C.18 yields a normal stress on the bed joints of $0.63 \tau_{np}$. This results in a shear stress on the head joints of $0.37 \tau_{np}$ and a

maximum shear stress on the units of $1.63 \, \tau_{np}$.

The equivalent shear modulus in this case, $(G_{np})_2$, also can be determined from the superposition of the deformations as follows:

$\Delta_t = \Delta_b + \Delta_m$, or

$$\frac{\tau_{np}}{(G_{np})_2} \frac{l_t}{t_m} = \frac{\tau_{np}}{G_b} \frac{l_b}{t_b} + \frac{(\tau_{np} - \sigma)}{G_m} \frac{h_m}{t_m} \qquad (C.21)$$

Which yields the following expression for the apparent shear modulus $(G_{np})_2$:

$$(G_{np})_2 = \frac{1}{\dfrac{l_b}{l_t} \dfrac{t_m}{t_b} + \dfrac{h_m}{l_t} \dfrac{G_b}{G_m} \dfrac{1 + 2 \dfrac{E_m}{G_b}}{1 + \dfrac{E_m}{G_m} + \dfrac{E_m}{G_b}}} \cdot G_b \qquad (C.22)$$

Then, it is assumed that due to both shears parallel and normal to the bed joints, the shear modulus may be approximately considered as the average of the two expressions in Equations C.16 and C.22. This results in the following expression for G_{np}:

$$G_{np} = \frac{1}{2} [(G_{np})_1 + (G_{np})_2]$$

from which

$$G_{np} = \frac{1}{2} \left[\cfrac{1}{\cfrac{h_b}{h_t} \cdot \cfrac{t_m}{t_b} + \cfrac{G_b}{G_m} \cdot \cfrac{h_m}{h_t}} \right.$$

$$\left. + \cfrac{1}{\cfrac{l_b}{l_t} \cdot \cfrac{t_m}{t_b} + \cfrac{h_m}{l_t} \cdot \cfrac{G_b}{G_m} \cdot \cfrac{1 + 2\cfrac{E_m}{G_b}}{1 + \cfrac{E_m}{G_m} + \cfrac{E_m}{G_b}}} \right] G_b \qquad (C.23)$$

This is the expression for the equivalent in-plane shear modulus in terms of the geometric and elastic properties of the masonry units and the mortar joints. The properties of the component materials used in this investigation yields a shear modulus of

$$G_{np} = \frac{1}{2} [0.61 + 0.97] G_b = 0.79 G_b = 5959 \text{ MPa}$$

After the head joints reach their shear capacity, both the stress distribution and the equivalent shear modulus change similar to the case for tension parallel to the bed joints. Assuming that nonlinear (plastic) deformations will take place in the head joints with zero stiffness, $G_m = 0$, Equation C.18 yields a normal stress on the bed joints of τ_{np}. This results in a zero shear stress increment at the head joints and a triangular stress distribution on the masonry unit similar to the case for tension parallel to the bed joints. The equivalent reduced shear modulus in this case is determined from the masonry unit shear deformations and the bed joints deformations due to

normal stresses. This yields the following expression:

$$G'_{np} = \frac{1}{2} \left[\cfrac{1}{\cfrac{h_b}{h_t} \cfrac{t_m}{t_b} + \cfrac{G_b}{G_m} \cfrac{h_m}{h_t}} \right.$$

$$\left. + \cfrac{1}{\cfrac{l_b}{l_t} \cfrac{t_m}{t_b} + \cfrac{h_m}{l_t} \cfrac{G_b}{G_m}} \right] G_b \qquad (C.24)$$

For the component materials used in this study, the previously mentioned data yields the following:

$$G'_{np} = \frac{1}{2} [0.61 + 0.95] G_b = 0.78 \, G_b = 5884 \text{ MPa}$$

and $\dfrac{G'_{np}}{G_{np}} = 0.99$

This means that, for the data for the component materials used in this investigation, even after head joint capacity is reached, the equivalent in-plane shear modulus may be kept the same as before the head joint strength limit without introducing any significant error in the calculations.

C.3.4 Equivalent Out-of-Plane Shear Modulii, G_{nz} and G_{pz}

The equivalent out-of-plane shear modulus for shearing in the plane of the bed joints, G_{nz}, may be considered to be the same as the shear modulus for shear parallel to the bed joints, (G_{np})₁. Accordingly, the expression given in Equation C.16 may be rewritten as:

$$G_{nz} = \cfrac{1}{\cfrac{h_b}{h_t}\cfrac{t_m}{t_b} + \cfrac{G_b}{G_m}\cfrac{h_m}{h_t}} \; G_b \tag{C.25}$$

For the component materials used in this study, Equation C.25 yields a value of

$$G_{nz} = 0.61 \; G_b = 4613 \; MPa$$

The out-of-plane shear modulus for shearing the planes of the head joints, G_{pz}, is not as easy to evaluate as the other constants. Therefore, it is suggested to be considered equal to the in-plane shear modulus, G_{np}. This approximation is thought to be acceptable because it seems to involve similar mechanisms due to the staggered head joint distribution and their influence on stresses within the masonry units.

C.4   FINITE ELEMENT ANALYSIS FOR MASONRY ASSEMBLAGES

Plane stress finite element analyses were performed for a small element of masonry assemblage subjected to uniform tension normal to the bed joints, uniform tension parallel to the bed joints and pure shear. The results of these analyses are used here to verify the suggested mechanisms for stress transfer within the assemblage and to check the approximate expressions given earlier in this appendix. As shown in Figure C.1, the masonry element considered in these analyses was chosen to be the smallest possible element which reasonably represents the masonry assemblage. Two bed joints and two head joints are included in this square element which is also symmetric with respect to the center line parallel to the bed joints. Due to the symmetry of loading about

this center line in the cases of tensile stresses normal or parallel to the bed joints and the antisymmetry in the case of shear stresses, it was possible to analyse only one half of the element shown in Figure C.1 with the appropriate boundary conditions imposed along this center line.

The edges of the assemblage were forced to deform uniformly so that the displacement profile can be considered representative for a part of an assemblage in a large structural element. These uniform deformations provide equal displacement at the nodes along the edges in the cases of tension normal or parallel to the bed joints and constant slopes along the edges in the case of pure shear. These uniform deformations were imposed by including a very rigid plate along the loaded edges which was connected to the assemblage using double nodes with the same degrees of freedom normal to the edge. However, these boundary and edge conditions as well as the assemblage size were thought to affect the results of the analysis close to these edges. Therefore, of the results obtained across the whole assemblage, only the results between the two bed joints and the two head joints will be considered for the comparison with the previous approximate analyses.

The finite element idealization of the upper half of the assemblage element shown in Figure C.5 consists of plane stress rectangular finite elements having bilinear displacement fields. As shown in Figure C.5, masonry units and mortar joints were modelled separately using the material properties given earlier in Section C.2 for concrete blockwork. Also, 32 mm minimum face shell thicknesses were used for mortar joint elements whereas the equivalent 35 mm uniform face shell thicknesses were used for block elements. In all analyses,
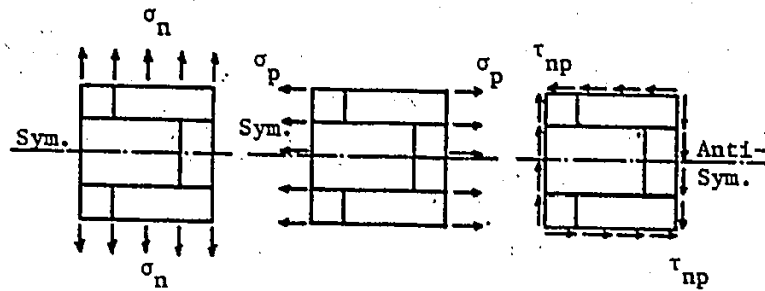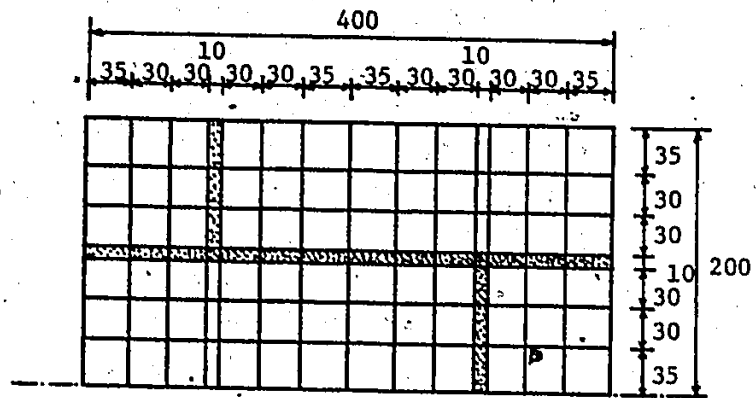
Figure C.5   Finite Element Idealization and Loading Cases
             for Masonry Assemblage

perfect bond was assumed between mortar joints and units. The cases of loading considered in these analyses and which are also shown in Figure C.5 were uniform-tension normal to the bed joints, uniform tension parallel to the bed joints and pure shear. The results of the analyses and discussions for these cases of loading are provided separately below.

C.4.1 Assemblage Subjected to Uniform Tension Normal to the Bed Joints

The assemblage element shown in Figure C.5 was analysed under uniform unit tension normal to the bed joints. The displacements and stresses normal to the bed joint orientation, as obtained from the finite element analysis for this case of loading, are shown in Figure C.6. The uniform displacements along the top edge shown in Figure C.6(b) was imposed to have deformations and stress distributions which are representative of large masonry assemblages. The distribution of tensile stresses normal to the bed joints along the mid height of the center block (Line A-A) is shown in Figure C.6(c). These tensile stresses were reasonably uniform except near the head joint. Also, the low stress values in head joints are attributed to the flexibility of the head joints relative to the face shells of the concrete blocks. This relative flexibility leads to increased stresses in the face shells close to the head joint locations. The distribution of tensile-stresses normal to the bed joints along an axis perpendicular to the bed joints mid way between the two head joints (Line I-I) is shown in Figure C.6(d). This stress distribution is uniform except at the bed joint where the 9% increase is attributed to the use of 9% less thicknesses
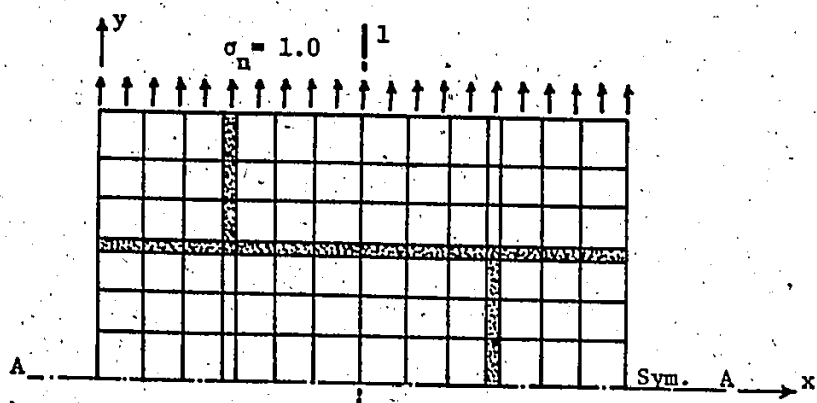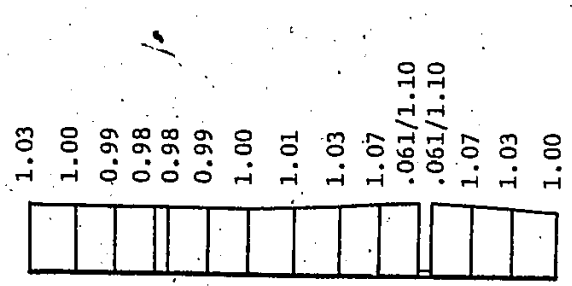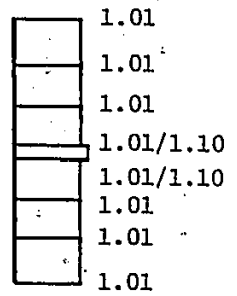
(a) Assemblage Under Unit Tension Normal to the Bed Joints
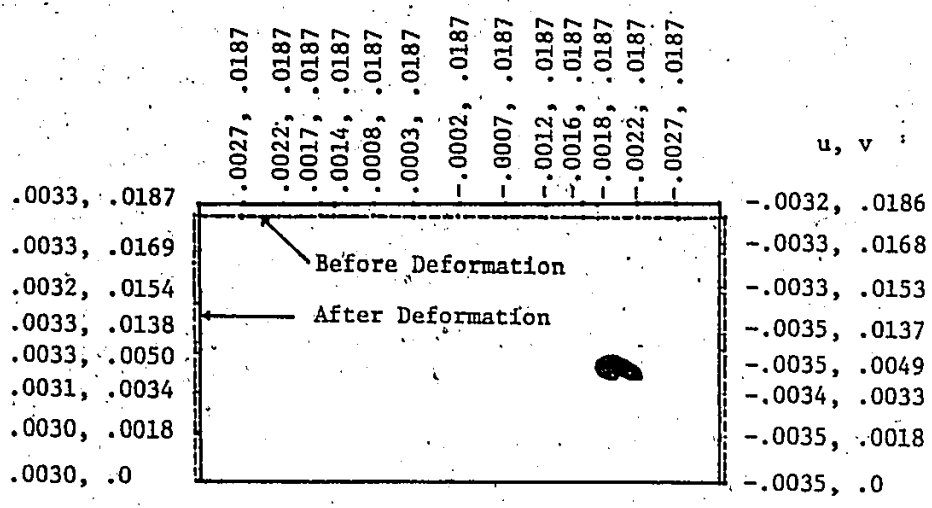
(b) Displacement Values Along Edges

(c) σ_y Along A-A

(d) σ_y Along 1-1

Figure C.6   Displacements and Stresses Under Uniform Tension Normal to the Bed Joints

for the mortar joints (i.e. (35-32)/35).

The equivalent modulus of elasticity normal to the bed joints can be estimated from the predicted displacement at the top edge of the assemblage. This yielded a value of 10700 MPa which is 8% less than the corresponding value estimated using the approximate expression in Equation C.3. The difference between the two values may be attributed to neglecting the head joints in the derivation of the approximate expression for this loading condition. In this regard, the 8% difference is considered to be insignificant compared to the variability of the stiffnesses normal to the bed joints reported earlier in the experimental part of this study. Accordingly, it may be concluded that the equivalent modulus of elasticity normal to the bed joints can be estimated reasonably using the approximate expression in Equation C.3.

The lateral deformations (parallel to the bed joints) of the two vertical edges are shown in Figure C.6(b). These lateral deformations were used to evaluate the Poisson's ratio, ν_{np}, of the equivalent masonry material. Based on the values of the longitudinal deformations (normal to the bed joints) and the average of the lateral deformations (parallel to the bed joints), Poisson's ratio was found to be 0.20. This value was used in the finite element analyses in Chapter 6.
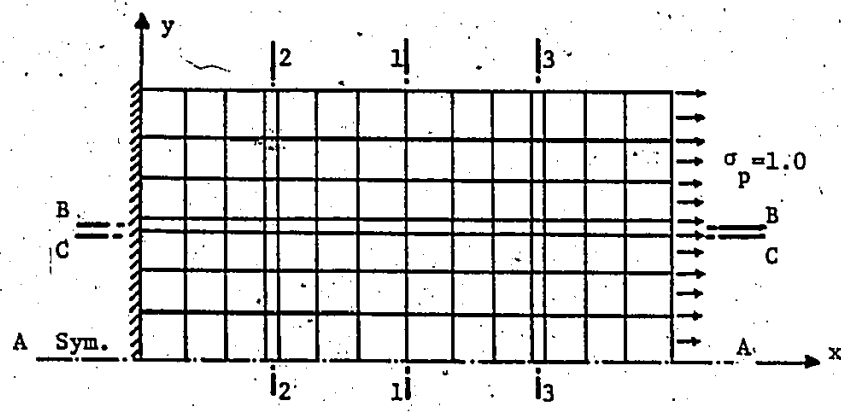
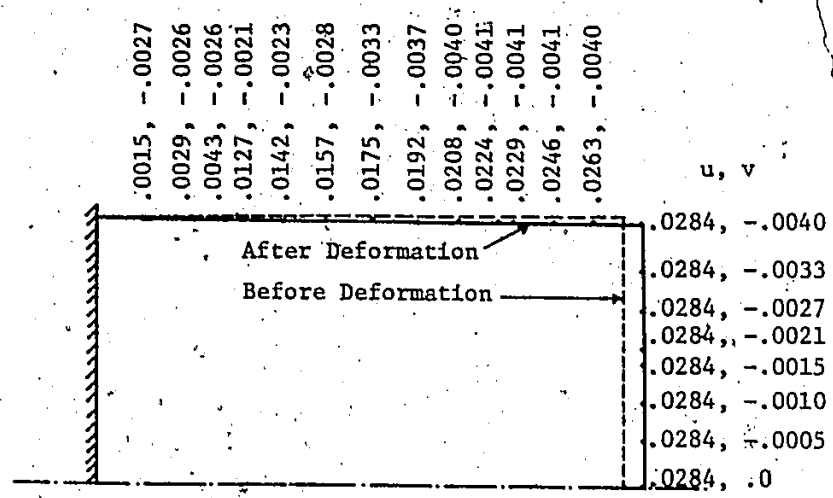## C.4.2 Assemblage Subjected to Uniform Tension Parallel to the Bed Joints

The assemblage element shown in Figure C.5 was analysed under uniform unit tension parallel to the bed joints where, beside the restraints provided along the axis of symmetry (center line parallel to

the bed joints), the nodes of the left vertical side were also restrained from horizontal displacements. The resulting displacements and tensile and shear stress distributions are shown in Figure C.7. Again here, the uniform displacement along the right vertical loaded edge shown in Figure C.7(b) was imposed to yield reasonably representative deformations and stress distributions within the assemblage.

As mentioned earlier, only the part between the two head joints was considered for the comparison with the approximate analysis. This was because of the effects of the boundary and edge conditions on the deformations and stress distributions near the edges. The tensile stress distribution along the center line parallel to the bed joints (Line A-A) is also shown in Figure C.7(b). This distribution was reasonably linear which confirms the linear distribution assumption made in the approximate analysis. However, the predicted stresses showed a variation of ±11% from the average which is significantly less than the ±27% obtained from the approximate expressions in Equations C.7 and C.8. This difference was attributed to the fact that, in the approximate analysis, the tensile capacity of the bed joints was neglected and the shear lag was not considered. This shear lag would result in nonuniform tensile stress distribution across the center block height which is different from the assumption made in the approximate analysis. This can be easily seen in the tensile stress distributions along the vertical lines 1-1, 2-2 and 3-3 shown in Figure C.6(d) where 8%, 25% and -25% differences respectively were predicted between the top edge of the

(a) Assemblage Under Unit Tension Parallel to the Bed Joints

.0015, −.0027
.0029, −.0026
.0043, −.0026
.0127, −.0021
.0142, −.0023
.0157, −.0028
.0175, −.0033
.0192, −.0037
.0208, −.0040
.0224, −.0041
.0229, −.0041
.0246, −.0041
.0263, −.0040

u, v

After Deformation

Before Deformation

.0284, −.0040
.0284, −.0033
.0284, −.0027
.0284, −.0021
.0284, −.0015
.0284, −.0010
.0284, −.0005
.0284, .0

(b) Displacement Values Along Edges

1.18
1.18
1.16
1.14
1.12
1.09
1.06
1.02
0.97
0.94
.91/1.01
.90/1.01
0.90
0.89
0.88
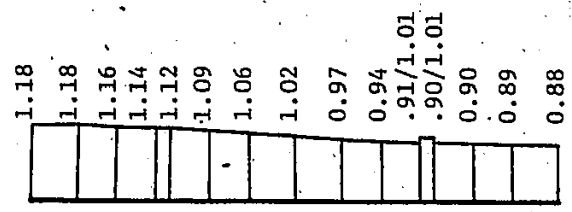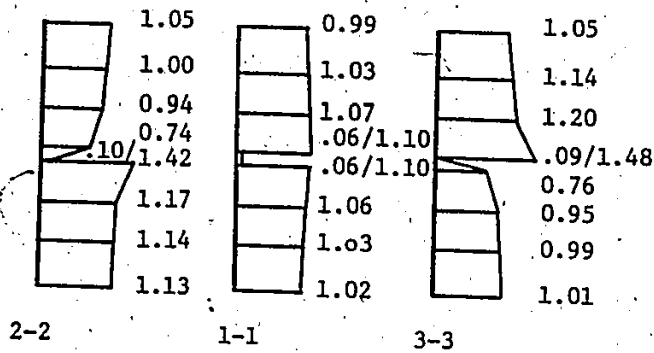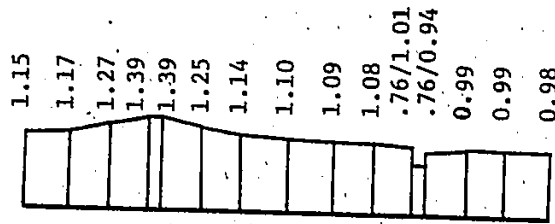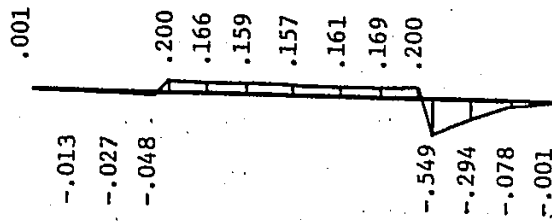
(c) σ_x Along A-A

Figure C.7   Displacements and Stresses Under Uniform Tension Parallel to the Bed Joints

(d) σ_x Along Vertical Lines

(e) σ_x Along C-C

(f) τ_{xy} Along B-B

Figure C.7   Continued

center block and the center line of the assemblage. The effect of the shear lag was also confirmed by investigating the tensile stress distribution along the top of the center block (Line C-C) shown in Figure C.6(e). As can be seen, the variation of the tensile stresses was significantly different from that along Line A-A. The shear stress distribution along the bed joint shown in Figure C.7(f) is nearly uniform between the head joints as was assumed in the approximate analysis. However, the predicted value was only 75% of the shear stress value from Equation C.6.

Finally, the average tensile stress and the average deformation for the central-part between the two head joints was used to calculate the equivalent modulus of elasticity parallel to the bed joints. This was 14400 MPa which is 13% less than was obtained from the approximate analysis in Equation C.10. It is suggested that this is a simple and acceptable approximation given the lack of available data.

C.4.3 Assemblage Subjected to Uniform In-Plane Pure Shear

For this loading condition, the assemblage element shown in Figure C.5 was analysed under uniform tangential unit shear stresses along the four sides. In this analysis, the center line parallel to the bed joints was utilized as an axis of antisymmetry which permitted the analysis of only half of the assemblage element. Moreover, for equilibrium requirements, the left vertical edge of the element was restrained from both horizontal and vertical displacements. The results of this analysis are shown in Figure C.8.

The displacements of the nodes along the element edges are shown

(a) Assemblage Under Unit Shear.

(b) Displacement Profile
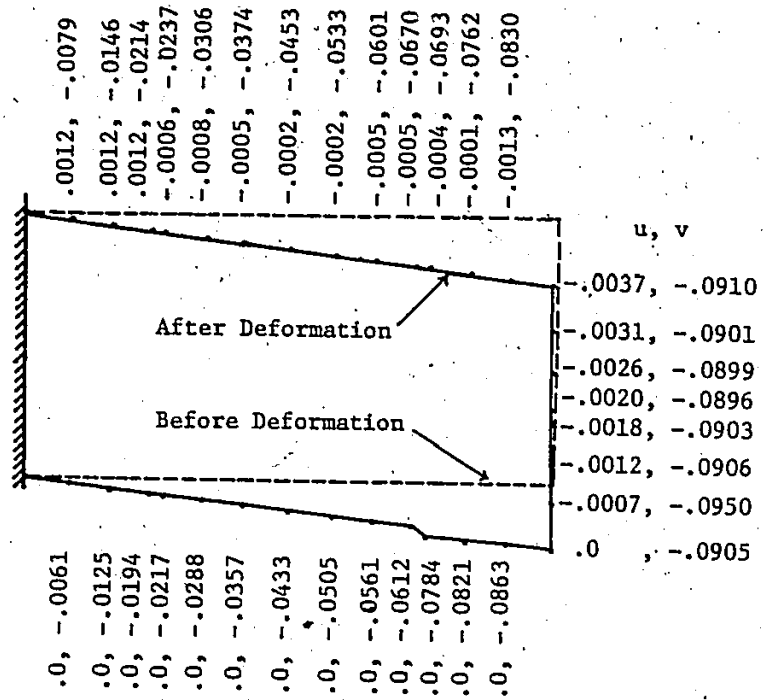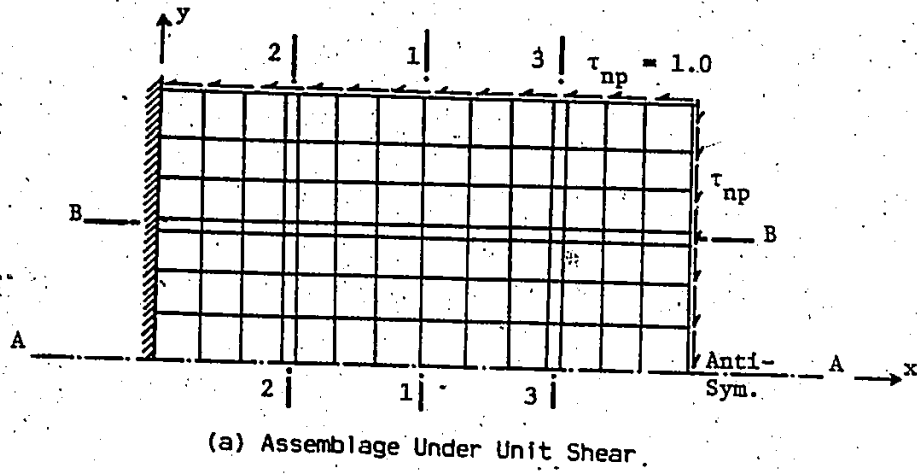
Figure C.8   Displacements and Stresses Under Uniform In-Plane Shear

1.33 1.28 1.35 1.33 1.32 1.22 1.13 1.04 0.95 0.85 .81/.82 .82/.83 0.95 1.03 1.08

(c) τ_{xy} Along A-A

.004 .040 .290 .699 .381 .187 .101

-.023 -.530 -.226 -.134 -.131 -.199 -.321 -.631

(d) σ_y Along B-B

.08   1.02   1.03
.38   0.99   1.14
.44   0.94   1.10
.76   .89/.93   .85/1.35
.79/1.12   .89/.93   1.00
1.07   0.94   0.73
1.27   1.01   0.79
1.34   1.04   0.82

2-2   1-1   3-3
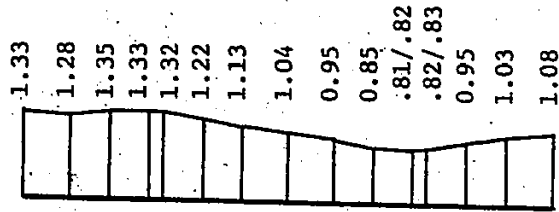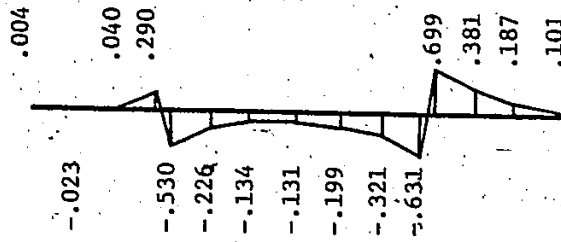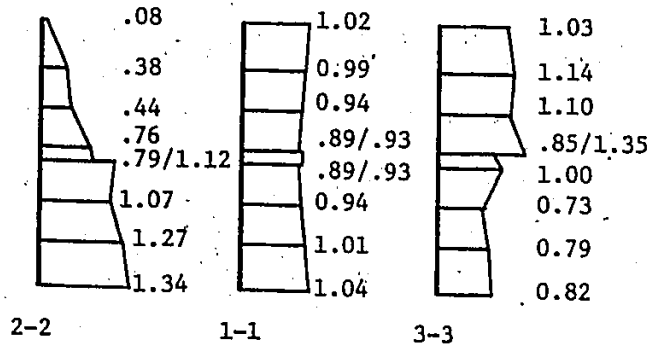
(e) τ_{xy} Along Vertical Lines

Figure C.8   Continued

in Figure C.8(b). The uniform shear distortion shown in this figure along the top and the right vertical edges was imposed to represent the large assemblage case. However, the change in slope along the center line parallel to the bed joints (Line A-A) was due to the presence of the relatively flexible head joint.

The shear stress distribution along the center line parallel to the bed joints (Line A-A) is shown in Figure C.8(c). The part between the two head joints was reasonably linear which confirms the assumption made earlier in the approximate analysis. However, the ±28% variations of the shear stresses is significantly less than the ±63% variations predicted using Equations C.19 and C.20. This difference may be also attributed to the fact that, in the approximate analysis, the bed joint was ignored in the case of shear normal to the bed joints and the shear lag effect was not considered. This shear lag is also thought to be the reason for the nonuniform normal stress distribution between the head joints along the bed joint (Line B-B) shown in Figure C.8(d). This is different from the assumed uniform normal stress distribution in the approximate analysis. Moreover, the shear stress distributions along vertical lines at the two head joints (Lines 2-2 and 3-3) and mid way between the joints (Line 1-1) are also shown in Figure C.8(e). The shear stress distributions along the vertical lines at the two head joints were markedly nonuniform. However, the distribution along the vertical line mid way between the joints (Line 1-1) showed a nearly uniform distribution within a 10% range. It also indicated a sudden increase in the shear stresses at the bed joints due to the use of the 32 mm thickness for the mortar joints compared to the 35 mm thick face

shells.

The in-plane equivalent shear modulus was calculated from these results and was found to be 5270 MPa which is 12% less than the value obtained from the approximate analysis using Equation C.23. Accordingly, it is suggested that this approximate expression may be used as an easy, simple and acceptable predictor.

APPENDIX D

FINITE ELEMENT SHAPE FUNCTIONS

AND

NON-ZERO ELEMENTS OF THE GENERALIZED STRAIN MATRIX

D.1   SHAPE FUNCTIONS FOR THE RECTANGULAR FINITE ELEMENT

(i)   For extension degrees of freedom (u^o, v^o)

$$N_1^o = (1-\xi)(1-\eta)$$

$$N_2^o = \xi(1-\eta)$$

$$N_3^o = \xi\eta$$

$$N_4^o = (1-\xi)\eta$$

(ii)   For transverse shear degrees of freedom (ϕ_x, ϕ_y)

$$N_1^S = -N_1^o \qquad\qquad N_5^S = N_1^o$$

$$N_2^S = -N_2^o \qquad\qquad N_6^S = N_2^o$$

$$N_3^S = -N_3^o \qquad\qquad N_7^S = N_3^o$$

$$N_4^S = -N_4^o \qquad\qquad N_8^S = N_4^o$$

(iii)   For Flexural degrees of freedom (w, $\partial w/\partial x$, $\partial w/\partial y$)

$$N_1 = 1-\xi\eta-(3-2\xi)\xi^2(1-\eta)-(1-\xi)(3-2\eta)\eta^2$$

$$N_2 = -a(1-\xi)^2\xi(1-\eta)$$

$$N_3 = b(1-\xi)\eta(1-\eta)^2$$

$$N_4 = (3-2\xi)\xi^2(1-\eta)+\xi\eta(1-\eta)(1-2\eta)$$

$$N_5 = a(1-\xi)\xi^2(1-\eta)$$

410

$$N_6 = b(1-\eta)^2\xi\eta$$

$$N_7 = (3-2\xi)\xi^2\eta - \xi\eta(1-\eta)(1-2\eta)$$

$$N_8 = a(1-\xi)\xi^2\eta$$

$$N_9 = -b(1-\eta)\xi\eta^2$$

$$N_{10} = (1-\xi)(3-2\eta)\eta^2 + \xi(1-\xi)(1-2\xi)\eta$$

$$N_{11} = -a(1-\xi)^2\xi\eta$$

$$N_{12} = -b(1-\xi)(1-\eta)\eta^2$$

D.2 NON-ZERO ELEMENTS OF THE GENERALIZED STRAIN MATRIX $[\bar{B}]$

$$B(1,1) = -\frac{1}{a}(1-\eta)$$

$$B(1,8) = \frac{1}{a}(1-\eta)$$

$$B(1,15) = \frac{1}{a}\eta$$

$$B(1,22) = -\frac{1}{a}\eta$$

$$B(2,2) = -\frac{1}{b}(1-\xi)$$

$$B(2,9) = -\frac{1}{b}\xi$$

$$B(2,16) = \frac{1}{b}\xi$$

$$B(2,23) = \frac{1}{b}(1-\xi)$$

$$B(3,1) = -\frac{1}{b}(1-\xi)$$

$$B(3,2) = -\frac{1}{a}(1-\eta)$$

$$B(3,8) = -\frac{1}{b}\xi$$

$$B(3,9) = \frac{1}{a}(1-\eta)$$

$$B(3,15) = \frac{1}{b}\xi$$

$$B(3,16) = \frac{1}{a}\eta$$

$$B(3,22) = \frac{1}{b}(1-\xi)$$

$$B(3,23) = -\frac{1}{a}\eta$$

$$B(4,3) = \frac{6}{a^2}(1-2\xi)(1-\eta)$$

$$B(4,4) = -\frac{2}{a}(2-3\xi)(1-\eta)$$

$$B(4,6) = \frac{3}{a}(1-2\xi)(1-\eta)$$

$$B(4,10) = -\frac{6}{a^2}(1-2\xi)(1-\eta)$$

$$B(4,11) = -\frac{2}{a}(1-3\xi)(1-\eta)$$

$$B(4,13) = \frac{3}{a}(1-2\xi)(1-\eta)$$

$$B(4,17) = -\frac{6}{a^2}(1-2\xi)\eta$$

$$B(4,18) = -\frac{2}{a}(1-3\xi)\eta$$

$$B(4,20) = \frac{3}{a}(1-2\xi)\eta$$

$$B(4,24) = \frac{6}{a^2}(1-2\xi)\eta$$

$$B(4,25) = -\frac{2}{a}(2-3\xi)\eta$$

$$B(4,27) = \frac{3}{a}(1-2\xi)\eta$$

$$B(5,3) = \frac{6}{b^2}(1-\xi)(1-2\eta)$$

$$B(5,5) = \frac{2}{b}(1-\xi)(2-3\eta)$$

$$B(5,7) = -\frac{3}{b}(1-\xi)(1-2\eta)$$

$$B(5,10) = \frac{6}{b^2}\xi(1-2\eta)$$

$$B(5,12) = \frac{2}{b}\xi(2-3\eta)$$

$$B(5,14) = -\frac{3}{b}\xi(1-2\eta)$$

$$B(5,17) = -\frac{6}{b^2}\xi(1-2\eta)$$

$$B(5,19) = \frac{2}{b}\xi(1-3\eta)$$

$$B(5,21) = -\frac{3}{b}\xi(1-2\eta)$$

$$B(5,24) = -\frac{6}{b^2}(1-\xi)(1-2\eta)$$

$$B(5,26) = \frac{2}{b}(1-\xi)(1-3\eta)$$

$$B(5,28) = -\frac{3}{b}(1-\xi)(1-2\eta)$$

$$B(6,3) = \frac{2}{ab}[1-6\xi(1-\xi)-6\eta(1-\eta)]$$

$$B(6,4) = -\frac{2}{b}(1-4\xi+3\xi^2)$$

$$B(6,5) = \frac{2}{a}(1-4\eta+3\eta^2)$$

$$B(6,6) = \frac{1}{b}(1-7\xi+6\xi^2)$$

$$B(6,7) = -\frac{1}{a}(1-7\eta+6\eta^2)$$

$$B(6,10) = -\frac{2}{ab}[1-6\xi(1-\xi)-6\eta(1-\eta)]$$

$$B(6,11) = \frac{2}{b} \xi(2-3\xi)$$

$$B(6,12) = -\frac{2}{a} (1-4\eta+3\eta^2)$$

$$B(6,13) = -\frac{1}{b} \xi(5-6\xi)$$

$$B(6,14) = \frac{1}{a} (1-7\eta+6\eta^2)$$

$$B(6,17) = \frac{2}{ab} [1-6\xi(1-\xi)-6\eta(1-\eta)]$$

$$B(6,18) = -\frac{2}{b} \xi(2-3\xi)$$

$$B(6,19) = \frac{2}{a} \eta(2-3\eta)$$

$$B(6,20) = \frac{1}{b} \xi(5-6\xi)$$

$$B(6,21) = -\frac{1}{a} \eta(5-6\eta)$$

$$B(6,24) = -\frac{2}{ab} [1-6\xi(1-\xi)-6\eta(1-\eta)]$$

$$B(6,25) = \frac{2}{b} (1-4\xi+3\xi^2)$$

$$B(6,26) = -\frac{2}{a} \eta(2-3\eta)$$

$$B(6,27) = -\frac{1}{b}(1-7\xi+6\xi^2)$$

$$B(6,28) = \frac{1}{a}\eta(5-6\eta)$$

$$B(7,6) = (1-\xi)(1-\eta)$$

$$B(7,13) = \xi(1-\eta)$$

$$B(7,20) = \xi\eta$$

$$B(7,27) = (1-\xi)\eta$$

$$B(8,7) = -(1-\xi)(1-\eta)$$

$$B(8,14) = -\xi(1-\eta)$$

$$B(8,21) = -\xi\eta$$

$$B(8,28) = -(1-\xi)\eta$$

REFERENCES

1. A.S.T.M., "A82-85 Specification for Steel Wire, Plain, for Concrete Reinforcement", Annual Book of A.S.T.M. Standards, Philadelphia, 1985.

2. A.S.T.M., "C67-85 Methods of Sampling and Testing brick and Structural Clay Tile", Annual Book of A.S.T.M. Standards, Philadelphia, 1985.

3. A.S.T.M., "C109-84 Compressive Strength of Hydraulic Cement Mortars (Using 2-in. or 5.0-mm Cube Specimens", Annual Book of A.S.T.M. Standards, Philadelphia, 1985.

4. A.S.T.M., "C952-76 Test Method for Bond Strength of Mortar to Masonry Units", Annual Book of A.S.T.M. Standards, Philadelphia, 1985.

5. A.S.T.M., "E518-80 Flexural Bond Strength of Masonry", Annual Book of A.S.T.M. Standards, Philadelphia, 1985.

6. ASCE Committee on Concrete and Masonry Structures, "State-of-the-Art Report on Finite Element Analysis of Reinforced Concrete", ASCE Special Publication, 1982.

7. Allen, H.G.,"Analysis and Design of Structural Sandwich Panels", Pergamon Press, Oxford, 1969.

8. American Concrete Institute Committee 531, Building Code Requirements for Concrete Masonry Structures, ACI 531-79, Detroit, MI, 1978.

9. Anderson,C., "Lateral Loading Tests on Concrete Block Walls", the Structural Engineer, Vol. 54, No. 7, July 1976, pp. 239 - 246.

10. Anderson, C., "Tensile Bond Tests with Concrete Blocks", Intern. Journal of Masonry Construc., Vol. 1, No. 4, 1981, pp. 134 - 148.

11. Arya, S.K. and Hegemier, G.A., "Finite Element Method for Interface Problems", Journal of Struc. Div., ASCE, Vol. 108, No. ST2, Feb. 1982, pp. 327 - 342.

12. Baker, L.R., "Flexural Sterngth of Brickwork Panels", Proc. of the 3rd. Intern. Brick Masonry Conf., Essen, W. Germany, April 1973, pp. 378 - 383.

13. Baker, L.R., "Design of Brickwork for Shear Wall and Panel Action", Seminar on Brickwork, Department of Housing and Construc., University of Melbourne, March 1975, pp. 23 - 35.

14. Baker, L.R. and Franken, G.L., "Variability Aspects of the Flexural Strength of Brickwork", Proc. of the 4th. Intern. Brick Masonry Conf., Brugge, April 1976, no. 2b4.

15. Baker, L.R., "The Latral Strength of Brickwork - An Overview", Report CE1, School of Engineering and Architecture, Deakin University, Geelong, Victoria, Australia, 1977, 16 pages.

16. Baker, L.R., "The Failure Criterion of Brickwork in Vertical Flexure", Report CE2, School of Engineering and Architecture, Deakin University, Geelong, Victoria, Australia, 1977, pp. 203 - 216.

17. Baker, L.R., "Precracking Behaviour of Laterally Loaded Brickwork Panels with In-Plane Restraints", Report CE3, School of Engineering and Architecture, Deakin University, Geelong, Victoria, Australia, 1977, pp. 129 - 145.

18. Baker, L.R., "A Failure Criterion for Brickwork in Bi-Axial Bending", Proc. of 5th. Intern. Brick Masonry Conf., Washington D.C., October 1979, pp. 37 - 40.

19. Baker, L.R., "Measurement of the Flexural Bond Strength of Masonry", Proc. of 5th. Intern. Brick Masonry Conf., Washington D.C., October 1979, pp. 41 - 43.

20. Baker, L.R., "Some Factors Affecting the Bond Strength of Brickwork", Proc. of 5th. Intern. Brick Masonry Conf., Washington D.C., October 1979, pp. 43 - 46.

21. Baker, L.R., "Lateral Loading of Masonry Panels", Structural Design of Masonry, Cement and Concrete Association of Australia, Sydney, Feb. 1980, 37 pages.

22. Baker, L.R., "The Flexural Action of Masonry Structures Under Lateral Load", Ph.D. Thesis Submitted to the School of Engineering and Architecture, Deakin University, Geelong, Victoria, Australia, July 1981, 389 pages.

23. Baker, L.R. (Ed.), "Masonry Code of Practice", Association of Consulting Engineers of New South Wales, 1984.

24. Baker, L.R.; Gairns; D.A.; Lawrence, S.J.; and Scrivener, J.C.; "Flexural Behaviour of Masonry Panels - A State of the Art", Proc. of the 7th. Intern. Brick Masonry Conf., Melbourne, Australia, Feb. 1985, pp. 27 - 55.

25. Balachandran, k., "An Investigation of the Strength of Concrete Masonry Shear Wall Structures", Ph.D. Thesis, University of Florida, 1974.

26. Basu, A.K. and Dawson, J.M., "Orthotropic Sandwich Plates- Part 1 : Dynamic Relaxation Treatment, Part 2 : Analysis and application to Multicell and Voided Bridge Decks", Proc. of Instn. of Civil Engrs., 1970, Suppl., pp. 87 - 115.

27. Borchelt, J.G., "Analysis of Shear Walls Subject to Axial Compression and In-Plane Shear", Proc. of the 2nd. Intern. Brick Masonry Conf., Stoke-on-Trent, April 1970, pp. 263 - 265.

28. British Standards Institution, "Code of Practice for Structural Use of Masonry- Part 1: Unreinforced Masonry", BS 5628: Part 1, London, 1978, 39 pages.

29. Cajdert, A. and Losberg, A., "Laterally Loaded Light Expanded Clay Block Masonry- the Effect of Reinforcement In Horizontal Joints", Proc. of 3rd. Intern. Brick Masonry Conf., Essen, W. Germany, April 1973, pp. 245 - 251.

30. Cajdert, A., "Laterally Loaded Masonry Walls", Chalmers Univ. of Technology, Div. of Concrete Structures, Publication 80:5, Goteberg, Sweden, 1980, 283 pages.

31. Canadian Standards Association, "Cold-Drawn Steel Wire for Concrete Reinforcement", CAN3 G30.3-M1983, Rexdale, Ontario, 1983.

32. Canadian Standards Association, "Mortar and Grout for Unit Masonry", CAN3 A179-M1976, Rexdale, Ontario, 1976.

33. Canadian Standards Association, "Masonry Design for Buildings", CAN3 S304-M84, Rexdale, Ontario, Nov. 1984, 70 pages.

34. Clough et al, "A Literature Survey- Transverse Strength of Masonry Walls", Report to the Department of Housing, U.O.C., Berkley, Calif., March 1977.

35. Cox, F.W. and Ennenga, J.L., "Transverse Strength of Concrete Block Walls", ACI Journal, Vol. 54, May 1958, pp. 951 - 960.

36. Crisfield, M.A., "Finite Element Methods for the Analysis of Multicellular Structures", Proc. of Instn. of Civil Engrs., Vol. 48, March 1971, pp. 413 - 437.

37. deVekey, R.C. and West, H.W.H., "The Flexural Strength of Concrete Blockwork", Magazine of Conc. Research, Vol. 32, no. 113, Dec. 1980, pp. 206 - 218.

38. Dhanasekar, M.; Page, A.W.; and Kleeman, D.W.; "The Failure of Brick Masonry Under Biaxial Stresses", Instn. of the Civil Engrs., Vol. 79, Part 2, June 1985, pp. 295 - 313.

39. Drysdale, R.G. and Hamid, A.A., "Influence of Block Properties on the Flexural Strength of Concrete Masonry", Proc. of 7th. Australian Conf. on Mechanics of Structures and Materials, Perth, Australia, 1980, pp. 179 - 184.

40. Drysdale, R.G. and Hamid, A.A., "Anisotropic Tensile Strength Characteristics of Brick Masonry", Proc. of the 6th. Inter. Brick Masonry Conf., Rome, May 1982, pp. 143 - 153.

41. Drysdale, R.G. and Hamid, A.A., "Proposed Tension Failure Criteria for Concrete Masonry", Journal of Struc. Div., ASCE, Vol. 110, Feb. 1984, pp. 228 - 244.

42. Drysdale, R.G. and Essawy, A.S., "Out-of-Plane Bending of Concrete Block Walls", Presented at Oct. 1984, ASCE Convention, San Francisco, California. Also, Accepted for Publication in the Journal of Struc. Div., ASCE, 14 pages.

43. Gairns,D.A. and Scrivener, J.C., "Local Research Into Concrete Masonry Subjected to Lateral Loading", Preliminary Draft, University of Melbourne, 32 pages.

44. Gairns, D.A., "Flexural Behaviour of Concrete Blockwork Panels", Master Thesis, University of Melbourne, Australia, April 1983, 287 pages.

45. Ganz, H.R. and Thurlimann, B., "Shear Design of Masonry Walls", Proc. of New Analysis Techniques for Structural Masonry, ASCE Structures Congress'85, Chicago, Illinois, Sept. 1985, pp. 56 - 70.

46. Gazzola, E.A.; Drysdale, R.G.; and Essawy, A.S., "Bending of Concrete Masonry Wallettes at Different Angles to the Bed Joints", Proc. of the Third North American Masonry Conf., Texas, June 1985, Paper No. 27, 14 pages.

47. Gazzola, E.A., "Macroscopic and Microscopic Failure Criteria for Concrete Block Masonry Subjected to General Biaxial Bending", M.Eng. Thesis, McMaster University, Hamilton, Ontario, 1986.

48. Goodman,R.E. and St. John, C., "Finite Element Analysis for Discontinuous Rocks", Numerical Methods in Geotechnical Eng., pp. 148 - 175. Also, "Deep Foundation", pp. 239 - 245.

49. Grimm, C.T., "Design of Non-Reinforced Masonry Panel Walls", Proc. of 2nd. North American Masonry Conf., Maryland, Aug. 1982, Paper No.11.

50. Hamid, A.A., "Behaviour Characteristics of Concrete Masonry", Ph.D. Thesis, McMaster University, Ontario, Canada, Sept. 1978, 445 pages.

51. Hamid, A.A. and Drysdale, R.G., "Proposed Failure Criteria for Concrete Block Masonry Under Biaxial Stresses", Journal of Struc. Div., ASCE, Vol. 107, No. ST8, Aug. 1981, pp. 1675 - 1687.

52. Hamid, A.A. and Drysdale, R.G., "Flexural Tensile Strength of Concrete Block Masonry", Accepted for Publication in the Journal of Struc. Division, ASCE, 1985.

53. Haseltine, A. and Hodgkinson, R., "Wind Effects Upon Brick Panel Walls - Design Information", Proc. of 3rd. Intern. Brick Masonry Conf., Essen, W. Germany, April 1973, pp. 399 - 406.

54. Haseltine,B.A., "Design of Laterally Loaded Wall Panels", Proc. of British Ceramic Society, Loadbearing Brickwork(5), No. 24, Stoke-on-Trent, Sept. 1975,pp. 115 - 126.

55. Haseltine, B.A.; West,H.W.H.; and Tutt, J.N., "The Resistance of Brickwork to Lateral Loading: part 2- Design of Walls to Resist Lateral Loads", the Structural Engineer, Vol. 55, No. 10, Oct. 1977, pp. 422 - 430.

56. Hedstorm, R.O., "Load Tests of Patterned Concrete Masonry Walls", ACI Journal, Vol. 57, March 1961, pp. 1265 - 1286.

57. Hendry, A.W., "The Lateral Strength of Unreinforced Brickwork", the Structural Engineer, Vol. 51, No. 2, Feb. 1973, pp. 43 - 50.

58. Hendry, A.W. and Kheir, A.M.A., "The Lateral Strength of Certain Brickwork Panels", Proc. of 4th. Intern. Brick Masonry Conf., Brugge, April 1976, No. 4.a.3.

59. Hinton, E.; Razzaque, A.; Zienkiewicz, O.C.; and Davis, J.D., "A Simple Finite Element Solution for Plates of Homogeneous, Sandwich and Cellular Construction", Proc. of Instn. of Civil Engrs., Vol. 59, Part 2, March 1975, pp. 43 - 65.

60. Hinton,E. and Owen, D.r.J., "Finite Element Programming", Academic Press, London, 1977.

61. Hoffman, O., "The Brittle Strength of Orthotropic Materials", Journal of Composite Materials, Vol. 1, No. 2, April 1967, pp. 200 - 206.

62. Hughes, D.M. and Zsembery, S., "A Method of Determining the Flexural Bond Strength of Brickwork at Right Angles to the Bed

Joint", Proc. of 2nd. Canadian Masonry Sympos., Ottawa, 1980, pp. 73 - 86.

63. Jones, L.L. and Wood, R.H., "Yield-Line Analysis of Slabs", Thames and Hudson, London, 1967.

64. Jones, R.M., "Mechanics of Composite Materials", Ist. Ed., McGraw-Hill Book Co., Washington D.C.,1975.

65. Korol, R.M. and Mirza, F.A., "Finite Element Analysis of RHS T-Joints", Journal of Struc. Div., ASCE, Vol. 108, No. ST9, Sept. 1982, pp. 2081 - 2098.

66. Lawrence, S.J., "Flexural Strength of Brickwork Normal to and Parallel to the Bed Joints", Journal of Australian Ceramic Society, Vol. 11, No. 1, May 1975, pp. 5 - 6.

67. Lawrence, S.J. and Morgan, J.W., "Investigations of the Properties of Small Brickwork Panels in Lateral Bending", Technical Record TR52/75/418, Exp. Building Station, Depart. of Housing and Construc., North Ryde, N.S.W., Australia, 1975, 40 pages.

68. Lawrence, S.J., "The Relationship Between the Strengths of Brickwork Bond Piers and Shear Couplets", Technical Record TR52/75/438, Experimental Building Station, North Ryde, N.S.W., Australia, Sept. 1977, 10 pages.

69. Lawrence, S.J., "Behaviour of a Brick Cavity Wall Under Lateral Load, Including the Effects of an Intermediate Steel Mullion", Technical Record 441, Experimental Building Station, Depart. of Construc., North Ryde, N.S.W., Australia, Feb. 1978, 28 pages.

70. Lawrence, S.J., "The Flexural Behaviour of Brickwork", Proc. of Ist. North American Masonry Conf., Boulder, Colorado, Aug. 1978, Paper No. 20.

71. Lawrence, S.J., "Lateral Loading of Masonry Infill Panels- A Literature Review", Technical Record 454, Experimental Building Station, Depart. of Housing and Construc., N.S.W., Australia, Nov. 1979, 38 pages.

72. Lawrence, S.J., "Design of Masonry Panels For Lateral Loading-Some Interim Recommendations", Technical Record 460, Experimental Building Station, Depart. of Housing and Construc., N.S.W., Australia, Nov. 1980, 20 pages.

73. Mindlin, R.D., "Influence of Rotatory Inertia and Shear on the Flexural Motions of Isotropic, Elastic Plates", Journal of Applied Mech. Div., ASME, Vol. 18, March 1951, pp. 31 - 38.

74. Mirza, F.A., "Finite Element Method and Basic Finite Element Computer Programs", Graduate Course Notes, Department of Civil Eng., McMaster University, 1981.

75. Nadai, A., "Theory of Flow and Fracture of Solids", Vol. 1, McGraw-Hill Book Co., New York, 1950.

76. National Research Council of Canada, "National Building Code of Canada", Associate Committee on the National Building Code, Ottawa, 1980.

77. Neville. A.M., "Properties of Concrete", Pitman Press, Metric Edition, England, 1973.

78. Nilsson, I.H.E. and Losberg, A., "The Strength of Horizontally Loaded Prefabricated Brick Panel Walls", Proc. of 2nd. Intern. Brick Masonry Conf., Stoke-on-Trent, England, April 1970, pp. 191 - 196.

79. Page, A.W., "Finite Element Model for Masonry", Journal of Struc. Div., ASCE, Vol. 104, No. ST8, Aug. 1978, pp. 1267 - 1285.

80. Page, A.W., "A Biaxial Failure Criterion for Brick Masonry in the Tension - Tension Range", Intern. J. of Masonry Construc., Vol. 1, No. 1, March 1980, pp. 26 - 29.

81. Page, A.W.; Kleemen, P.W.; and Dhanasekar, M., "An In-plane Finite Element Model for Brick Masonry", Proc. of New Analysis Techniques for Structural Masonry, ASCE Structures Congress'85, Chicago, Illinois, Sept. 1985, pp. 1 - 18.

82. Pryor, Jr., C., "Finite Element Analysis of Laminated Anisotropic Plates Including Transverse Shear Deformations", Ph.D. Thesis, Virginia Polytechnic Institute, 1970, 130 pages.

83. Pryor, Jr., C.W. and Barker, R.M., "A Finite-Element Analysis Including Transverse Shear Effects for Applications to Laminated Plates", AIAA Journal, Vol. 9, No. 5, May 1971, pp. 912 - 917.

84. Sahlin, S., "Structural Masonry", Prentice-Hall, New Jersey, 1971.

85. Samarasinghe, W.; Page, A.W.; and Hendry, A.W., "Behaviour of Brick Masonry Shear Walls", the Structural Engineer, Vol. 59B, No. 3, Sept. 1981, pp. 42 - 48.

86. Satti, K.M.H. and Hendry, A.W., "The Modolus of Rupture of Brickwork", Proc. of 3rd. Intern. Brick Masonry Conf., Essen, W. Germany, April 1973, pp. 155 - 160.

87. Sawko, F. and Cope, R.J., "Analysis of Multi-Cell Bridges Without Transverse Diaphragms- A Finite Element Approach", the Structural Engineer, Vol. 47, No. 11, Nov. 1969, pp. 455 - 460.

88. Self, M.W., "Structural Properties of Loadbearing Concrete Masonry", A.S.T.M. STP589, Masonry: Past and Present, Philadelphia, 1973.

89. Seward, D.W., "A Developed Elastic Analysis of Lightly Loaded Brickwork Walls With Lateral Loading", Intern. J. of Masonry Construc., Vol. 2, No. 3, 1982, pp. 129 - 134.

90. Shanley, F.R., "Mechanics of Materials", McGraw-Hill Book, New York, 1967.

91. Shehata, A.A., "Finite Element Modelling and Elasto-Plastic Analysis of RHS Double Chord T-Joints", Ph.D. Thesis, McMaster University, 1983.

92. Sinha, B.P., "A Simplified Ultimate Load Analysis of Laterally Loaded Model Orthotropic Brickwork Panels of Low Tensile Strength", The Structural Engineer, Vol. 56B, No.4, Dec. 1978, pp. 81 - 84.

93. Sinha, B.P., "An Ultimate Load Analysis of Laterally Loaded Brickwork Panels", Intern. Journal of Masonry Construction, Vol. 1, No. 2, 1980.

94. Soliman, M.I., "Behaviour and Analysis of a Reinforced Concrete Box Girder Bridge", Ph.D. Thesis, McGill University, Montreal, 1979.

95. Standards Association of Australia, "Australian Standard Rules for Brickwork in Buildings", AS1640- 1974, 1974, 126 pages.

96. Standards Association of Australia, "S.A.A. Blockwork Code, Part I-Unreinforced Blockwork", AS1475, Part 1-1977, North Sydney, Australia, 1977, 32 pages.

97. Standards Association of Australia, "Draft Australian Standard for Masonry in Buildings", Sydney, Australia, April 1984.

98. Standards Association of New Zealand, "Draft New Zealand Standard Specification for Design of Reinforced Masonry", DZ4210 Part 8, 1981, 71 pages.

99. Suwalski, P.D., "Capacity of Eccentrically Loaded Slender Concrete Block Walls", M.Eng. Thesis, McMaster University, Hamilton, Ontario, 1986.

100. Szilard, R., "Theory and Analysis of Plates: Classical and Numerical Methods", Prentice-Hall, New Jersey, 1974.

101. Timoshenko, S.P. and Krieger, W., "Theory of Plates and Shells", Second Edition, McGraw-Hill Book, New York, 1959.

102. Turkstra, C.J. and Thomas, G.R., "Strain Gradient Effects in Masonry", Proc. of 1st. North American Masonry Conf., Boulder, Colorado, Aug. 1978, pp. 22.1 - 22.21.

103. West, H.W.H.; Hodgkinson, H.R.; and Webb, W.F., "The Resistance of Brick Walls to Lateral Loading", Proc. of British Ceramic Society, Loadbearing Brickwork (4), No. 21, Stoke-on-Trent, April 1973, pp. 141 - 164.

104. West, H.W.H.; Hodgkinson, H.R.; and Webb, W.F., "Lateral Loading Tests on Walls With Different Boundary Conditions", Proc. of 3rd. Intern. Brick Masonry Conf., Essen, W. Germany, April 1973, pp. 180 - 186.

105. West, H.W.H., "The Flexural Strength of Clay Masonry Determined from Wallette Specimens", Proc. of 4th. Intern. Brick Masonry Conf., Brugge, April 1976, No. 4.a.6.

106. West, H.W.H. and Haseltine, B.A., "The Design of Laterally Loaded Walls", Proc. of 4th. Intern. Brick Masonry Conf., Brugge, April 1976, No. 4.b.10.

107. West, H.W.H.; Hodgkinson, H.R.; and Haseltine, B.A., "The Resistance of Brickwork to Lateral Loading: Part 1-Experimental Methods and Results of Tests on Small Specimens and Full Sized Walls", the Structural Engineer, Vol. 55, No. 10, Oct. 1977, pp. 411 - 421.

108. Discussion of References 55 and 107, "The Resistance of Brickwork to Lateral Loading", The Structural Engineer, Vol. 56A, No. 2, 1978.

109. Whang, B., "Elasto-Plastic Orthotropic Plates and Shells", Proc. of Sympos. on Application of F.E. Methods in Civil Eng., ASCE, Nashville, Tennessee, Nov. 1969, pp. 481- 515.

110. Wong, H.E., "Compression Characteristics of Concrete Block Masonry Prisms", M.Eng. Thesis, Depart. of Civil Eng., McMaster University, Draft, 1985.

111. Yokel, F. and Fattal,G., "Failure Hypotheses for Masonry Shear Walls", Journal of Struc. Div., ASCE, Vol. 102, No. ST3, March 1976, pp. 515 - 532.

112. Zia, P., "Torsional Strength of Prestressed Concrete Members", Magazine of Concrete Research, No. 14, 1953, pp. 75 - 86.

113. Zienkiewicz, O.C. and Cheung, Y.K., "The Finite Element Method for Analysis of Elastic Isotropic and Orthotropic Slabs", Proc. of Instn. of Civil Engrs., Vol. 28, Aug. 1964, pp. 471 - 488.

114. Zienkiewicz, O.C., "The Finite Element Method", McGraw-Hill Book, London, 1977.